



Statistical analysis of traffic loads and their effects on bridges

Xiao Yi Zhou

► To cite this version:

Xiao Yi Zhou. Statistical analysis of traffic loads and their effects on bridges. Other. Université Paris-Est, 2013. English. NNT : 2013PEST1041 . tel-00862408

HAL Id: tel-00862408

<https://theses.hal.science/tel-00862408>

Submitted on 16 Sep 2013

HAL is a multi-disciplinary open access archive for the deposit and dissemination of scientific research documents, whether they are published or not. The documents may come from teaching and research institutions in France or abroad, or from public or private research centers.

L'archive ouverte pluridisciplinaire **HAL**, est destinée au dépôt et à la diffusion de documents scientifiques de niveau recherche, publiés ou non, émanant des établissements d'enseignement et de recherche français ou étrangers, des laboratoires publics ou privés.

STATISTICAL ANALYSIS OF TRAFFIC LOADS AND TRAFFIC LOAD EFFECTS ON BRIDGES

Using Weigh-in-Motion data collected in France

by

Xiao Yi ZHOU

A Thesis Submitted to

the École Doctorale Sciences Ingénierie et Environnement of
the Université Paris-Est in Partial Fulfillment of the Requirements for
the Degree of Doctor of Philosophy

Reviewers:	Prof.	E. Brühwiler	EPFL, Switzerland
	Prof.	T. Vrouwenvelder	TU Delft, Netherlands
Examinators:	Prof.	P. Croce	University of Pisa, Italy
	Prof.	B. Jourdain	CERMICS, ENPC
Supervisor	HDR	F. Toutlemonde	IFSTTAR
Advisors		B. Jacob	IFSTTAR
	Dr.	F. Schmidt	IFSTTAR

Paris, France

May 15, 2013

Abstract

It is vital to ensure highway structures to cater for increasing demand in transport capacity. This involves the precise estimation of structural load-carrying capacity to withstand potential maximum load effects in residual lifetime. The scope of this research thus addresses estimation of traffic load effect. Many different methods have been used to model extreme traffic load effects on bridges for estimating characteristic value or distribution, including fitting a Normal or Gumbel distribution to the upper tail of load effects, the use of Rice formula based level crossing method, the block maxima method and the peaks over threshold (POT) method. A review of the mathematic and engineering background of these methods is presented with qualitative analysis. In addition, a quantitative comparison is carried out to evaluate the performances of these methods on estimating characteristic value and probability of failure. Results show that the POT method provides relatively good estimation.

A thorough study on POT method is thus carried out in this thesis. Estimation of generalized Pareto distribution parameters is a crucial step in the application of POT method. Available methods include the method of moments (MM), the probability weighted moments (PWM), the maximum likelihood (ML), the penalized maximum likelihood (PML), the minimum density power divergence (MDPD), the empirical percentile method (EPM), the maximum goodness-of-fit statistic and the likelihood moment (LM). In order to provide guidance on selecting appropriate method when applying POT to bridge traffic load effects, we evaluate their performance by estimating characteristic values through three studies with: numerical simulation data, Monte Carlo simulated and measured traffic load effect measurements. From the simulated traffic load effect, the ML and PML provide more accurate estimates for large size sample, while the MM and PWM are better than others for small size sample. Moreover, results from monitored traffic load effects indicate that outliers or large observations have significant influence on the parameter estimators.

A common cause of outliers or larger observation is observed when the traffic is a mixture of two distributions, which may be two distinct sub-populations. Traffic load effects induced by different numbers of vehicles are not identically distributed, and this violates basic assumption in the use of the classic extreme value theory to estimate the distribution of extreme bridge traffic load effects. A new method named mixture peaks over threshold (MPOT) is proposed which enables to estimate the distribution of extreme traffic load effects from mixture loading events. Its performance is evaluated by theoretical and traffic load effect examples, and results

Abstract

show that MPOT can provide sufficiently accurate estimation.

A precise method can improve the accuracy on modeling traffic load effects, while the epistemic assumption may be also important. In traffic load effect calculation, vehicles are generally assumed to cross over the bridge along the lane centerline which may not influence the global load effects but is important to study transverse bending and local effects as significantly considered for orthotropic steel decks. Due to the advance of weigh-in-motion technique, vehicle lateral position in lane can be measured with sufficient accuracy. We investigate the influence of the vehicle lateral position in lane on bridge local effects by comparing simulated effects based on measured traffic loads with Eurocode recommended model.

Résumé

Il est essentiel de s'assurer que les infrastructures et particulier les ponts européennes sont en mesure de répondre à la demande croissante en capacité de transport. Différentes méthodes d'extrapolation ont déjà été utilisées pour modéliser les effets extrêmes du trafic, afin de déterminer les effets caractéristiques pour de grandes périodes de retour. Parmi celles-ci nous pouvons citer l'ajustement d'une gaussienne ou d'une loi de Gumbel sur la queue de distribution empirique, la formule de Rice appliquée à l'histogramme des dépassements de niveaux, la méthode des maxima par blocs ou celle des dépassements de seuils élevés. Les fondements et les utilisations faites de ces méthodes pour modéliser les effets extrêmes du trafic sur les ouvrages sont donnés dans un premier chapitre. De plus, une comparaison quantitative entre ces méthodes est réalisée. Deux études sont présentées, l'une basée sur un échantillon numérique et l'autre sur un échantillon réaliste d'effets du trafic. En général, bien qu'aucune méthode n'ait réalisée des extrapolations de manière correcte, les meilleures sont celles qui s'intéressent aux queues de distributions, et en particulier des dépassements au-dessus d'un seuil élevé.

Ainsi une étude de cette dernière méthode est réalisée : en effet, cette méthode, nommée «dépassements d'un seuil élevé», considère que les valeurs au-dessus d'un seuil correctement choisi, assez élevé, suivent une distribution de Pareto généralisée (GPD). Beaucoup de facteurs influencent le résultat lorsqu'on applique cette méthode, comme la quantité et la qualité des données à notre disposition, les critères utilisés pour déterminer les pics indépendants, l'estimation des paramètres et le choix du seuil. C'est pour cette raison qu'une étude et une comparaison des différentes méthodes d'estimation des paramètres de la distribution GPD sont effectuées : les conditions, hypothèses, avantages et inconvénients des différentes méthodes sont listés. Différentes méthodes sont ainsi étudiées, telles la méthode des moments (MM), la méthode des moments pondérés (PWM), le maximum de vraisemblance (ML), le maximum de vraisemblance pénalisé (PML), le minimum de la densité de la divergence (MDPD), la méthode des fractiles empiriques (EPM), la statistique du maximum d'adaptation et la vraisemblance des moments (LM). Pour comparer ces méthodes, des échantillons numériques, des effets de trafic simulés par méthode de Monte Carlo et des effets mesurés sur un ouvrage réel sont utilisés. Pour des effets du trafic simulés, ML et PML donne des valeurs de retour meilleures lorsque le nombre de valeurs au-dessus du seuil est supérieur à 100 ; dans le cas contraire, MM et PWM sont conseillés. De plus, comme c'est

prouvé dans l'étude de valeurs réelles mesurées, les valeurs atypiques («outliers») ont une influence notable sur le résultat et toutes les méthodes sont moins performantes.

Comme cela a été montré dans la littérature, ces «valeurs atypiques» proviennent souvent du mélange de deux distributions, qui peuvent être deux sous-populations. Dans le cas de l'effet du trafic sur les ouvrages, cela peut être la raison d'une estimation des paramètres non correcte. Les articles existant sur le sujet soulignent le fait que les effets du trafic sont dus à des chargements indépendants, qui correspondent au nombre de véhicules impliqués. Ils ne suivent pas la même distribution, ce qui contredit l'hypothèse classique en théorie des valeurs extrêmes que les événements doivent être indépendants et identiquement distribués. Des méthodes permettant de prendre en compte ce point et utilisant des distributions mélangées (exponentielles ou valeurs extrêmes généralisées) ont été proposées dans la littérature pour modéliser les effets du trafic. Nous proposons une méthode similaire, que nous appelons dépassement de seuils mélangés, afin de tenir des différentes distributions sous-jacentes dans l'échantillon tout en appliquant à chacune d'entre elles la méthode des dépassements de seuil.

Une méthode précise peut améliorer la précision sur les effets calculés des charges de trafic, alors que l'hypothèse épistémique peut être aussi importante. Dans le calcul de l'effet des charges de trafic, les véhicules sont généralement supposés traverser l'ouvrage le long de l'axe de la voie, ce qui peut ne pas influencer sur l'effet global. Mais il est important d'étudier l'effet local de la position transversale des charges, comme pour les ponts métalliques à dalle orthotrope. En raison des avancées des techniques du pesage en marche, la position latérale du véhicule peut être mesurée avec une précision suffisante. Nous étudions l'influence de la position latérale du véhicule dans la voie en comparant les effets obtenus avec des charges mesurées et modèle recommandé par l'Eurocode.

Acknowledgments

I would like to thank the members of the examination committee for time spent reading and commenting on this dissertation: Emeritus Professor Ton VROUWENVELDER from Delft University of Technology, Professor Eugen BRÜWHILER from École Polytechnique Fédérale de Lausanne, Professor Pietro CROCE from Università di Pisa and Professor Benjamin JOURDAIN from École des Ponts ParisTech.

This work has been carried out under the supervision of Dr. François TOUTLEMONDE and I would like to thank him for all his help and encouragement. His numerous advice, attention to detail and thorough proof reading ensure the thesis to be completed on time. Mr. Bernard JACOB has made valuable comments of the thesis. There is no doubt that Dr. Franziska SCHMIDT has had the greatest influence on my work. Responsible for overseeing the thesis, she has consistently provided sound advice throughout my work.

I would like to express my gratitude to Dr. Christian CREMONA from SETRA, Professor Airong CHEN and Professor Xin RUAN from Tongji University for their recommendations to let me have the opportunity to begin my doctoral study at IFSTTAR. Professor Robert EYMARD and Professor Florence MERLEVÈDE at Université Paris-Est Marne-la-Vallée are appreciated for their supervisions during the first year of my PhD period.

I would like to express my appreciation of the support I have received from my colleagues at Département Structures et Ouvrages d'Art (SOA) in IFSTTAR - particularly Jean-François SEIGNOL, Minh ORCESI, Véronique BOUTEILLER, Anne-Sophie COLAS, Nina COULATY-CHIN, Nadia KAGHO, Lucas ADELAIDE, Cédric DESPREZ, Umair IFTIKHAR, Bruno KOUBI, André ORCESI, Adam OUMAROY Marc QUIERTANT and Binh TA. Merci bien! The supports from my friends are also greatly appreciated - especially Boke, João, Sio-song, Su, Suzhe, Weichao, Xiaowei, Xiaoyan, Zhangli and Zhidong.

This thesis is a part of TEAM project which is a Marie Curie Initial Training Network funded by the European Commission FP7 which is greatly appreciated. All members of TEAM project have been very helpful. Special thanks are directed to my TEAM secondment advisors: Professor Eugen BRÜWHILER at École Polytechnique Fédérale de Lausanne (EPFL) and Professor Eugene O'BRIEN at University College Dublin (UCD). Co-workers Donya HAJIALIZADEH at UCD and Mark TREACY at EPFL are particularly appreciated for their contribution and useful

Acknowledgments

discussion on works of Chapter 2 and Chapter 5, respectively.

I would like to thank the CETE de l'Est for the data provided to accomplish this research, especially Mr. Eric KLEIN and Mr. Daniel STANCZYK for all of their helps with obtaining the data needed.

Finally, I would like to thank all my family, and particularly my parents, Yunhe and Fengzi, for teaching me the value of hard work, my wife, Xi, for her infinite patience and support over the last three years while I have been working on this research, and my son, Yuxuan.

Contents

Abstract	iii
Résumé	v
Acknowledgments	vii
Introduction	1
Background and Motivation	3
Thesis Objective	5
Structure of the Thesis	6
1 Extreme Value Modeling - A Review in Bridge Traffic Load Effects Analysis	9
1.1 Introduction	11
1.2 Extreme Value Modeling	11
1.3 Collecting and Using Weigh-in-Motion Data in Bridge Design and Assessment .	19
1.4 Extreme Values in Bridge Traffic Load Effects	21
1.5 Summary	38
2 Performances of Some Prediction Methods for Bridge Traffic Load Effects	39
2.1 Introduction	41
2.2 Data Description, and Characteristic Value and Probability of Failure Calculation	41
2.3 Results for Simulation Study Case I: Theoretical Examples	46
	ix

Contents

2.4	Results for Simulation Study Case II: Traffic Load Effect Examples	48
2.5	Conclusion	53
3	A Comparative Evaluation for the Estimators of the GPD	59
3.1	Introduction	61
3.2	Methods for estimating GPD parameters	62
3.3	Evaluating the Performance of Estimators	74
3.4	Conclusion	96
4	Mixture Peaks over Threshold Approach to Model Extreme Bridge Traffic Load Effect	99
4.1	Introduction	101
4.2	Methodology	101
4.3	Theoretical Examples	103
4.4	Discussion	116
4.5	Simulated Traffic Load Effects	119
4.6	Conclusion	134
5	Effects of Distribution of Vehicle Lateral Position in Lane on Bridge Local Effects from WIM Measurements	139
5.1	Introduction	141
5.2	Related Research	142
5.3	Measurements	143
5.4	Sensitivity of Local Effects to VLP Case I: RC Bridge Deck Slab	149
5.5	Sensitivity of Local Effects to VLP Case II: Orthotropic Bridge Deck	151
5.6	Conclusion	164
	Conclusions and Perspectives	167
	Conclusions of the Thesis	169

Perspectives for Future Research	171
Bibliography	185
Appendix A Weigh-in-Motion Data and its Statistical Analysis	187
A.1 WIM data	189
A.2 Cleaning Unreliable WIM Data	190
A.3 Statistical Description of WIM Data	192
Appendix B Bridge Traffic Load Effect Calculation and Simulation Program	199
B.1 Introduction	201
B.2 Program Description	201
B.3 Traffic Files	206
B.4 Output	209
Appendix C Mixture Peaks over Threshold Method	219
Résumé Long	225
List of Figures	229
List of Tables	233
Curriculum Vitae	239

Definitions

List of Terminology

Term	Definition
Probability of exceedance	probability that a given value is exceeded
Return period	an average time interval between two occurrences of a given value
Return level or	a value that is expected to be exceeded once in a given return period
Characteristic value	
Heavy-vehicle	vehicle having a total weight greater than 3.5 t

List of Special Symbols

Symbol	Definition
F	cumulative distribution function (CDF), other symbols like G are used also;
f	probability density function (PDF), density of CDF F ;
F^m	m^{th} power of distribution function F
F^{-1}	quantile function (qf) pertaining to the CDF F ;
$F^{[u]}$	exceedance distribution function at u (left truncation at F of u);
Φ	standard normal (Gaussian) distribution function;
$x_{i:n}$	i^{th} ordered value of data x_1, \dots, x_n (in ascending order);
\hat{F}_n	empirical distribution function;
\hat{F}_n^{-1}	empirical quantile function;
$E(X)$	mean value or expectation of a random variable X ;
$V(X)$	variance of a random variable X ;
ν	intensity of level crossing;
x_p	p^{th} quantile;
X^*	bootstrap data set generated from the data set X ;
θ	parameter or parameter vector;
$\hat{\theta}$	estimate of parameter or parameter vector;
$T(F)$	parameter as function of distribution function F ;
I_A	indicator function of the set A ;
Pr	probability.

Definitions

List of Abbreviations

Term	Definitions
df	distribution function
iid	independent and identically distributed
rv	random variable
AASHTO	American Association of State Highway and Transportation Officials
AD	Anderson-Darling test
BM	block maximum (method)
EC	Eurocode
CDF	cumulative distribution function
CDS	composite distribution statistics
CM	Camera von-Mises test
CLT	central limit theorem
EDF	empirical distribution function
EPM	elemental percentile method
EVD	extreme value distribution
EVT	extreme value theory
GEV	generalized extreme value
GMM	generalized method of moments
GP(D)	generalized Pareto (distribution)
GPWM	generalized probability weighted moments
GVW	gross vehicle weight
KS	Kolmogorov Smirnov test
LE	load effect
LM	likelihood moment
LLN	law of large number
LSM	least squares method
MC	Monte Carlo simulation method
MDPD	minimum density power divergence
MGF	maximum goodness-of-fit
ML(E)	maximum likelihood
MM	method of moments
MPOT	mixture peaks over threshold method
PDF	probability density function
PML	penalized maximum likelihood
POT	peaks over threshold (method)
PWM	probability weighted moments
OSD	orthotropic steel deck
RMSE	root-mean-square error
WIM	Weigh-in-Motion



Introduction

Background and Motivation	3
Thesis Objective	5
Structure of the Thesis	6

Background and Motivation

Road is the by far the dominant mode (45.8%) of freight transport in almost all of the European countries. Road freight transport has increased by 36.2% in terms of tonne-kilometres (t.km) between 1995 and 2010 in Europe, and the trend is projected to continue with the rate of 1.7% per year between 2005 and 2030 [European Commission, 2008, 2012]. It is thus vital to ensure highway structures availability to cater for this increasing demand in transport capacity, especially as they are aging and deteriorating due to environment aggression (corrosion, loss of resistance).

For the design of new bridges, the codified load model should guarantee all newly designed bridge to have at least a minimum safety under future traffic. Therefore, the load model should be periodically calibrated using modern collected traffic data [Fu and van de Lindt, 2006; Ghosn et al., 2012; Jacob and Kretz, 1996; Kwon et al., 2011a; O'Connor et al., 2001; Pelphrey et al., 2008; van de Lindt et al., 2005].

For existing bridges, the task is to assess their safety under current and future traffic, and a prioritization of the measures necessary to ensure their structural integrity and safety. In 2002, the economic cost of bridge repair, rehabilitation and maintenance in the Europe of 27 is estimated to be in the value of 2-3 billion € annually [COST 345, 2002b]. However, the budgets available for bridge management are usually limited, for example, the total rehabilitation expenditure is evaluated in 2006 to be 635 million € but the annual budget of maintenance is 45 million € for national bridges in France [Cremona, 2011]. It is thus crucial to allocate the available budgets reasonably. The use of design standards for assessment is too conservative and can lead to considerable unnecessary expenditure. Indeed bridges can often be shown to be safe for the individual site-specific traffic loading to which they are subject, even if they do not have the capacity to resist to the notional assessment load for the network or road class [Getachew and O'Brien, 2007; O'Connor and Eichinger, 2007; O'Connor and Enevoldsen, 2008]. Hence, a site-specific assessment is a solution to quantify the safety of an existing bridge structure. Many works have been conducted to improve the assessment of highway bridges, and the procedures for the assessments of highway structures in Europe have been proposed under the European research COST 345 [COST 345, 2002a; O'Brien et al., 2005].

In addition, to address this growth without compromising the competitiveness of European, some countries are encouraging the introduction of longer and heavier trucks, with up to 9 axles and gross weights of up to 60 t. It has the advantage of reducing the number of vehicles for a given volume or mass of freight and reducing labor, fuel and other costs. This thesis originated in the need to assess the impacts of traffic evolution on bridges safety [Ghosn and Moses, 2000; Jacob and Kretz, 1996; O'Brien et al., 2008; Sivakumar and Ghosn, 2009], costs [Hewitt et al., 1999] and policy [Fekpe, 1997].

Clearly, issues caused by the increasing of traffic depend on the accurate knowledge of traffic loads and traffic load effects on bridges. For assessment of existing bridges, by deterministic approach, a bridge can be considered safe when its resistance exceeds the possible experienced

load effect, while a bridge is safe when the resistance is exceeded with a legally defined low probability in probabilistic approach. Whatever choice is made to conduct a deterministic or probabilistic site-specific assessment, the loading capacity and the possible loads need to be established as accurately as possible. Understanding of load carrying capacity has greatly improved in recent decades that a number of works have been carried out on methods to model the load capacity of bridges and the associated uncertainties. However, an important component of applied load effects on bridges from traffic loading has not received enough attention until recent years. To know and establish the maximum lifetime distribution of traffic load effects is crucial to carry out the assessment of bridge structures. This can be done by using huge number of measurements [Eymard and Jacob, 1989], Monte Carlo simulation [Enright and O'Brien, 2012], and statistical analysis. Although WIM techniques have been advanced in recent years, the relative recent adoption of WIM makes it hard to obtain long term measurements. Monte Carlo simulation can extend the size of measured data, but the simulated data has the same statistical feature as the measurements that cannot reflect real traffic evolution.

A suitable way is to use simulation to extend the data to a certain size, then use statistics of extremes to project them to remote future. Due to the theoretical and application development in WIM techniques [Jacob, 2000; Jacob et al., 2000], even a relative short term measurement can well model the statistics of traffic. Statistical methods have been introduced to model traffic load effects on bridges [Cremona, 2001; Nowak et al., 1993], but extreme value modeling methods have just been used since the 1980s [Bailey and Bez, 1999; Messervey et al., 2010; Siegert et al., 2008]. Extreme value modeling techniques have become widely used in the last 50 years in many disciplines, such as extreme levels of a river in hydrology, the largest claim in actuarial analysis, the failure load of material [Cebrian et al., 2003; Holmes and Moriarty, 1999; Huang et al., 2012]. The objective of extreme value modeling is to quantify rare events and the extreme events outside the scope of being observed. Modeling the tails of distributions is important in bridge engineering and the study of extreme loading events in reliability analysis. Extreme value models provide an asymptotic approximation for the tail distributions, which are very flexible in terms of the allowable tail shape behavior. The attraction of the extreme value theory based methods is that they can provide mathematically and statistically justifiable parametric models for the tail distributions, which can give reliable extrapolations beyond the range of the observed data.

Extreme value modeling techniques have been shown to be a very useful tool in estimating and predicting the extremal behavior of traffic loads or load effects, such as predicting the 1000-year return level, Caprani et al. [2008]. However, applying extreme value models is not always straightforward and there are common issues in applications. The typical problem is the correlation of extreme data, which will lead the feasibility problem of the model. The inherent sparsity of extremal data is another common issue, which can result in the model identification and parameter estimation problem, particularly with a complex structure. Traffic load effects are actually of this type [Caprani et al., 2008], the load effects may be induced by traffic flow with traffic volume of 5000 trucks today and 3000 trucks tomorrow. Additionally, other

issues such as sampling the extremes and the choice of threshold can also be problematic. Therefore, applying extreme value models is not always straightforward and the modification of traditional extreme value models needs to be considered to minimize the impact of these issues.

Thesis Objective

The rapid increase of global economics has induced growth in transportation demand. Safety assessment appears more and more important for both investors and regulators. In this thesis, we have applied the extreme value modeling to bridge traffic load effects with application in bridge engineering and focus on solving extreme value modeling issues such as complex model structure and parameter estimation.

The available traffic data is always limited in duration of measurement, which may impact representativity for studying traffic load effects. The live load model of AASHTO was developed based on 9250 trucks representing 2-week heavy traffic [Nowak and Hong, 1991]. The traffic load model of EC is mainly developed based on 2 weeks traffic collected from A6 highway in France [Sedlacek et al., 2006]. Sivakumar et al. [2011] suggest to collect one year's continuous data for load modeling. However, obtaining such long term measurements is time consuming and expensive. A suitable statistical tool needs to be introduced in order to acquire reliable extreme value modeling with short term measurements. Using Monte Carlo simulation to extend the data is a recently popular way in bridge traffic load effect analysis [Enright and O'Brien, 2012], however, it should be borne in mind the limitation of the Monte Carlo simulation that the generated data have the same statistical features as the measurements. In addition, the generalized Pareto distribution based extreme value modeling method is more suitable to small size sample of extremes than the generalized extreme value distribution based block maxima method as it uses all extremes over a certain high threshold. Usually, it will use the data more efficient. In this thesis, we try to use the generalized Pareto distribution based Peaks over threshold (POT) method to establish the extreme value model of traffic load effect. The common issues of threshold choice, especially parameter estimation, have been discussed in this thesis to propose a suitable parameter estimation method in applying POT method to traffic load effects.

Caprani et al. [2008]; Harman and Davenport [1979] point out that the traffic load effect is not identically distributed, which violates the assumption of classic extreme value theory that the underlying distribution should be identically independently distributed [Leadbetter et al., 1983]. With respect to non-identical distribution in bridge traffic load effects, non-identical distribution needs to be addressed in extreme modeling to account for the impacts in inference. Harman and Davenport [1979] propose a mixture exponential distribution to model the extreme value, Caprani et al. [2008] propose a mixture generalized extreme value distribution. Stimulated by their works, we have aimed to explicitly model the non-identically distributed behavior of extremes for a stationary extreme time series within a mixture peaks

over threshold model to avoid the loss of information. This constitutes one of the main original developments of this thesis.

In many situations, the governing traffic load effect is the possible extreme value in service period, but components like orthotropic steel decks are governed by traffic induced fatigue load effects. In this thesis, we have attempted to explore the influence of traffic load on the fatigue behavior of orthotropic steel decks, especially the influence of the loading position in terms of transverse location of vehicle.

Structure of the Thesis

The thesis focuses on applying statistical techniques in extreme value modeling on safety assessment in bridge engineering studies. The research presented in the thesis involves a variety of statistical methods, including extreme value theory. The outline of the thesis are as follows.

Chapter 1 reviews the relevant background to this work. Particular attention is given to statistical background of extreme value modeling methods and their applications on estimating the distribution of extreme bridge traffic load effects.

Except extreme value modeling methods, other statistical methods are also used for traffic load effects. A quantitative investigation of extreme value modeling methods and historical methods is carried out in Chapter 2 through two examples. The first example uses numerical simulated theoretical sample, and the second example uses Monte Carlo simulated traffic load effect sample. The performances of the methods are evaluated, and recommendations are given to improve the applicability.

The qualitative and quantitative evaluation in Chapters 1 and 2 indicate that peaks over threshold method has well performance in modeling extreme traffic load effect. A further exploration is carried out on this method. The use of POT method is limited by two critical issues: threshold choice and parameter estimation. There are a number of parameter estimation methods available in the literature, and each method has its advantages and disadvantages. In order to provide a guide to select appropriate parameter estimation method in the use of peaks over threshold method for bridge traffic load effects. Several parameter estimation methods are presented in Chapter 3. Especially, their performances are evaluated using numerical simulation data, simulated traffic load effect and monitored load effects.

A new method is proposed in Chapter 4 to simultaneously model both tails using GPD and to account for the non-identically distribution feature of traffic load effects. More specifically, we define a mixture generalized Pareto distribution with certain components corresponding to different types of loading events. The proposed method is firstly examined by using numerical simulation sample. Its performance is reported and comparison with standard POT is presented in this chapter. Furthermore, the proposed method is applied to traffic load effects

data. The load effects and corresponding information of loading event are obtained by passing the WIM data or synthetic traffic data over influence lines.

Bridge structural components like orthotropic steel deck frequently encounter fatigue problems that relate to local effects induced by wheel load. In Chapter 5, the influence of distribution of lateral position in lane of wheel load on effects on orthotropic steel decks and reinforced concrete bridge decks are investigated through statistical analysis and fatigue damage analysis.

Finally, the conclusions are drawn from this work along with areas in which further research may be directed.

1 Extreme Value Modeling - A Review in Bridge Traffic Load Effects Analysis

1.1	Introduction	11
1.2	Extreme Value Modeling	11
1.2.1	Asymptotic Models of Extremes and Block Maxima Method	11
1.2.2	Generalized Pareto Distribution and Peaks over Threshold Method	15
1.2.3	Level Crossings and Rice's Formula	17
1.3	Collecting and Using Weigh-in-Motion Data in Bridge Design and Assessment	19
1.3.1	Developing of Load Model for Bridge Design and Assessment	19
1.3.2	Calibrate Traffic Load Model	20
1.3.3	Evaluating Bridge Safety	21
1.4	Extreme Values in Bridge Traffic Load Effects	21
1.4.1	Tail of Parent Distribution Method	22
1.4.2	Block Maxima Method	26
1.4.3	Peaks over Threshold Method	33
1.4.4	Level Crossing Method	35
1.5	Summary	38

1.1 Introduction

The objective of extreme value modeling is to quantify the outcome of a stochastic process for events which have a small probability of occurring and even to extrapolate outside the scope of observations. The issue belongs to extreme value statistics, which has been developed in the last 60 years. Since they have been developed, extreme value techniques have been used in many disciplines such as the hydrology [Deidda, 2010], insurance [Cebrian et al., 2003], and structural engineering [Pisarenko and Sornette, 2003]. Of course, they have been used in civil engineering, for instance traffic load effect [Messervey et al., 2010], wind loading [Holmes and Moriarty, 1999]. In the definition of live load for design or the evaluation of bridge safety, a critical step is to estimate maximum traffic load or load effects for long return periods that represent the events possible occur in future during the expected life span or operational period of structures. The extrapolation for the tail behavior is performed by the asymptotic extreme value theory (EVT) which supplies the asymptotic justified distribution for extrapolating the underlying data generating process for these extremes providing a flexible and simple parametric model for capturing tail-related behaviors.

The study of extreme traffic load or load effects on bridges is important for bridge design and assessment. The increase of traffic demand, evolution of truck configuration and degradation of structural loading capacity have stimulated the interest in accurate modeling. In this thesis, extreme value modeling in the traffic loads or load effects on bridge is of interest, especially we are interested in estimating characteristic values for long return period. In this chapter, we review the extreme value theory and modeling with focus on traffic load effect applications with the discussion of issues in applying extreme value modeling in bridge traffic load effect.

The rest of this chapter is organized as follows: Section 1.2 reviews the EVT based distributions and Rice formula. Section 1.3 reviews the use of WIM data in bridge engineering. A review on modeling extreme bridge traffic loads is given in Section 1.4. Section 1.5 summarizes the chapter.

1.2 Extreme Value Modeling

1.2.1 Asymptotic Models of Extremes and Block Maxima Method

Let X_1, \dots, X_n be a sequence of independent random variables having a common distribution function F , and let M_n be the maximum value of this sequence:

$$M_n = \max\{X_1, \dots, X_n\}. \quad (1.1)$$

In theory, there is no difficulty in writing down the distribution function of M_n exactly for all values of n :

$$\begin{aligned}
 Pr\{M_n \leq x\} &= Pr\{X_1 \leq x, \dots, X_n \leq x\} \\
 &= Pr\{X_1 \leq x\} \times \dots \times Pr\{X_n \leq x\} \\
 &= \{F(x)\}^n.
 \end{aligned} \tag{1.2}$$

From Eq. (1.2), it is straightforward to obtain the maximum value distribution by raising the parent distribution to a certain power. However, the distribution function F is always unknown in practice, it is thus needed to estimate F from observed data, and then to obtain the maximum distribution by substituting this estimate into Eq. (1.2). Due to the need to raise the parent distribution function to a certain power, it may lead to an inaccurate estimation of F^n if the estimate \hat{F} is insufficiently accurate, and only the upper tail governs the behavior of extreme value, see Figure 1.1. For example, to estimate the daily maximum distribution of traffic load effects induced by traffic from a site of 5000 average daily truck traffic (ADTT), it is needed to raise the parent distribution to a power of 5000. It is clear that majority of F^n will suddenly lead to 0. The F needs to be close to 1 or larger than 0.999539 for F^n to be greater than 0.1, and more accuracy of F is required to well approximate the upper tail of F^n .

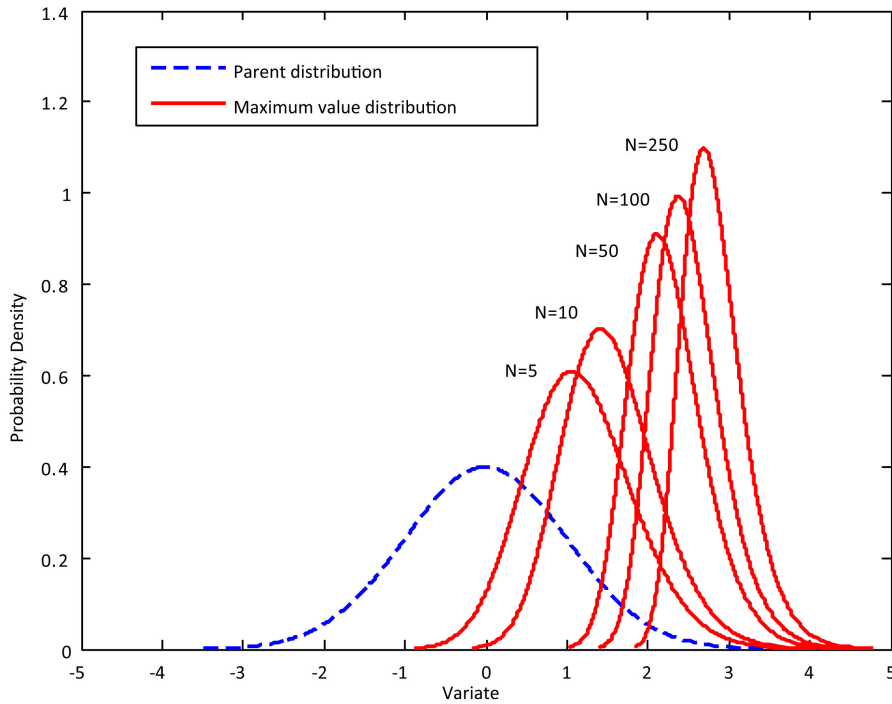


Figure 1.1: Maximum value distribution PDF for varying N

Fortunately, the advance in statistics of extreme makes it possible to estimate the distribution of M_n . In fact, one does not have to know the CDF, F , precisely to obtain the distribution of M_n as it can be obtained through asymptotic theory. If the distribution function, F , belongs to maximum attraction domain (Table 1.1 gives the commonly used maximum attraction

domain.), the F^n converges to three types of extreme value distributions, Gumbel, Fréchet and Weibull distributions (see Figure 1.2) as follows:

$$\text{Type I: Gumbel} \quad G(x) = \exp \left\{ -\exp \left[-\left(\frac{x-\mu}{\sigma} \right) \right] \right\} \quad \text{for } -\infty < x < \infty. \quad (1.3)$$

$$\text{Type II: Frechet} \quad G(x) = -\exp \left[-\left(\frac{x-\mu}{\sigma} \right)^{-\alpha} \right] \quad \text{for } x > \mu. \quad (1.4)$$

$$\text{Type III: Weibul} \quad G(x) = -\exp \left[-\left(\frac{x-\mu}{\sigma} \right)^\alpha \right] \quad \text{for } x < \mu. \quad (1.5)$$

for parameters $\sigma > 0$, μ and in case of types II and III, $\xi \neq 0$.

Table 1.1: Domains of Attraction of the Most Common Distributions [Castillo et al., 2004]

Distribution	Domain Attraction	
	Maximum	Minimum
Exponential	Gumbel	Weibull
Lognormal	Gumbel	Gumbel
Gamma	Gumbel	Weibull
Gumbel	Gumbel	Gumbel
Uniform	Weibull	Weibull
Pareto	Fréchet	Weibull
Weibull _M	Weibull	Gumbel
Fréchet _M	Fréchet	Gumbel
M=maxima, m=minima		

In early applications of extreme value theory, it was usual to adopt one of the three types, and then to estimate the relevant parameters of that distribution. But there are two weaknesses: first, a technique is required to choose which of the three families is most appropriate for the data at hand; second, once such a decision is made, subsequent inferences presume this choice to be correct, and do not allow for the uncertainty such a selection involves, even though this uncertainty may be substantial. These three families were combined into a single distribution by von Mises [1936] (see Jenkinson [1955] for an explanation in English), now universally known as the generalized extreme value (GEV) distribution:

$$G(x; \xi, \sigma, \mu) = \exp \left\{ -\left(\frac{x-\mu}{\sigma} \right)^{-1/\xi} \right\}, \quad (1.6)$$

defined on the set $\{z : 1 + \xi(z - \mu)/\sigma > 0\}$, where the parameter satisfy $-\infty < \mu < \infty$, $\sigma > 0$ and $-\infty < \xi < \infty$. It has three parameters: a shape parameter, ξ ; a location parameter, μ ; a scale parameter, σ . The type II and type III classes of extreme value distribution correspond respectively to the cases $\xi > 0$ and $\xi < 0$ in this parameterization. The subset of the GEV family with $\xi = 0$ is interpreted as the limit of Eq. (1.6) as $\xi \rightarrow 0$, leading to the Gumbel family as Eq. (1.3).

As the GEV is an approximation for maximum, M_n , of n observations, it thus suggests the use of GEV family for modeling the distribution of long sequences. Let x_1, x_2, \dots be a series

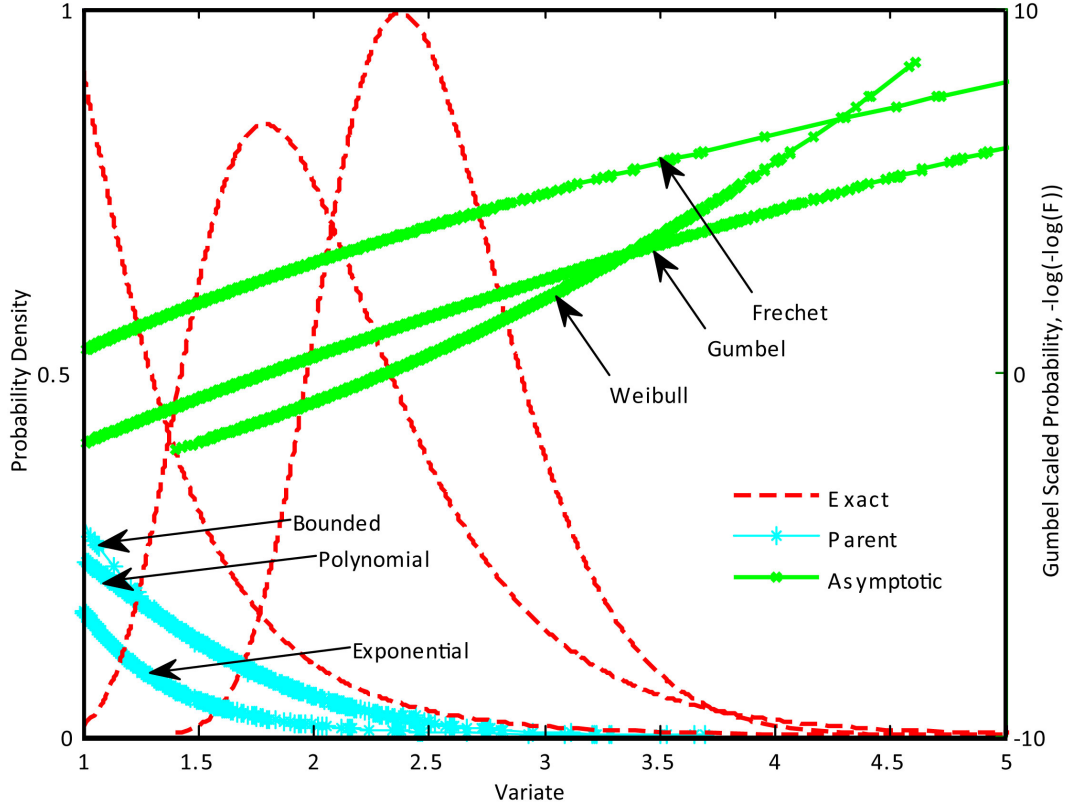


Figure 1.2: GEV distribution

of independent observations. Data are blocked into sequences of observations of length n generating a series of block maxima, $M_{n,1}, \dots, M_{n,m}$ as

$$M_{n,i} = \max\{x_{i,1}, \dots, x_{i,n}\}. \quad (1.7)$$

These block maxima M_n s can fit to GEV distribution, this method is called block maxima method (BM). In practice, the BM is often used to model extremes of natural phenomena such as river heights, sea levels, stream flows, rainfall and air pollutants, in order to obtain the distribution of daily or annual maxima.

The inverse of the distribution function of GEV for the maxima, $G^{-1}(1 - p)$ represents the quantile of $1 - p$, here p is the small probability as $P(x > x_p) = p$, which can be calculated as:

$$x_p = \begin{cases} \mu - \sigma \log[-\log(1 - p)], & \text{for } \xi = 0, \\ \mu - \frac{\sigma}{\xi} \left\{ 1 - [-\log(1 - p)]^{-\xi} \right\}, & \text{for } \xi \neq 0. \end{cases} \quad (1.8)$$

x_p is also known as return level with the return period of $1/p$. For example, if the GEV represents yearly maximum distribution, then x_p is the $\frac{1}{p}$ -year return level. It can be interpreted as it will appear an extreme value greater than the return level x_p once every $1/p$ period (e.g.,

years) on average, or as the mean time interval between specific extremal events. In traffic load effect on bridges, x_p is known as the characteristic value to denote the maximum possible load or load effect within a certain period $1/p$. For example, an allowed maximum load effect for a period of 50 years should not be greater than R_p , which is assumed to have a probability of exceedance of 5% in the 50 years. This implies that a return level of R_p with a return period 1000 years ($p = 0.001$) as solved for $P(LE(R_p) \leq 50) = 1 - (1 - p)^{50} = 0.05$, and $LE(R_p)$ denotes the time of first exceedance which assumed a Bernoulli distribution.

1.2.2 Generalized Pareto Distribution and Peaks over Threshold Method

It should be noticed that the BM method does not use information efficiently and correctly. Only the maximum were kept in each block or time interval. Even if there are second, third largest values larger than the selected maxima in some blocks, these second, third largest values will not be considered to model maximum value distribution. If the block where the maximum is taken has a large sample size, m , then an extreme value distribution function can be accurately fitted to the actual CDF F^m of the maximum. Yet, one must cope with the disadvantage that the number of maxima, k , is small. In Figure 1.3a for example, three 10-second maxima were drawn from a set of load effects as given in the left panel, while eight peaks were drawn when setting the threshold equals to the minimum of the three 10-second maxima in Figure 1.3b; five more extremes can thus be used for POT than BM method. If the block values is kept small there is a risk that some important data are discarded: if two unrelated extreme loading events occur in the same block of time, only one of the resulting load effect is retained. In such a case, the POT approach would retain both as valid data.

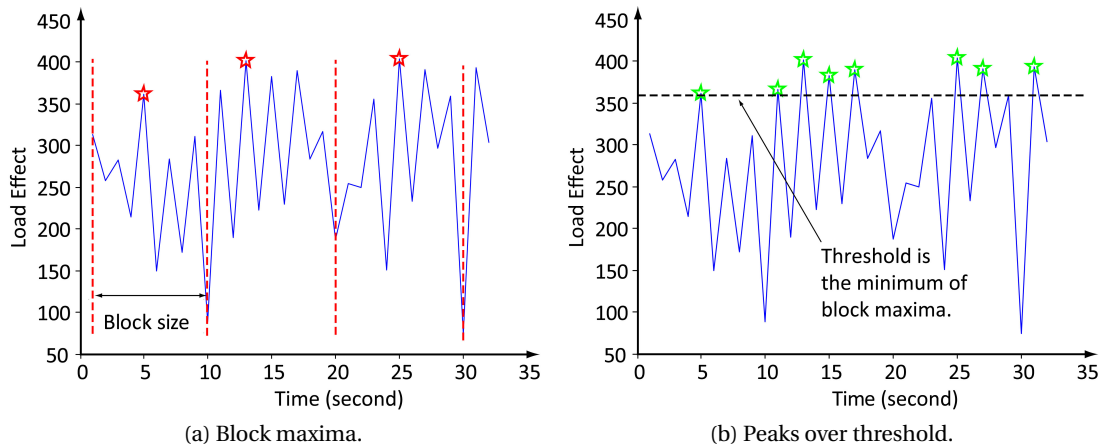


Figure 1.3: Extreme value modeling methods: block maxima and peaks over threshold

As been noted, POT approach is to use, instead of block maxima, all exceedances over a high threshold, u . This threshold method has been developed by hydrologists over the last 40 years. Early versions of the method assumed a non-homogeneous Poisson process to model the times of exceedances over the high thresholds in conjunction with independent exponentially

distributed excesses. The first systematic developments are in Todorovic and Zelenhasic [1970]. This approach was generalized in Davison and Smith [1990] where excesses, $X - u$, are modeled as independent generalized Pareto random variables. The use of GPD to model excesses is a natural as the GPD has an interpretation as a limiting distribution to that which motivates the GEV [Davison and Smith, 1990; Pickands III, 1975]. The cumulative distribution function of the GPD with shape and scale location parameters ξ and σ , respectively, is defined as

$$H(x|\xi, \sigma, u) = \begin{cases} 1 - \left[1 + \xi \frac{(x-u)}{\sigma}\right]^{-1/\xi}, & \text{for } \xi \neq 0, \\ 1 - \exp\left(-\frac{x-u}{\sigma}\right), & \text{for } \xi = 0. \end{cases} \quad (1.9)$$

and its probability density function (PDF) is

$$h(x|\xi, \sigma, u) = \begin{cases} \frac{1}{\sigma} \left[1 + \xi \frac{(x-u)}{\sigma}\right]^{-1/\xi-1}, & \text{for } \xi \neq 0, \\ \frac{1}{\sigma} \exp\left(-\frac{x-u}{\sigma}\right), & \text{for } \xi = 0. \end{cases} \quad (1.10)$$

For $\xi \leq 0$, the distribution function is defined in the range of $[u, \infty]$, while for $\xi < 0$, the range

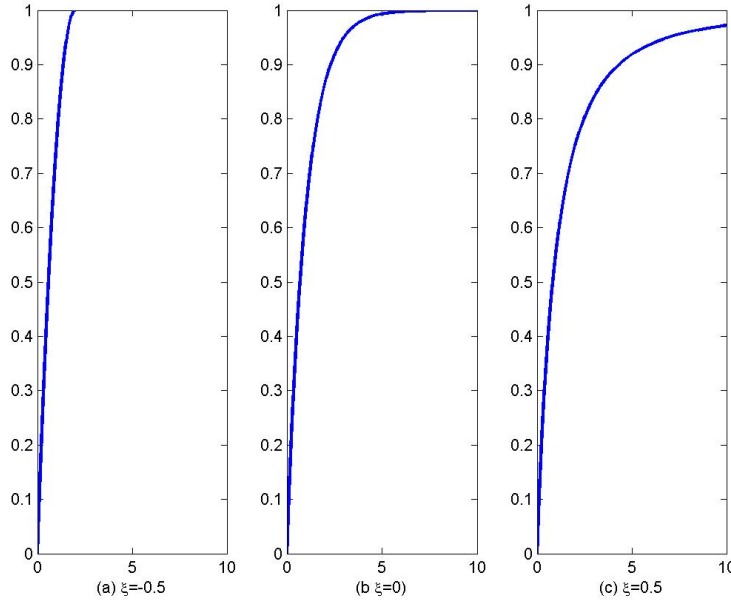


Figure 1.4: Cumulative distribution function for generalized Pareto distribution

is $[u, u - \frac{\sigma}{\xi}]$. Similarly to GEV distribution, there are three types of tail distributions associated with GPD depending on the shape parameter value. When $\xi \rightarrow 0$, the GPD converges to exponential distribution. If $\xi > 0$, the excesses above the threshold have a slowly decaying tail and no upper bound. In contrast, the distribution of excesses has an upper bound of the

distribution if $\xi < 0$. Therefore, the shape parameter of GPD is dominant in determining the qualitative behavior of the tail.

Similar to the GEV, the inverse of distribution function of GPD for the upper tail, $H^{-1}(1 - p)$ represents the quantile of $1 - p$ for the excess over threshold, here p is the small probability of exceedance as $P(x > x_p) = p$. Given that $x > u$, the conditional quantile or return level of x_p can be calculated as:

$$x_p = \begin{cases} u - \frac{\sigma}{\xi}(1 - p^{-\xi}), & \text{for } \xi \neq 0, \\ u - \sigma \log(p), & \text{for } \xi = 0. \end{cases} \quad (1.11)$$

According to

$$\begin{aligned} Pr\{X > u + y | X > u\} &= \frac{Pr\{X > u + y\}}{Pr\{X > u\}} \\ &= \frac{1 - F(u + y)}{1 - F(u)} \\ &\approx 1 - H(y; \xi, \sigma, u), \end{aligned} \quad (1.12)$$

assuming $Pr(X > u) = \zeta_u$, the unconditional return level of x_m is given by:

$$x_m = \begin{cases} u - \frac{\sigma}{\xi} [1 - (p/\zeta_u)^{-\xi}], & \text{for } \xi \neq 0, \\ u - \sigma \log(p/\zeta_u), & \text{for } \xi = 0. \end{cases} \quad (1.13)$$

For bridge traffic load effect, the quantile x_m refers to the maximum load effect within a period of $1/p$ days, years and so on.

1.2.3 Level Crossings and Rice's Formula

In the previous section we have answered the question of the distribution of the maxima of n iid random variables. We will now consider extremal properties of stochastic processes $X(t, t \in R)$ whose index set are the positive real numbers. The theory of stochastic processes provides a useful tool for analyzing civil engineering structures subjected to random loadings, such as the dynamic response of highway bridges under random truck loading.

In practice, level crossing counting is often used to describe the extremal behavior of a continuous stochastic processes. Since it is often easier to find the statistical properties of the number of level crossings than to find the maximum distribution, level crossing methods are of practical importance. For sample functions of a continuous process $\{X(t), t \in R\}$ we say that $X(t)$ has an up-crossing of the level u at t_0 if, for some $\epsilon > 0$, $X(t) \leq u$ for all $t \in (t_0 - \epsilon, t_0]$ and $X(t) \geq u$ for all $t \in (t_0, t_0 + \epsilon]$. For any interval $I = [a, b]$, write $N_I^+(x, u)$ for the number of

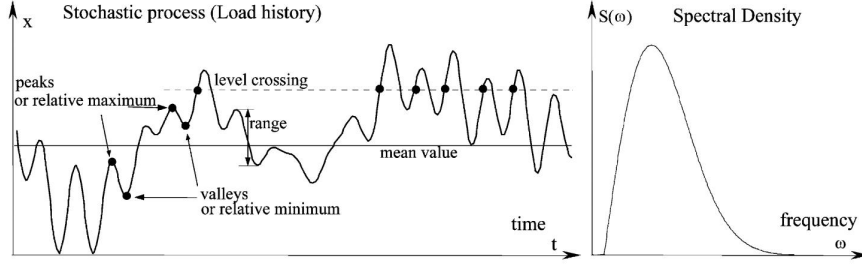


Figure 1.5: Principal parameters of a stochastic proces

up-crossings of level u by $x(t)$ in I [Lindgren, 2006],

$$N_I^+ = N_I^+(x, u) = \text{the number of } u\text{-up-crossings by } x(t), t \in I.$$

By the intensity of up-crossings we mean any function $\nu_t^+(t)$ such that

$$\int_{t \in I} \nu_t^+(u) dt = E[N_I^+(x, u)].$$

For a stationary process, $\nu_t^+(u) = \nu^+(u)$ is independent of t . In general, the intensity is the mean number of events per time unit.

In reliability applications of stochastic processes one may want to calculate the distribution of the maximum of a continuous process $X(t)$ in an interval $I = [0, T]$. The following approximation is then often useful, and also sufficiently accurate for short intervals,

$$\begin{aligned} P(\max_{0 \leq t \leq T} X(t) > u) &= P(\{X(0) \leq u\} \cap \{N_I^+(x, u) \geq 1\}) + P(x(0) > u) \\ &\leq P(N_I^+ \geq 1) + P(x(0) > u) \\ &\leq E(N_I^+(x, u)) + P(x(0) > u) \\ &= T \cdot \nu^+(u) + P(x(0) > u). \end{aligned} \quad (1.14)$$

Studies on level-crossings in stationary Gaussian processes began about sixty years ago. Different approaches have been proposed. The intensity function of up-crossings, $\nu^+(u)$, were obtained by Rice [1944, 1945] for Gaussian processes, and the function is named in the literature Rice's formula as expressed:

$$\nu^+(u) = \frac{1}{2\pi} \frac{\sigma_{\dot{X}}}{\sigma_X} \exp\left(-\frac{(u - \mu_X)^2}{2\sigma_X^2}\right) = \frac{1}{2\pi} \left[\frac{-R_X''(0)}{R_X(0) - \mu_X^2} \right]^{0.5} \exp \frac{-(u - \mu_X)^2}{2[R_X(0) - \mu_X^2]}. \quad (1.15)$$

where t = time; $X = X(t)$, a continuous stationary normal process; u = a fixed threshold level; ν^+ = instantaneous up-crossing rate of X over u , a constant due to the stationarity of X ; $\dot{X} = \dot{X}(t)$, the derivative process of X ; μ_X = the mean of X ; R_X = the autocorrelation function of X ; R_X'' = the second-order derivative function of R_X ; σ_X = the standard deviation of X ; and

1.3. Collecting and Using Weigh-in-Motion Data in Bridge Design and Assessment

$\sigma_{\dot{X}}$ = the standard deviation of \dot{X} . See more details of the derivation of the formula in Rice [1944, 1945]. Note that down crossings and up crossings are studied in the same way.

For the stationary stochastic process, the mean number of up-crossings over a period, R_t , is, $R_t \cdot \nu^+(u)$. According to the definition of return period, R_t , which is the mean period between two occurrences of the value x , the return level can be obtained using the concept of level crossing:

$$R_t \cdot \nu^+(u) = R_t \frac{1}{2\pi} \frac{\sigma_{\dot{X}}}{\sigma_X} \exp\left(-\frac{(u - \mu_X)^2}{2\sigma_X^2}\right) = 1, \quad (1.16)$$

thus, the return level for the return period R_t is:

$$u = \mu_X \pm \sigma_X \sqrt{-2 \log \left[\frac{2\pi \sigma_X}{R_t \sigma_{\dot{X}}} \right]} \quad (1.17)$$

1.3 Collecting and Using Weigh-in-Motion Data in Bridge Design and Assessment

Weigh-in-Motion of road vehicles is essential for the management of freight traffic, road infrastructure design and maintenance and the monitoring of vehicle and axle loads. Literature for the collection, analysis and application of bridge-related WIM data concern all topics for example bridge health monitoring and enforcement. According to the cope of this thesis, this literature review concentrated on the following WIM data research topics concerning the use of WIM to: (a) develop load model for bridge design or evaluation; (b) calibrate current used load model; (c) evaluate safety of bridge; (d) study the evolution of traffic like the growth in truck weights.

1.3.1 Developing of Load Model for Bridge Design and Assessment

Nowak and Hong [1991] have used truck measurements, which consist of 9250 heavily trucks representing 2 weeks traffic collected in 1975 at Ontario, to develop a probability based live load model for bridge design. Due to change of traffic and more available traffic data can be used, Kozikowski [2009] has developed a live load model for highway bridges followed Nowak and Hong method based on newly collected WIM data in America. Three types of live load models have been developed for considering heavy, medium, and light traffic situations. European researchers also use collected traffic data to develop traffic load model for bridge design in Europe. The basis for the preparation of the traffic loads model in EN 1991-Part 2 has been developed in parallel at various locations in Europe with studies performed at SETRA, LCPC, University of Pisa, University of Liege, RWTH Aachen, TU Darmstadt, Flin & Neil, London [Sedlacek et al., 2006]. In order to determine the target values, researchers from these institutions independently studied the effect values that should reproduce the future

European load system by considering various traffic scenarios based on traffic measurements at Liege, Paris, Pisa and Aachen [Bruls et al., 1996; Flint and Jacob, 1996; Jacob, 1991; Jacob et al., 1989]. Miao and Chan [2002] have used 10 years Hong Kong WIM data collected by WIM station located at Tolo Highway, Tun Mun Road, Lung Cheung Road, Island Eastern Corridor, and Kwai Chung Road to derive highway bridge live load models for short span (less than 40 m) bridges.

1.3.2 Calibrate Traffic Load Model

Fu and van de Lindt [2006]; Kwon et al. [2011a,b]; Pelphrey and Higgins [2006]; Pelphrey et al. [2008]; van de Lindt et al. [2005] use WIM data to calibrate live load factors for use on state-specific bridges. Pelphrey and Higgins [2006]; Pelphrey et al. [2008] use WIM data that collected at four WIM sites in Oregon state, including state and interstate routes, considering possible seasonal variation, and different WIM data collection windows. Kwon et al. [2011a,b] use WIM data collected at WIM sites in Missouri to calibrate live load factor for Strength I Limit State in the AASHTO-LRFD Bridge Design Specifications. 105 of representative bridges are selected considering number of spans, maximum span length, and number of lanes. Approximately 41 million WIM data were collected from 24 WIM stations in Missouri. Based on the evaluated distribution of 75-year maximum live load, dead load, and minimum required resistance, reliability analyses were carried out and live load calibration factors proposed as a function ADTT (average daily truck traffic). Results of first stage reliability analysis show that most reliability indexes for positive moments and shear forces are higher than the target reliability index of 3.5. van de Lindt et al. [2005, 2002] present the process and results to examine the adequacy of current vehicle loads used to design bridges in the State of Michigan. Reliability indices were calculated for twenty different bridges selected randomly from the Michigan inventory of new bridges including types of steel girder, prestressed I-beam, prestressed adjacent box-girder, and prestressed spread box girder. WIM data procured from nine different bridge site belonging to five different functional classes in the Detroit area was processed to statistically characterize the truck load effect. To cover the variation of truck traffic volume, two values of truck traffic were used in the reliability analysis. The reliability indices were calculated for two cases of traffic: entire state of Michigan and Metro Region. The reliability indices were found to vary from bridge type to bridge type. Finally, the authors recommend that a new design load level be considered for bridge beam design in the Metro Region. A continuous research project [Fu and van de Lindt, 2006] was conducted to determine what scaling of the HL93 bridge design load configuration will provide Michigan's trunk line bridges designed using the LRFD bridge design code a consistent reliability index of 3.5. 20 typical bridges as same as the pervious study [van de Lindt et al., 2005, 2002] were used again. Five years of truck data were procured from MDOT's Bureau of Transportation Planning, Asset Management Division. The data was organized again into 5 functional classifications of roadway. The total number of trucks was approximately 101 million. Critical load effects were calculated by using these recorded WIM data. The target reliability index used in AASHTO LRFD code was utilized in the study as the criterion for evaluating the adequacy. Reliability

indices were calculated for the twenty selected bridges. The calibration results show that for the Metro Region, bridge design requires an additional live load factor of 1.2 to provide a reliability index consistent with the rest of the state. For the recommended live load increase for the Metro Region, a cost impact of 4.5% was estimated in order to achieve the higher bridge capacity.

1.3.3 Evaluating Bridge Safety

Fu and You [2009] evaluated the bridge capacity using WIM data gathered from stations on highways in three provinces of China. The WIM data were collected continuously over 1-16 months in 2006 and 2007. But the time stamp is 1 second, which is impossible to estimate simultaneous presence of trucks on a bridge span of short- or medium-length. A set of WIM consisting of data from five New York stations were used to investigate the behavior of simultaneous truck presence. The data were processed and projected to model the live-load spectrum over 3-year and 100-year periods, respectively. The former is the required bridge inspection interval and the latter the bridge design lifetime, according to current Chinese maintenance and design specifications. The calculated traffic load effects were projected to obtain corresponding maximum distribution functions for using to reliability assessment. Four most representative highway bridges in China, reinforced concrete beams (RC), prestressed concrete T beams (PCT), prestressed concrete box beam (PCB), and steel I beam (SI), were selected. Guo et al. [2011] present a probabilistic procedure for the assessment of the time-dependent reliability of existing prestressed concrete box-girder bridges. These bridges are subject to increased traffic loads and an aggressive environment, which result in structural deterioration such as cracking and corrosion. To obtain maximal vehicle loads during the remaining life of bridges, a renew load model established based on measured traffic data from WIM systems. Time-dependent corrosion models were adopted to account for pitting corrosion because of chloride attack as well as uniform corrosion because of concrete carbonation. A degenerated shell element was used for accurate and efficient modeling of the PSC box-girder. The time-dependent reliabilities were calculated by an adaptive importance sampling method.

1.4 Extreme Values in Bridge Traffic Load Effects

Due to the need for developing traffic load model for bridge design or evaluation, integration of calculated load effects from collected traffic data or measured load effects and extreme value statistics to estimate the distribution of extreme bridge traffic load effects have gained many attentions. Statistical methods have been introduced to model traffic load effects on bridges including historical methods [Cremona, 2001; Flint and Jacob, 1996; Jacob, 1991; Nowak and Hong, 1991] and modern methods based on extreme value theory [Bailey and Bez, 1999; Cooper, 1997; Grave et al., 2000; Messervey et al., 2010; O'Brien et al., 2003, 1995; Siegert et al., 2008]. A review on the methods for modeling extreme bridge traffic load effects are given

in the following.

1.4.1 Tail of Parent Distribution Method

It is straightforward to get the maximum distribution through Eq. (1.2) if the underlying parent distribution function, F , is known. Perhaps inspired by this, the extreme value distribution is realized by finding the parent distribution in the early stage of extreme traffic load effect modeling [Flint and Jacob, 1996; Jacob, 1991; Nowak, 1993; Nowak and Hong, 1991; Nowak et al., 1993].

As a comparison method to predict extreme traffic load effects in the background study of the development of current used Eurocode 1 traffic load model in early 1990's [Flint and Jacob, 1996; Jacob, 1991], the normal distributions of traffic load effects were found by fitting the distribution to the upper tail of histogram using the least square method.

During the development of live load model for AASHTO LRFD code, [Nowak, 1993; Nowak and Hong, 1991; Nowak et al., 1993] have used the tail distribution method to predict the mean 75-year maximum load effects. The truck data used to predict these mean 75-year maximum level were collected over a period of approximately 2 weeks consisting of 9250 trucks [Nowak and Hong, 1991]. Due to limitation of sample size, Nowak et al. [1993] point out that the traditional histogram method can not provide a sufficient accuracy in fitting the particular important upper tails, thus the parameter estimates may not be accurate. They propose to use an alternative method, which is based on plotting the empirical CDF on normal probability paper, to fit the upper tail. Each vehicle from truck survey was run over the influence lines to determine the calculated maximum bending moment, shear force and negative moment at the interior support of two span bridges. The calculations were carried out for span length from 10 ft through 200 ft to simple span and two-span continuous bridges. The resulting cumulative distribution functions were plotted on the normal probability paper as shown in Figure 1.6. The upper tails were assumed to have normal distribution as straight lines are superimposed on them. Therefore, the effects corresponding to the probability of occurrence can be read directly from the plots. For a design lifetime of 75 years, the total number of trucks will be 15 million [Nowak and Hong, 1991] or 20 million [Nowak, 1993], and the corresponding exceedance probability are therefore $1/15000000 = 7e-8$ and $1/20000000 = 5e-8$, respectively. The return levels for various return periods from 1 day to 75 year were graphically shown in the plots.

To improve accuracy of Monte Carlo simulation of traffic loading on bridges, [O'Brien et al., 2010] have proposed to model gross vehicle weight (GVW) with a semi-parametric method, which uses the measured histogram where there are sufficient data and parametric fitting to a Normal distribution in the tail region where there are less data. The parameters of the normal distribution is estimated by the maximum likelihood method with a constraint equation:

$$|\hat{F}(x_0) - \tilde{F}(x_0)| \leq \epsilon. \quad (1.18)$$

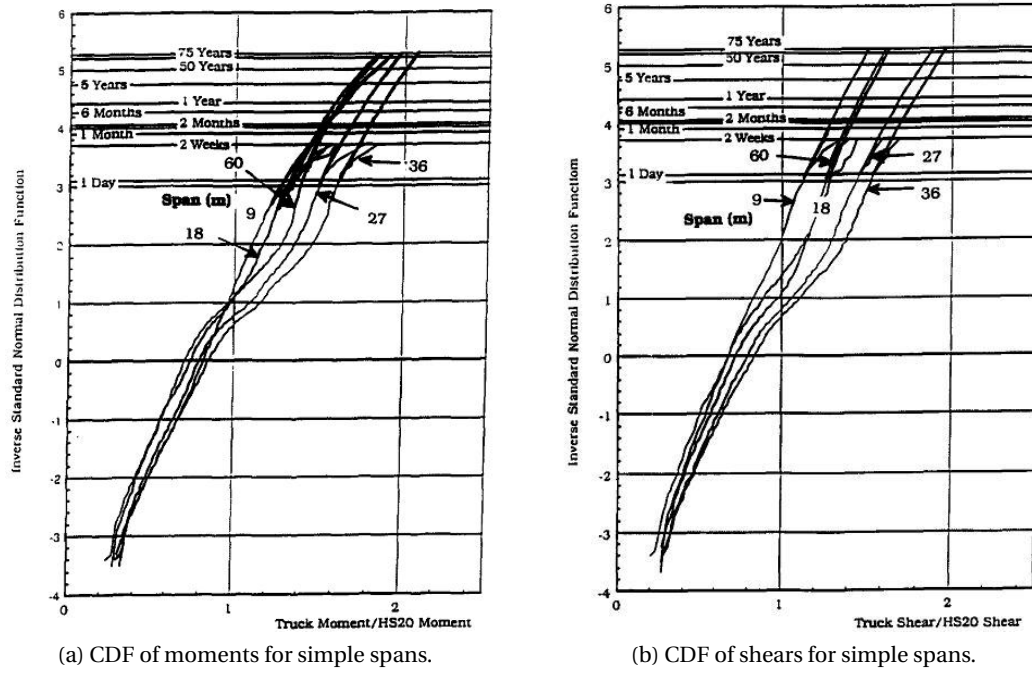


Figure 1.6: CDF of moment and shear effect on normal probability paper. Reproduced from [Nowak and Hong, 1991]

where $\hat{F}(x_0)$ is the fitted normal distribution function, ϵ is a tolerance value of a small positive number (e.g., 1×10^{-8}) and $\tilde{F}(x_0)$ is the empirical distribution function. The maximum likelihood method based fitting is compared with others like least square method and Chi-square statistic method as shown in Figure 1.7. The authors have stated that the fitting of tail of GVW has significant influence on bridge assessment.

The previous methods that extend the upper tail of CDF with a normal distribution involves a considerable dose of engineering judgment. Indeed, the load effects do not follow a normal distribution as the curves on normal probability paper do not appear as straight lines, and also for the tails (see Figure 1.8). To avoid this subjective aspect, Kozikowski [2009] proposes to use a nonparametric approach of Kernel density estimation to fit the data. The best fit to the whole data was found by using kernel function as normal and selecting certain bandwidth for the distribution of live load. However, for the important tail, trend of the end of the fit tail depended on the distance of the last point of the data set from the other points. Then the characteristic value for long return period was interpolated according to its probability of occurrence.

Sivakumar et al. [2011] evaluated the performance of the normal fit of the tail method on estimating maximum load effects for long return periods (see Figure 1.9). The verification results show that the method can obtain good estimates for short return period like less than 1 month, but is not accurate enough to obtain the maximum load effect for longer return period.

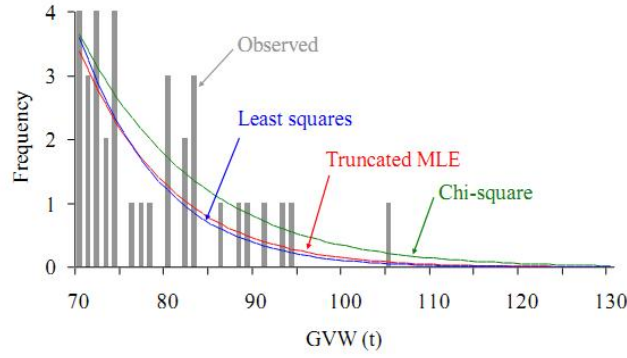


Figure 1.7: Fitting normal distribution to upper tail of GVW histogram. Reproduced from [O'Brien et al., 2010]

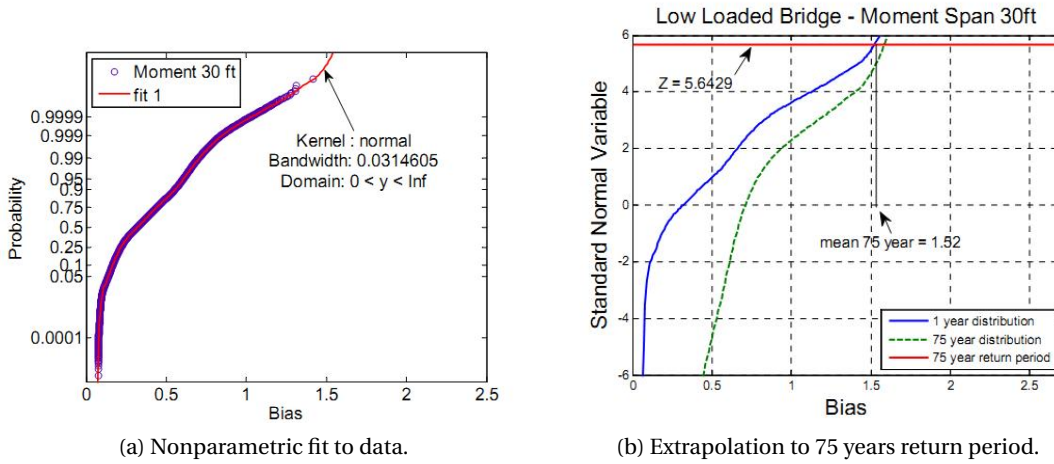


Figure 1.8: Extrapolation with nonparametric fit. Reproduced from [Kozikowski, 2009]

Therefore, an alternative more analytic and better founded method is proposed in [Sivakumar et al., 2011]. The fitted normal distribution is raised to a power to obtain the maximum distribution, which is the Extreme Value Type I (Gumbel) distribution according to the attraction domain. The parent distribution of the initial variable is a general normal distribution with mean, μ , and standard deviation, σ , then the maximum value after N repetitions approaches asymptotically an Extreme Value Type I (Gumbel) distribution. Its mean μ_{max} and standard deviation, σ_{max} , are derived analytically as follows related to the mean and standard deviation of parent distribution:

$$\mu_{max} = \mu + \sigma \sqrt{2 \ln(N)} - \sigma \frac{\ln[\ln(N)] + \ln(4\pi)}{2\sqrt{2 \ln(N)}}, \quad (1.19)$$

$$\sigma_{max} = \frac{\sigma}{\sqrt{2\ln(N)}}. \quad (1.20)$$

In Cooper [1997], histograms of 2-week traffic load effects are established from WIM data. The

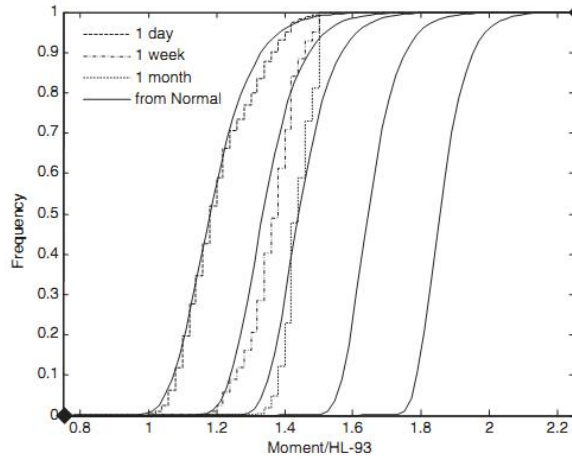


Figure 1.9: Cumulative distribution maximum load effect of single lane events for different return periods. Reproduced from [Sivakumar et al., 2011]

histograms were then converted into CDFs, which are then raised to a power equal to number of daily trucks, to obtain the distribution of daily maxima. The points of the CDF of daily maxima are then plotted on Gumbel paper and a straight line is fitted. Although this approach is straightforward, it has risk to obtain unreasonable estimation as the CDF needs to be raised to a high power such as average daily truck traffic. 2-week WIM data is short comparing with the required daily maxima distribution. However, this method can have better performance when large amount of WIM data is available.

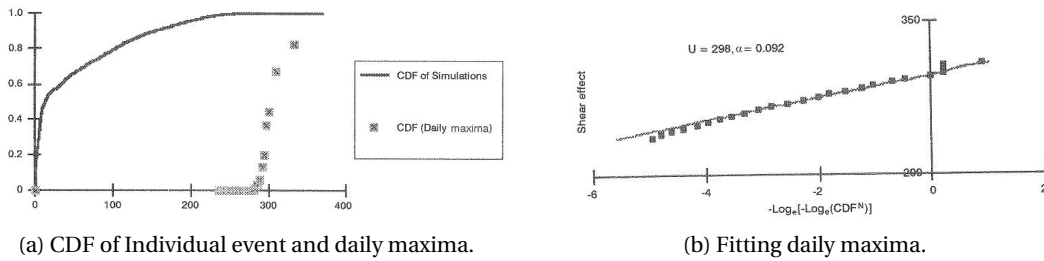


Figure 1.10: Daily maxima CDF fitted to Gumbel distribution (Reproduced from [Cooper, 1997])

1.4.2 Block Maxima Method

The extreme value theory used for extrapolating data to the required/considered return period is well established. It has been widely applied to model traffic load effects on bridges in recent years. Many authors approach the problem by identifying the maximum load effect recorded during a loading event or in a reference period such as a day or a week, and then fit these maxima to an extreme value distribution. In all cases, the fitted distributions are extrapolated to obtain an estimate of the lifetime maximum load effect. This approach is based on the assumption that individual loading events are independent and identically distributed.

Standard Block Maxima Method

In the early application of BM method, it was usual to fit one of the three extreme value distributions to data of traffic loads or load effects from measurements or Monte Carlo Simulation. Due to the tail behavior, the Gumbel and Weibull distributions were the most adopted. Cooper [1997]; Grave et al. [2000]; O'Brien et al. [2003, 1995] have fitted Gumbel distribution to their data, and Bailey [1996] has used Weibull distribution to approximate his data. Both Gumbel and Weibull distributions have been investigated in Enright [2010]; Grave et al. [2000], and it seems that both methods can be used to model extreme traffic load effects. However, these two types of distribution have distinct shapes of behavior, corresponding to the different forms of tail for the underlying parent distribution function. Weibull has a finite upper bound with value of $\frac{\mu}{\sigma}$, while the tail of Gumbel distribution is infinite, see Figure 1.2. Actually, many of the governing factors like GVWs follow normal distribution or have normal distribution type tail [O'Brien et al., 2010], thus it is reasonable that the maximum distributions of load effect follow a Gumbel law. In addition, due to the length of effective influence lines or the size of influence areas, the total number of heavy-vehicles on bridges and their total weight have a finite limit, thus the induced load effects should converge to an extreme value distribution with upper bound.

However, it is hard to say which type of extreme value distribution the extreme traffic load effect belongs to. Therefore, once unsuitable type distribution is chosen, doubtful inferences are gained. A better choice is to use the generalized form of extreme value distribution of generalized extreme value (GEV) distribution. The most appropriate type of tail behavior can be determined through parameter estimation, it thus avoids to make a priori judgment on which family of extreme value distribution to be adopted. In the recent publications [Caprani, 2005; Gindy, 2004; James, 2003; Siegert et al., 2008], GEV distribution has been widely adopted to model extreme bridge traffic load effects.

The use of extreme value distribution to model extreme bridge traffic load effects is more rational than directly model them by some distributions like normal, but the data should be independent and identically distributed. A practical method, which is named block maxima method (BM), is to fit GEV distribution to maxima taken out of blocks with sufficient number of data. In the literature on studying bridge traffic load effects, the block maxima of traffic load

1.4. Extreme Values in Bridge Traffic Load Effects

effects are drawn from different sizes of block like an hour [Caprani et al., 2002; O'Brien et al., 2003], daily maxima [Caprani, 2005], a week [Siegert et al., 2008], a year [Enright, 2010]. There seems to be no uniform criteria for determining how large or how long the interval should be to draw the maximum. However, the condition that block maxima can well converge to an asymptotic extreme value distribution is that the maximum should be taken out of a sample with sufficient large block size to ensure the data is independent.

Many researchers have noticed that their data do not really follow asymptotic extreme value distribution, the extreme value distributions are thus used to fit only the upper tails of their data. For instance, O'Brien et al. [2003] assume that the upper $2\sqrt{n}$ points follow Gumbel distribution according to the suggestion provided by Castillo et al. [2004]. Although this empirical tail fraction satisfies the application of extreme value modeling, the source of a formal derivation of this rule is lacked.

When block maxima are well prepared, the problem to obtain well modeled distribution of load effect is decided by the estimates of the parameters of the distribution. Maximum likelihood estimation, method of moments and probability weighted moments are preferred by statisticians. However, the graphic method, which is used to check the quality of the modeling, is used widely in the papers on bridge traffic loads related topics. To determine the characteristic deflection of the Foyle Bridge, which has a total length of 866 m, O'Brien et al. [1995] used 8 minute periods of measurements taken during each 4 hour rush hour period of a day. Each day of measurement is then represented by a 48 minute sample. 155 daily samples were recorded. The authors then consider the daily maximum deflection, from which the effect induced by wind and temperature is removed, as an extreme value population. The data is plotted on a Gumbel probability paper, and the parameters of the distribution are determined directly from the plot by linear regression as shown in Figure 1.11.

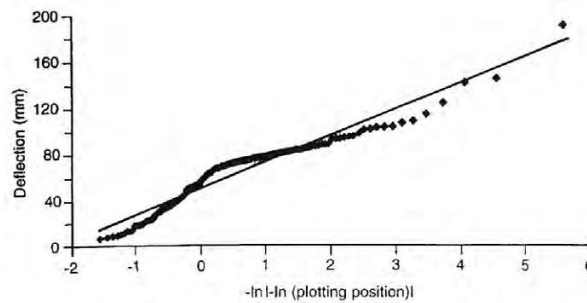


Figure 1.11: Gumbel extrapolation for the Foyle bridge, Reproduced from [O'Brien et al., 1995]

In [O'Brien et al., 2003], hourly maximum strain values are plotted on Gumbel probability paper. Through least-squares method, straight line is used to the upper $2\sqrt{n}$ data points as shown in Figure 1.12.

To predict extreme load effects, Caprani et al. [2002] use a sample of two-week simulated traffic. The authors assume maxima hourly load effect induced by the traffic conform to an extreme

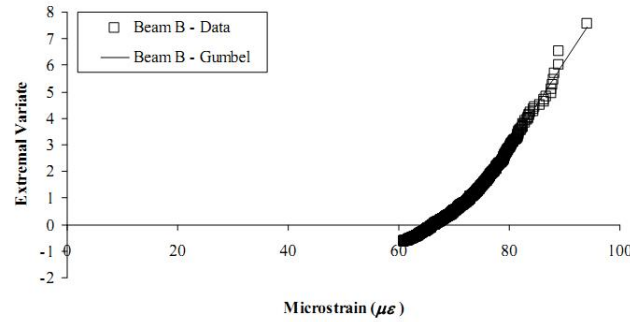


Figure 1.12: Gumbel extrapolation for the strain, Reproduced from [Grave et al., 2000]

value distribution. Hence, 240 maxima for each type of load effect are generated. Gumbel probability paper is used to determine the parameters of presumed Gumbel distribution of hourly maxima. The author then carries out a least squares fit to the upper $2\sqrt{n}$ point as suggest by Castillo. In the simulations carried out as part of his work, O'Connor [2001] has

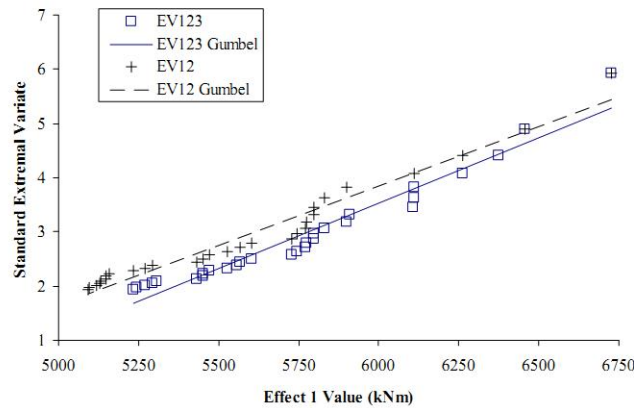


Figure 1.13: Gumbel plot of load effect, Reproduced from [Caprani et al., 2002]

fitted Gumbel and Weibull distribution to a population of 'extreme' load effects. Maximum likelihood fitting is carried out on a censored population. O'Connor [2001] has censored for the upper \sqrt{n} , $2\sqrt{n}$ and $3\sqrt{n}$ data points, and noted that different estimates of lifetime load effect result from different censoring.

Siegert et al. [2008] fit Gumbel distribution to daily or weekly maximum measurements of deformation at mid-span of a prestressed concrete bridge, which is located on a heavy trafficked highway in Northern France. The deformations at mid-span were measured during a 256 days period in 2004 and 2005. The return values for long return periods in the range from 50 years to 1000 years are estimated by using both maximum likelihood and least squares methods. The parameter estimates are similar from both methods.

Two Steps Block Maxima Method

The reliability of extrapolation obtained by block maxima method depends on the way to use the data. In practice, the number of available data is always limited. To use the block maxima method, if the block size is large, then an EV distribution function can be accurately fitted to the actual CDF F^m of the maximum. However, the smaller the number of maxima with increasing block size, the larger bias and variance are introduced to estimates for distribution parameters or quantile. More truck load data have been available in recent years due to the wide use of WIM system. As an example Gindy and Nassif [2006] have collected 11-year WIM data from sites at the State of New Jersey. It is possible to obtain more accurate parent distribution. However, the data are insufficient to ensure to obtain accurate maximum distribution when the estimated distribution has to be raised to a large power. Fu and You [2010] state that reduction of the power N can significantly lower the requirements on fitting quality for the parent distribution. To obtain the N -event maximum distribution, the authors propose to group the N measurements into n subset with sample size of M and to take out the maximum of each group, then fitting GEV distribution to the n maxima of M -event maximum, therefore the M -event maximum distribution can be obtained and the N -event maximum is easier to obtain by raising the M -event maximum distribution to power N/M . The principle of the method is to reduce the raised power to improve the fitting accuracy. The method is applied to traffic load effects induced by traffic load collected from different sites, the difference between the proposed method and the method directly raising a large power is shown in Figure 1.14. It has been found that the difference of the estimated PDFs from the proposed method and the NCHRP 12-76 method is significant. The method proposed by Fu and You [2010] has better performance on estimating the maximum distribution. As the authors stated, the possible reason is the proposed method reduce the power needed to raise the parent distribution to obtain the maximum distribution.

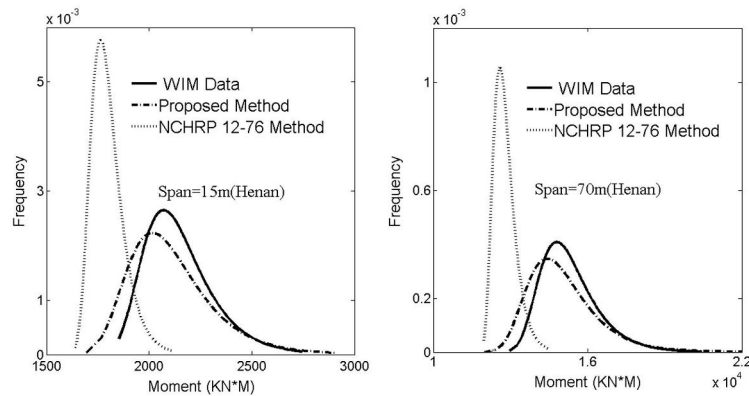


Figure 1.14: A comparison of extrapolated PDF by NCHRP 12-76 method and the two steps block maxima method for load effect, Reproduced from [Fu and You, 2010]

Composite Distribution Statistics

Harman and Davenport [1979] state that traffic load effects are not identically distributed as the load effects are induced by different loading events, which are identified by the number of involved trucks. The histograms for load effects caused by five different types of loading event are shown in Figure 1.15. It can be seen that they are considerably different in the histograms either from the measured traffic configuration (in full line) or from simulated traffic (in dash line). Harman and Davenport [1979] have noted that each mechanism may be represented by a negative exponential function. Hence, the authors use a mixture distribution to model the upper tail of the load effect distribution, and then the maximum distribution is obtained by raising the mixture model to a given power. Caprani et al. [2002, 2008] confirm this statement (see Figure 1.16), but suggest to characterize the extreme traffic load effects with a mixture models that is a linear combination of GEV distribution. The distribution of each component is obtained by fitting GEV to the daily maxima of the load effect induced by the corresponding loading events. The proposed method is applied to model traffic load effects and compared with the conventional method. Their results show that the proposed method provides much more reasonable prediction especially when the mixed distributions are quite different. As shown in Figure 1.16-b, the fitting to a single GEV is governed by mixed maxima in the range between 1600 and 1650, which are mainly from 2-truck and 3-truck event. However, the load effects from 4-truck loading events actually govern the upper tail. The difference between the conventional method and mixture distribution on characteristic value prediction are shown in Figure 1.16-c.

Other Works

The relatively new theory of predictive likelihood can be used to estimate the variability of the predicted value, or predictand. Fisher [1973] is the first clear reference to the use of likelihood as a basis for prediction in a frequentist setting. A value of the predictand z is postulated and the maximized joint likelihood of the observed data y and the predictand is determined, based on a probability distribution with given parameters. The graph of the likelihoods thus obtained for a range of values of the predictand, yields a predictive distribution. Such a predictive likelihood is known as the profile predictive likelihood. Denoting a normed likelihood by $\bar{L}(\theta; x)$, this is given by:

$$L_p(z|y) = \sup_{\theta} \bar{L}_y(\theta; y) \bar{L}_z(\theta; z) \quad (1.21)$$

This formulation states that the likelihood of the predictand, z , given the data, y , is proportional to the likelihood of both the data (L_y) and the predictand (L_z) for a maximized parameter vector [Caprani and O'Brien, 2010].

Caprani and O'Brien [2010] use the Predictive Likelihood method proposed by Butler [1986], based on that of Fisher [1973] and Mathiasen [1979]. This Predictive Likelihood is the Fisherian approach, modified so that the variability of the parameter vector resulting from each

1.4. Extreme Values in Bridge Traffic Load Effects

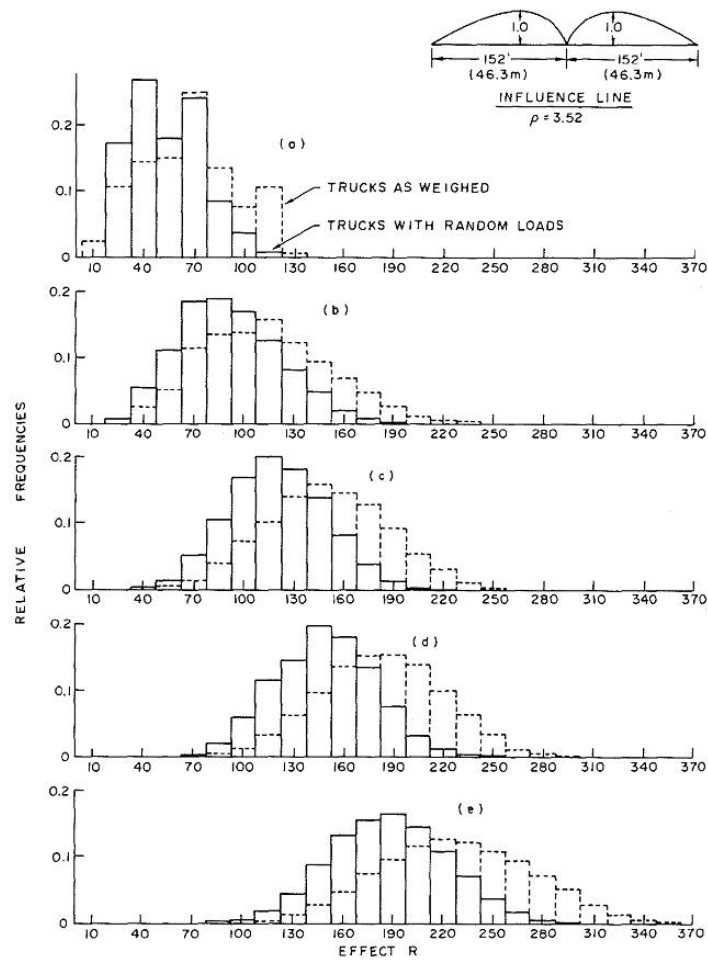
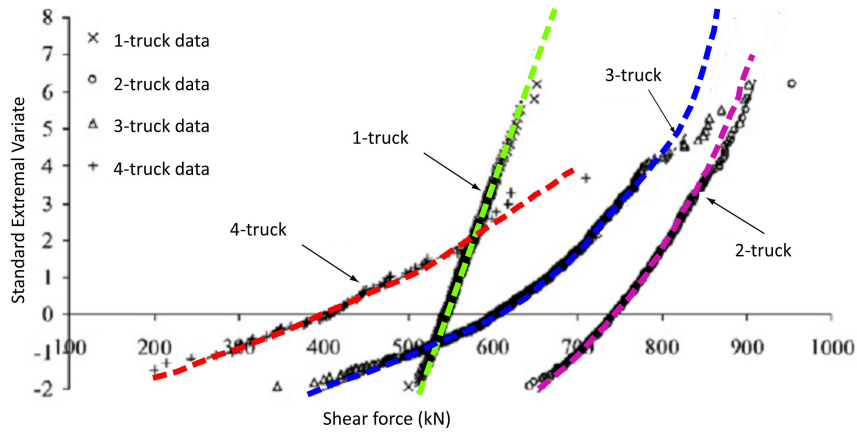
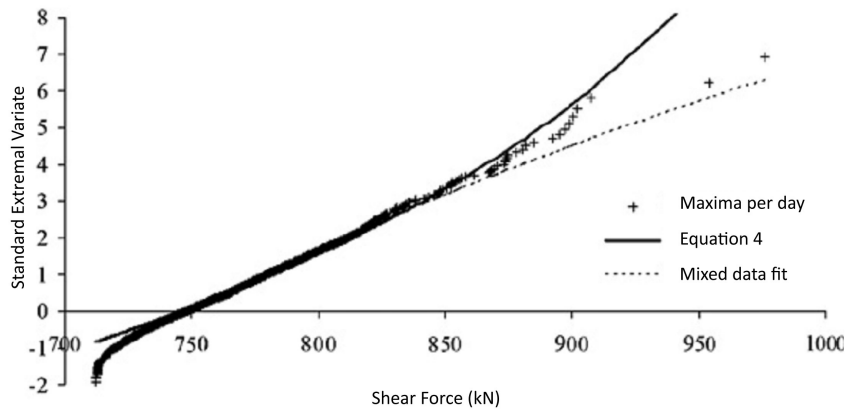


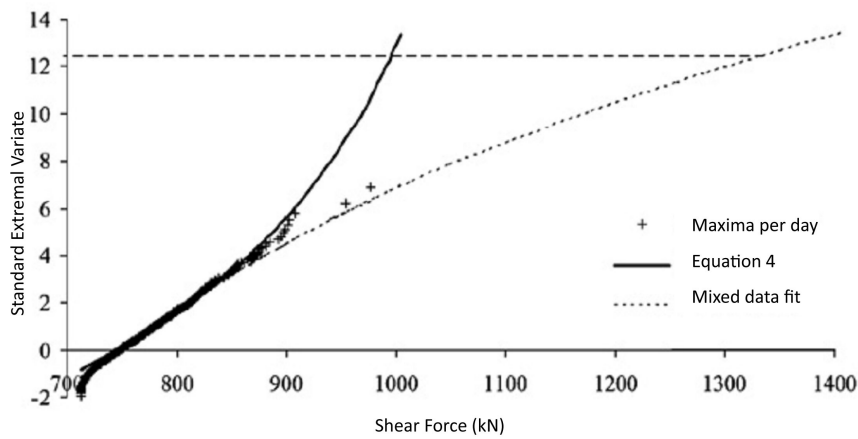
Figure 1.15: Histograms of load effect for different loading events, (a)-(e) represent 1- to 5-truck events, Reproduced from [Harman and Davenport, 1979]



(a) Daily maxima by event type.



(b) Mixed daily maxima.



(c) Mixed daily maxima extrapolation to characteristic value.

Figure 1.16: Mixture model of loading events, Reproduced from [Caprani et al., 2008]

maximization is taken into account.

As been stated in Eq. (1.21), the main advantage of this method is that it involves the predictand like 1000-year return level into the process of parameter estimation. Therefore the estimated parameters are more suitable to estimate the maximum distribution function. However, it should be noticed, this method is very time consuming as it needs to test a number of possible predictand to find the optimal one.

1.4.3 Peaks over Threshold Method

To the best of our knowledge, GPD for the extreme traffic load effect was not addressed until the article by Crespo-Minguillon and Casas [1997]. The authors point out that: (i) the method of raising parent distribution to a power needs a large size of sample to obtain accurate parent data, (ii) the way of using information of the block maxima method is rather uneconomical, (iii) the method of fitting an extreme type I distribution to upper endpoints of maxima lacks of theoretical supporting bases and also lacks of objectiveness when setting the threshold value from where the fitting starts. The POT method is applied to weekly maxima of internal force induced by simulated traffic load. Gindy [2004] use POT method to predict maximum live load and load effect. James [2003] use POT method to analyze traffic load effects on railway bridges.

Threshold selection is an important step in the use of POT method. [Gindy, 2004] uses two typical graphical methods of mean residual life plot and stability plot of estimates of parameter. Crespo-Minguillon and Casas [1997] use a graphical method that is based on both function, $L(x_i|u, \xi, \sigma)$ and $L_i(i = 1, n)$, for different threshold, u_j , which $F_x(u_j) > 0.90$. The optimal threshold value is selected by approximating both curves. An example of fitting of a GPD to a load effect of bending moment is presented in Figure 1.17. [James, 2003] states that using only the graphical method cannot make a good decision on threshold selection. Therefore, the author proposes a hybrid method that combines graphical methods with computational methods. The mean exceedance plot was used for the first criterion, attempting to locate signs of linearity, while a plot of the estimated shape parameter versus the threshold level was used in assessing the second criterion. Figure 1.18a shows the mean exceedance plot for the 20 m span case. As one can see from this plot, linearity occurs at approximately $u = 0.42$. A plot of the estimated against the threshold level can be seen in Figure 1.18b. From this figure it can be seen that $\hat{\xi}$ remains relatively constant over a range of threshold level from approximately 0.42 – 0.49. Also for varying values of threshold, goodness-of-fit statistics were also evaluated and used in the decision process. Figure 1.18c shows these plots for the 20 m span. The uppermost sub-figure shows the R^2 value versus threshold. A value of $R^2 = 1$ represents a perfect fit, likewise the KS test indicates a good fit as the significance level Q_{KS} approaches 1. For the Anderson-Darling test, at the 5% significance level, the value of 2.492 is suggested in literature, i.e. the test value should fall below this level if there is no significant difference at this probability level. In the third sub-figure the Anderson-Darling test value falls below this value for all the threshold values $u > 0.41$. In the case of the χ^2 goodness-of-fit test the test value, shown continuous in the sub-figure, should fall below the χ^2 distribution value, for the

correct degree of freedom, at the required significance level. This value is shown dashed in the sub-figure. The test value falls below the χ^2 value shortly after 0.38. Another measure of the goodness-of-fit used in this process was the mean square error (MSE). This is a measure of the variation of the data from that predicted by the fitted theoretical model, and small values of MSE indicate a good fit. Figure 1.18d shows the MSE versus the threshold level and as can be seen from this figure a threshold of between 0.40 and 0.47 may be justified. Finally, the author states that a value of anywhere in the range of $0.42 < u < 0.46$ would therefore seem a reasonable choice, and the final choice was $u = 0.458$ which was quite long into the tail, thus hopefully avoiding bias, but still had a large number of data points (695) on which to make the parameter estimates. The procedure was applied to other cases of load effects in the thesis.

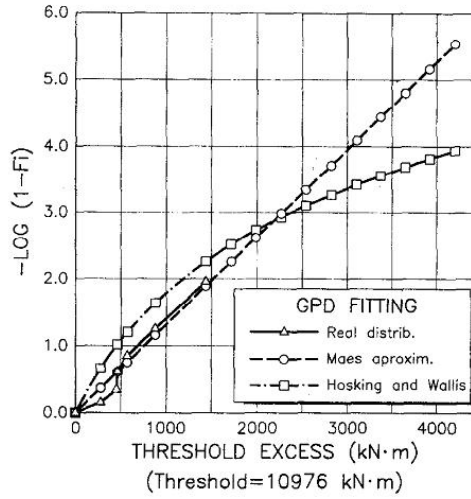


Figure 1.17: Example of fitting a generalized Pareto distribution, Reproduced from [Crespo-Minguillon and Casas, 1997]

After determining the threshold, the next step is to estimate the parameters for the GPD. A number of methods are available in the literature, maximum likelihood, probability weighted moments and method of moments are the most frequently used amongst. It does not exist a method that is available for all, therefore the choice of the parameter estimation method is also important to utilize POT method. Maximum likelihood estimation is used in [Gindy, 2004]. The three typical methods are used to estimate the parameters in [James, 2003]. Crespo-Minguillon and Casas [1997] adopt an estimator proposed by Maes [Maes, 1995] that is based on the minimization of the weighted sum of square errors:

$$SWSE = \sum_{i \in T} w_i [L_i - L(x_i|u, \xi, \sigma)]^2 \quad (1.22)$$

where the function $L(x_i|u, \xi, \sigma)$ refers to the value of the minus logarithm of the probability of exceedance of x_i , given a chosen threshold, u , and the parameters of the GPD, ξ and σ .

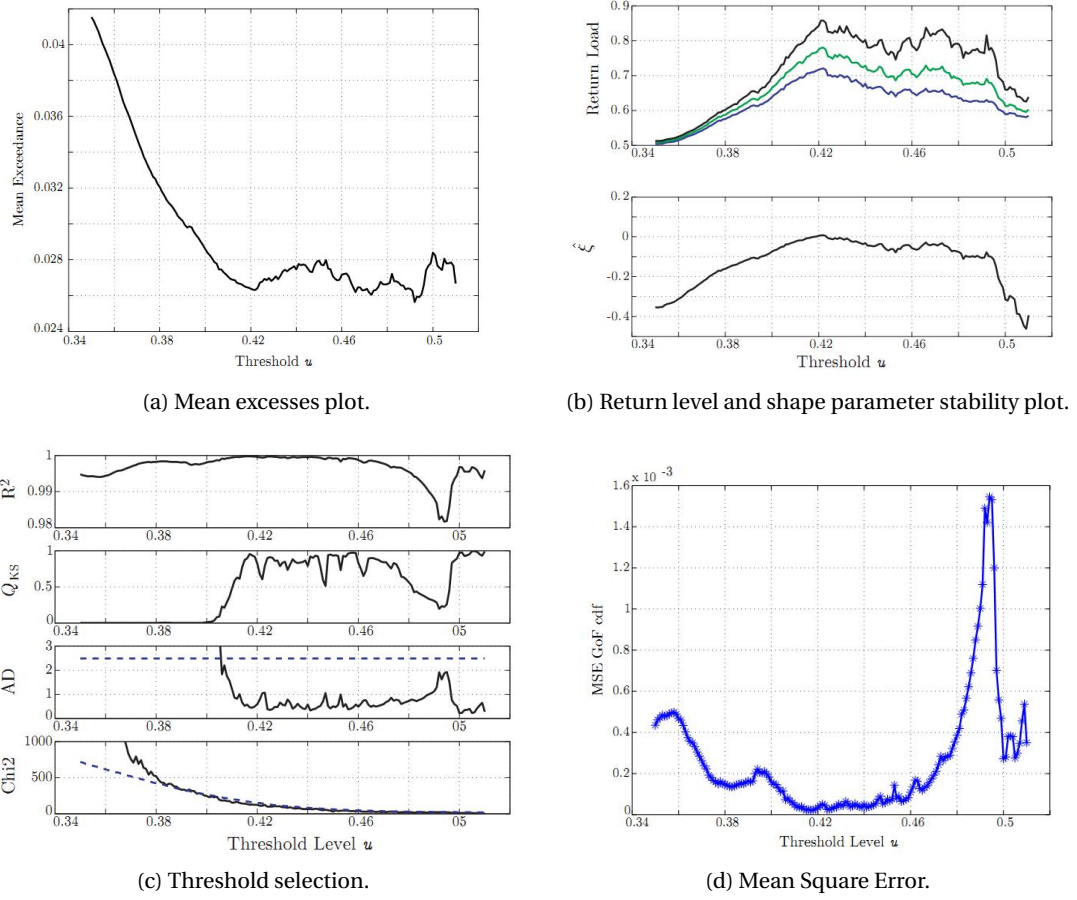


Figure 1.18: Application of POT to load effect for a 20 m span, Reproduced from [James, 2003].

1.4.4 Level Crossing Method

Although the classic extreme value theory based methods are the natural choice to model maximum distribution of traffic load effect, level crossing method has also got some attention by researchers. The level crossing method deals with the full time history of load effect or load process, more information are involved in the analysis. However, this method is more popular with analyzing simulation data than with measured data as the full time history is always impossible to obtain in practice. In developing the theoretical model to traffic load effect, Ghosn and Moses [1985] have used Rice formula to approximate the maximum distribution of load effect. Using Rice's formula to approximate the level crossing rates is one of the five methods adopted to develop load model for Eurocode during the background study, its performance is presented in [Jacob, 1991] on extrapolating traffic load effects. O'Connor et al. [1998, 2001] use the method in the study of re-calibration of the normal load model with modern traffic. The method is introduced to evaluate the safety of bridge structures under site-specific traffic [Cremona, 1995; Cremona and Carracilli, 1998; Getachew, 2003].

The condition to use Rice's formula to approximate the level crossing rates is well known. It consists in assuming that the effect should be a stationary Gaussian process Bulinskaya [1961]; Ito [1963]; Ivanov [1960]; Ylvisaker [1965]. Ditlevsen [1994] state that if the influence function for the considered load effect is slowly varying along the lane over steps not containing a discontinuity and of length as the mean distance between consecutive vehicles and the contributing lane length is large compared to this mean vehicle distance, the load effect can be modeled to be Gaussian.

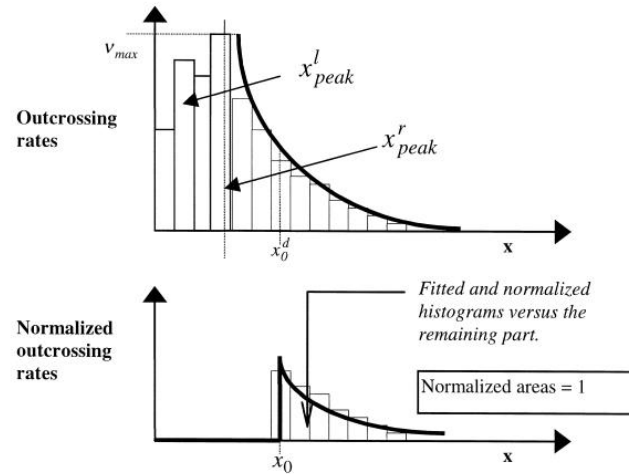


Figure 1.19: Principles of optimal fitting. Reproduced from [Cremona, 2001]

As the stochastic processes of traffic load effects satisfy the condition of stationary Gaussian processes, therefore Rice's formula can be used to estimate the up-crossing rate. However, it is hard to obtain the \dot{X} , $\sigma_{\dot{X}}$, and R_X'' , and therefore the implementation of Rice formula is still difficult. Cremona [2001] proposes to use the level crossing histogram to estimate the parameters of the Rice formula. The author simplifies the Rice formula into a second order polynomial function by taking the logarithm of Rice's formula, and thus the problem becomes to fit a curve to the level crossing histogram. The determination of the polynomial coefficients can easily be carried out by the least squares method. The goal of extrapolation is to estimate as accurately as possible the high quantile, thus only the upper tail should be concerned. However, the selection of tail fraction is problematic. Cremona [2001] points out that the crucial point for the use of Rice's formula is the selection of proportion of upper tail to be approximated by Rice's formula. The choice of the starting point should be a trade off variation and bias. If the starting point is chosen very close to the tail end, the fitting is expected to be a good approximation of the very far tail, but it introduces large variation as few points involved. In contrast, if the starting point is far from the end of tail, the fitting can be expected to be more representative for extrapolating load effects, but would increase the bias of approximation. In the preparatory studies of Eurocodes, the choice of the optimal starting point was performed by successive tests [Jacob, 1991], it is very time consuming when many datasets need to be dealt with. An automatic selection method is presented in [Cremona, 2001], the principle of this automatic optimal starting point selection (see Figure 1.19) is to use KS test

to select automatically the optimal starting based on the KS statistic $D(x)$, which represents the supremum of the set of distance, $S(x) - F(x)$, provided by the fitted and empirical level crossing rates. As a result, each selected starting point has a corresponding P-value of KS (see Figure 1.20), the point can be selected by relative optimal fitting or absolute optimal fitting. The absolute optimal fitting is to select the smallest start point corresponding to the highest P -value; while the relative optimal fitting is to select the smallest starting point with P -value over a given reference value.

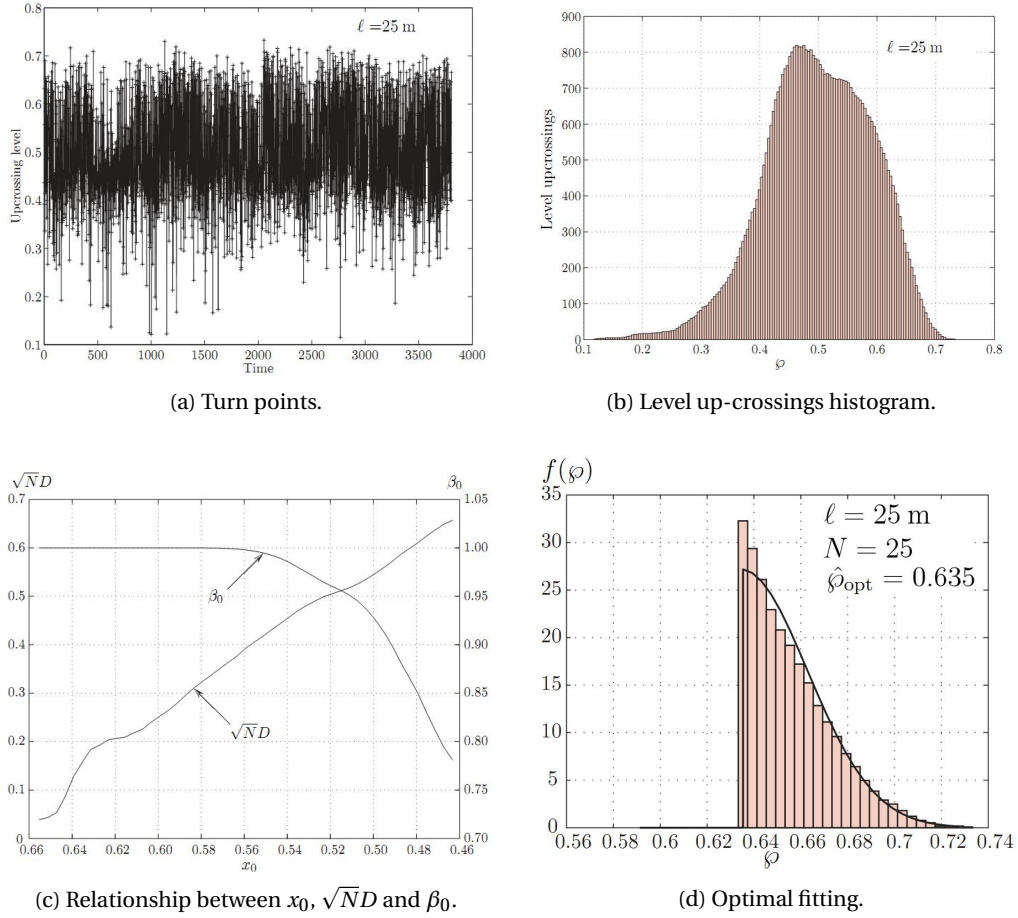


Figure 1.20: Application of fitting Rice's formula to level crossing histogram. For queue length of 25 meters. Each value is a yearly maximum value, therefore the figure shows values that represent 3805 years' signal with one year interval. Reproduced from [Getachew, 2003]

After obtaining the optimal starting point, the parameters of Rice's formula can be calculated simply. When the optimal fitting is obtained, the extrapolation of maximal and minimal effects, for any return period, R , can be assessed according to the definition of the return period that is the mean period between two occurrences of a value x . The value, x , therefore can directly be calculated from $R \cdot \nu(x) = 1$. In O'Connor and O'Brien [2005], the extremes predicted by level crossing method (or Rice's formula) are compared with those calculated using extreme value distributions of Gumbel and Weibull, some extent differences have been found. The

author does not state which method gives more precise prediction. Indeed, the extrapolated extremes from Rice's formula follow Gumbel distribution as been demonstrated in [Cremona, 2001] with an effective variable of $\frac{1}{2} \left(\frac{x-m}{\sigma} \right)^2 - \lg(v_0 T_{ref})$.

1.5 Summary

Many different methods have been used in modeling the extreme traffic loads or load effects. All of them focus on the tail behavior. However, the early stage used fitting tail distribution approach needs to pre-select the type of distribution and choose the suitable fraction to be fitted, thus subjective judgments are involved in the modeling. Level crossing method needs full time history of stochastic process, and the available method to model the level crossing histogram requires the stochastic process to be stationary and Gaussian. These methods are restricted to use in specific situations. However, extreme value modeling makes it possible to concentrate on the tail behavior suited towards tail-related inference. For measurements from bridge structures, such as traffic loads and load effects, extreme value based models are advantageous in reliable extrapolation to rare events as they turn out flexible of the tail behaviors. The GEV distribution is feasible to any shape of tail behavior, therefore the extreme value can be easily modeled if enough information for the tail is obtained. However, the typical problems in tail related inferences is the inherent lack of extreme informations. The period of available data is always very short compared to the expected lifetime of the structure. Therefore, attentions should be put on using short term measurement to model the extreme value as accurately as possible. The literature review on extreme bridge traffic load effect modeling reveals that it is possible to achieve the objectivity. The extensively used extreme value modeling method is block maximum method, which deals with the extreme data in a very waste manner. We will focus on introducing POT method to model extreme bridge traffic load effects. In applying this method, difficulties like applicability of parameter estimation method, optimal threshold choice and mixture behavior of traffic load effects needs to be solved. We will focus on these issues in the following chapters with application to problems in bridge traffic load effects.

2 Performances of Some Prediction Methods for Bridge Traffic Load Effects

2.1	Introduction	41
2.2	Data Description, and Characteristic Value and Probability of Failure Calculation	41
2.3	Results for Simulation Study Case I: Theoretical Examples	46
2.4	Results for Simulation Study Case II: Traffic Load Effect Examples	48
2.4.1	Effect of Prediction Methods	48
2.4.2	Effect of Time Interval or Block Size	50
2.5	Conclusion	53

2.1 Introduction

Methods used to estimate extreme bridge traffic load effects and their corresponding statistical theory have been carefully reviewed in Chapter 1. Historical methods: fitting distribution to upper tail [Nowak, 1993; Nowak and Hong, 1991; Nowak et al., 1993] and Rice formula based level crossing method [Cremona, 2001; Flint and Jacob, 1996; Ghosn and Moses, 1985; Jacob, 1991; O'Connor et al., 1998, 2001], have been criticized for their inappropriateness since strict mathematic assumptions are required. Two modern methods related to the extreme value theory (EVT): the block maxima (BM) [Bailey, 1996; Cooper, 1997; Enright, 2010; Gindy and Nassif, 2006; Grave et al., 2000; O'Brien et al., 2003, 1995; Siebert et al., 2008] and the peaks over threshold (POT) [Crespo-Minguillon and Casas, 1997; Gindy, 2004; James, 2003] have received more and more attention in recent years, and considerable efforts have been recently devoted to improve their performance in studying bridge traffic load effects e.g. statistical assumption [Caprani et al., 2002; Fu and You, 2010], parameter estimation [Caprani and O'Brien, 2010]. Evolution on the methods for characterizing the extreme bridge traffic load effects is due to its importance in verifying the performance of bridge structures for either deterministic or probabilistic domain [Melchers, 1987], and increased awareness of economic and social effects of bridge structures.

In this chapter, we intend to investigate the relative performance of reviewed methods, which includes (1) method fitting normal distribution to upper tail (Normal), (2) Rice formula based level crossing method (Rice), (3) peaks over threshold (POT), (4) block maxima method with parameters estimated by maximum likelihood estimation (BM-ML), (5) predictive likelihood estimation (BM-PL) and (6) Bayesian method (BM-Bayes), in estimating the distribution of extreme bridge traffic load effect with two simulation studies. The two studies includes two types of data that consist of random numbers from distribution with known parameter and the Monte Carlo simulated bridge traffic load effects. Both studies evaluates the performance of predictions methods by comparing the estimates of characteristic value for 75-year return period and annual probability of failure, which represent deterministic and probabilistic assessment respectively, with corresponding exact values.

The chapter is structured as follows. In Section 2.2, we present the data sets; in Sections 2.3 and 2.4 we display the results, and finally, Section 2.5 concludes.

2.2 Data Description, and Characteristic Value and Probability of Failure Calculation

Two cases of simulation studies have been carried out and reported in this chapter: theoretical study with known distribution parameters and bridge traffic load effect study. A main aim is to estimate 75-year characteristic values of bridge traffic load effects or, in different terminology, the 75-year return levels. By definition these are the annual maximum traffic load effects which, on average, are exceeded once every 75 years. Correspondingly, the 75-year return

Chapter 2. Performances of Some Prediction Methods for Bridge Traffic Load Effects

values are the $1 - 1/75$ quantiles of the distribution of the annual maximum bridge traffic load effect.

We evaluate also the performance of these methods used to estimate extreme bridge traffic load effects on the computation of probability of failure, p_f , which is defined as probability that the load effect S applied to a structure exceeds the resistance R of the structure and can be formulated as $p_f = Pr[R < S]$. To calculate this probability both the distribution function of the resistance F_R and the distribution function of the load effect F_S are required. In this study, in order to retain the focus on traffic load effects, the probability density function of resistance f_R is assumed to be a mirrored version of the probability density function of annual maximum load effect with respect to symmetry axis $x = k$ as illustrated in Figure 2.1. The relation between f_R and f_S can thus be expressed as $f_S(x) = f_R(2k - x)$. The aim is to compare the probability of failure estimated by the six methods with exact probability of failure, therefore we kept the distribution function F_R or probability density function f_R unchanged through the study. For instance, the f_R is obtained by symmetrizing the exact PDF of annual maximum load effect, f_S , with respect to axis which leads to a probability of failure of $p_f = 1 \times 10^{-6}$.

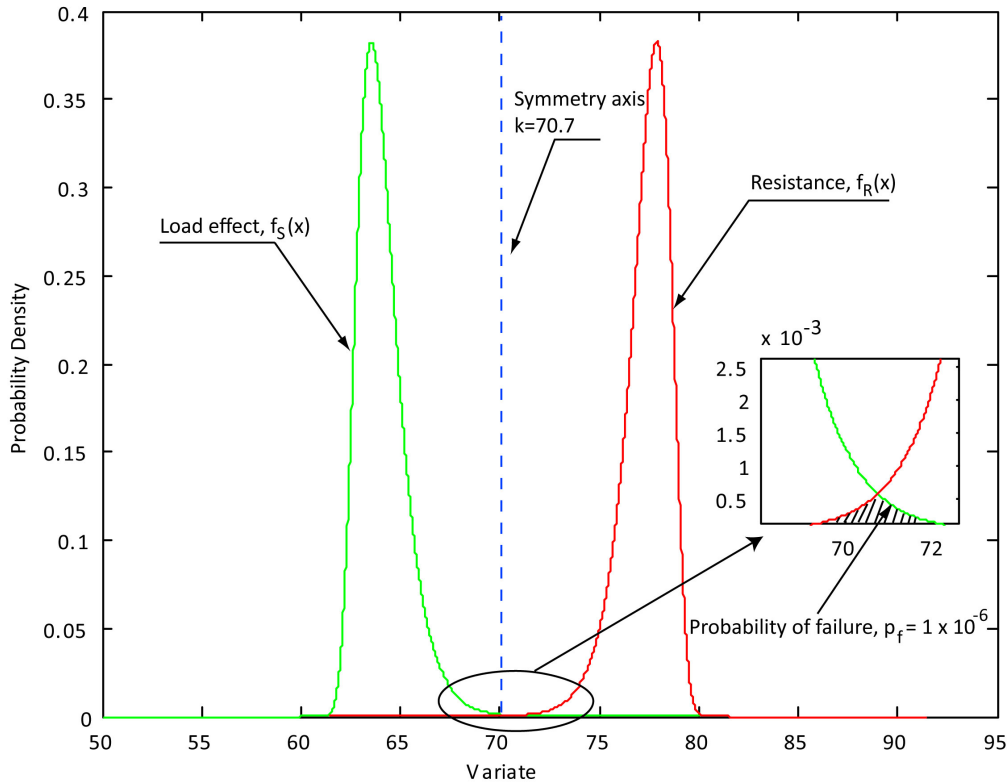


Figure 2.1: Symmetrizing probability density function of load effect to obtain probability density function of resistance

The first study aims to evaluate the performance by comparing the estimates from the six methods with known values, data from distribution with known parameters are thus used. It is thus assumed that an event, Z , has been recorded like the gross vehicle weight of fully

2.2. Data Description, and Characteristic Value and Probability of Failure Calculation

loaded 5-axle truck, which follows normal distribution, $F(z; \mu, \sigma)$, with mean value $\mu = 40$ and standard deviation, $\sigma = 5$, the event occurs $n_d = 3000$ times every day. According to the extreme value theory, the daily maximum, $X = \max\{Z_1, \dots, Z_{3000}\}$ follows the distribution of $F^{3000}(40, 5)$, which approximates to Gumbel distribution, $G(x; \mu_{d,max}, \sigma_{d,max})$, with location parameter, $\mu_{d,max} = 57.13$, and scale parameter, $\sigma_{d,max} = 1.25$ estimated by using Eq. (1.19) and (1.20), and the distribution of annual maximum approximates to Gumbel distribution, $G(x; \mu_{y,max}, \sigma_{y,max})$, also with $\mu_{y,max} = 63.54$ and $\sigma_{y,max} = 0.96$ when assuming 250 days per year by excluding holidays and weekends. The exact characteristic value for 75-year return period can be straightforwardly calculated by $G^{-1}(1 - 1/75; 0, 0.96, 63.54) = 67.7$, and the symmetry axis for obtaining distribution function of "resistance" is $x = 70.7$ as shown in Figure 2.1.

The second study investigates the performance of the six methods in estimating the distributions of bridge traffic load effects generated by combining Monte Carlo simulated traffic and influence lines. Five load effects have been considered with varying types of effects and bridge lengths: (LE1-15 and LE1-35) bending at mid-span and (LE2-15 and LE2-35) shear force at left support of simply support bridges with span length of 15 m and 35 m respectively, and (LE3-35) hogging moment at central support of two-span continuous bridge with span length of 35 m. 75000 trucks collected at WIM site in Slovakia from 2005 and 2006 were used as the basis to statistically describe the feature of traffic, in this case for vehicle and axle weight, axle spacing, vehicle speed, headway distance between successive vehicles, etc. Due to the lack of exact distribution of traffic load effect, 5000 years of traffic were simulated to approximate the exact distribution of annual maximum traffic load effects as it can describe the distribution with sufficient accuracy by using 5000 annual maxima of traffic load effects as shown in Figure 2.2. The parameters of exact distributions of annual maximum traffic load effects considered are given in Table 2.1, and the corresponding 75-year characteristic values are given also. As known the distribution function of load effects, the probability density function of "resistance" can be calculated by the previous described method illustrated in Figure 2.1, and the symmetry axis to obtaining the probability of failure of $p_f = 1 \times 10^{-6}$ for each types of load effects are given in Table 2.1. Hence, the performance of the six methods can be evaluated by comparing the estimates of characteristic values and probability of failure with the "exact" values. The six methods were applied to the five cases of traffic load effects induced by 1000 days simulated traffic, and the procedure was repeated 20 times to examine the inherent variation. The used simulated traffic were generated by using simulation program developed by [Enright, 2010; Enright and O'Brien, 2012]. A detailed description of the simulation methodology adopted has been given by Enright and O'Brien [2012], and is summarized here with emphasizing on critical factors which may influence the accuracy on predicting extreme bridge traffic load effects:

Characters of vehicle: gross vehicle weight, axle weight and axle spacing: Due to the correlation between gross vehicle weight and vehicle class (generally, the number of axles), [Enright, 2010; Enright and O'Brien, 2012] propose to use a bivariate distribution to model them,

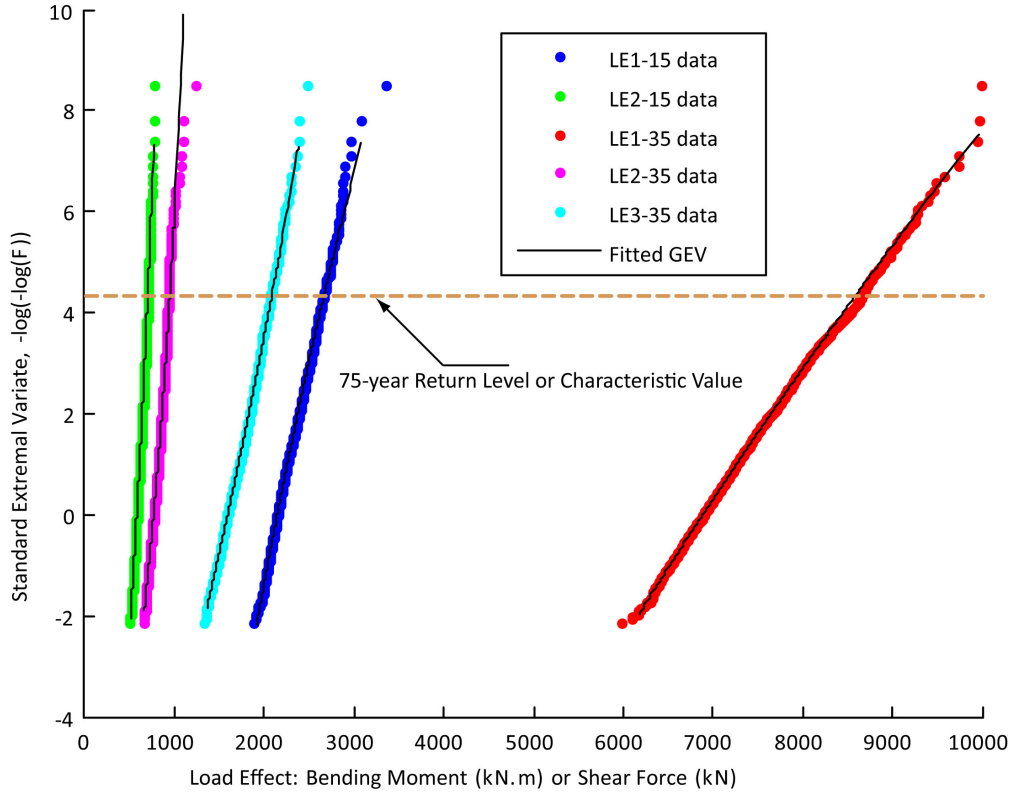


Figure 2.2: Fit of the estimated generalized extreme value distribution for annual maxima from 5000 years of simulation

and a semi-parametric approach is used to model the distribution $F(x_{weight}, x_{vehicle}; \theta)$, where x_{weight} is the gross vehicle weight, $x_{vehicle}$ is the number of axle and θ is the vector of distribution parameters. This involves using a bivariate empirical frequency distribution, $F(x_{weight}, x_{vehicle})$, in the regions where there are sufficient observations and using a parametric distribution function, here a bivariate normal distribution, $F(x_{weight}, x_{vehicle}; \mu_{weight}, \sigma_{weight}, \mu_{vehicle}, \sigma_{vehicle})$. Commonly a large amount of trucks with weight less than or around the truck weight limit can be recorded, while the extremely heavy trucks are rare with weight greater than weight limit. In the use of the semi-parametric approach, O'Brien et al. [2010] propose an empirical method to choose the threshold by using coefficient of variation of GVW. This mixture model allows simulated vehicles have GVW heavier and number of axles more than any measured vehicle. However, the simulated vehicles may have unreasonable GVW or number of axle due to the infinite tail behavior of normal distribution, restriction rules are also proposed to prevent the occurrence of this situation by setting maximum GVW to each type of vehicles. This maximum is calculated (in tonnes) as $15N_{axles} + 40$ up to 6 axles and $10N_{axles} + 70$ for 7 axles or more, where N_{axles} is the number of axles.

Bridge load effects for the short spans, e.g. 15 m and 35 m considered here, are very sensitive to wheelbase and axle layout as the influence lines are a function of $\frac{1}{l}$, where l

2.2. Data Description, and Characteristic Value and Probability of Failure Calculation

Table 2.1: Statistics (distribution parameters, symmetry axis, 75-year return level) of annual maximum traffic load effects from 5000 years of simulation

Load Effect	GEV Distribution Parameters			Symmetry Axis	Return Level (kN or kN.m)
	Shape, ξ	Scale, σ	Location, μ		
LE1-15	0.04	109.9	2145.5	3314.14	2662.9
LE2-15	-0.058	31.6	579.5	780.13	700.2
LE1-35	0.025	370.8	6887.5	10458.26	8575.7
LE2-35	-0.089	50.1	767.1	1049.18	946.6
LE3-35	-0.035	122.1	1593.6	2448.96	2082.5

is the span length. In the program, special emphasis is paid on inter-axle spacing and axle weight. For axle weight, it is considered by the percentage of the GVW carried by each axle and is modeled by using a bimodal normal distribution for each axle for each type of vehicle. Moreover, there is high correlation between weight carried by adjacent axles, and this generally increases when the axles are closely spaced. The coefficients of correlation between adjacent pairs of axles are calculated for each type of vehicle by using the measurements, and the correlation matrix is established and used in the simulation using the technique described by Iman and Conover [1982]. Within each vehicle class, empirical distributions are used for the maximum axle spacing for each GVW range. Axle spacings other than the maximum are less critical and trimodal Normal distributions are used to select representative values.

Traffic flow and headway model: An important parameter in the micro simulation of traffic is the headway in terms of distance or time between successive vehicles in lane. The headway model proposed by O'Brien and Caprani [2005] has been used, but a slightly modification is considered in this simulation program by replacing the time in seconds between the front axles of two successive vehicles arriving at a point on the road with the time between the rear axle of the leading vehicle and the front axle of the following vehicle. It can more reasonably model the clear gap between vehicles as it is independent on the vehicle length and reduces the possibility of vehicle overlap. The model is to fit quadratic curves to the cumulative distribution functions of headways up to a certain threshold, here is 2.6 seconds, and to fit a negative exponential distribution for those above the threshold. Traffic flows measured at the site are reproduced in the simulation by fitting Weibull distributions to the daily truck traffic volumes in each direction, and by using hourly flow variations based on the average weekday traffic patterns in each direction.

Lateral load distribution factor: The modeled traffic is bidirectional, with one lane in each direction, and independent streams of traffic are generated for each direction. In simulation, many millions of loading events are analyzed, and for efficiency of computation, it is necessary to use a reasonably simple model for transverse load distribution on two-lane bridges. For bending moment the maximum load effect is assumed to occur at the center of the bridge, with equal contribution laterally from each lane. In the case of

shear force at the supports of a simply supported bridge, the maximum occurs when each truck is close to the support, and the lateral distribution is very much less than for mid-span bending moment. In this case a reduction factor of 0.45 is applied to the axle weights in the second lane. This factor is based on finite element analyses performed for different types of bridge [O'Brien and Enright, 2013].

2.3 Results for Simulation Study Case I: Theoretical Examples

The (1) method fitting normal distribution to upper tail (Normal), (2) Rice formula based level crossing method (Rice), (3) peaks over threshold (POT), and (4) block maxima method with parameters estimated by maximum likelihood estimation (BM-ML), (5) predictive likelihood estimation (BM-PL) and (6) Bayesian method (BM-Bayes) were used to estimate the annual maximum distribution for the theoretical example, and their performances were evaluated by comparing the estimates of characteristic value for 75-year return period and annual probability of failure with exact values from the known distribution. The results were graphically presented by error bar plot, which is a commonly used tool to graphically report how far the estimates from the true value and represents one standard deviation of uncertainty, as given in Figures 2.3 and 2.4.

Influence of amount of data used: In order to investigate the effects of amount of data on estimating the distribution, three different numbers of days of with 200, 500 and 1000 days were considered. Both Figures 2.3 and Figure 2.4 show that the mean values of estimates of 75-year characteristic value and annual probability of failure are closer to the exact value with the increase of amount of data, and the uncertainty of the estimates reduce as expected with smaller standard deviation when increase the number of data. In the following analysis, the results from 1000 days of simulation are used in order to reducing the influence of size of data on the estimates.

Normal and Rice methods: In this study, the two methods were applied to 1000 daily maxima, and the parameters were obtained by fitting Normal distribution to upper tail of distribution function of daily maxima for the Normal methods and by fitting Rice formula to the upper tail of level crossing histogram of daily maxima. The choice of fraction of upper tail in both cases was determined by using KS goodness-of-fit test. The mean values of characteristic value for 75-year return period are 67.54 and 67.47 for the Normal and Rice methods, respectively, and the standard deviations are 0.23 and 0.42. Similarly, the mean values of Gumbel scaled annual probability of failure are -2.6252 and -2.6138 , and corresponding standard deviations are 0.0159 and 0.0166. The differences between the mean values of estimates from these two methods and the true value were quite small for 75-year characteristic value of about -0.02% and -0.13% , and for probability of failure of -0.02% and -0.46% .

POT method: The threshold for selecting the peaks in POT method was determined by KS goodness-of-fit test, and the parameters of generalized Pareto distribution were calculated by maximum likelihood method. The mean value of estimated 75-year return value was 67.49

2.3. Results for Simulation Study Case I: Theoretical Examples

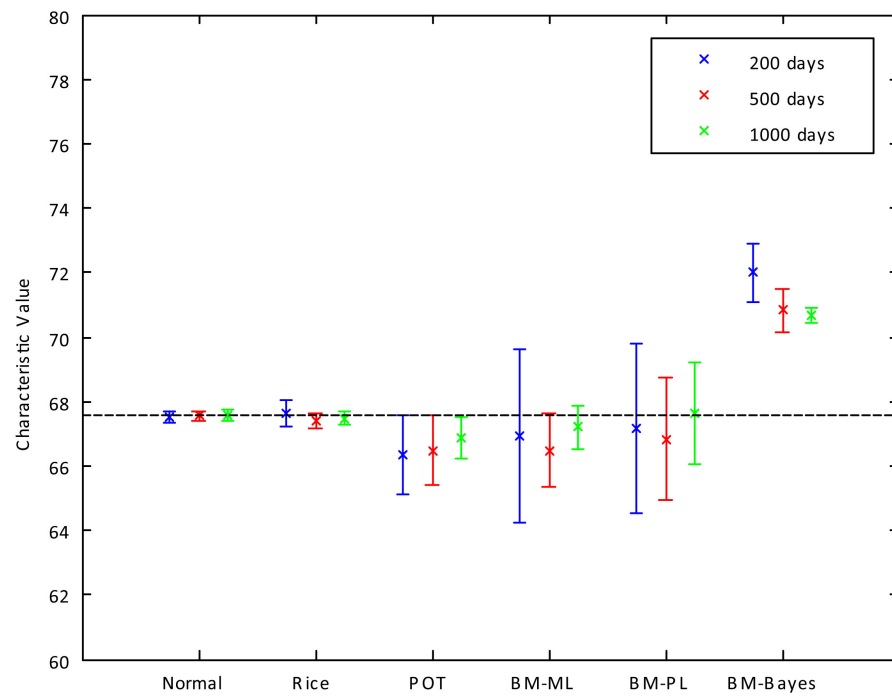


Figure 2.3: Error bar plot for inferred 75-year characteristic values

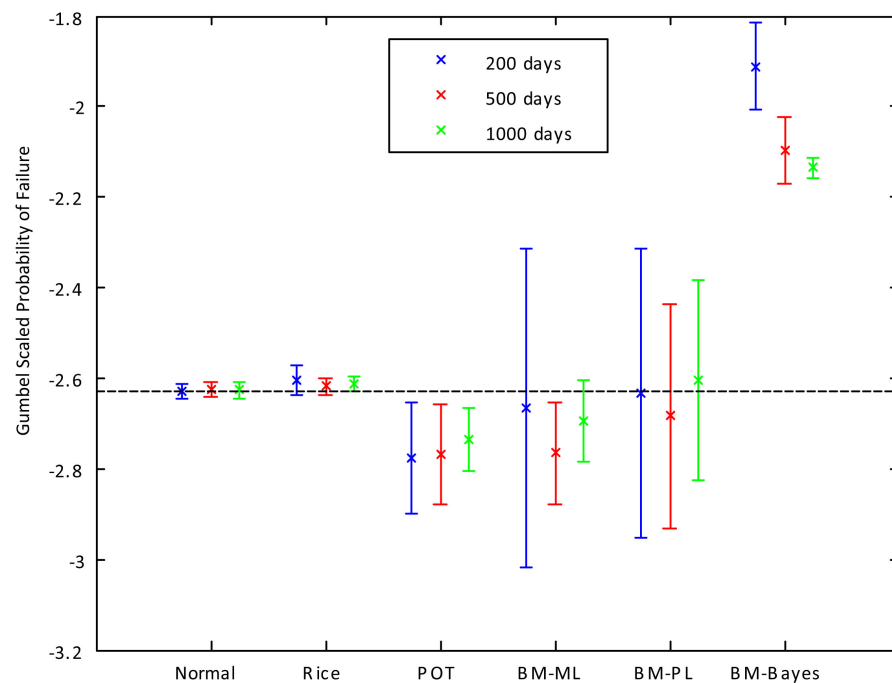


Figure 2.4: Error bar plot for inferred probabilities of failure

and the corresponding difference from true value was -1.01% , and the mean value of Gumbel scaled probability of failure was -2.74 and the corresponding difference from true value was 4.16% .

BM method: Using the BM method the differences between the estimates obtained from the maximum likelihood (ML), the predictive likelihood (PL) and the Bayesian were apparently and the true values were about, 1.37% , -0.1% and 4.6% for the mean value of 75-year characteristic value respectively. The difference between estimates of Gumbel scaled annual probability of failure and true values were similar but slightly larger of -3.94% , 1.13% and -18.68% .

Comparison of results: From the results, the Normal and Rice method is relatively good, while the two extreme value theory based methods provides larger differences. However, the results are moderately accurate in most cases, most falling in the 64 to 73 range with difference less 5% for mean value of 75-year characteristic value. Hence, there is no significant difference between these six methods in estimating characteristic value.

For the results of annual probability of failure, the difference between estimates and true values are larger than those for characteristic value. The Rice and Normal methods are again better than the other four methods. POT method is also relatively good with difference less than 5%. For the group of BM methods, the two traditional parameter estimation method provides smaller difference than the modern Bayesian estimation.

2.4 Results for Simulation Study Case II: Traffic Load Effect Examples

2.4.1 Effect of Prediction Methods

For the tail fitting method of normal distribution, the distribution is fit to the upper tail. The fraction of upper tail is selected by using KS test statistic based method. For POT method, the optimal threshold is chosen also by using KS test statistic based criteria. For Rice formula, the histogram of level crossing is generated firstly, then the Rice formula is fitted to the upper tail of the histogram, and the optimal starting point is chosen by using the method proposed by [Cremona, 2001] that is based on the KS statistic also. For the BM method, GEV is fitted to the daily maxima, and the parameters of GEV distribution are estimated by ML, PL and Bayesian methods. The results are illustrated in Figure 2.6. These figures show, in each case (i) the median value (red line), (ii) the 25% to 75% range (boxed), (iii) the 0.7% to 99.3% range (median ± 2.7 standard for normally distributed data) (dashed lines) and (iv) individual outliers (red plus sign) beyond that range.

Figure 2.6 shows that the three tail fitting methods (Normal, Rice, POT) are reasonably good, with modest range and median value close to the benchmark result from the 5000 year run. As for the simple example, fitting to a Normal distribution gives a smaller range of results which, in this case, are all reasonably close to the benchmark. The Rice method is generally better

2.4. Results for Simulation Study Case II: Traffic Load Effect Examples

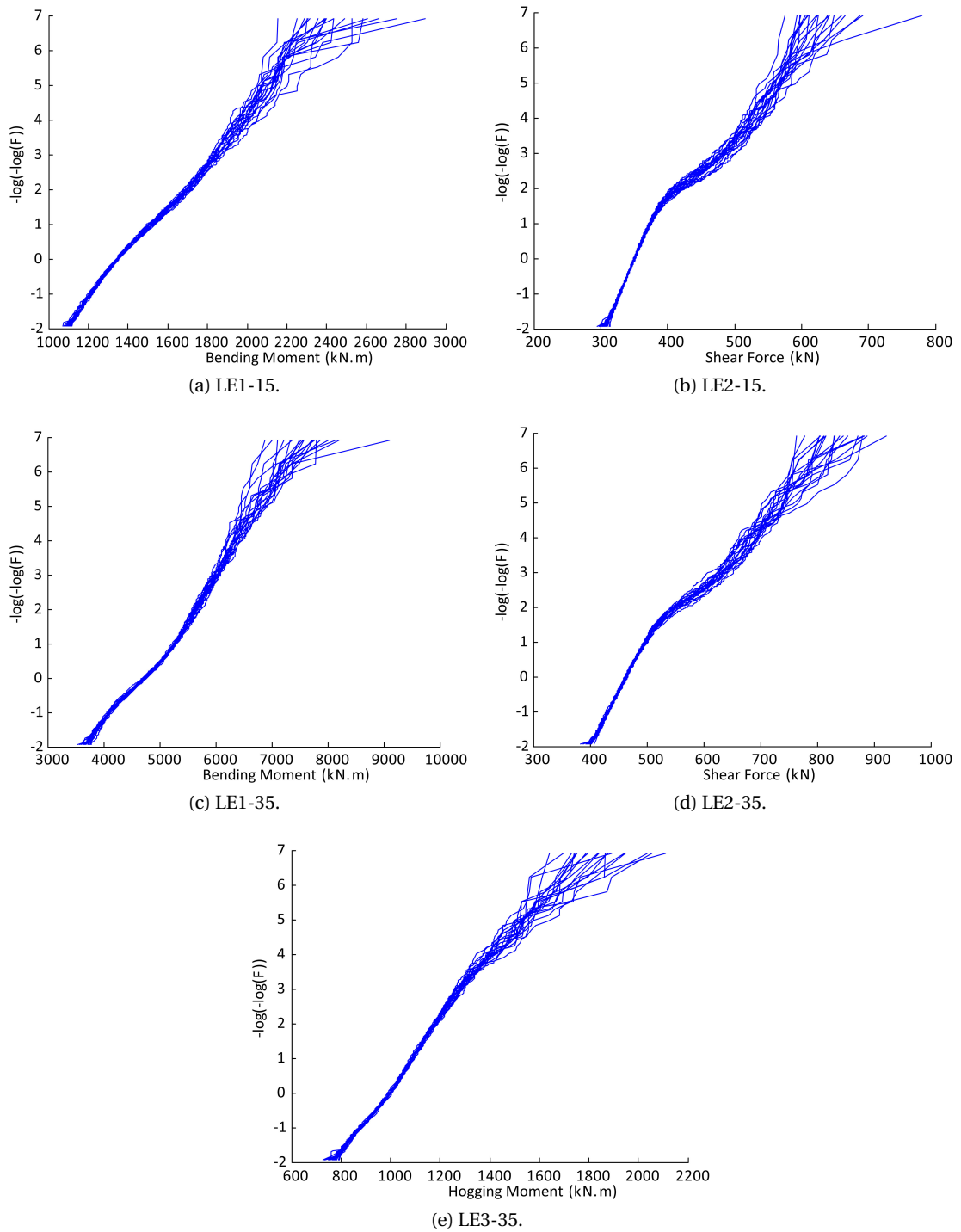


Figure 2.5: Daily maxima of load effects for 20 sets of 1000 days of simulation on Gumbel probability paper

than all the others. The two BM methods that estimate the distribution parameters by maximum likelihood and predictive likelihood give poor results for these traffic loading problems. Characteristic values are sometimes under-estimated and other times over-estimated, with no clear trend.

Annual probabilities of failure are also inferred for the five cases of load effects. The results are illustrated in Figure 2.7. As for the simple example, the errors in the probabilities, even when plotted on an Gumbel scale, are much higher than for characteristic values. Most of the tail fitting methods - POT and Rice - give relatively good results, with the Rice formula generally beating the others. As before, when fitting to a Normal distribution, the benchmark result is sometimes outside the 25% – 75% range, but not by a great deal. As for the characteristic values, BM-Bayes and BM-PL are less accurate than the other methods.

2.4.2 Effect of Time Interval or Block Size

The previous results show that the tail fitting methods have better performance than the methods fitting distribution to the whole data. The possible reason can be read from the Figure 2.5. Some types of load effect, i.e shear force at left support for a simply supported bridge, is multi-modal distribution as the plotted curves on Gumbel probability paper change direction - around 400 kN. However, it should be noted that the curves on Gumbel probability paper for yearly maxima seems have a single distribution. The change in slope is possibly caused change in daily traffic, side-by-side truck occurrence, and the effects of vehicle speeds. For example, daily truck volume may be 300 trucks today and 500 trucks tomorrow, thus the daily maxima may not be identically distributed. In the literature, the extreme value distribution or the generalized extreme value distribution is proposed to fit on the upper tail. For instance Enright [2010] proposed to fit distribution to the top 30% after comparing with the empirical fraction of $2\sqrt{n}$ recommended by Castillo et al. [2004]. Although this method can facilitate and improve the application of GEV distribution on traffic load effect, it is lack of theory background.

The principle of BM method is that the maxima should be identically and independently distributed. Therefore, when this condition is violated then the fit of extreme value distribution to data is inaccurate. As mentioned, the variation of daily traffic volume and the mixture of loading events may lead to non-identically distributed daily maximum. The comparison between of daily maxima in Figure 2.5 and yearly maxima in Figure 2.2 demonstrates that maxima taken over different years are likely to more independent and identically distributed than daily measurements. Hence, it is acceptable that the dependence and non-identification decrease suitably fast with increasing time separation. Although a longer observation time interval is generally more desirable, the amount of observations is always limited. Thus, it must be balanced against the fact that it reduces the number of maximum values available to determine the parameter using the same amount of data. In the following, we intend to illustrate how time interval influence the fitting of GEV or EV distributions to data.

2.4. Results for Simulation Study Case II: Traffic Load Effect Examples

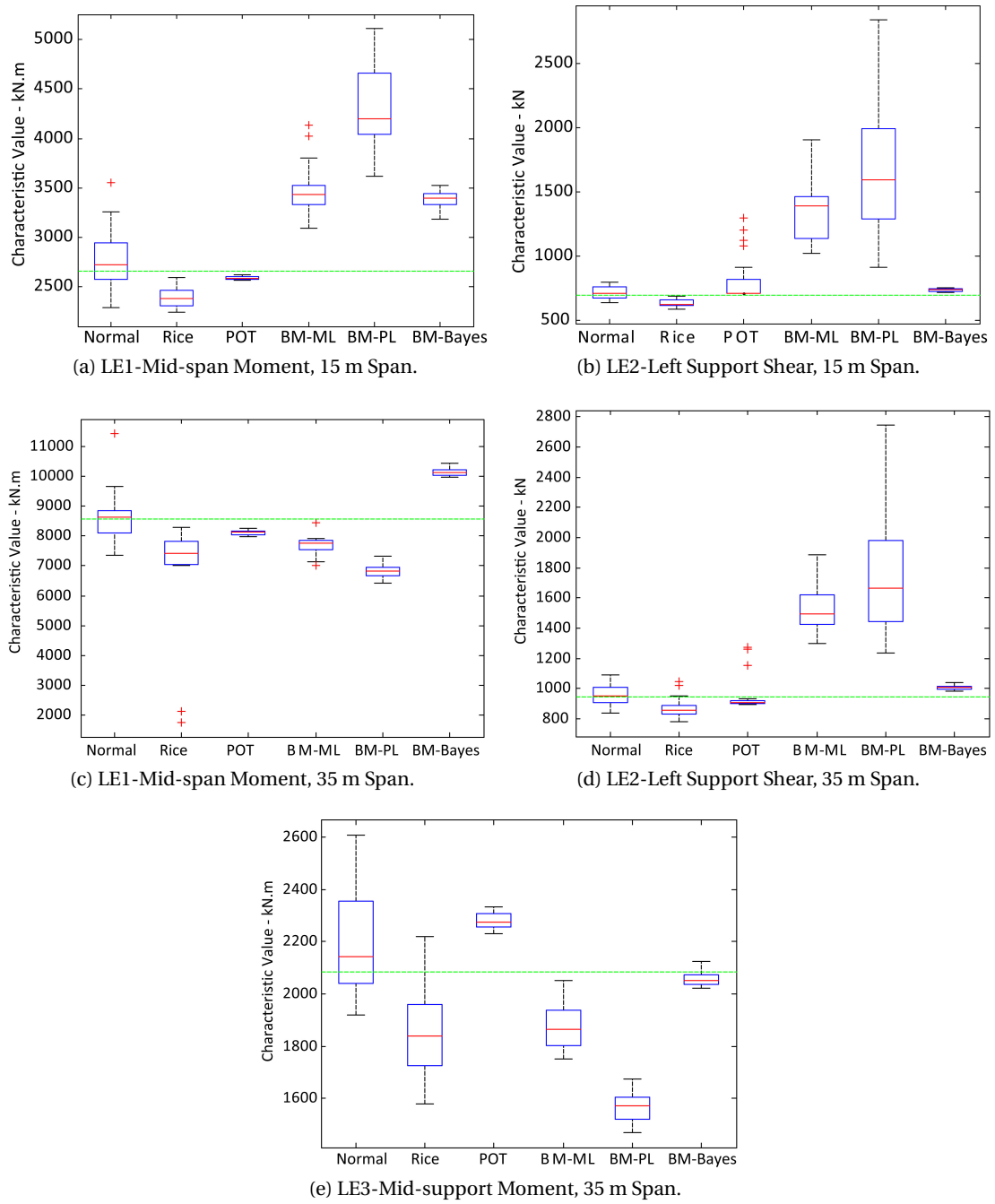


Figure 2.6: Boxplots for 75-year return levels from 1000 days of simulation

Chapter 2. Performances of Some Prediction Methods for Bridge Traffic Load Effects

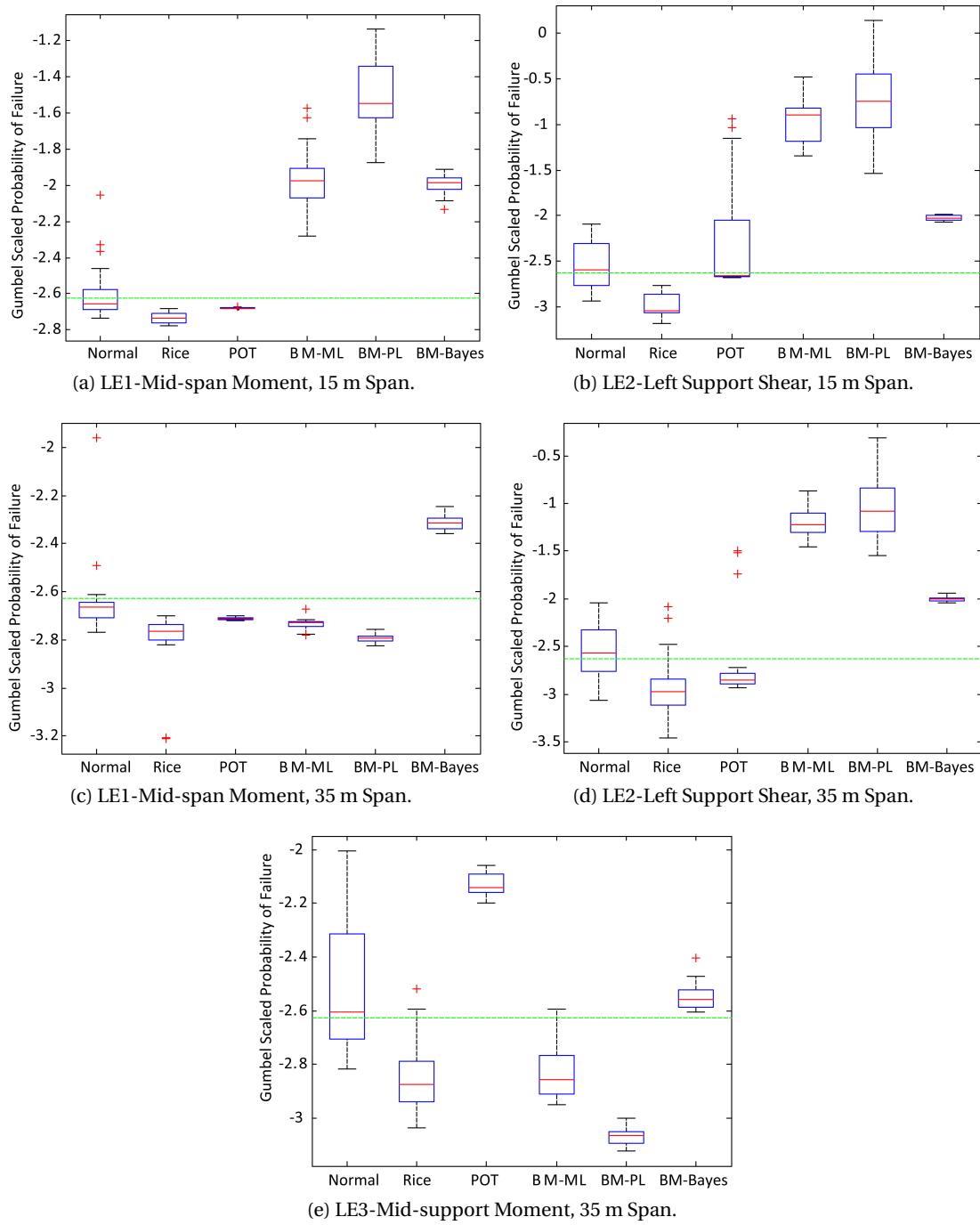


Figure 2.7: Boxplots for annual probabilities of failure from 1000 days of simulation

For this purpose, maxima are selected from the same data sets by picking the maximum value from time intervals of increasing length (e.g. every five days and so on) creating a new vector of maximum values for each time interval. Once each vector is established, the GEV distribution is fitted to them to define the respective EVDs. The results from these calculations are shown in Figure 2.8 for all the five types of load effects. As expected, each successive distribution shifts slightly to the right on the abscissa as maxima are taken out of longer observation time intervals. The impact of the choice of time interval on the estimation of annual maximum distribution is illustrated in Figure 2.9, which shows the transformation of 1 day, 5 day, 10 day, 25 day and 50 day EVDs to an annual maximum distribution by raising to a certain power. It is seen that a selection of daily observation time interval for this data would result in a significantly greater mean value and standard deviation for the annual EVD. Moreover, the true annual EVDs obtained from the 5000-year long term simulation run are given in Figure 2.9 as references, and it indicates that the annual EVDs transformed from 10-day maxima are very close to the true distribution. Further investigating the various time intervals, Table 2.2 provides the 75-year return levels estimated from the BM method. The percentage differences between estimated return level from various time intervals and exact value given from long term simulation indicates that longer time interval can improve the prediction accuracy. For example, the return level provided by max-per-day data is 113% larger than exact value for effect of LE2-15, while the difference significantly reduce to around 2% when the distribution is fitted to max-per-10 days' data.

Table 2.2: Percentage differences in 75-year return levels for various time intervals (%)

Load Effect	LE1-15 (kN.m)	LE2-15 (kN)	LE1-35 (kN.m)	LE2-35 (kN)	LE3-35 (kN.m)
Benchmark	2651	701	8646	928	2070
Max-per-day	3341 (26.05)	1498 (113.82)	7791 (-9.89)	1372 (47.85)	1713 (-17.24)
Max-per-5 days	2445 (-7.76)	866 (23.60)	7935 (-8.22)	1389 (49.68)	2320 (12.11)
Max-per-10 days	2607 (-1.65)	714 (1.93)	7927 (-8.31)	851 (-8.27)	2126 (2.73)
Max-per-25 days	2638 (-0.47)	669 (-4.48)	8037 (-7.04)	855 (-7.86)	2428 (17.29)
Max-per-50 days	2785 (5.06)	711 (-4.48)	8753 (1.24)	904 (-2.57)	2093 (1.14)

The previous results show that extending time interval to 10-day can reasonably improve the extrapolation. For the 20 sets of 1000 daily maxima, three types of time interval of 1 day, 5 day and 10 day are used to drawn maxima, and the GEV distributions are fitted to the data. The results are given in Figure 2.10 in term of boxplot again. From these results, the 10 day distribution is selected as the optimal time interval from which to select the maximum values because it provides reasonable estimates of return level and maximizes the number of available maxima.

2.5 Conclusion

In this chapter, six methods of statistical inference were quantitatively evaluated by two simulation studies. The first study was based on sample derived from a Normal distribution

Chapter 2. Performances of Some Prediction Methods for Bridge Traffic Load Effects

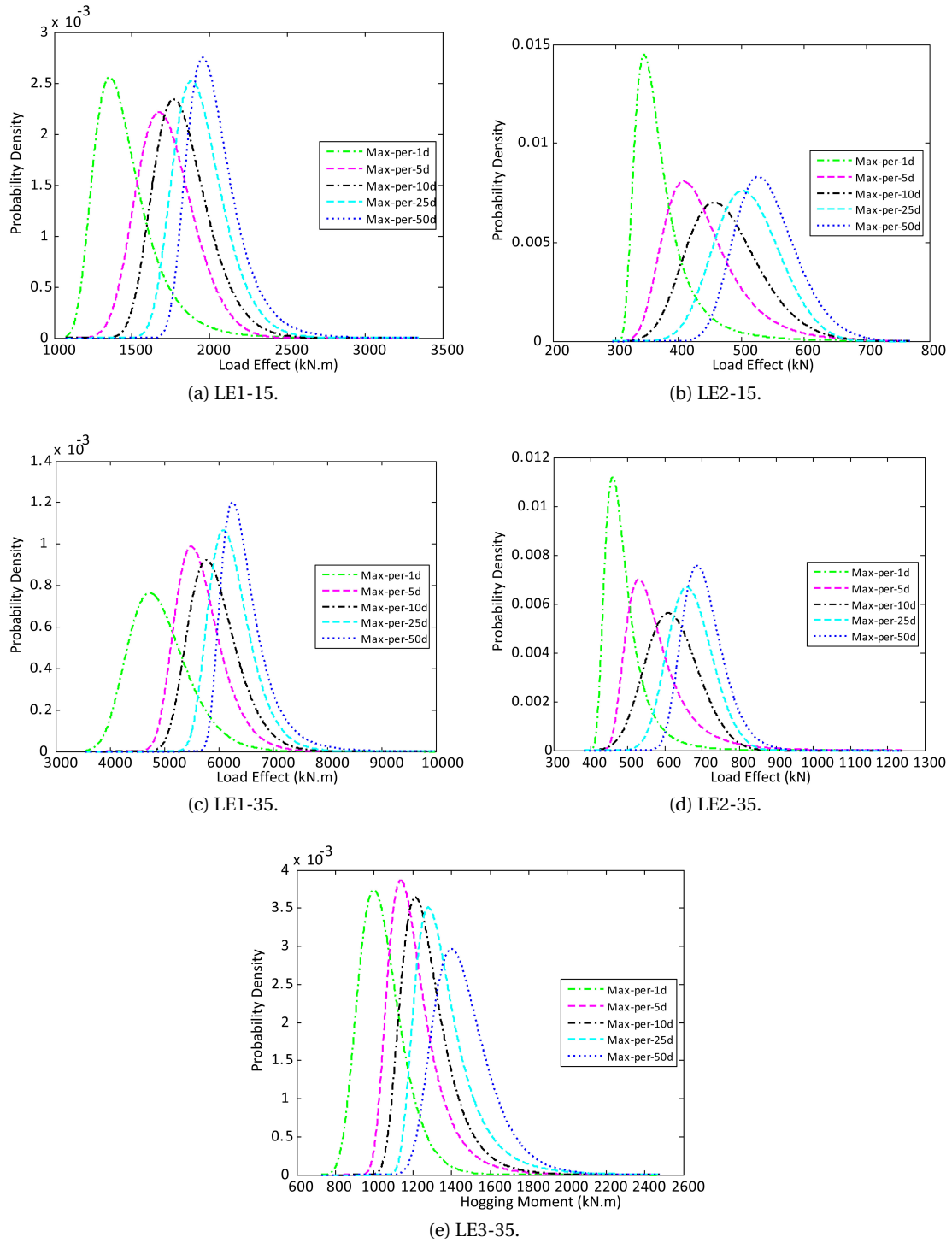


Figure 2.8: Estimated distribution for maxima taken out of various time intervals for data from 1000 days of simulation

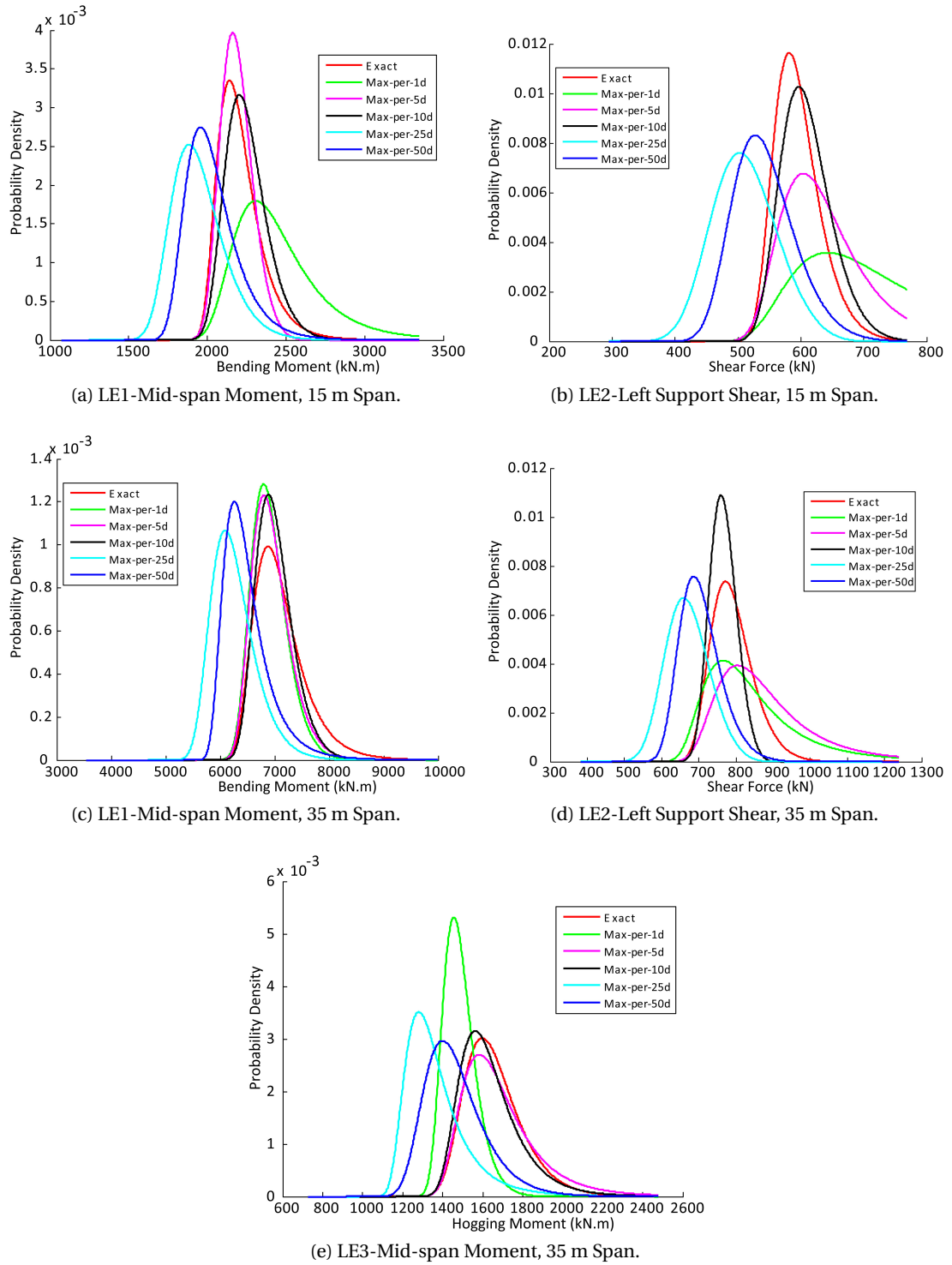


Figure 2.9: Estimated annual maximum distribution from distributions fitted to block maxima taken out of various time intervals for data from 1000 days of simulation

Chapter 2. Performances of Some Prediction Methods for Bridge Traffic Load Effects

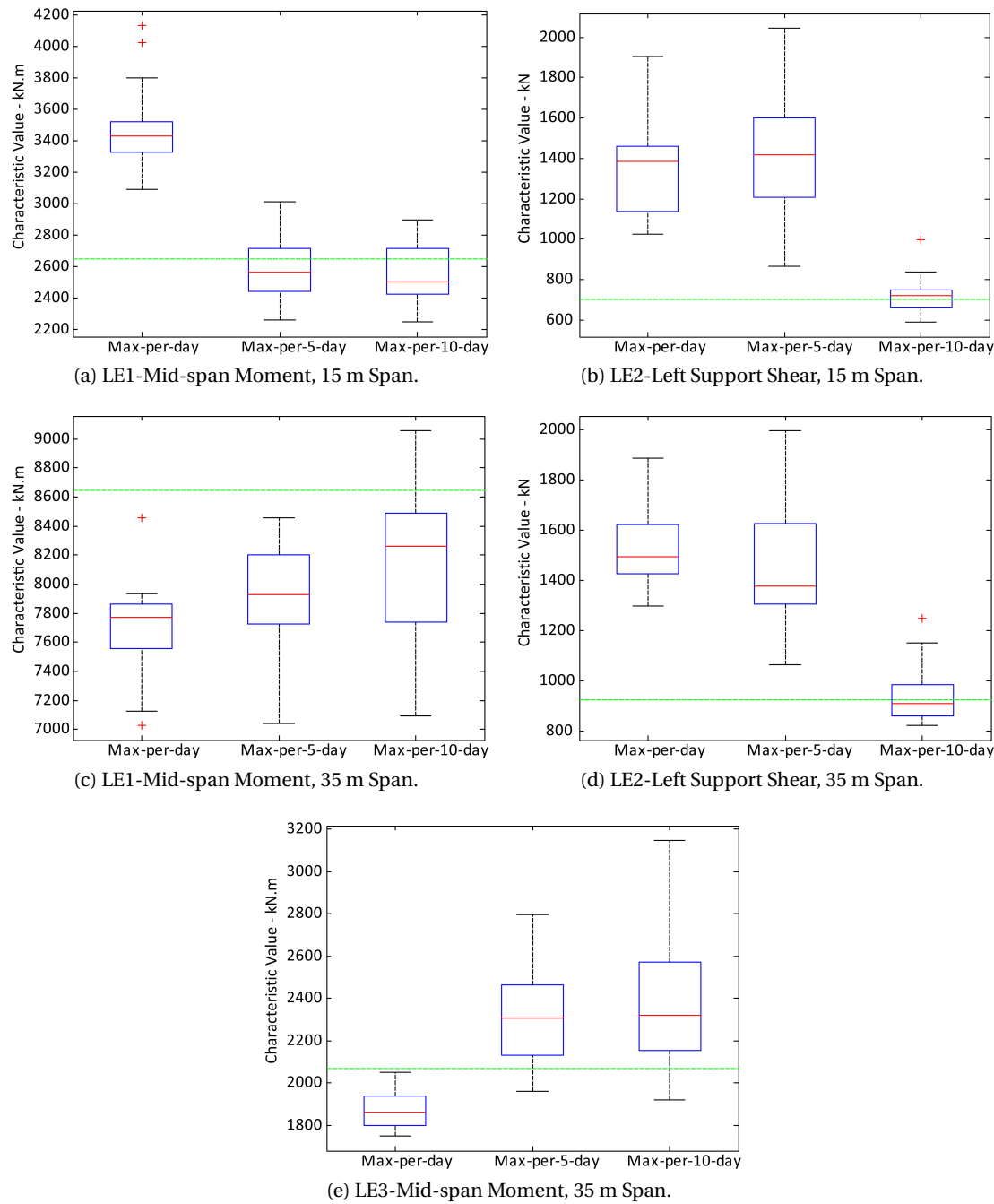


Figure 2.10: Boxplots for 75-year return levels for annual maximum distribution from different time intervals

with known parameters. A total of 3000 normally distributed values (e.g., vehicle weights) were generated every day and the daily maxima were used to infer the characteristic maximum for 75-year return period and annual probability of failure, and the estimates were compared with the corresponding true values to evaluate the performance of the six methods. In the second study, a Monte Carlo traffic loading simulation program was used to generate a traffic stream with vehicle weights and axle configurations consistent with measured Weigh-in-Motion data. Five different load effect/span combinations were considered, and characteristic values and annual probability of failure were calculated in each case by using the six methods again. In the second example, the exact solutions cannot be obtain, and a long-run simulation of 5000 years was carried out to approximate true values. Hence the performance of the six methods were evaluated by comparing the estimates from 1000 days measurements with the long-run simulation generated true values. In the probability of failure calculation, to avoid the need for any assumption on the distributions for resistance, the benchmark load effect distribution is mirrored.

The Normal and Rice methods are generally good for inferring the characteristic values and probability of failure for the two studies as expected due to the underlying Normal distribution properties of the samples. BM method is popular in recent years in studying bridge traffic load effects. Except for maximum likelihood method, the predictive likelihood and Bayesian methods have been introduced to estimate the parameters of GEV distribution in BM method. BM also shows good performance in theoretical study case, but results have shown that the BM method does not perform well in the second study of traffic load effect as directly fitting GEV distribution to commonly obtained daily maxima may not capture the distribution well, because the commonly used daily maxima of traffic load effect usually does not follow a single distribution. Through a sensitive analysis, increasing the time separation of maximum taken can significantly improve the performance of BM method, such here maximum taken out of a 10-day time frame capture the maximum distribution well for 1000 daily maxima. POT method is popular in some domains but receives less attention in bridge traffic load effect study, but it almost has the same performance as the Normal and Rice methods. However, the POT has same statistical background as BM method, and it is not restricted that the data should be normally distributed. Moreover, the POT method use the data more efficiently than BM method. Therefore, it is an interesting task to further explore the use of POT method for bridge traffic load effect study.

3 A Comparative Evaluation for the Estimators of the GPD

3.1	Introduction	61
3.2	Methods for estimating GPD parameters	62
3.2.1	Method of Moments	62
3.2.2	Method of Probability Weighted Moments	64
3.2.3	Maximum Likelihood	66
3.2.4	Likelihood Moment Estimator	68
3.2.5	Maximum Goodness-of-Fit Statistic	69
3.2.6	Elemental Percentile Method	70
3.2.7	Minimum Density Power Divergence Estimator	71
3.2.8	Other Estimation Methods	74
3.3	Evaluating the Performance of Estimators	74
3.3.1	Simulation Study Case I: Theoretical Examples	75
3.3.2	Simulation Study: Case II - Simulated Traffic Load Effects	77
3.3.3	Measured Traffic Load Effects	89
3.4	Conclusion	96

3.1 Introduction

The qualitative and quantitative evaluation results in Chapter 1 and 2 point out that generalized Pareto distribution (GPD) based POT method is deemed to approximate the CDF of excesses well. There are numerous factors, which affect the accuracy of estimates of the expected return values, such as the length and accuracy of data available, the criteria used to identify independent traffic load effects, the choice of threshold. For the choice of threshold, there is still no one that can be suitable for all situations, thus even the graphic diagnosis approaches are still used. Hence it is still an open topic in statistic of extremes [Scarrott and MacDonald, 2012]. Even though we assume that a sample follows generalized Pareto distribution, the estimated parameters can be very different as numerous parameter estimation methods exist in the literature.

In this chapter, we focus on the influence that the method used to estimate the parameters of the GPD has on the accuracy of the estimated return values. Each parameter estimation methods has its advantages and disadvantages. Traditional methods such as maximum likelihood and method of moments are undefined in some regions of the parameter space. Alternative approaches exist but they lack robustness (e.g., PWM) or efficiency (e.g., method of medians), or present significant numerical problems (e.g., minimum divergence procedures). In the domains of the applications of GPD, there are some preferred parameter estimators according to the statistical properties. For instance, the probability weighted moment (PWM) is extensively used in hydrological applications [Moharram et al., 1993], the ML is a common choice for engineering, weather, insurance, etc. Since the application of GPD on traffic load effects is still not very active, it is necessary to provide some guidance in the choice of the most suitable estimators for its application. The performance of various estimation methods for parameter and quantile estimators will be investigated in terms of their bias, variance, and their sensitivity to threshold choice and consequently affect the accuracy of the estimated return values. In addition, the specific goodness-of-fit tests for the GPD have been established by Choulakian and Stephens [2001] for the shape parameter space that either maximum likelihood (ML) or method of moments (MM) estimates exists, and Villasenor-Alva and Gonzalez-Estrada [2009] proposed a method that is valid for a wider shape parameter space. It makes the possibility to evaluate the performance of the estimation method through goodness-of-fit test.

The rest text of this chapter is organized as follows: an overview of parameter estimation methods is presented in Section 2. In section 3, the performance of the estimators is compared using the Monte Carlo simulation. The results are discussed in Section 4 and an example is presented to illustrate the difference in practical situations. Finally, conclusions are presented in Section 5.

3.2 Methods for estimating GPD parameters

Numerous methods have been proposed for estimating the parameters of the GPD from data, statistics of an observed process, since Pickands III [1975] introduced it to model exceedances over thresholds. The methods can be grouped into those for three-parameter GPD and those for two-parameter GPD. The difference is that the former has to estimate the shape, the scale and the location parameters, while the latter assumes that the location parameter is known. Several estimators have been proposed for the threshold, u , at which GPD can be considered a valid model for the data Singh and Ahmad [2004]. The parameter estimators for two-parameter GPD were extensively developed in the literature. For instance, Hosking and Wallis [1987] investigated the method of moments (MM) and the method of probability weighted moments (PWM). Rasmussen [2001] proposed the use of the generalized probability weighted moments (GPWM) to estimate the shape and scale parameters of the GPD as he notes that the standard PWM method may not be suitable to some shape space like $\xi < 0$. Dupuis and Tsao [1998] introduced hybrid-MM and PWM estimators. Dupuis [1996] observed that the MM and PWM fitting methods may produce estimates of the GPD upper bound that are inconsistent with the observed data. A review of the various methods existing in the literature for that type of GPD has been presented by de Zea Bermudez and Kotz [2010], the mathematical advantages and disadvantages of each method were listed in the article. However, it may not be easy to identify which estimation method is better for modeling GPD to bridge traffic load effects due to their properties. In this section, we qualitatively and quantitatively review the estimation methods that may be the most suitable for estimating characteristic values of extreme bridge traffic load effects. Moreover, the newly proposed methods, like Luceno [2006]; Zhang [2007], which were not considered by de Zea Bermudez and Kotz [2010], are considered in addition and compared all of them.

3.2.1 Method of Moments

The method of moments is a method to estimate population parameters such as mean, variance, etc., by equating sample moments with underlying theoretical moments and then solving these equations for the quantities to be estimated. The principle is very clear that the theoretical moments can be equated to the sample moments, and thus the parameters can be obtained through these equation. The moments of the GPD are given by

$$E \left[\left(1 + \xi \frac{X}{\sigma} \right)^r \right] = \frac{1}{1 + r\xi} \quad \text{for } 1 + \xi r > 0 \quad (3.1)$$

and the r th moments around zero is given as

$$E(X^r) = r! \frac{\sigma^r}{(-\xi)^{r+1}} \frac{\Gamma\left(-\frac{1}{\xi} - r\right)}{1 - \frac{1}{\xi}} \quad \text{for } 1 + \xi r > 0 \quad (3.2)$$

where $\Gamma(\cdot)$ stands for the Gamma function. From Eq. (3.1) or Eq. (3.2), we can easily obtain some commonly used characteristics of the GPD. The mean, variance, skewness and kurtosis have the following expressions:

$$E(x) = \frac{\sigma}{1-\xi}, \quad \xi < 1, \quad (3.3)$$

$$Var(X) = \frac{\sigma^2}{(1-\xi)^2(1-2\xi)}, \quad \xi < \frac{1}{2}, \quad (3.4)$$

$$Skew(X) = \frac{2(1+\xi)(1-2\xi)^{1/2}}{1-3\xi}, \quad \xi < \frac{1}{3}, \quad (3.5)$$

$$Kurt(X) = \frac{3(1-2\xi)(3+\xi+2\xi^2)}{(1-3\xi)(1-4\xi)} - 3, \quad \xi < \frac{1}{4}, \quad (3.6)$$

The MM estimates of parameters ξ and σ can be easily obtained by utilizing these moments, for instance, the shape parameter, ξ , can directly be obtain from Eq. (3.5), and the scale parameter σ can be obtained if ξ is known. The classical MM estimator uses the first two moments of mean and variance since the other two moments are restricted to a narrower shape parameter space. The corresponding estimates for ξ and σ are, therefore,

$$\hat{\xi} = \frac{1}{2} \left(1 - \frac{\bar{x}^2}{s^2} \right), \quad (3.7)$$

$$\hat{\sigma} = \frac{1}{2} \bar{x} \left(1 + \frac{\bar{x}^2}{s^2} \right), \quad (3.8)$$

where \bar{x} and s^2 are the sample mean and variance, respectively.

Ashkar and Ouarda [1996] point out that the order of the moments that the classic MM uses to estimate the parameters of a given distribution is somewhat arbitrary. The use of the first two moments may not be the best option for some distributions, while other combination of moments can be more efficient. The authors propose to address this issue of estimating the parameters of GPD by using generalized method of moments (GMM). Actually, this method is originally proposed to other types of distributions (e.g., Gamma distribution). The performance of the GMM has been assessed by means of simulation studies. Based on the results from the simulation studies, the authors conclude that using the traditional MM estimators is optimal for GPDs with $\xi < 0$ but has less performance than the GMM with pair $(r = 0, r = -1)$ of the moments combination for GPDs with $\xi > 0$.

Although the MM estimator is very simple and easy to implement, it is strictly restricted in the

shape parameter space of $\xi < 1/2$ since the variance is undefined for $\xi \geq 1/2$. This limitation may have no influence on the application for traffic load effects since it is commonly accepted that the asymptotic distributions of extreme traffic load effects belongs to upper-bound type extreme value distribution (see e.g., Bailey [1996]). Nevertheless, another drawback of the MM estimators should be noted for bridge traffic load effect applications. Outliers in the sample may cause considerable distortion of the results, because the MM estimators involve squaring the sample observations. Three types of abnormal observations may exist in sample of traffic loads or load effects. The first type is that some trucks may load much more than others. For example, [O'Brien et al., 2010] report that majority truck weighed less than 70 t in the Netherlands, while 892 vehicles weighted over 70 t, with a maximum recorded weight of 165 t. The second type may be arose from different traffic conditions. Load effects induced by free flowing traffic are quite different from those induced by congested traffic for certain types of load effects; the traffic in weekdays differ from those in weekends or holidays, even the night traffic is different from the daily one. The third type may be caused by the mixture of loading events as the load effects induced by different loading events are generally different, such the effects caused by single truck events are lesser than those from multiple trucks events [Caprani et al., 2008; Ghosn and Moses, 1985; Harman and Davenport, 1979].

According to the conditions and assumptions of MM estimator, it needs to take following considerations when applying to estimate parameters of GPD for traffic loads or load effects. The data should have light tails or medium as the MM estimator is restricted to $\xi < 0.5$. The abnormal observations may have significant influence on the estimates, for example special permission vehicle like low crane with GVW much higher than weight limit should be excluded from the WIM if it is recorded. This do not mean to eliminate the extreme highly loaded truck, but these observation should be treat in other manner.

3.2.2 Method of Probability Weighted Moments

Probability weighted moments (PWM) were first introduced for estimating parameters of the GPD by Hosking and Wallis [1987] when the GPD was applied to hydrological data. Before it was applied on GPD, the PWM was already extensively used in hydrological applications. The PWM was introduced by Greenwood et al. [1979] as a tool for estimating the parameters of probability distributions, especially for those distributions which are easier to be expressed in the inverse form as $x = x(F)$ than the conventional, while these types of distribution are commonly used in hydrology like the generalized lambda distribution. In such situations, it is easier to express the parameters of a distribution as function of the PWM, rather than through the ordinary moments. Although the GPD is not a distribution that can be expressed only in its inverse distribution function, the parameter estimators are convenient to compute through its PWMs [Hosking and Wallis, 1987]. The PWM of a continuous variable X with cdf F is defined as

$$M_{p,r,s} = E \left[X^p (F(X))^r (1 - F(X))^s \right], \quad (3.9)$$

where p, r, s are real numbers. For the generalized Pareto distribution, it is convenient to work with the PWM given as follows

$$\alpha_s = E[X(1 - F(X))^s] = \frac{\sigma}{(s+1)(s+1-\xi)}, \xi < 1, s = 0, 1, 2, \dots, \quad (3.10)$$

and the parameters can be obtained

$$\hat{\xi} = 2 - \frac{\alpha_0}{\alpha_0 - 2\alpha_1}, \quad (3.11)$$

$$\hat{\sigma} = \frac{2\alpha_0\alpha_1}{\alpha_0 - 2\alpha_1}. \quad (3.12)$$

The quantities α_0 and α_1 are then replaced by appropriate sample estimates denoted by α_s :

$$\alpha_s = \frac{1}{n} \sum_{i=1}^n x_{i:n} (1 - p_{i:n})^s \quad (3.13)$$

with $s = 0$ and $s = 1$. The plotting positions, $p_{i:n}$, imply that $1 - p_{i:n}$ estimates $1 - F$, the tail of the distribution. Various expressions for $p_{i:n}$ are available in the literature, for example Hosking and Wallis [1987] recommend to use

$$p_{i:n} = \frac{i + \gamma}{n + \delta} \quad (3.14)$$

with $\gamma = -3.5$, and $\delta = 0$. An estimate of the upper limit $-\sigma/\xi$ is then given by

$$-\frac{2\alpha_0\alpha_1}{4\alpha_1 - \alpha_0},$$

where α_0 and α_1 are presented in Eq. (3.13).

Actually, the method is similar in nature to the aforementioned method of moments but has advantage of avoiding the squaring of observations, which in case of bridge traffic load effects may give undue weight to large observations from abnormal loading or loading events.

Several transformations of the PWM were proposed for estimating the parameters of GPD. The first was actually a transformation of MM but has similar structure as the PWM, therefore we discussed it here. The estimator proposed by Hosking [1990] is based on linear combinations of the expectations of order statistic, and is named as L-moments. L-moments are more easily related to distribution shape and spread than PWMs. Refer to [Hosking, 1990] for more details and the exact expressions for the estimators of the GPD parameters, using the L-moments. Following a similar idea to the L-moments, high order linear combination of moments (LH-moments) were proposed by Wang [1997] to characterize generalized extreme value distribution, by using the upper part of the distributions. Meshgi and Khalili [2009] extend them to the GPD, and the estimators for the GPD parameters are provided. Actually,

the objective of using these moments to parameter estimation is to be able to use them in the situations where observations have large size. Since the L-moments and LH-moments can actually be expressed as linear combinations of the PWMs, there is no reason to distinguish them from PWMs for the purpose of parameter estimation, and hence we will not consider them further.

As found by Rasmussen [2001], the moments used by Hosking and Wallis [1987] are actually a particular case based on the principle of analytical simplicity, but this may not be the best option. Rasmussen states that any pair M_{1,r_1,s_1} and M_{1,r_2,s_2} for $(r_1, s_1) \neq (r_2, s_2)$ can be used to estimate the parameters of the GPD. Therefore, a generalized probability weighted moments (GPWM) based estimator was proposed in [Rasmussen, 2001].

Although the available shape parameter space for the PWM is restricted to $\xi < 1$, which is wider than the one provided by the MM, simulation studies [Castillo and Hadi, 1997] have shown that the PWMs perform especially well when the sample size is not large and $0 < \xi < 0.5$, and the PWM is recommended for estimating parameters under these situations. For the shape parameter space of $\xi < 0$, the GPWM outperforms the traditional PWM as shown by the simulation presented by Rasmussen [2001].

Even though the existing estimators can cover a wide range of shape parameter, the PWM and MM methods have infeasible problem that is the estimates of shape and scale parameters of the GPD are inconsistent with the observed data. To the best of our knowledge, the feasibility of estimation for the GPD was not addressed until the articles by Dupuis [1996] and Ashkar and Nwentsa Tatsambon [2007]. Dupuis points out that the infeasibility of PWM and MM when $\xi < 0$, Ashkar and Nwentsa Tatsambon [2007] study the other two extensively used estimators of ML and GPWM and find that the GPWM also provides estimates that are inconsistent with the observed data. Dupuis [1996] states that may be caused by the fact that one or more sample observations are greater than the estimated upper bound of X , which is $-\frac{\sigma}{\xi}$, and the finding is confirmed by Ashkar and Nwentsa Tatsambon [2007] via simulation studies. It is a notable issue that may be encountered when applying these moment based methods to fit GPD to traffic load effects. As been stated before, some effects caused by abnormal loadings or loading events may be greater than the estimated upper bound which relies on the majority of the data. Moreover, Dupuis and Tsao [1998] state that the infeasible problem cannot be avoided by collecting more samples.

3.2.3 Maximum Likelihood

The maximum likelihood estimators (ML) of ξ and σ have been considered by many authors, including Chaouche and Bacro [2006]; Grimshaw [1993]; Husler et al. [2011]; Smith [1984], and this approach has become the most extensively used parameter estimation method in applications like rainfall, assurance.

For a sample of \mathbf{x} of size n form a GPD, the logarithm of the likelihood can be expressed as

$$l(\xi, \sigma) = \begin{cases} -n \ln \sigma - \left(1 + \frac{1}{\xi}\right) \sum_{i=1}^n \ln \left(1 + \frac{\xi x_i}{\sigma}\right), & \text{for } \xi \neq 0, \\ -n \ln \sigma - \frac{1}{\sigma} \sum_{i=1}^n x_i, & \text{for } \xi = 0. \end{cases} \quad (3.15)$$

The maximum likelihood estimators are considered to be the values $\hat{\xi}$ and $\hat{\sigma}$, which yield a local maximum of the log-likelihood of Eq. (3.15). However, no explicit nor exact solutions for Eq. (3.15) can be exhibited. In practice, graphical or numerical methods are used and approximate solutions are considered. In the most cited reference on fitting the GPD model, Hosking and Wallis [1987] use a procedure based on Newton-Raphson algorithm to find the local maximum of $\log L$. By comparing the other two estimators of the MM and the PWM, the ML is recommended for sample with large size that is suspected to have $\xi < -0.2$. This algorithm encounter convergence problems in other situations. Due to this reason, at the GPD application active domain of hydrology, the ML is almost ignored, and the PWM and its relevant estimators are extensively used.

The issue of the high rate of failure is due to the algorithm used to find the local maximum of log-likelihood. A handy method is the one proposed by Grimshaw [1993] which has the benefit of reducing a two-dimensional maximum search to an one dimensional, by applying an appropriate transformation. Ashkar and Nwentsa Tatsambon [2007] adopt the algorithm proposed by Smith [1984] to find estimates by ML, their study show that this algorithm has excellent performance as it never encounters convergence problem. Chaouche and Bacro [2006] also proposed a new algorithm to overcome the non-convergence issues during finding the local maximum of log-likelihood, but the authors point out that although their method seems to be theoretically sound and promising, several issues are still to be solved. Therefore, in our study, we will use the algorithm proposed by Smith [1984] to find estimates of the GPD parameters.

Except improvement of the algorithm to find local maximum of log-likelihood, another improvement of ML has been conducted by Coles and Dixon [1999]. Coles and Dixon have noted that superior performance of the MM and the PWM estimators to the ML estimator for small sample size is due to the assumption of a restricted parameter space, corresponding to finite population moments. To incorporate similar information into likelihood-based inference they suggest to use a likelihood function, which penalizes larger estimates of ξ (with an infinite penalty at $\xi = 1$), similar to assuming a prior distribution for ξ . The corresponding penalized likelihood function is given by

$$l_{pen}(\xi, \sigma) = l(\xi, \sigma) P(\xi) \quad (3.16)$$

where $P(\xi)$ is the penalty function. Estimators are found as the values of σ and ξ , which maximize Eq.(3.16). In the following we will refer to these estimators as the penalized maximum likelihood (PML) estimators. Coles and Dixon [1999] states the PML performs very well for

$\xi > 0$, and the performance of the PML is the same as the regular ML for $\xi < 0$.

The tails of traffic loads or load effects are always around medium and light, which have shape parameter ξ around zero. Therefore the PML should at least have same performance as the ML and even better performance than ML if the data have shape parameter greater than zero. Additionally, the PML has better performance than ML for small size sample.

3.2.4 Likelihood Moment Estimator

Zhang [2007] has noted the defects of the traditional PWM, MM and ML methods, and an estimator has been proposed to replace the PWM and MM methods through combining likelihood with moments. The author uses the method proposed by Smith [1984] to reduce the two-dimensional optimization to find local maximum of log-likelihood, Eq. (3.15), to one-dimension, by introducing $b = \frac{\xi}{\sigma}$.

$$\frac{1}{n} \sum_{i=1}^n \frac{1}{1+bx_i} - \left(1 + \frac{1}{n} \sum_{i=1}^n \log(1+bx_i) \right)^{-1} = 0 \quad (3.17)$$

The author then introduce

$$\frac{1}{n} \sum_{i=1}^n (1+bx_i)^p - \frac{1}{1+r} = 0 \quad (3.18)$$

where

$$p = \frac{-rn}{\sum_{i=1}^n \log(1-bx_i)}$$

and $r > -1$ is chosen before estimation. Having solved this equation and found the unknown b , the GPD parameter estimators are given by

$$\hat{\xi} = \frac{1}{n} \sum_{i=1}^n \log 1 - bx_i \quad (3.19)$$

$$\hat{\sigma} = -\frac{\xi}{b} \quad (3.20)$$

Zhang [2007] shows that the solution to Eq.(3.18) is simply obtained since it is a smooth monotonous function of b with a unique solution in $(-\infty, \frac{1}{x(n)})$, unless $r = 0$ or $x_1 = x_2 = \dots = x_n$. He notes that a Newton-Raphson method will usually converge within 4-6 iterations to a margin of relative errors less than 10^{-6} .

3.2.5 Maximum Goodness-of-Fit Statistic

The infeasible issue motivates several new estimators, like the previous presented Likelihood moments approach. Luceno [2006] has proposed to use statistics based on the empirical distribution function to estimate the parameters of probability distribution. The estimators were found by minimizing the squared differences between empirical and model distribution functions, given in terms of various goodness-of-fit statistics. Luceno consider several goodness-of-fit statistics, including the three classical statistics of Kolmogorov distance, Cramer-von Mises (CM) and Anderson-Darling (AD), and the modified versions of AD (right-tail AD (ADR), left-tail AD (ADL), right-tail AD of second degree (AD2R), left-tail AD of second degree (AD2L), and AD of second degree (AD2)). The three classical EDF statistics and the five modified EDF statistics are given in Tables 3.1 and 3.2, and their computational forms are given in Table 3.3 by using the notation $z_i = F(x_{(i,n)})$ and considering that $S_n(x)$ is a step function with jumps at the order statistics $x_{(1,n)}, \dots, x_{(n,n)}$ for a set of observations x_1, \dots, x_n .

Table 3.1: Three classical EDF statistics

Statistic	Acronym	Formula
Kolomogrov distance	KS	$D_n = \sup F(x) - S_n(x)$
Cramer-von Mises	CM	$W_n^2 = n \int_{-\infty}^{\infty} \{F(x) - S_n(x)\}^2 dF(x)$
Anderson-Darling	AD	$A_n^2 = n \int_{-\infty}^{\infty} \frac{\{F(x) - S_n(x)\}^2}{F(x)\{1-F(x)\}} dF(x)$

Table 3.2: Modified Anderson-Darling statistics

Statistic	Acronym	Formula
Right-tail AD	ADR	$R_n^2 = n \int_{-\infty}^{\infty} \frac{\{F(x) - S_n(x)\}^2}{1-F(x)} dF(x)$
Left-tail AD	ADL	$L_n^2 = n \int_{-\infty}^{\infty} \frac{\{F(x) - S_n(x)\}^2}{F(x)} dF(x)$
Right-tail AD of second degree	AD2R	$r_n^2 = n \int_{-\infty}^{\infty} \frac{\{F(x) - S_n(x)\}^2}{\{1-F(x)\}^2} dF(x)$
Left-tail AD of second degree	AD2L	$l_n^2 = n \int_{-\infty}^{\infty} \frac{\{F(x) - S_n(x)\}^2}{\{F(x)\}^2} dF(x)$
AD of second degree	AD2	$a_n^2 = r_n^2 + l_n^2$

Table 3.3: Computational forms for the EDF statistics

Acronym	Formula
KS	$D_n = \frac{1}{2n} + \max_{1 \leq i \leq n} \left z_i - \frac{i-1/2}{n} \right $
CM	$W_n^2 = \frac{1}{12n} + \sum_{i=1}^n \left(z_i - \frac{i-1/2}{n} \right)^2$
AD	$A_n^2 = -n - \frac{1}{n} \sum_{i=1}^n (2i-1) \{ \ln z_i + \ln(1 - z_{n+1-i}) \}$
ADR	$R_n^2 = \frac{n}{2} - 2 \sum_{i=1}^n z_i - \frac{1}{n} \sum_{i=1}^n (2i-1) \ln(1 - z_{n+1-i})$
ADL	$L_n^2 = -\frac{3n}{2} + \sum_{i=1}^n z_i - \frac{1}{n} \sum_{i=1}^n (2i-1) \ln z_i$
AD2R	$r_n^2 = 2 \sum_{i=1}^n \ln(1 - z_i) + \frac{1}{n} \sum_{i=1}^n \frac{2i-1}{1-z_{n+1-i}}$
AD2L	$l_n^2 = 2 \sum_{i=1}^n \ln z_i + \frac{1}{n} \sum_{i=1}^n \frac{2i-1}{z_i}$
AD2	$a_n^2 = 2 \sum_{i=1}^n \{ \ln z_i + \ln(1 - z_i) \} + \frac{1}{n} \sum_{i=1}^n \left(\frac{2i-1}{1-z_{n+1-i}} + \frac{2i-1}{z_i} \right)$

Luceno [2006] demonstrated that the estimators can be used for any types of distribution, and even these estimators show better performance than the ML method in the types of

distribution considered in the simulation study. As the author emphasized, unlike the aforementioned estimation methods that can just be used for single distribution, the MGF based estimators could be applied also in the case where the dataset results from a combination of several statistic processes. Therefore, in the simulation study, in addition to evaluating the performance of the maximum goodness-of-fit estimation methods on standard homogeneous population, the author also assesses their performance for the heterogeneous populations, which are generated by using generalized linear models based on the GPD. The performance of the MGF estimators are evaluated by RMSE and Bias with two samples. Simulation results show that the AD statistics has the better performance.

3.2.6 Elemental Percentile Method

The ML method encounters convergence problem for $\xi < -1$ as stated by Chaouche and Bacro [2006]; Smith [1984]. Both MM and PWM estimates do not exist when $\xi \geq 1/2$. Even when the MM and PWM estimates exist, a serious problem with the MM and PWM estimates is that they may not be consistent with the observed sample values; that is, some of the sample values may fall outside the range suggested by the estimated parameter values. To address these issues, Castillo and Hadi [1997] have proposed an estimator by equating percentiles of the empirical and evaluated distribution. It was named elemental percentile method (EPM). The EPM is developed from a reparameterized version of the GPD with $\mu = 0$ by substituting σ/ξ by δ . The cdf is then given by

$$F(x) = 1 - \left(1 + \frac{x}{\delta}\right)^{-1/\xi}, \xi \neq 0. \quad (3.21)$$

The procedure starts with equating the cdf in Eq. (3.21) to two percentile values

$$F(x_{i:n}) = p_{i:n}$$

and

$$F(x_{j:n}) = p_{j:n} \quad (3.22)$$

where $x_{i:n}$ and $x_{j:n}$ are the i th and j th order statistics in a sample of size n , respectively. The authors suggest using

$$p_{i:n} = \frac{i - \gamma}{n + \beta}$$

with $\gamma = 0$ and $\beta = 1$. Taking the logarithm, the last two expressions can be rewritten as

$$\ln\left(1 - \frac{x_{i:n}}{\delta}\right) = kC_i \quad (3.23)$$

and

$$\ln\left(1 - \frac{x_{j:n}}{\delta}\right) = kC_j, \quad (3.24)$$

where $i \neq j$ and the constants C_i and C_j are functions of $p_{i:n}$ and $p_{j:n}$, respectively, given by

$$C_i = \ln(1 - p_{i:n})$$

and

$$C_j = \ln(1 - p_{j:n}).$$

Solving Eqs. (3.23) and (3.24) for ξ and σ . We arrive at

$$C_j \ln\left(1 - \frac{x_{i:n}}{\delta}\right) = C_i \ln\left(1 - \frac{x_{j:n}}{\delta}\right) \quad (3.25)$$

and

$$x_{i:n} \left[1 - (1 - p_{j:n})^\xi\right] = x_{j:n} \left[1 - (1 - p_{i:n})^\xi\right] \quad (3.26)$$

The solutions of Eqs. (3.25) and (3.26), which can be obtained by using the bisection method, provide a procedure for obtaining estimates for ξ and σ corresponding to the two selected order statistics, $x_{i:n}$ and $x_{j:n}$. The estimate of ξ and σ will be of the following form:

$$\hat{\xi}(i, j) = -\frac{\ln\left(1 - \frac{x_{i:n}}{\hat{\delta}(i, j)}\right)}{C_i} \quad (3.27)$$

and

$$\hat{\sigma}(i, j) = \hat{\delta}(i, j) \hat{\xi}(i, j). \quad (3.28)$$

Castillo and Hadi [1997] proposed an algorithm for computing the estimates of ξ and σ described above. They recommend applying the algorithm for all possible pairs of order statistics $x_{i:n}$ and $x_{j:n}$ for all $i, j = 1, 2, \dots, n$. After computing $\hat{\delta}(i, j)$ and $\hat{\xi}(i, j)$ for all values i and j , the final EPM estimates for ξ and σ are given by the median of the $\hat{\delta}(i, j)$ and $\hat{\xi}(i, j)$, respectively. The number of pairs of order statistics involved in this algorithm could be quite large, especially for large n . To overcome this technical difficulty, the authors suggest various alternatives. Possibly the simplest one is to consider only the pairs $(x_{i:n}, x_{n:n})$, $i = 1, 2, \dots, n-1$, which would correspond to setting $j = n$.

3.2.7 Minimum Density Power Divergence Estimator

Even though the non-robustness of maximum likelihood and probability weighted moments was pointed out in Davison and Smith [1990], only recently have robustness issues come into

consideration for fitting the GPD. Robust estimation for the GPD was firstly addressed by Peng and Welsh [2001], who have proposed rather complicated estimators for the shape and scale parameters of the GPD that are obtained by using the method of the medians (MM). Basing on a simulation study by comparing with ML estimator and the optimal bias robust estimator (OBRE), the authors showed that the MM is superior to the ML estimation and to the OBRE in the intervals in which the ML is not regular. Juárez and Schucany [2004] showed that the minimum density power divergence estimator (MDPD) is more efficient than the ML for the contaminated data, while the ML has the highest efficiency under uncontaminated GPDs. It is interesting to consider such kind of robust estimator for practical use as the observations always have some extent of contamination.

Let X_1, X_2, \dots, X_n be a random sample of size n from a distribution G with probability density function (pdf) g and let

$$F = \{f(x|\theta), x \in \chi, \theta \in \Theta\}$$

be a parametric family of pdfs. This family is supposed to be identifiable in the sense that, for $\theta_1 \neq \theta_2$,

$$\{x \in \chi : f(x|\theta_1) \neq f(x|\theta_2)\}$$

has a positive Lebesgue measure.

The density power divergence (DPD) between two pdfs f and g is defined as:

$$d_\alpha(g, f) = \begin{cases} \int_X [f^{1+\alpha}(x) - (1 + \frac{1}{\alpha})g(x)f^\alpha(x) + \frac{1}{\alpha}g^{1+\alpha}(x)] dx, & \text{for } \alpha > 0, \\ \int_X g(x) \log \left[\frac{g(x)}{f(x)} \right] dx, & \text{for } \alpha = 0. \end{cases} \quad (3.29)$$

The expression for $\alpha = 0$ is obtained as the $\lim_{\alpha \rightarrow 0} d_\alpha(g, f)$ and is known as Kullback-Leibler divergence. For $\alpha = 1$, the divergence is the well known mean square error,

$$d_1(g, f) = \int_\chi [f(x) - g(x)]^2 dx.$$

We search for a pdf f , amongst the parametric family of pdfs F defined above, which is as close as possible (in a certain sense) to the pdf g . Formally, for a given $\alpha > 0$, the aim is to search, within the parameter space Θ , for the minimum DPD functional T_α at G given as

$$d_\alpha(g, f(\cdot | T_\alpha(G))) = \inf_{\theta \in \Theta} d_\alpha(g, f(\cdot | \theta)).$$

The minimum DPD function, $\theta_0 = T_\alpha(G)$, is then the parameter of interest. [Basu et al., 1998] propose using $\hat{\theta}_{\alpha,n} = T_\alpha(G_n) \in \Theta$, where G_n is the empirical cdf. Consequently, $\hat{\theta}_{\alpha,n}$ is considered to be the value of θ associated with the pdf $f \in F$ which bears the greatest similarity with the empirical pdf g_n . The minimum density power divergence estimator (MDPDE) is

then the value of θ which minimizes, over the space Θ ,

$$H_\alpha = \int_{\chi} f^{\alpha+1}(x|\theta) dx - \left(1 + \frac{1}{\alpha}\right) \frac{1}{n} \sum_{i=1}^n f^\alpha(X_i|\theta).$$

In the framework of the GPD parameter estimation, the parametric family F is the collection of the two-parameter GPD pdfs defined in Eq.(1.9). According to Juárez and Schucany [2004], and for $\xi \neq 0$, the estimator of the pair (ξ, σ) is obtained by minimizing the function

$$H_\alpha(\xi, \sigma) = \frac{1}{\sigma^\alpha(1 + \alpha + \alpha\xi)} - \left(1 + \frac{1}{\alpha}\right) \frac{1}{n} \sum_{i=1}^n \left(1 + \xi \frac{X_i}{\sigma}\right)^{(-1/\xi - 1)\alpha} \quad (3.30)$$

over

$$\{(\xi, \sigma) \in \Theta : \sigma > 0, \xi X_{n:n} < \sigma, (1 + \alpha)/\alpha < \xi < 0 \text{ and } \xi > 0\}.$$

For traffic load effects on bridges, the issue that of the data violates the condition of identically independent distribution was pointed in the literature. Caprani et al. [2008]; Harman and Davenport [1979] have pointed out that load effects can be treated as independently distributed, but they are unsuitable to say that they are identically distributed. Caprani et al. [2008] proposed to use a composite extreme value distribution to characterize the load effects from a mixture loading events, their results show that the characteristic values from standard block maxima are drastically different from those obtained using the new proposed method. However, the parameters were fitted by ML estimators, therefore, this results in a robustness problem as been demonstrated in Dupuis and Field [1998]. As the load effects in Caprani et al. [2008] are calculated by Monte Carlo simulation, therefore it is possible to identify the loading events and group the load effects by loading events. However, it is always impossible from monitoring to identify what are the loading events which induce the considered effect, therefore it is impossible to apply the mixture GP distribution or composite GEV distribution to predict long term characteristic value. Using the classical single component POT method is a better choice, although it avoid the underlying rule of identical distribution.

In recent years, the statisticians have noticed that the data may come from mixture populations, and methods have been proposed to solve the problem. They have defined the data coming from a mixture populations as one data contaminated by the other. A single extreme that is not consistent with the bulk of extremes may jeopardize the inferences drawn, since the traditional estimators like maximum likelihood, method of moments, and probability weighted moment are not robust. Dupuis and Field [1998] has implemented Hampel's optimally-biased robust estimator (OBRE), the algorithm is based on the algorithm given by Victoria-Feser and Ronchetti [1994] in the context of estimating income distributions. Peng and Welsh [2001] derive an estimator named Medians from equating medians of sample and population score functions. This method was originally proposed by He and Fung [1999] in a survival analysis context. Juárez and Schucany [2004] use the concept of density power divergence, originally proposed by Basu et al. [1998], to derive a class of estimators (MDPDE).

A numerical study has been performed to evaluate the performance of these three estimators in Juárez and Schucany [2004]. The Medians and the OBRE encounter convergence problem when $\xi < -1$. The author also reported that the MDPDE has better performance when the severe contaminated by the performance improves when the amount of contamination data increased from 10% to 20%. Finally, the author conclude: if the true GPD model is not very heavy-tailed and contaminated by a heavier-tailer distribution, the MDPDE or the OBRE should be used; and when the GPD model has a positive upper bound and is contaminated by another GPD with upper bound then the MDPDE is the recommended method [de Zea Bermudez and Kotz, 2010]. The bridge traffic load effects were recommended to be modeled by Weibull distribution that has a upper bound. Therefore, the MDPDE is the proper method for our study.

3.2.8 Other Estimation Methods

Bayesian techniques have seen increasing applications with the development in computers' technology in the last decades. Several but not many parameter estimation approaches for the GPD parameters are developed in the Bayesian framework. A review on Bayesian methods for estimating the parameters of the GPD was provided in de Zea Bermudez and Kotz [2010]. They state that the Bayesian approach can provide satisfactory estimates as it uses all available information, but they also clarify that the Bayesian methods can be very time-consuming to implement and, most of the times, they require the use of Markov chain Monte Carlo algorithm. In addition, the parameter space is also limited such as the one provided by Eugenia Castellanos and Cabras [2007] can only be used for $\xi > 0.5$. We will not consider Bayesian methods further more in the following study as the traffic load effect shows light tail behavior that has shape value less than zero or around zero. In additional, the current available algorithm on implementing Bayesian method is too time consumption. It should be noticed that it works in many situations better or at least as well as the traditional approaches and provides much lower variance [de Zea Bermudez and Turkman, 2003].

3.3 Evaluating the Performance of Estimators

A qualitative evaluation of the performance the estimators has been conducted in the previous section, and estimators of MM, PWM, ML, PML, LM, MGF, EPM and MDPD are expected to have good performance on fitting GPD to exceedance of bridge traffic load effects over threshold. Simulation studies are commonly used to assess the performance of estimators among others, for instance Ashkar and Nwentsa Tatsambon [2007]; Ashkar and Ouarda [1996]; Castillo and Hadi [1997]; Hosking and Wallis [1987]; Moharram et al. [1993]; Singh and Ahmad [2004]. However, these studies have either compared only a few estimators or compared more estimators but for a limited range of sample sizes or GPD shape parameters. Two recently published articles on parameter estimators comparison involve more estimators. Deidda and Puliga [2009] evaluate the performance of the MM, the ML, the PWM, the MDPD,

the LM and the PML estimators for estimating parameters of the GPD for over rounded-off samples, the performance is evaluated by bias and RMSE for shape and scale parameters. Mackay et al. [2011] also assess the performance of several existing methods in literature, but the performance is evaluated through the bias and RMSE of quantiles at a non-exceedance probability of 0.999. Existing simulation results in the literature confirm that the performance of an estimator can vary considerably with both the sample size and the value of the GPD shape parameter. Moreover, Ashkar and Nwentsa Tatsambon [2007] show that the measure used to evaluate the performance of estimators is also very important. Ashkar and Nwentsa Tatsambon utilize bias and RMSE for quantiles with different return period to perform the comparison. They note that the considered four estimators of the MM, the PWM, the ML and the GPWM have litter difference on estimating quantiles with a return period that is smaller than the sample size, while the difference between various methods of estimation arise when the required quantiles are for longer return period that is greater than the sample size.

In this section, we will conduct a quantitative evaluation of the performance through applying them to model GPDs to numerical simulation samples, Monte Carlo simulated bridge traffic load effects and measured realistic traffic load effects on bridges. The purpose of this comparison study is thus to evaluate the performance of the estimators by using bias and RMSE of shape parameter, quantile with shorter and longer return period. The Bias and the root mean square error (RMSE) are:

$$Bias = E(\theta_{est} - \theta_{true}) \quad (3.31)$$

$$RMSE = \sqrt{E[(\theta_{est} - \theta_{true})^2]} \quad (3.32)$$

where $\theta_{est}, \theta_{true}$ are the estimated and the true values of the parameter respectively. In our case θ can be the ξ , the σ parameter and/or quantile of the GPD.

3.3.1 Simulation Study Case I: Theoretical Examples

Using numerical simulation samples to evaluate the performance of proposed method and compare with the existing is a common approach (see e.g., Hosking and Wallis [1987]), and it is also used to evaluate the performance of methods adapted in applications (see e.g., Deidda and Puliga [2009]). In Hosking and Wallis [1987], simulations were performed for sample sizes $n = 25, 50, 100, 200, 500$. The scale parameter σ was set to 1. The range of shape parameter is always set in $[-0.5, 0.5]$ to ensure the existence of estimates for various methods, regardlessly, there are some exception such as Castillo and Hadi [1997] who considered the range of $-2 < \xi < 2$. In particular the values of ξ observed for significant traffic load effect are usually in the range of $-0.5 \leq \xi \leq 0.5$. In this section we also carry out a simulation study to compare the reviewed methods for the generalized Pareto distribution. We have restricted our interest to this range with $\xi = -0.5, -0.25, 0, 0.25, 0.5$. For each combination of values of

n and ξ , 10000 random samples were generated from the generalized Pareto distribution. For each sample, comparisons were made the parameters σ and ξ and the quantiles at non-exceedance probabilities of 0.9 and 0.999 between true values and estimated values from methods described in Section 3.2. The true values for quantiles at 0.9 are 1.368, 1.751, 2.303, 3.113 and 4.325, and those at 0.999 are 1.937, 3.289, 6.908, 18.494 and 61.246.

Our simulation results are summarized in Tables 3.4-3.11 which present the bias and root mean squared error (RMSE) of estimates for the shape parameters ξ , the scale parameter σ and the upper-tail quantiles at non-exceedance probability of 0.9 and 0.999. Biases and RMSE's of quantile estimators have been scaled by the true value of the quantile being estimated. Some observations can be drawn from the results:

Parameter estimator

- Overall, the bias and RMSE become smaller with sample size increasing. Most of methods perform better for large size sample than small size sample. The bias and RMSE decrease as the size of sample increases, which is an indication that all the estimates are consistent.
- For the MM and the PWM, it seems that the PWM has better performance than the MM with lower bias.
- For the three commonly used methods of MM, PWM and ML, all of them have low bias the MM outperforms than the others when $\xi \leq 0.25$ for small size sample, and it has better performance than PWM when $\xi \leq 0$. The PWM estimator almost possesses the smallest RMSE when $\xi \geq 0.25$. The ML possesses the smallest RMSE when $\xi \leq -0.25$, and it outperforms than MM and PWM for samples with size of 500. These findings confirm the conclusion made by Hosking and Wallis [1987].
- For the four selected maximum goodness-of-fit statistics based methods of MGF-KS, MGF-CM, MGF-AD, MGF-ADR, the parameter estimators with the smallest RMSE are generally the MGF-ADR, but the MGF-CM estimators outperform the MGF-ADR when $\xi \geq 0.4$ for large size samples. The second best estimator appears to be the MGF-AD estimator, and the KS statistics based MGF-KS estimator always provides the worst estimator. As known, the KS method takes the same weight, while CM and AD give more weight to the tail. AD statistics give even more weight to the tails of the CDF than the CM statistics, while the ADR assigns more weight to the selected tail of the CDF. Overall, the ADR statistics outperform the others.
- The ML and MPLE estimators have almost the same performance among all the considered cases with similar RMSE's and biases. The two methods provide the best estimator for shape parameter in the case of large size samples.

Quantile estimator

- The estimators seem to have similar performance on the estimating quantile at lower non-exceedances probability, here is 0.9. The estimators show very consistent features that the bias and RMSE decrease with increasing of sample size.
- The MM and PWM estimators have low bias but has a larger RMSE than other methods in small samples.
- Amongst all estimators, the LM estimator consistently has the lowest RMSE and a small negative bias.
- The sample has a great influence on quantile estimates as smaller size samples generate larger RMSE than the larger size samples. For $\xi < 0$, the RMSE's are always greater than 0.20 (or 20%) when sample size is 25, and the RMSE's are less than 0.10 (or 10%) when sample size is 500. For $\xi > 0$, all estimators have a high RMSE.
- Once again, the present findings confirm the conclusions of Hosking and Wallis [1987] for the three commonly used estimators of MM, PWM and ML. Moment estimators of quantiles have large negative biases, however, the PWM estimators also have the smallest bias when $\xi \geq 0.25$.
- The well performed maximum goodness-of-fit statistics based estimators for shape parameters do not have the consistent performance in quantile estimation situation, the estimators place is below 6th on the rank table.

Above simulation results indicate that there is not a single estimator better than all the others in all the situations considered. Actually, it is not a surprising conclusion. First, the extensively stated disadvantages of the traditional methods indicate that they cannot cover all situation. Second, the revised form of the traditional methods were designed to address the unsatisfied factors of the traditional methods.

3.3.2 Simulation Study: Case II - Simulated Traffic Load Effects

In this section, we fit the GPD to traffic load effects data calculated by combining measured traffic data and influence lines of interest load effects. The dataset present here is the hourly maximum bending moment at mid-span of a simply supported bridge with span of 30m and carrying 4 lanes of traffic.

Traffic data, taken from a piezo-ceramic weigh-in-motion system on the A9 motorway near Saint Jean de Védas, in the South-East of France, is used to validate the proposed method on the estimation of characteristic bridge traffic load effects. This WIM station is very close to the famous station at which WIM data collected in 1986 was used to develop current traffic load model of Eurocode. It can have the same manner as a representative of current

Table 3.4: Bias of estimators of shape parameter for GPD

Shape	n	Estimator										
		MM	PWM	ML	PML	LM	MGF-KS	MGF-CM	MGF-AD	MGF-ADR	EPM	MDPD
	25	-0.06	-0.05	-0.18	-0.19	0.63	0.14	-0.08	0.01	-0.02	0.02	-0.16
	50	-0.03	-0.03	-0.09	-0.09	0.62	0.10	-0.04	0.01	0.00	0.01	-0.08
	100	-0.01	-0.01	-0.04	-0.04	0.62	0.05	-0.01	0.02	0.01	0.01	-0.03
	200	-0.01	-0.01	-0.03	-0.03	0.63	0.02	-0.01	0.01	0.00	0.00	-0.02
	500	0.00	0.00	-0.01	-0.01	0.62	0.01	0.00	0.01	0.00	0.00	-0.01
-0.25	25	-0.06	-0.05	-0.16	-0.16	0.18	0.07	-0.06	0.03	-0.01	0.05	-0.13
	50	-0.03	-0.02	-0.08	-0.08	0.09	0.06	-0.03	0.02	0.00	0.03	-0.06
	100	-0.02	-0.02	-0.04	-0.04	0.04	0.04	-0.02	0.00	0.00	0.02	-0.03
	200	0.00	0.00	-0.02	-0.02	0.01	0.04	0.00	0.01	0.01	0.02	-0.01
	500	0.00	0.00	-0.01	-0.01	0.00	0.02	0.00	0.00	0.00	0.01	-0.01
0	25	-0.08	-0.06	-0.13	-0.15	-0.03	-0.02	-0.06	0.03	0.00	0.28	-0.09
	50	-0.05	-0.03	-0.06	-0.07	-0.03	-0.01	-0.02	0.02	0.01	0.19	-0.04
	100	-0.02	-0.01	-0.03	-0.03	-0.01	-0.01	-0.01	0.01	0.01	0.13	-0.02
	200	-0.01	-0.01	-0.01	-0.02	-0.01	-0.01	0.00	0.01	0.00	0.10	-0.01
	500	-0.01	0.00	-0.01	-0.01	0.00	0.00	0.00	0.00	0.00	0.07	0.00
0.25	25	-0.16	-0.09	-0.12	-0.19	-0.08	-0.13	-0.07	0.02	-0.01	0.12	-0.08
	50	-0.11	-0.06	-0.06	-0.11	-0.05	-0.11	-0.04	0.01	0.00	0.09	-0.04
	100	-0.07	-0.02	-0.02	-0.05	-0.02	-0.07	0.00	0.01	0.01	0.07	-0.01
	200	-0.04	-0.01	-0.01	-0.02	-0.01	-0.05	-0.01	0.01	0.00	0.06	0.00
	500	-0.02	0.00	0.00	-0.01	0.00	-0.03	0.00	0.00	0.00	0.05	0.00
0.5	25	-0.29	-0.15	-0.11	-0.26	-0.10	-0.32	-0.10	0.01	-0.01	0.16	-0.07
	50	-0.22	-0.08	-0.04	-0.15	-0.04	-0.23	-0.03	0.02	0.01	0.12	-0.02
	100	-0.18	-0.06	-0.02	-0.09	-0.02	-0.13	-0.02	-0.02	-0.02	0.08	-0.01
	200	-0.15	-0.04	-0.01	-0.05	-0.01	-0.08	-0.01	-0.07	-0.06	0.09	-0.01
	500	-0.12	-0.02	-0.01	-0.02	-0.01	-0.05	-0.01	-0.16	-0.16	0.07	-0.01

Table 3.5: Bias of estimators of scale parameter for GPD

Shape	n	Estimator										
		MM	PWM	ML	PML	LM	MGF-KS	MGF-CM	MGF-AD	MGF-ADR	EPM	MDPD
-0.5	25	0.06	0.05	0.18	0.19	-0.39	-0.02	0.08	0.02	0.04	0.02	0.16
	50	0.03	0.03	0.09	0.09	-0.39	-0.03	0.03	0.00	0.01	0.00	0.07
	100	0.01	0.01	0.04	0.04	-0.39	-0.02	0.01	-0.01	0.00	0.00	0.03
	200	0.01	0.01	0.02	0.02	-0.39	-0.01	0.01	0.00	0.00	0.00	0.02
	500	0.00	0.00	0.01	0.01	-0.39	0.00	0.00	0.00	0.00	0.00	0.01
-0.25	25	0.06	0.05	0.16	0.17	-0.13	0.01	0.07	0.02	0.04	0.00	0.13
	50	0.03	0.02	0.08	0.08	-0.07	0.00	0.03	0.01	0.01	0.00	0.06
	100	0.02	0.02	0.04	0.04	-0.03	0.00	0.02	0.01	0.01	0.00	0.03
	200	0.01	0.00	0.02	0.02	0.00	-0.01	0.00	0.00	0.00	0.00	0.01
	500	0.00	0.00	0.01	0.01	0.00	0.00	0.00	0.00	0.00	0.00	0.01
0	25	0.08	0.06	0.14	0.16	0.04	0.05	0.07	0.02	0.04	0.02	0.11
	50	0.04	0.02	0.06	0.07	0.03	0.02	0.03	0.00	0.01	-0.01	0.04
	100	0.02	0.01	0.02	0.03	0.01	0.01	0.01	0.00	0.00	-0.01	0.01
	200	0.01	0.01	0.02	0.02	0.01	0.01	0.01	0.00	0.00	-0.01	0.01
	500	0.01	0.00	0.01	0.01	0.00	0.00	0.00	0.00	0.00	-0.01	0.00
0.25	25	0.19	0.09	0.15	0.21	0.10	0.11	0.10	0.04	0.06	-0.02	0.11
	50	0.13	0.05	0.07	0.10	0.05	0.07	0.05	0.02	0.02	-0.02	0.05
	100	0.08	0.01	0.02	0.04	0.01	0.03	0.01	0.00	0.00	-0.03	0.01
	200	0.05	0.01	0.01	0.02	0.01	0.03	0.01	0.01	0.01	-0.02	0.01
	500	0.03	0.00	0.00	0.01	0.00	0.01	0.00	0.01	0.01	-0.02	0.00
0.5	25	0.50	0.16	0.15	0.28	0.13	0.31	0.14	0.06	0.08	-0.01	0.14
	50	0.40	0.08	0.06	0.14	0.05	0.20	0.05	0.08	0.08	-0.03	0.06
	100	0.30	0.04	0.02	0.07	0.02	0.08	0.02	0.10	0.08	-0.02	0.02
	200	0.27	0.03	0.02	0.05	0.02	0.05	0.02	0.21	0.18	-0.02	0.03
	500	0.22	0.01	0.01	0.02	0.01	0.03	0.01	0.39	0.38	-0.03	0.02

Table 3.6: Bias of estimators of quantile at non-exceedance probability of 0.9

Shape	n	Estimator										
		MM	PWM	ML	PML	LM	MGF-KS	MGF-CM	MGF-AD	MGF-ADR	EPM	MDPD
	25	-0.01	-0.01	-0.02	-0.02	0.22	0.11	-0.01	0.02	0.00	0.02	-0.02
	50	-0.01	-0.01	-0.01	-0.01	0.20	0.07	-0.01	0.01	0.00	0.01	-0.01
	100	-0.01	0.00	-0.01	-0.01	0.19	0.03	0.00	0.00	0.00	0.00	-0.01
	200	0.00	0.00	0.00	0.00	0.19	0.02	0.00	0.00	0.00	0.01	0.00
-0.5	50	0.00	0.00	0.00	0.00	0.19	0.00	0.00	0.00	0.00	0.00	0.00
	25	-0.02	-0.02	-0.03	-0.03	0.05	0.08	0.00	0.03	0.01	0.04	-0.03
	50	-0.01	-0.01	-0.02	-0.02	0.02	0.05	0.00	0.01	0.00	0.02	-0.02
	100	-0.01	-0.01	-0.01	-0.01	0.01	0.04	0.00	0.01	0.00	0.01	-0.01
-0.25	200	0.00	0.00	0.00	0.00	0.00	0.03	0.00	0.01	0.00	0.01	0.00
	500	0.00	0.00	0.00	0.00	0.00	0.01	0.00	0.00	0.00	0.01	0.00
	25	-0.02	-0.02	-0.02	-0.03	-0.01	0.02	0.02	0.06	0.03	0.09	-0.01
	50	-0.02	-.02	-0.02	-0.02	-0.02	0.01	0.01	0.02	0.01	0.05	-0.01
0	100	-0.01	-0.01	-0.01	-0.01	-0.01	0.00	0.00	0.01	0.00	0.03	-0.01
	200	0.00	0.00	0.00	0.00	0.00	0.00	0.01	0.01	0.01	0.03	0.00
	500	0.00	0.00	0.00	0.00	0.00	0.00	0.00	0.00	0.00	0.02	0.00
	25	-0.01	-0.03	-0.01	-0.05	-0.01	-0.03	0.04	0.08	0.05	0.18	0.01
0.25	50	-0.01	-0.0	-0.01	-0.04	-0.01	-0.05	0.02	0.04	0.02	0.12	0.00
	100	-0.01	-0.01	-0.01	-0.02	0.00	-0.04	0.01	0.02	0.01	0.08	0.00
	200	0.00	0.00	0.00	0.00	0.00	-0.04	0.01	0.01	0.01	0.06	0.00
	500	0.00	0.00	0.00	0.00	0.00	-0.02	0.00	0.01	0.00	0.04	0.00
0.5	25	0.07	-0.03	0.01	-0.09	0.01	-0.10	0.07	0.12	0.09	0.37	19.73
	50	0.08	-0.02	0.02	-0.06	0.02	-0.09	0.05	0.10	0.08	0.19	0.07
	100	0.04	-0.03	-0.01	-0.06	-0.01	-0.07	0.01	0.05	0.03	0.13	0.00
	200	0.05	-0.01	0.00	-0.02	0.00	-0.04	0.01	0.06	0.05	0.13	0.01
0.5	500	0.05	-0.01	0.00	-0.01	0.00	-0.03	0.00	0.06	0.06	0.09	0.00

Table 3.7: Bias of estimators of quantile at non-exceedance probability of 0.999

Shape	n	Estimator										
		MM	PWM	ML	PML	LM	MGF-KS	MGF-CM	MGF-AD	MGF-ADR	EPM	MDPD
-0.5	25	0.03	0.07	-0.09	-0.09	3.36	0.69	0.43	0.82	0.09	0.13	-0.07
	50	0.01	0.02	-0.06	-0.06	2.85	0.41	0.07	0.08	0.03	0.05	-0.05
	100	0.01	0.02	-0.03	-0.03	2.63	0.20	0.04	0.04	0.02	0.02	-0.03
	200	0.00	0.01	-0.02	-0.02	2.56	0.09	0.02	0.02	0.01	0.01	-0.02
	500	0.00	0.00	-0.01	-0.01	2.48	0.02	0.01	0.01	0.00	0.01	-0.01
-0.25	25	0.01	0.09	-0.10	-0.11	0.82	0.93	2.43	1.76	0.26	0.36	0.01
	50	0.00	0.04	-0.07	-0.08	0.33	0.39	0.26	0.20	0.09	0.13	-0.04
	100	-0.01	0.01	-0.04	-0.04	0.13	0.22	0.07	0.06	0.03	0.07	-0.03
	200	0.01	0.02	-0.02	-0.02	0.03	0.16	0.05	0.05	0.03	0.05	-0.01
	500	0.00	0.01	-0.01	-0.01	0.00	0.07	0.02	0.02	0.01	0.03	0.00
0	25	-0.06	0.07	-0.01	-0.15	0.15	0.89	3.49	633.16	0.68	1.08	1162.60
	50	-0.04	0.03	-0.03	-0.09	0.03	0.40	1.00	0.64	0.25	0.47	0.07
	100	-0.01	0.02	-0.01	-0.03	0.02	0.13	0.20	0.16	0.10	0.25	0.02
	200	-0.01	0.02	-0.01	-0.02	0.01	0.07	0.11	0.09	0.06	0.17	0.01
	500	-0.01	0.00	-0.01	-0.01	0.00	0.03	0.04	0.03	0.02	0.12	0.00
0.25	25	-0.24	0.05	0.38	-0.28	0.33	2.94	6.84	5.15	1.34	7.27	1.48
	50	-0.20	0.01	0.18	-0.17	0.16	0.62	2.31	1.42	0.65	1.88	0.55
	100	-0.12	0.03	0.06	-0.06	0.08	0.13	0.47	0.35	0.23	0.97	0.13
	200	-0.07	0.03	0.04	-0.02	0.05	0.00	0.19	0.15	0.11	0.55	0.07
	500	-0.04	0.01	0.01	-0.01	0.02	-0.04	0.07	0.05	0.03	0.35	0.03
0.5	25	-0.47	-0.05	1.04	-0.49	0.87	6.70	18.15	11.09	2.47	144.74	366126600.00
	50	-0.41	0.00	0.49	-0.33	0.45	0.65	2.69	1.90	1.03	5.88	1.96
	100	-0.39	-0.04	0.21	-0.23	0.19	0.39	0.79	0.53	0.38	2.91	0.34
	200	-0.34	-0.03	0.07	-0.13	0.07	0.04	0.29	0.10	0.06	2.81	0.12
	500	-0.29	0.01	0.02	-0.06	0.02	-0.04	0.09	-0.21	-0.21	1.15	0.03

Table 3.8: RMSE of estimators of shape parameter for GPD

Shape	n	Estimator										
		MM	PWM	ML	PML	LM	MGF-KS	MGF-CM	MGF-AD	MGF-ADR	EPM	MDPD
-0.5	25	0.30	0.32	0.31	0.31	0.65	0.40	0.42	0.30	0.25	0.25	0.30
	50	0.19	0.21	0.17	0.18	0.63	0.31	0.26	0.18	0.15	0.15	0.17
	100	0.14	0.15	0.10	0.10	0.63	0.22	0.18	0.12	0.10	0.10	0.09
	200	0.09	0.11	0.06	0.06	0.63	0.15	0.12	0.08	0.07	0.06	0.06
	500	0.06	0.07	0.04	0.04	0.63	0.09	0.07	0.05	0.04	0.04	0.04
-0.25	25	0.25	0.28	0.30	0.31	0.27	0.33	0.42	0.31	0.26	0.25	0.30
	50	0.16	0.19	0.18	0.18	0.19	0.25	0.27	0.19	0.17	0.16	0.17
	100	0.11	0.13	0.10	0.10	0.12	0.19	0.18	0.12	0.11	0.10	0.10
	200	0.07	0.09	0.07	0.07	0.07	0.14	0.12	0.09	0.07	0.07	0.07
	500	0.05	0.06	0.04	0.04	0.04	0.09	0.08	0.05	0.05	0.04	0.04
0	25	0.22	0.24	0.30	0.28	0.21	0.30	0.43	0.31	0.26	0.28	0.31
	50	0.14	0.17	0.18	0.17	0.16	0.22	0.29	0.21	0.18	0.19	0.18
	100	0.10	0.12	0.11	0.11	0.11	0.16	0.19	0.14	0.12	0.13	0.11
	200	0.07	0.08	0.08	0.07	0.08	0.12	0.14	0.10	0.09	0.10	0.08
	500	0.04	0.05	0.05	0.04	0.05	0.07	0.08	0.06	0.05	0.07	0.05
0.25	25	0.25	0.25	0.33	0.31	0.27	0.37	0.46	0.34	0.30	0.37	0.33
	50	0.18	0.18	0.21	0.20	0.19	0.29	0.32	0.24	0.21	0.25	0.21
	100	0.12	0.12	0.13	0.13	0.13	0.20	0.20	0.16	0.14	0.20	0.14
	200	0.09	0.09	0.09	0.09	0.09	0.16	0.15	0.12	0.10	0.15	0.09
	500	0.06	0.05	0.05	0.05	0.06	0.10	0.09	0.08	0.07	0.11	0.06
0.5	25	0.33	0.29	0.35	0.35	0.32	0.62	0.71	0.37	0.33	0.46	0.38
	50	0.25	0.19	0.23	0.22	0.22	0.53	0.47	0.26	0.24	0.32	0.23
	100	0.20	0.15	0.16	0.15	0.16	0.35	0.23	0.22	0.19	0.25	0.17
	200	0.16	0.11	0.11	0.10	0.10	0.25	0.16	0.22	0.20	0.22	0.11
	500	0.13	0.08	0.07	0.07	0.07	0.18	0.10	0.29	0.29	0.17	0.08

Table 3.9: RMSE of estimators of scale parameter for GPD

Shape	n	Estimator										
		MM	PWM	ML	PML	LM	MGF-KS	MGF-CM	MGF-AD	MGF-ADR	EPM	MDPD
-0.5	25	0.32	0.33	0.37	0.38	0.40	0.31	0.35	0.29	0.28	0.29	0.36
	50	0.21	0.21	0.22	0.22	0.39	0.23	0.22	0.19	0.18	0.19	0.21
	100	0.14	0.15	0.13	0.13	0.39	0.16	0.15	0.13	0.12	0.13	0.13
	200	0.10	0.11	0.09	0.09	0.39	0.12	0.11	0.09	0.09	0.09	0.09
	500	0.06	0.07	0.05	0.05	0.39	0.07	0.07	0.06	0.06	0.06	0.06
-0.25	25	0.32	0.34	0.39	0.39	0.26	0.34	0.37	0.32	0.31	0.29	0.38
	50	0.22	0.23	0.24	0.24	0.19	0.24	0.25	0.22	0.21	0.20	0.23
	100	0.14	0.16	0.14	0.14	0.13	0.17	0.17	0.15	0.14	0.14	0.14
	200	0.10	0.11	0.10	0.10	0.10	0.12	0.11	0.10	0.10	0.10	0.10
	500	0.06	0.07	0.06	0.06	0.06	0.08	0.07	0.07	0.06	0.06	0.06
0	25	0.32	0.34	0.40	0.40	0.30	0.36	0.40	0.33	0.33	0.32	0.38
	50	0.20	0.22	0.23	0.23	0.21	0.23	0.25	0.22	0.21	0.21	0.23
	100	0.14	0.15	0.15	0.15	0.15	0.17	0.18	0.16	0.15	0.15	0.15
	200	0.10	0.11	0.10	0.10	0.10	0.12	0.13	0.11	0.11	0.11	0.10
	500	0.06	0.07	0.06	0.06	0.06	0.07	0.08	0.07	0.07	0.07	0.06
0.25	25	0.38	0.35	0.44	0.45	0.36	0.40	0.42	0.36	0.36	0.34	0.42
	50	0.25	0.24	0.25	0.26	0.24	0.28	0.28	0.25	0.24	0.23	0.25
	100	0.17	0.16	0.16	0.17	0.16	0.18	0.18	0.17	0.16	0.16	0.16
	200	0.12	0.11	0.11	0.11	0.11	0.13	0.13	0.12	0.12	0.12	0.11
	500	0.08	0.07	0.07	0.07	0.07	0.09	0.08	0.10	0.09	0.08	0.07
0.5	25	0.83	0.40	0.44	0.49	0.41	1.11	0.70	0.39	0.39	0.38	0.79
	50	0.63	0.26	0.27	0.30	0.26	0.78	0.37	0.82	0.82	0.26	0.45
	100	0.40	0.17	0.18	0.18	0.17	0.33	0.20	0.55	0.52	0.18	0.21
	200	0.33	0.13	0.13	0.13	0.13	0.24	0.14	0.61	0.59	0.14	0.27
	500	0.26	0.08	0.08	0.08	0.08	0.16	0.09	0.72	0.72	0.10	0.19

Table 3.10: RMSE of estimators of quantile at non-exceedance probability of 0.9

Shape	n	Estimator										
		MM	PWM	ML	PML	LM	MGF-KS	MGF-CM	MGF-AD	MGF-ADR	EPM	MDPD
	25	0.12	0.12	0.11	0.11	0.33	0.23	0.16	0.15	0.11	0.11	0.11
	50	0.08	0.08	0.08	0.08	0.26	0.16	0.10	0.08	0.08	0.08	0.08
	100	0.05	0.06	0.05	0.05	0.22	0.11	0.07	0.05	0.05	0.06	0.05
	200	0.04	0.04	0.04	0.04	0.21	0.07	0.05	0.04	0.04	0.04	0.04
	500	0.03	0.03	0.02	0.02	0.19	0.04	0.03	0.02	0.03	0.03	0.03
	25	0.15	0.15	0.15	0.15	0.20	0.24	0.23	0.18	0.16	0.17	0.15
	50	0.11	0.11	0.11	0.11	0.13	0.16	0.15	0.12	0.11	0.12	0.11
	100	0.07	0.08	0.07	0.07	0.08	0.12	0.10	0.08	0.08	0.08	0.07
	200	0.05	0.05	0.05	0.05	0.05	0.09	0.07	0.06	0.05	0.06	0.05
	500	0.03	0.03	0.03	0.03	0.03	0.05	0.04	0.03	0.03	0.04	0.03
	25	0.20	0.20	0.21	0.20	0.21	0.26	0.30	0.37	0.23	0.27	0.36
	50	0.14	0.14	0.14	0.14	0.14	0.19	0.21	0.17	0.16	0.18	0.15
0	100	0.10	0.10	0.10	0.10	0.10	0.13	0.13	0.11	0.11	0.13	0.10
	200	0.07	0.07	0.07	0.07	0.07	0.09	0.10	0.08	0.08	0.10	0.07
	500	0.04	0.04	0.04	0.04	0.04	0.06	0.06	0.05	0.05	0.07	0.04
	25	0.27	0.25	0.26	0.24	0.26	0.38	0.42	0.37	0.31	0.48	0.29
0.25	50	0.20	0.19	0.19	0.18	0.19	0.27	0.29	0.25	0.22	0.31	0.21
	100	0.14	0.13	0.14	0.13	0.14	0.18	0.19	0.16	0.15	0.22	0.14
	200	0.10	0.09	0.09	0.09	0.09	0.13	0.12	0.11	0.10	0.16	0.10
	500	0.06	0.06	0.06	0.06	0.06	0.09	0.08	0.07	0.07	0.12	0.06
	25	0.65	0.34	0.38	0.30	0.38	0.53	0.57	0.51	0.44	0.95	622.41
	50	0.50	0.24	0.27	0.22	0.27	0.35	0.36	0.50	0.48	0.46	1.11
	100	0.28	0.17	0.18	0.16	0.18	0.25	0.24	0.28	0.27	0.36	0.19
	200	0.21	0.13	0.13	0.12	0.13	0.18	0.16	0.23	0.22	0.32	0.17
0.5	500	0.16	0.08	0.08	0.08	0.08	0.12	0.10	0.18	0.17	0.21	0.10

Table 3.11: RMSE of estimators of quantile at non-exceedance probability of 0.999

Shape	n	Estimator										
		MM	PWM	ML	PML	LM	MGF-KS	MGF-CM	MGF-AD	MGF-ADR	EPM	MDPD
-0.5	25	0.25	0.36	0.17	0.17	4.22	1.23	3.27	9.95	0.47	0.33	0.21
	50	0.17	0.21	0.11	0.11	3.28	0.78	0.49	0.37	0.18	0.13	0.11
	100	0.12	0.15	0.06	0.06	2.88	0.49	0.26	0.16	0.10	0.07	0.06
	200	0.08	0.10	0.04	0.04	2.68	0.32	0.14	0.08	0.06	0.04	0.04
	500	0.05	0.06	0.02	0.02	2.52	0.15	0.08	0.04	0.03	0.02	0.02
-0.25	25	0.33	0.48	0.36	0.30	1.69	7.35	35.71	26.99	1.26	0.80	1.55
	50	0.22	0.31	0.21	0.20	0.77	0.89	1.28	1.01	0.42	0.34	0.24
	100	0.16	0.21	0.14	0.14	0.41	0.51	0.45	0.29	0.21	0.19	0.14
	200	0.11	0.15	0.09	0.09	0.15	0.37	0.27	0.18	0.13	0.13	0.10
	500	0.07	0.09	0.05	0.05	0.06	0.22	0.15	0.09	0.08	0.08	0.06
0	25	0.43	0.63	0.84	0.45	0.95	5.12	40.43	19907.05	3.58	2.79	36758.19
	50	0.33	0.44	0.49	0.36	0.51	2.25	8.35	4.40	1.01	1.12	0.87
	100	0.25	0.30	0.29	0.26	0.30	0.84	0.86	0.56	0.41	0.58	0.32
	200	0.18	0.22	0.19	0.18	0.21	0.42	0.52	0.35	0.28	0.41	0.21
	500	0.12	0.13	0.12	0.11	0.12	0.23	0.25	0.18	0.15	0.28	0.12
0.25	25	0.57	1.00	3.37	0.58	2.34	31.20	52.40	35.12	5.54	40.17	14.26
	50	0.47	0.72	2.75	0.53	1.77	4.07	25.32	11.21	5.53	5.72	7.81
	100	0.37	0.47	0.56	0.40	0.55	1.39	1.77	1.19	0.81	2.50	0.70
	200	0.30	0.34	0.37	0.32	0.37	0.73	0.82	0.60	0.48	1.33	0.42
	500	0.22	0.21	0.21	0.20	0.21	0.38	0.40	0.30	0.26	0.84	0.23
0.5	25	0.78	1.26	4.90	0.64	3.97	133.03	355.83	166.25	8.35	2175.97	11577940000.00
	50	0.66	1.03	2.11	0.53	1.92	4.43	18.58	9.67	3.45	23.51	32.18
	100	0.51	0.71	1.15	0.47	1.10	3.42	3.08	2.10	1.61	10.73	1.54
	200	0.44	0.55	0.58	0.37	0.57	1.01	1.17	0.85	0.71	19.79	0.67
	500	0.37	0.46	0.32	0.27	0.32	0.53	0.53	0.53	0.51	3.66	0.34

European traffic. Weight and dimensional data were collected for trucks traveling in the slow and fast lanes in one direction of the 6-lane motorway from January 2010 to May 2010. Unreliable data (e.g. inter-axle spacing greater than 20 m) were eliminated from records under the recommended WIM data cleaning criteria [Enright and O'Brien, 2011; Sivakumar et al., 2011]. Measurements for days during which the WIM system may not be active for some hours were excluded also, as it is important to exclude these days to ensure having a series of homogeneous traffic days and maximum determination. In the data, the truck traffic on weekends shows different pattern from those on weekdays, and this results in difference in extreme traffic load and load effects between weekdays and weekends traffic [Zhou et al., 2012]. Finally, 581011 trucks for 86 days were kept from the original 138 days' measurements excluding data of error, weekends and system inactive days. The more details of the statistics of the data are presented in Appendix A.

To obtain representative information on bridges, a large amount of data is required to figure out the actual situation on load carrying capacity, load subjected. Although traffic collections from WIM system have excellent quality, it is still very expensive to collect data in long term. The 86 days valid data is insufficient to estimate characteristic values or extreme value distributions of traffic load effect required to evaluate and design bridge structure, but it can help adjusting statistical models of traffic characteristics. Long term traffic can be obtained by using Monte Carlo method based on these mathematical models. Using Monte Carlo method to simulate traffic loads or load effects has been demonstrated as efficient and accurate by many authors in recent years [Caprani, 2005; Enright and O'Brien, 2012; O'Connor and O'Brien, 2005]. The description of the method is provided in Appendix B, but a simple summary of the models used is presented. The vehicles are classified by their silhouettes, and to each vehicle type we attached statistical models for gross vehicle weight, percentage of GVW taken by axle load and inter-axle spacing. The best fit is selected among the normal, bi- and tri-modal normal distribution. For the circulation characteristics, a refined hourly truck flow rate depended headway model proposed by O'Brien and Caprani [2005] is adopted. The observed gap distributions up to 4 seconds are modeled using quadratic curves for different flow rates, and a negative exponential distribution is used for larger gaps.

In order to verify the performance of the Monte Carlo traffic simulation program, a comparison was carried out between the measurements and simulated traffic. Traffic load effects (here are bending moment at mid-span and shear force at right end of simply supported bridge) were calculated by combining the simulated traffic and corresponding influence lines, and the effects are illustrated on mean excess plot in Figure 3.1. The figures show that load effects from simulation in red dots have reasonable agreement with those calculated from measured data in blue dots. However, the tails do not match very well, the possible reasons is that the number of simulation days is too small. Therefore, 1500 days traffic were simulated for the following analysis in order to reduce the dispersion.

We adopt the forecast accuracy measure proposed by Hyndman and Koehler [2006], which is called mean absolute scaled error (MASE) that measures the forecast accuracy by scaling

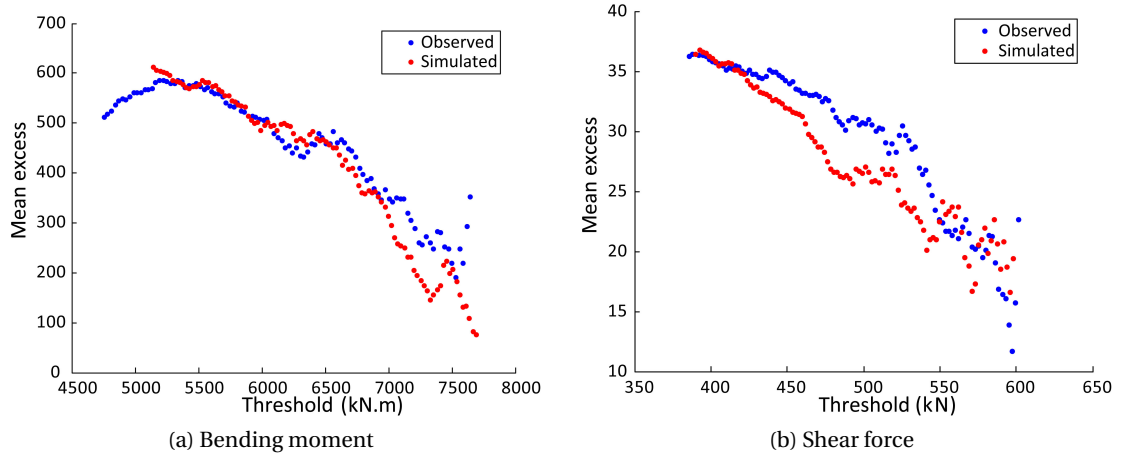


Figure 3.1: Comparison of simulated and observed load effects on ME plot

the error based on the mean absolute error (MAE) from the benchmark forecast method, to judge the performance of estimation methods. The commonly used RMSE is useful when comparing different methods applied to the same set of data, but is sensitive to outliers. A scaled error is defined as

$$q_t = \frac{Y_t - F_t}{\frac{1}{n-1} \sum_{i=2}^n |Y_i - Y_{i-1}|}, \quad (3.33)$$

which is independent of the scale of the data. A scaled error is less than one if it arises from a better forecast than the benchmark method. Conversely, it is greater than one if the forecast is worse than the benchmark. In this study, linear interpolated empirical quantiles are used as the benchmarks.

The MASEs, $mean(|q_t|)$, are given in Table 3.12 for several threshold values u and corresponding number of exceedance m , and some remarks can be drawn from the results:

- For all estimators, the MASEs decrease as the value of threshold increases, it is an indication that the GPD fits well the high tail.
- The ML and MPLE almost provide the smallest MASE for the samples with size greater than 100. Thus the two estimators perform better than the others for larger size samples. It confirms the conclusion from numerical simulations that MPLE has excellent performance for quantile estimation.
- In contrast, the PWM appears to provide the smallest MASE for the samples with size smaller than 100, and the MM, MGF-AD, and MDPD estimators have similar performance. Note that the bad performing MDPD method in the numerical case has well performance here.

Table 3.12: Mean absolute scaled error for the competition of estimators traffic load effect data

Threshold	Num	MM	PWM	ML	MPLF	MDPD	MGF-KS	MGF-CM	MGF-AD	MGF-ADR	EPM
4737	619	17.36	28.28	13.11	13.11	25.26	47.34	55.00	44.73	28.36	31.09
4804	528	9.75	15.01	7.16	7.16	18.15	48.14	50.74	27.14	28.52	28.75
4872	462	7.49	11.93	7.99	8.00	16.25	47.10	49.46	26.75	28.40	26.99
4940	398	3.08	4.30	3.19	5.22	12.48	53.20	48.01	24.61	24.43	24.59
5007	351	3.66	3.51	5.30	5.28	10.85	47.91	44.71	21.43	14.64	22.71
5075	316	3.92	5.65	5.05	5.34	10.70	36.19	42.03	7.27	21.87	21.70
5143	283	4.93	8.04	3.81	3.82	10.29	37.34	40.78	22.82	22.18	21.03
5210	244	4.06	6.20	3.94	3.94	9.29	39.23	39.17	23.11	19.97	19.13
5278	207	3.33	3.34	2.90	2.90	7.30	41.09	35.25	17.14	14.45	16.51
5346	182	3.50	3.93	2.92	2.92	6.24	30.84	33.90	13.84	11.83	14.82
5414	156	5.48	6.91	2.84	2.79	5.02	48.62	30.03	3.74	3.45	11.54
5481	139	5.93	7.51	2.96	2.81	4.66	51.09	23.71	4.91	9.13	10.06
5549	126	4.64	6.48	2.97	2.98	3.95	46.44	22.84	8.25	6.92	9.90
5617	113	3.81	5.69	2.92	2.93	3.65	35.40	16.67	6.19	5.42	9.22
5684	102	2.24	4.33	2.32	3.35	3.27	23.83	9.14	2.89	4.16	8.43
5752	91	2.10	1.61	2.65	2.65	3.03	9.57	6.80	1.65	3.51	8.22
5820	79	2.52	2.41	2.66	2.66	2.85	5.55	5.27	3.54	3.55	7.82
5887	62	2.34	1.96	2.55	2.55	2.70	7.58	4.98	1.82	3.34	6.42
5955	51	2.07	1.53	2.04	2.12	2.16	5.01	2.85	2.70	2.74	5.73
6023	42	2.57	2.63	2.43	2.43	2.51	2.07	2.16	2.77	2.70	6.62

3.3.3 Measured Traffic Load Effects

To evaluate the performance of visited estimators for realistic observations, we consider the measured maximum deformations analyzed by Siegert et al. [2008] using block maxima method. The measurements were from a highway prestressed concrete bridge, which consists of five simply supported concrete girders connected by an overall concrete deck and five cross beams as shown in figure. The instrumented span is 33 m long and carries three one way lanes. The bridge is located on a heavy trafficked motorway in the North of Paris.



Figure 3.2: View of the instrumented Roberval Bridge

Figure 3.3 shows a scheme of the instrumented span with three resistive strain gauges J1, J2 and J3, which were on the mid-span of girder P1 under the slow lane. Bending deformations were measured, and the measurements were processed to filtrate the thermal effects and electrical drift. The monitoring system has a sampling frequency of 75 Hz, but only the maximum and minimum values of 120s duration signals were recorded for the purpose to study extreme traffic load effects. Considering the length and type of instrumented bridge, the 2-minute maxima load effects can be treated as independently distributed population. 256 days' measurements were collected during two periods, one was conducted from February, 2004 to June, 2004, and the other was from January, 2005 to June 2005. Due to traffic patterns, the load effects collected on weekends and holidays differ from those from weekdays, these days' measurement were excluded and 178 days were kept finally. The histogram for these filtrated measurements is given in Figure 3.4.

Two observations, which are $95.2 \mu m/m$ and $99.4 \mu m/m$, measured in June 2004 were close to $100 \mu m/m$ and were much larger than the others less than $70 \mu m/m$. Siegert et al. [2008] kept them in the extreme value extrapolation by using block maxima method, but their influence on

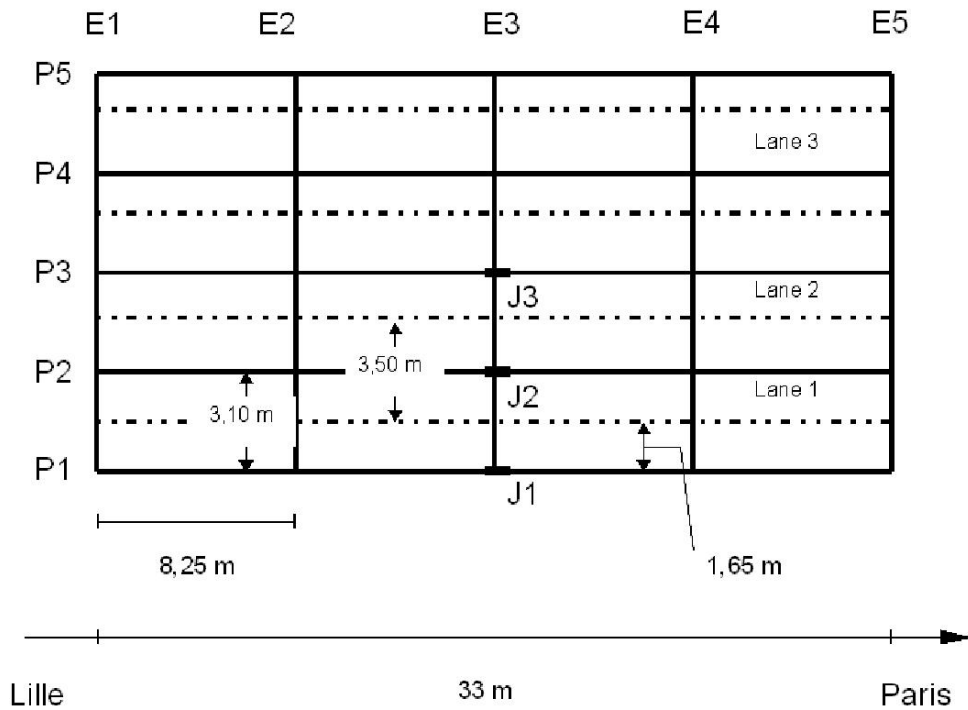


Figure 3.3: Instrumented span, after Siegert et al. [2008]

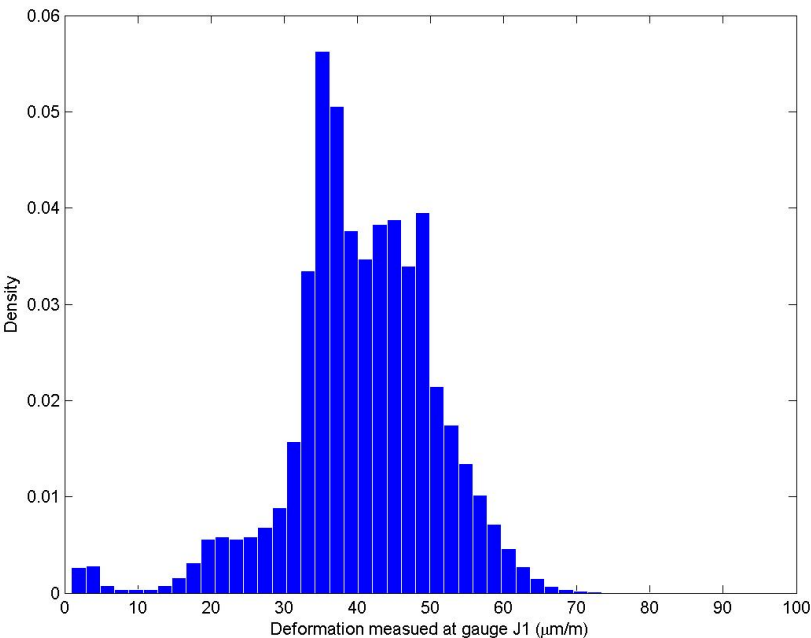


Figure 3.4: Histogram of the measured bending deformations

Table 3.13: Inconsistency rate for each method of parameter estimation

Threshold	MM	PWM	ML	PML	MDPD	LM	MGF-AD	MGF-ADR
56	100 (99.5)	100 (100)	13.4 (0)	13.4 (0)	37.5 (2.3)	37.5 (13.7)	37.5 (14)	37.5 (14)
57	97.9 (39.2)	100 (100)	14.5 (0)	14.5 (0)	37.3 (0)	39 (4.9)	39.1 (12.5)	39.1 (11.1)
58	67.1 (1.2)	100 (99.4)	8.4 (0)	8.4 (0)	24.4 (0)	33.7 (0)	35.8 (10.9)	35.8 (1.7)
59	11.7 (0)	99.3 (34.2)	2.6 (0)	2.6 (0)	6.9 (0)	15.2 (0.2)	34.9 (1.8)	28.9 (0)
60	0.79 (0)	60.8 (1)	0.1 (0)	0.13 (0)	0.6 (0)	2.7 (0.3)	22.7 (0)	6.9 (0)
61	0 (0)	4.3 (0)	0 (0)	0 (0)	0 (0)	0 (0)	1.3 (0)	0.2 (0)
62	0 (0)	0.3 (0)	0 (0)	0 (0)	0 (0)	0 (0)	0 (0)	0.4 (0)
63	0 (0)	0.8 (0)	0 (0)	0 (0)	0 (0)	0 (0)	0 (0)	0 (0)
64	0 (0)	0 (0)	0 (0)	0 (0)	0 (0)	0 (0)	0 (0)	0 (0)
65	0 (0)	0 (0)	0 (0)	0 (0)	0 (0)	0 (0)	0 (0)	0 (0)
66	0 (0)	0 (0)	0 (0)	0 (0)	0 (0)	0 (0)	0 (0)	0 (0)
67	7.7 (0)	8.9 (0)	9.3 (0)	8.6 (0)	7.8 (0)	11.1 (0)	9.1 (0)	4.5 (0)
68	0 (0)	0 (0)	0 (0)	0 (0)	0 (0)	0 (0)	0 (0)	0 (0)
69	5.9 (0)	25 (0)	5.6 (0)	4.3 (0)	14.3 (0)	14.3 (0)	0 (0)	6.5 (0)
70	5.6 (0)	0 (0)	9.1 (0.7)	8.3 (0.7)	18.2 (0)	0 (0)	0 (0)	17.3 (0)

the extrapolation was not reported. As noted, the outliers have great influence on estimation methods like MM in application of POT method. Therefore, our first objective will be to test how they influence the parameter estimates through consistency analysis. The inconsistency issue refers to the upper bound defined by $\frac{\mu}{\sigma}$ is less than the data considered.

Table 3.13 shows, for each threshold, the percentage of times that each method of estimation produced an estimate of the GPD upper bound that is inconsistent with the data. The values in parentheses are those for data when the two outliers are removed. It is apparent that the two outliers have severe influence on the consistency issue, the rates of inconsistency for basis data including the two outliers are larger than those for data excluding the two outliers. Especially, only the ML and PML encounter feasibility problems for data without the two outliers when threshold is higher than 61, while all methods report the feasibility problem for data with two outliers. Moreover, for all methods considered, it can be seen that the inconsistency rate increases with decreasing threshold level or increasing sample size. Although it is counterintuitive, similar observations were reported in [Ashkar and Nwentsa Tatsambon, 2007; Dupuis, 1996]. Therefore, the outliers should be dealt with very carefully, it is better to keep them to capture information on extreme if they do not induce feasibility problem in parameter estimation. The same consideration should be made in threshold selection, since lower threshold may induce feasibility problem.

We used the GPD model to fit the exceedances over high threshold. To study the sensitivity of the estimates to the specification of the threshold, we repeated the calculations for several thresholds and monitored the effect of changing the threshold on the obtained results. Following the consistency analysis, the two outliers were removed in following analysis. Further, the thresholds were set between $62 \mu m/m$ and $69 \mu m/m$ to avoid infeasible modeling. The statistics of estimated parameters and return levels from various estimation methods based on 1000 bootstrap samples are given in Tables 3.14 to 3.16. Estimation methods including the MM, the PWM, the ML, the PML, the LM, the MDPD, the MGF-AD and the MGF-ADR were used. The MGF-KS and MGF-CM were abandoned as they do not work well in previous preliminary studies comparing with the others, while the EPM also had similar performance as the MGF-KS estimator. From the results remarks were made as follows:

- For different threshold levels, the mean value and standard deviation of the shape parameter increase with increasing threshold values; the scale parameter has similar feature but the mean value decreases with increasing thresholds. It seems that a threshold over $67 \mu m/m$ leads to unreasonable modeling of GPD to the exceedances, the mean value shape parameters are greater than 0.1 that violates the conclusions that the type of extreme value distribution of traffic load effect should be upper bounded (see e.g., Bailey [1996]). In contrast, the shape parameter estimates for exceedances with thresholds less than $67 \mu m/m$ are negative or close to zero.
- For parameter estimates, it turns out that all methods have similar performance except the standard Anderson-Darling test statistic based MGF estimator, which gives a larger

Table 3.14: Measurements of Roberval bridge: mean and standard deviation of estimated shape and scale parameters

Parameter	Threshold	Mean $\mu m/m$								Standard deviation $\mu m/m$							
		62	63	64	65	66	67	68	69	62	63	64	65	66	67	68	69
Shape	No.	1719	1243	904	654	462	320	243	175	1719	1243	904	654	462	320	243	175
	MM	0.00	0.01	0.03	0.05	0.03	0.00	0.05	0.05	0.02	0.02	0.03	0.03	0.04	0.05	0.05	0.05
	PWM	-0.01	0.01	0.06	0.11	0.09	0.04	0.13	0.15	0.03	0.03	0.03	0.04	0.05	0.06	0.07	0.08
	Hybrid	-0.01	0.01	0.06	0.11	0.09	0.04	0.13	0.15	0.03	0.03	0.03	0.04	0.05	0.06	0.07	0.08
	ML	0.00	0.02	0.04	0.08	0.05	0.01	0.09	0.11	0.02	0.03	0.03	0.05	0.06	0.06	0.08	0.11
	PML	0.00	0.01	0.04	0.08	0.05	0.01	0.08	0.09	0.02	0.03	0.03	0.05	0.05	0.06	0.08	0.10
	MDPD	0.01	0.02	0.06	0.12	0.09	0.03	0.15	0.20	0.02	0.03	0.04	0.05	0.07	0.07	0.11	0.16
	LM	0.01	0.03	0.06	0.12	0.09	0.04	0.14	0.16	0.02	0.03	0.04	0.05	0.06	0.06	0.09	0.11
	MGF-AD	0.02	0.06	0.13	0.26	0.25	0.13	0.38	0.53	0.03	0.04	0.05	0.07	0.11	0.10	0.18	0.27
	MGF-ADR	0.01	0.03	0.08	0.13	0.07	0.02	0.11	0.13	0.03	0.04	0.04	0.06	0.07	0.07	0.10	0.12
Scale	MM	2.90	2.82	2.70	2.58	2.69	2.81	2.51	2.47	0.09	0.11	0.12	0.15	0.18	0.22	0.22	0.28
	PWM	2.92	2.81	2.62	2.43	2.53	2.72	2.31	2.23	0.10	0.12	0.13	0.16	0.20	0.25	0.25	0.31
	Hybrid	2.92	2.81	2.62	2.43	2.53	2.72	2.31	2.23	0.10	0.12	0.13	0.16	0.20	0.25	0.25	0.31
	ML	2.89	2.81	2.67	2.52	2.64	2.81	2.43	2.35	0.10	0.12	0.14	0.18	0.22	0.25	0.29	0.37
	PML	2.90	2.81	2.67	2.53	2.65	2.81	2.45	2.38	0.10	0.12	0.14	0.17	0.21	0.24	0.28	0.36
	MDPD	2.88	2.79	2.62	2.43	2.56	2.75	2.31	2.19	0.10	0.12	0.14	0.18	0.23	0.25	0.31	0.41
	LM	2.88	2.78	2.61	2.43	2.54	2.73	2.31	2.22	0.10	0.12	0.13	0.17	0.22	0.25	0.28	0.35
	MGF-AD	2.86	2.74	2.51	2.23	2.30	2.59	1.99	1.79	0.11	0.13	0.15	0.18	0.25	0.29	0.34	0.44
	MGF-ADR	2.90	2.79	2.64	2.49	2.68	2.82	2.47	2.43	0.10	0.12	0.14	0.18	0.23	0.25	0.29	0.36

Chapter 3. A Comparative Evaluation for the Estimators of the GPD

Table 3.15: Measurements of Roberval bridge: mean of return levels for various return periods ($\mu m/m$)

Method	Threshold	Mean							
		62	63	64	65	66	67	68	69
	No.	1719	1243	904	654	462	320	243	175
MM	10	92	93	94	96	94	91	94	93
	100	99	100	103	106	103	99	103	103
	1000	106	108	113	119	113	106	115	115
PWM	10	91	93	98	104	100	95	102	103
	100	97	101	110	122	116	105	122	126
	1000	103	109	124	147	136	117	151	161
ML	10	92	93	95	99	96	92	98	101
	100	99	101	106	114	107	100	114	123
	1000	106	109	117	132	120	109	137	166
PML	10	92	93	95	99	95	92	97	98
	100	99	101	105	113	106	99	111	116
	1000	106	109	117	130	119	108	131	145
MDPD	10	92	94	98	107	101	94	109	129
	100	100	103	111	128	118	104	144	269
	1000	107	112	126	159	142	116	213	1129
LM	10	92	94	99	105	101	95	105	108
	100	100	103	111	126	117	105	129	141
	1000	107	113	126	153	139	117	167	205
MGF-AD	10	95	99	114	154	155	111	269	839
	100	104	112	141	248	265	143	977	9825
	1000	114	127	181	441	534	197	5040	166872
MGF-ADR	10	93	96	102	110	100	95	104	106
	100	101	106	117	134	115	104	126	136
	1000	109	117	136	169	134	116	162	194

3.3. Evaluating the Performance of Estimators

Table 3.16: Measurements of Roberval bridge: standard deviation of return levels for various return periods ($\mu m / m$)

Method	Threshold	Standard deviation							
		62	63	64	65	66	67	68	69
	No.	1719	1243	904	654	462	320	243	175
MM	10	2.67	2.93	3.11	3.51	3.57	3.57	3.84	3.83
	100	4.19	4.76	5.30	6.34	6.36	6.21	7.34	7.61
	1000	6.10	7.14	8.31	10.46	10.29	9.76	12.67	13.57
PWM	10	3.19	3.85	4.80	6.42	6.44	5.69	8.05	8.96
	100	4.95	6.32	8.65	13.04	13.01	10.76	18.55	22.51
	1000	7.13	9.56	14.33	24.22	23.88	18.44	38.75	51.20
ML	10	2.88	3.42	4.37	6.66	6.21	4.91	10.06	17.15
	100	4.55	5.64	7.72	13.11	12.00	8.99	24.40	59.54
	1000	6.65	8.55	12.51	23.60	21.14	14.89	56.25	219.03
PML	10	2.84	3.36	4.28	6.44	5.90	4.64	8.77	11.93
	100	4.48	5.53	7.54	12.58	11.31	8.41	20.30	33.28
	1000	6.54	8.38	12.18	22.50	19.74	13.81	43.88	90.50
MDPD	10	3.20	4.01	5.70	10.55	10.44	6.69	25.02	134.35
	100	5.11	6.71	10.49	22.74	22.75	13.02	85.14	1314.78
	1000	7.54	10.36	17.76	45.35	46.08	23.08	302.34	13763.98
LM	10	3.21	3.94	5.29	8.39	8.19	6.14	12.71	18.50
	100	5.12	6.60	9.71	17.59	17.07	11.80	32.60	58.93
	1000	7.55	10.19	16.37	33.88	32.55	20.60	78.45	185.84
MGF-AD	10	5.07	6.97	13.49	39.14	61.64	22.51	322.36	2573.30
	100	8.38	12.40	28.86	116.45	222.56	60.68	2520.62	60698.45
	1000	12.84	20.44	57.56	331.45	797.54	160.98	20543.59	1564691.00
MGF-ADR	10	4.04	5.19	7.53	12.41	9.69	7.19	14.71	21.30
	100	6.48	8.84	14.29	27.35	20.05	13.73	37.89	66.44
	1000	9.62	13.91	25.06	56.16	38.53	24.03	95.11	205.36

mean value for shape parameter but a smaller mean value for the scale parameter for all threshold levels considered.

- For return level, values for three different return periods, which are 10 years, 100 years and 1000 years, and represent short term and remote term, have been considered. It can be seen that the extrapolated values for 10-year and 100-year return period are stable with thresholds and estimation methods, but the predictands for 1000-year return periods are sensitive to the thresholds and also the estimation methods. Hence, one must cope with the disadvantage that the number of available measurements is relatively small when extrapolating return level for a long period compared with the measured period. Again, the MGF-AD has worse performance than the others, thus it should not be considered as an estimator for GPD in the traffic load effect applications. In addition, it is seen that the moments based estimation methods provide smaller estimates for return level.
- The MDPD does not perform as well as expected, even if it provides unreasonable return level for 1000-year return period.

3.4 Conclusion

One of the main problems in using POT to model extreme events is the need to obtain optimal parameters for generalized Pareto distribution. The parameters are important to describe the model of extremes and to predict extreme quantiles. A number of estimation methods exist in the literature, some have extensive application, while some are just applied to numerical samples. The main objective of the study presented was to provide an evaluation of the relative performance of methods for estimating parameters and quantiles of the GPD through numerical samples and realistic traffic load effects, and it can provide a guidance to apply the POT method to traffic load effects. The forecast accuracy measures of RMSE, bias and MASE were introduced to perform the evaluation.

Although no method is uniformly best based on the simulation results and realistic applications, there are still some valuable findings. The MGF-KS, MGF-CM, MGF-AD and EPM do not seem to be the optimal for modeling GPD of traffic load effects among these considered in this study. Sample size has a great influence on the accuracy of parameter estimation, almost all estimators perform better for larger size sample than smaller, that is illustrated by the decreasing of bias and RMSE. However, the different methods have a various sensitivity to size of sample. The most influenced method is ML, which has extremely different performance between small size sample and large size sample. The PWM and MM have the best performance in small size sample, while the ML and MPLE are the optimal choice for large sample. Although the quantile is a function of parameters, the performance of estimators differs according to the considered parameter and quantile. The PWM and MM seem the better choice for parameter estimations than others, while MPLE shows excellent performance for quantile estimation. These findings based on simulations are confirmed by realistic applications. An interesting

finding to be noted is the worst performing MDPD method in simulation study has a better performance in realistic application. The realistic data are always contaminated, while the better performance of the MDPD for contaminated data has been demonstrated by Juárez and Schucany [2004]. For modeling traffic load effects, the MDPD method is an optimal choice. However, the traditional methods can also be a option. The ML and MPLE are preferable methods for large size sample as the shape parameter is always in the range of $[-0.5, 0.5]$; the MM method is proposed to be used in the case of small size samples only.

4 Mixture Peaks over Threshold Approach to Model Extreme Bridge Traffic Load Effect

4.1	Introduction	101
4.2	Methodology	101
4.3	Theoretical Examples	103
4.3.1	Sample Problems and Examples	104
4.3.2	Study 1: GPD Distributed Sample	104
4.3.3	Study 2: GEV Distributed Sample	108
4.3.4	Study 3: Normal Distributed Sample	113
4.4	Discussion	116
4.4.1	Effect of Sample Size	116
4.4.2	Composition	118
4.5	Simulated Traffic Load Effects	119
4.5.1	Introduction	119
4.5.2	Composition of Loading Event	122
4.5.3	Applicability of Conventional POT Method in Extreme Traffic Load Effect Modeling	124
4.5.4	Threshold Selection Approach in the Use of Mixture POT method	128
4.5.5	Results of Simulation	131
4.6	Conclusion	134

4.1 Introduction

As concluded in Chapter 3, the outliers cause feasible problem on estimating the parameters of GPD distribution. While a frequent cause of outlier is a mixture of two distributions, which may be two distinct sub-populations. The aim of this chapter is to introduce a modification to the POT method to address the mixture feature of traffic load effects on short to medium span bridges. Caprani et al. [2008]; Harman and Davenport [1979] have pointed out that the traffic load effects are induced by loading events that involve different numbers of vehicles, and the distribution of the load effects from different loading events are not identically distributed. Hence, it violates the assumption of classic extreme value theory that the underlying distribution should be identically independent distributed. With respect to non-identical distribution in bridge traffic load effects, non-identical distribution needs to be addressed in extreme modeling to account for the impacts in inference. Harman and Davenport [1979] have proposed to model the traffic load effect with an exponential distribution. Caprani et al. [2008] have addressed the maximum distribution of mixing of non-identically distributed load effects by a composite generalized extreme value distribution.

However, it should be noticed that the generalized extreme value distribution is fitted to block maxima, which implies the possibility of losing some extremes, and the use of exponential distribution is objective. We have attempted to explicitly model the non-identically distributed behavior of extremes for a stationary extreme time series with a mixture peaks over threshold (MPOT) model to avoid the loss of information and predetermination of distribution type in the present chapter. The new method is to simultaneously model both tails using GPD and to account for the non-identically distribution feature of traffic load effects. More specifically, we have defined a mixture generalized Pareto distribution with certain components corresponding to different types of loading events. To illustrate the behavior and accuracy of the proposed method, numerical simulation data generated from three commonly used types of distributions (GPD, GEV and Normal) are used as it is possible to compare with the true value. Comparison has also been conducted to investigate the difference between the mixture peaks over threshold method and the conventional peaks over threshold. Finally, the method has been applied to model the extreme traffic load effects on bridges.

4.2 Methodology

Bridge traffic load effects can be classified by number of simultaneous presence of trucks on the deck, which is called bridge loading event (BLE). Let load effect be a random variable, X , it can be induced by random number of trucks, and its probability should be expressed as a sum of:

$$F(x) = \sum_{j=1}^m F_j(x) \cdot \varphi_j \quad (4.1)$$

where m is the number of loading events in the mixture, $F_j(\cdot)$ is the cumulative distribution function (CDF) associated with the j -truck event and $\varphi_j (j = 1, \dots, m)$ are the mixing proportions, and x is a d -dimensional vector of feature variables.

$$\bar{F}(x) = 1 - F(x) = \sum_{j=1}^m [1 - F_j(x)] \varphi_j \quad (4.2)$$

According to the classic extreme value theory, the CDF of the maximum load effect from a sample with distribution function F of size n is then given by:

$$G(x) = F^n(x) = \left[\sum_{j=1}^m F_j(x) \varphi_j \right]^n \quad (4.3)$$

Reiss and Thomas [2007] have stated that if the iid condition fails, then the F^n may still be an accurate approximation of the maximum distribution. For independent, yet heterogeneous random variables X_j with df F_j , the previous equation holds with F^n replaced by $\prod_{j \leq n} F_j$. Caprani et al. [2008] obtain similar functions from the GEV distribution, and the parameters are found by fitting GEV to block maxima of each BLE types. According to Eq.(1.2), the distribution function of block maximum value can be expressed:

$$Pr[M_n \leq x] = \left[\sum_{j=1}^m F_j(x) \varphi_j \right]^n \approx \prod_{j=1}^m G_j(x) \quad (4.4)$$

where

$$G_j(x) = \exp \left\{ - \left[1 + \xi_j \left(\frac{x - \mu_j}{\sigma_j} \right) \right]^{-\frac{1}{\xi_j}} \right\}$$

where μ_j is the location parameter; σ_j is the scale parameter; and ξ_j is the shape parameter for effect from j -th loading event.

The maximum distribution function can also be expressed as:

$$G(x) = F^n(x) = [1 - F(x)]^n, \quad (4.5)$$

where $\bar{F}(x) = 1 - F(x)$ is the survivor function given in Eq. (4.2). The parameter, n , is the number of loading events for a reference period such as 1 day, which is a sufficiently large value. For sufficiently large x , its probability can be expressed in a Taylor expansion as:

$$G(x) \approx \exp[-n\bar{F}(x)] \quad (4.6)$$

Harman and Davenport [1979] approximate it by a sum of exponential distributions:

$$G(x) = \exp[-n\bar{F}(x)] = \prod_{j=1}^{n_t} \exp[-n\varphi_j \bar{F}_j(x)] \quad (4.7)$$

Therefore, the authors used negative exponential distribution to fit the upper tail of each effect induced by corresponding type of loading event, and the distribution parameters were estimated by a graphic method. Actually, the exponential distribution is a special case of the GPD and is obtained from CDF of GPD by taking the limit as $\xi \rightarrow 0$. The use of CDF of GPD to model excesses is a natural as GPD has an interpretation as a limit distribution similar to that which motivates the GEV distribution. See Pickands III [1975] and Davison and Smith [1990] for further developments and applications. However, from extreme value theory, the tail distribution has the following relationship with GPD:

$$Pr(X > u) = \frac{1 - F(x)}{1 - F(u)} = 1 - H(y) \quad (4.8)$$

Thus, the survivor function is

$$1 - F_j(x) = [1 - H_j(y)][1 - F_j(u_j)] \quad (4.9)$$

Then,

$$\bar{F}(x) = \sum_{j=1}^{n_t} [1 - H_j(x - u_j)][1 - F_j(u_j)]\varphi_j \quad (4.10)$$

Therefore,

$$F(x) = 1 - \bar{F}(x) = 1 - \sum_{j=1}^{n_t} [1 - H_j(x - u_j)][1 - F_j(u_j)]\varphi_j \quad (4.11)$$

Substitution into Eq. (4.7) yields:

$$G(x) = \exp - \sum_{j=1}^{n_t} n\varphi_j [1 - F_j(u_j)] [1 + \xi_j \left(\frac{x - u_j}{\sigma_j} \right)]^{-\frac{1}{\xi_j}} \quad (4.12)$$

There is no need to know the underlying parent distribution function of F , the parameters of the distribution are determined by fitting the upper tail of load effects induced by each type of loading event to GPD separately.

4.3 Theoretical Examples

Theoretical example representing load effects were generated by distributions with known parameters, and true values for statistics like quantile can be calculated by via Eq. (4.11) or Eq. (4.3). Such samples form the basis for the application of mixture peak-over-threshold (MPOT) and the conventional peak-over-threshold (CPOT) methods; the results from both methods are compared to the exact return level for a given return period, or the exact distribution. For CPOT method, the GPD is fit to the mixed data. For MPOT method, data are classified according to underlying event type, then those coming from same event are fitted to a standard GPD. The parameters of GPD are estimated by the method of moments (MM), the probability-weighted

moment (PWM), the maximum likelihood (ML), the Right-tail Anderson-Darling (ADR), and the minimum density power divergence (MDPD). These estimators have shown their excellent performance in estimating parameters of GPD either for numerical sample or traffic load effects in Chapter 3, and also they are representative of the most commonly used estimators [de Zea Bermudez and Kotz, 2010]. The MM, PWM, and ML are the most common and quite useful ones in practice. The MM and PWM methods use the first and second order moments to estimate the parameters, and they have good performance in the situations of small size samples. The ML is the most efficient method for estimating the parameters of the GPD for sample size larger than 500. From these examples the performance of the proposed method (MPOT) can be evaluated, and its behavior in solving realistic problems can be explored.

4.3.1 Sample Problems and Examples

In what follows we show simulation results for 1000-year return level for three samples generated by generalized Pareto, generalized extreme value, and normal distributions, respectively. The three samples were designed to reflect different properties. The first was designed to explore the performance of MPOT on Monte Carlo samples drawn by GPDs with different combination of parameters. Specifically, we compared MPOT results with those of a standard fit with a single distribution. The second and the third studies were designed to reflect the true relationships between mechanisms that comprise the loading events and to provide insight into the nature of the asymptotic theory of extreme order statistics.

4.3.2 Study 1: GPD Distributed Sample

In this section we assess the performance of the conventional POT approach and the mixture POT approach on quantile estimation when the underlying generalized Pareto distribution is not identically distributed. Dupuis and Field [1998]; Juárez and Schucany [2004]; Peng and Welsh [2001] call that one distribution of $F_1(\xi_1, \sigma_1)$ is contaminated by another $F_2(\xi_2, \sigma_2)$, and the distribution $F_2(\xi_2, \sigma_2)$ is called contamination distribution. Both Peng and Welsh [2001] and Juárez and Schucany [2004] state that the slight change of scale parameter has small influence on shape parameter estimates, hence, only a change of shape parameter is considered in this study. We have generated five hundred samples of size $n = 2000$ from the 10% mixture distribution $0.90F_1(\xi_1, \sigma_1) + 0.1F_2(\xi_2, \sigma_2)$ and applied the estimators MM, PWM, ML, MDPD and ADR to estimate parameters for the cases $(\xi_1, \sigma_1, \epsilon, \xi_2, \sigma_2) = (-1/3, 1, 0.1, -1/2, 1), (-1/3, 1, 0.1, -1/3, 1), (-1/3, 1, 0.1, -1/6, 1), (-1/3, 1, 0.1, 0, 1), (-1/3, 1, 0.1, 1/12, 1)$, and $(-1/3, 1, 0.1, 1/6, 1)$, where ϵ is the probability weight of contamination distribution. The data generated by $F_1(\xi_1, \sigma_1)$ are denoted as event 1, and those generated by $F_2(\xi_2, \sigma_2)$ are denoted as event 2. Therefore, it is possible to identify the data through the denoted type of events. In order to avoid the influence of threshold estimation on modelling, the distributions are set to have the same threshold. In all cases, the contamination is chosen to be fairly mild as the objective is to reflect its influence on extreme value prediction and modelling. However, in practice like traffic load effects may comprise of several types of loading events with almost

the same weight, another sensitivity study is given in Section 4.4.2 to discuss the influence of component composition on modelling.

Results are presented here in terms of the quantile estimates from CPOT and MPOT approaches, since most often we are interested in the accuracy of the predicted extreme values. Quantile estimators from CPOT approach are obtained by using Eq. (1.13), while quantile estimators from MPOT are obtained by using Eq. (4.11). Substituting the parameters of the six cases into Eq. (4.11) and equating to a probability of $1 - 1/(1000 \times 250 \times 2000/500)$ (assuming the number of working days is 250 working days per year excluding weekends and holidays, and the 2000 events are observed in 500 days.) gives the 1000-year return levels, x_{1000} , of 2.9689, 5.1193, 11.5129, 19.3219, and 34.8775, respectively for the five contaminated cases, while the corresponding return level for uncontaminated case is 2.97. The return levels are reported in terms of the ratio of predicted values with respect to the corresponding accuracy values as $r = \hat{x}_{1000}/x_{1000}$. When the ratio is less than one, the predicted value is smaller than accuracy ones. We consider the root mean squared errors of the estimators in Table 4.1, the biases in Table 4.2, the means in Table 4.3 and their standard errors in Table 4.4 of parameter and quantile estimates. For a subset of the estimators results are presented graphically in Figure 4.1 - 4.4 for all cases considered.

Table 4.1: Simulation results for the estimation methods of MM, PWM, ML, MDPD and ADR. The results presented are the RMSEs over 500 replicates.

$(\xi_0, \sigma_0, \epsilon, \xi_1, \sigma_1)$	Parameter	MM	PWM	ML	MDPD	ADR
$(-1/3, 1, 0.1, -0.5, 1)$	CPOT	0.0517	0.0626	0.0330	0.0318	0.0454
	MPOT	0.0486	0.0614	0.0299	0.0318	0.0471
$(-1/3, 1, 0.1, -1/3, 1)$	CPOT	0.0476	0.0603	0.0280	0.0297	0.0461
	MPOT	0.1093	0.1538	0.0485	0.0577	0.1325
$(-1/3, 1, 0.1, -1/6, 1)$	CPOT	0.3719	0.3805	0.2746	0.2865	0.3019
	MPOT	0.2206	0.3242	0.2034	0.2449	0.4310
$(-1/3, 1, 0.1, 0, 1)$	CPOT	0.6589	0.6940	0.5118	0.5473	0.5584
	MPOT	0.3483	0.4359	0.3731	0.4211	0.5816
$(-1/3, 1, 0.1, 1/12, 1)$	CPOT	0.7487	0.8016	0.6401	0.6837	0.6883
	MPOT	0.4329	0.5561	0.5810	0.8206	1.3039
$(-1/3, 1, 0.1, 1/6, 1)$	CPOT	0.8012	0.8787	0.7537	0.7991	0.7991
	MPOT	0.5588	0.6063	0.6451	0.7931	1.0792

An overall look at the tables clearly reveals how performances can drastically change depending on the shape parameter value of contaminated distributions. Consider first the case that core distribution with $\xi_0 = -1/3$ is contaminated by a distribution with only a slightly less shape parameter, $\xi_0 = -1/2$, it has little effect on the estimation of quantile. The statistics of RMSE, bias, mean and standard deviation are almost the same as the no contamination form. When the contaminated distribution has a larger shape parameter, the difference becomes apparent. The CPOT method is insensitive to the contamination, and hence the performance of the CPOT becomes worse as the shape parameter increases. Even though the proportion of

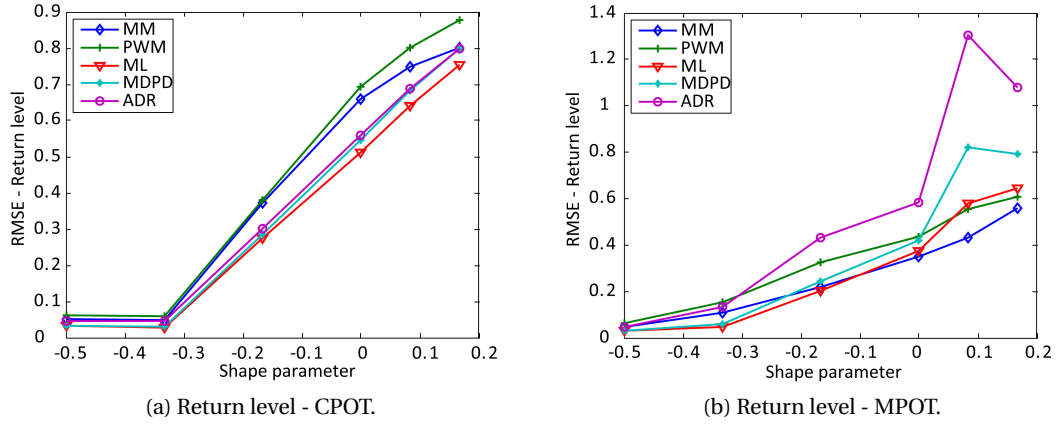


Figure 4.1: RMSE of quantile estimators.

Table 4.2: Simulation results for the estimation methods of MM, PWM, ML, MDPD and ADR. The results presented are the biases over 500 replicates.

$(\xi_0, \sigma_0, \epsilon, \xi_1, \sigma_1)$	Parameter	MM	PWM	ML	MDPD	ADR
$(-1/3, 1, 0.1, -0.5, 1)$	CPOT	-0.0267	-0.0303	-0.0131	-0.0124	-0.0231
	MPOT	0.0023	0.0050	-0.0047	-0.0043	0.0031
$(-1/3, 1, 0.1, -1/3, 1)$	CPOT	0.0023	0.0035	-0.0046	-0.0037	0.0037
	MPOT	0.0574	0.0802	0.0175	0.0233	0.0687
$(-1/3, 1, 0.1, -1/6, 1)$	CPOT	-0.3705	-0.3786	-0.2644	-0.2788	-0.2946
	MPOT	0.0163	0.0519	-0.0191	0.0061	0.0944
$(-1/3, 1, 0.1, 0, 1)$	CPOT	-0.6579	-0.6936	-0.5062	-0.5444	-0.5547
	MPOT	0.0038	0.0443	-0.0005	0.0342	0.1225
$(-1/3, 1, 0.1, 1/12, 1)$	CPOT	-0.7468	-0.8014	-0.6371	-0.6826	-0.6865
	MPOT	-0.0057	0.0871	0.0597	0.1335	0.2889
$(-1/3, 1, 0.1, 1/6, 1)$	CPOT	-0.7936	-0.8786	-0.7521	-0.7987	-0.7984
	MPOT	-0.0430	0.0895	0.0855	0.1642	0.3130

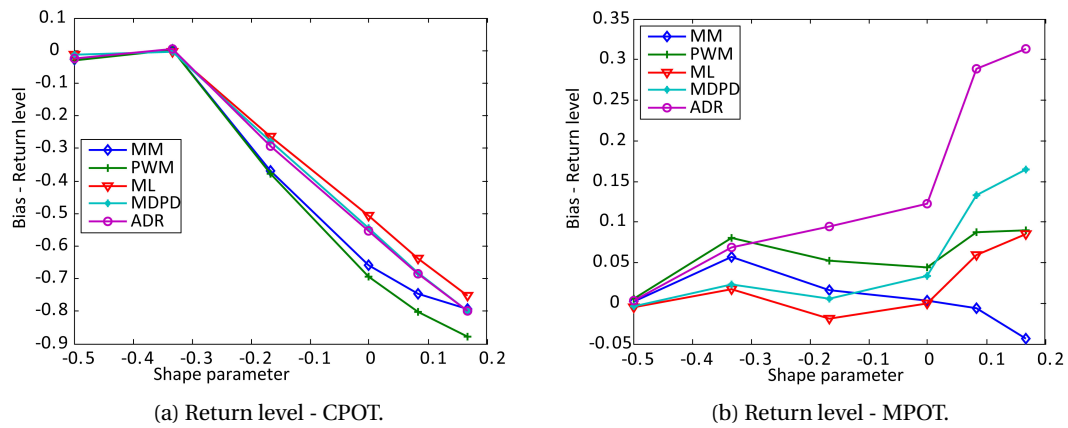


Figure 4.2: Bias of quantile estimators.

Table 4.3: Simulation results for the estimation methods of MM, PWM, ML, MDPD and ADR. The results presented are the means over 500 replicates.

$(\xi_0, \sigma_0, \epsilon, \xi_1, \sigma_1)$	Parameter	MM	PWM	ML	MDPD	ADR
$(-1/3, 1, 0.1, -0.5, 1)$	CPOT	0.9733	0.9697	0.9869	0.9876	0.9769
	MPOT	1.0023	1.0050	0.9953	0.9957	1.0031
$(-1/3, 1, 0.1, -1/3, 1)$	CPOT	1.0023	1.0035	0.9954	0.9963	1.0037
	MPOT	1.0574	1.0802	1.0175	1.0233	1.0687
$(-1/3, 1, 0.1, -1/6, 1)$	CPOT	0.6295	0.6214	0.7356	0.7212	0.7054
	MPOT	1.0163	1.0519	0.9809	1.0061	1.0944
$(-1/3, 1, 0.1, 0, 1)$	CPOT	0.3421	0.3064	0.4938	0.4556	0.4453
	MPOT	1.0038	1.0443	0.9995	1.0342	1.1225
$(-1/3, 1, 0.1, 1/12, 1)$	CPOT	0.2532	0.1986	0.3629	0.3174	0.3135
	MPOT	0.9943	1.0871	1.0597	1.1335	1.2889
$(-1/3, 1, 0.1, 1/6, 1)$	CPOT	0.2064	0.1214	0.2479	0.2013	0.2016
	MPOT	0.9570	1.0895	1.0855	1.1642	1.3130

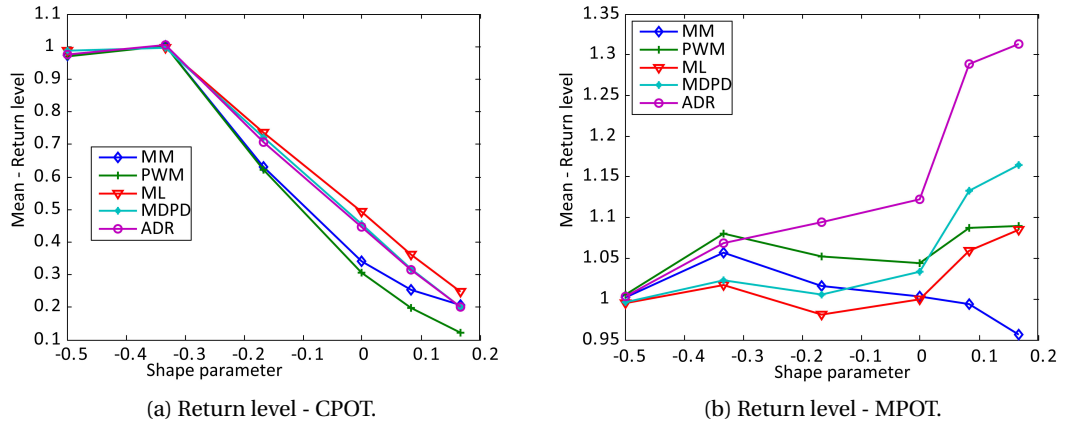


Figure 4.3: Mean of quantile estimators.

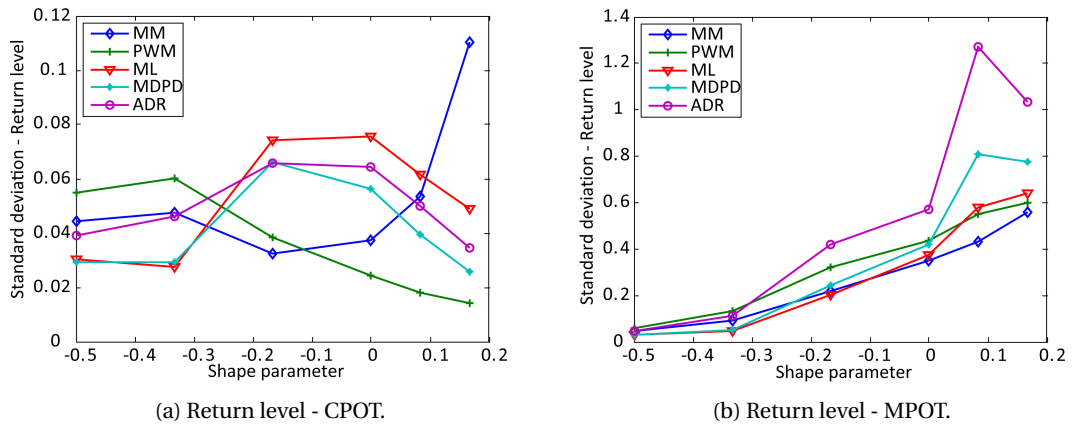


Figure 4.4: Standard deviation of quantile estimators.

Chapter 4. Mixture POT Approach to Model Extreme Bridge Traffic Load Effect

Table 4.4: Simulation results for the estimation methods of MM, PWM, ML, MDPD and ADR. The results presented are the standard deviations (STDs) over 500 replicates.

$(\xi_0, \sigma_0, \epsilon, \xi_1, \sigma_1)$	Parameter	MM	PWM	ML	MDPD	ADR
$(-1/3, 1, 0.1, -0.5, 1)$	CPOT	0.0444	0.0548	0.0303	0.0293	0.0391
	MPOT	0.0486	0.0613	0.0295	0.0315	0.0471
$(-1/3, 1, 0.1, -1/3, 1)$	CPOT	0.0476	0.0603	0.0277	0.0295	0.0460
	MPOT	0.0931	0.1313	0.0453	0.0528	0.1134
$(-1/3, 1, 0.1, -1/6, 1)$	CPOT	0.0325	0.0384	0.0740	0.0662	0.0658
	MPOT	0.2202	0.3203	0.2027	0.2451	0.4210
$(-1/3, 1, 0.1, 0, 1)$	CPOT	0.0372	0.0243	0.0758	0.0564	0.0643
	MPOT	0.3486	0.4341	0.3735	0.4202	0.5692
$(-1/3, 1, 0.1, 1/12, 1)$	CPOT	0.0535	0.0179	0.0618	0.0396	0.0500
	MPOT	0.4333	0.5497	0.5785	0.8105	1.2728
$(-1/3, 1, 0.1, 1/6, 1)$	CPOT	0.1105	0.0143	0.0490	0.0257	0.0345
	MPOT	0.5577	0.6002	0.6401	0.7767	1.0339

contaminated distribution is only 10 percent, it dominates the tail distribution. The high quantile is rather close to the contaminated distribution than to the core distribution. From Table 4.4 and Figure 4.3 it is apparent that the MPOT method estimates the return level with good accuracy. The CPOT method does not estimate the return level accurately but has a lower coefficient of variation as shown in Figure 4.4. The mean for the CPOT method are less than the accuracy estimates. For parameter estimators, various estimators give consistent estimates of quantile for either conventional POT or mixture POT.

From these results, it is clear that the "contamination" distribution has severely distorted the quantile estimates. Thus there is no doubt about the advantage of applying the MPOT approach on samples with non-identical distributions. In light of these results we strongly suggest the use of the MPOT in the case when the main distribution is contaminated by distribution with larger shape parameter. While for the case that the main distribution is contaminated by distribution with smaller shape parameter, the conventional POT method can model the data with sufficient accuracy, similar conclusion is remarked in Dupuis and Field [1998]; Juárez and Schucany [2004]; Peng and Welsh [2001].

4.3.3 Study 2: GEV Distributed Sample

In this study, we used several of the parameter values from Caprani et al. [2008] to evaluate the performance of MPOT comparing with conventional POT method, and also comparing with approach proposed by Caprani et al. [2008], which models the mixture traffic load effects with a composite generalized extreme value distribution. Two examples are used to conduct this study. The first represents the core distribution contaminated by distributions with small shape parameters, while the second represents that the main distribution slightly contaminated by a distribution from different loading event. The distribution parameters and weight

of each component event for these two examples are listed in Table 4.5. The first example represents load effects due to three loading event types. Type 1 events are more than twice as probable as type 2 events and type 3 events only occur 2% of the time. The total number of events per day of all types is specified as $n_d = 2800$. Similar, the second example represents load effects due to two types of loading events. The type 1 event contributes 95% to the total, while the type 2 takes the rest 5%. Monte Carlo simulation is used to sample the distributions for each event-type. This is repeated for a total of 1000 days to obtain a 1000-day sample. Additionally, the procedure is repeated 100 times to consider the variation.

Table 4.5: Parameters of mechanisms for Study 2

Example	Event type number	Shape ξ	Scale σ	Location μ	Probability of occurrence f_j	Daily number of events n_d
First	Type 1	0.07	31	370	0.7	2800
	Type 2	-0.19	127	300	0.28	
	Type 3	-0.19	128	380	0.02	
Second	Type 1	-0.18	270	610	0.95	800
	Type 2	-0.21	310	840	0.05	

For adopting standard block maximum method, GEV distribution is fitted to the maximum-per-day data regardless of the event types. On each sample we estimate the shape parameter, ξ , scale parameter, σ , and location parameter, μ , with maximum likelihood estimator. For applying Eq. (4.4), Maximum-per-day data for each of the event types are drawn, and these data are fit to GEV distributions. The parameters of the GEV distributions are used to calculate the 1000-year return level. In the case using POT method to model the data, the entire data of each simulation sample is used. For applying the CPOT approach, a series of thresholds is investigated and an optimal threshold is selected by using KS test. The parameters of the GPD are estimated by five previous utilized estimators. For applying the proposed MPOT approach, GPD is fitted to the exceedances over high threshold for data with respect to type of loading event. The threshold selection method is also based on the statistics of KS test. Then the estimated parameters are used to calculate 1000-year return level.

We firstly present the result for the first example. Substituting the parameters of Table 4.5 into Eq. (4.3) and equating to a probability of $1 - 1/(250 \times 1000)$ (assuming 250 working days per year excluding weekends and holidays) gives the exact characteristic value for 1000-year return period, here is 1724. In Figure 4.5, the estimated 1000-year return levels are presented in terms of ratio with respect to the exact return level, and the performances of the prediction methods are assessed by this ratio. From Figure 4.5 it is apparent that neither the conventional block maxima method nor the conventional POT method estimates the return level accurately. The return levels estimated by the conventional methods are less than the exact solution. However, it should be noticed that the POT has better performance than the BM even in the standard use. Among the convention methods, the return level found from the BM method is about 30% less than the exact solution, while these found from the POT method are closer to the

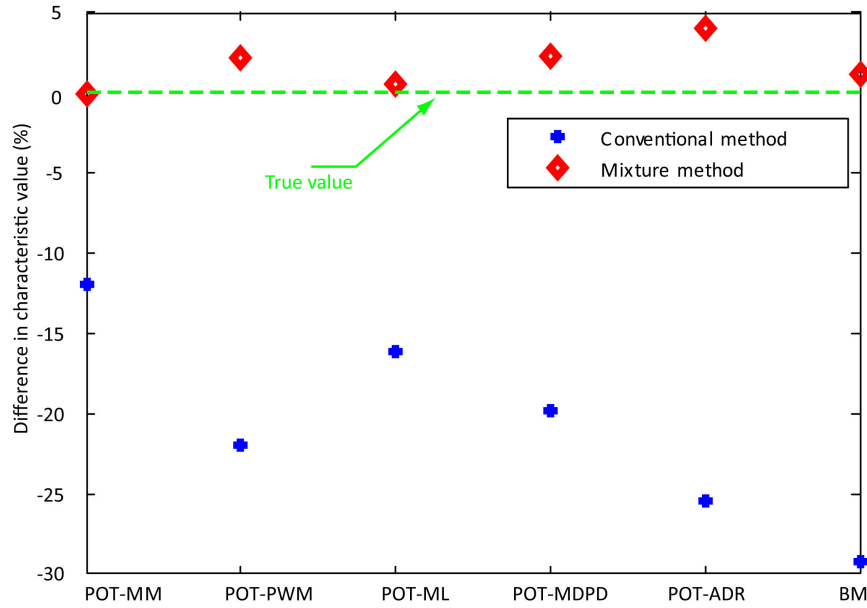


Figure 4.5: Comparison of estimates of characteristic value between conventional methods vs. mixture methods for Study 2, Example 1

exact value with ratio ranging from 0.75 to 0.9. The POT with parameter estimator of method of moments is the best one which provides the return level only about 10% less than the exact value.

Although the POT method performs better than the BM method, the assumption of convergence to a single GPD or GEV distribution is not valid as the sources data are mixed. The mean ratios from mixture POT or mixture BM method indicate that these methods provide more accurate prediction of return level with a maximum error of 5%. From Figure 4.5, the POT method with estimator of MM have better performance than the mixture POT method with other parameter estimators; even the mixture POT method with ML has slightly better performance than the mixture BM method.

The variation of mixture methods is illustrated with box plot given in Figure 4.6. The box plot is a standard technique for exploiting data variation. It presents the commonly used five characteristic features which consists of the minimum and maximum range values, the upper and lower quartiles and the median. On each box, the central mark is the median, the edges of the box are the 25th and 75th percentiles, the whiskers extend to the most extreme data points not considered outliers, and outliers are plotted individually with red plus sign.

Figure 4.6 shows that all the methods estimate the return level with good accuracy as the median value close to the exact value from analytical model. Among these methods, mixture GEV distribution gives a lesser range of results which, in this case, are reasonably close to the

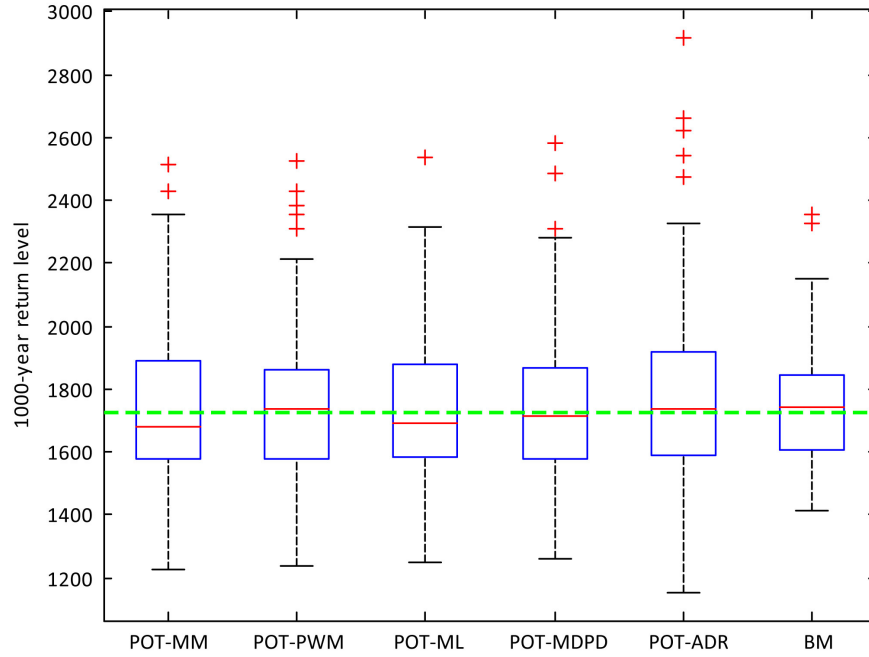


Figure 4.6: Estimated 1000-year return levels in boxplots for Study 2, Example 1

exact value. The mixture GEV distribution method seems to provide much stable prediction. It is reasonable that the rule to draw data in mixture GEV method is much clearer. The block maxima are used to fit GEV distribution, while the selected threshold is variable from sample to sample. In this case study, 1000 daily maxima are used to fit to GEV distribution; hence, the block maxima method can reasonably model the extreme value distribution. However, it has the risk to give worse modeling when the sample size is smaller, it will be studied in next section that how the methods reflect to sample size. The MPOT method using MDPD estimator and PWM estimator provide similar narrow range of results as the mixture GEV method. Therefore, the predictions from extreme value theory based models can be considerably good, the return levels predicted by mixture GPD model are relatively close to those predicted using mixture GEV model.

The same procedure is conducted on the second example are got by the same procedure. The comparison of prediction methods is presented in Figure 4.7 and 4.8. It can be seen that the mixture model methods provide better prediction. However, the conventional methods also provide a very accurate estimation with a maximum error of about 8%. These results indicate that the conventional methods can model the data with sufficient accuracy when the distribution composition is not very different like the shape parameters are close for the two types of loading events in this example, and also demonstrate the statement given by Reiss and Thomas [2007] that the form F^m may still serve as an approximation of the actual df of the maximum if a slight mixture in the data.

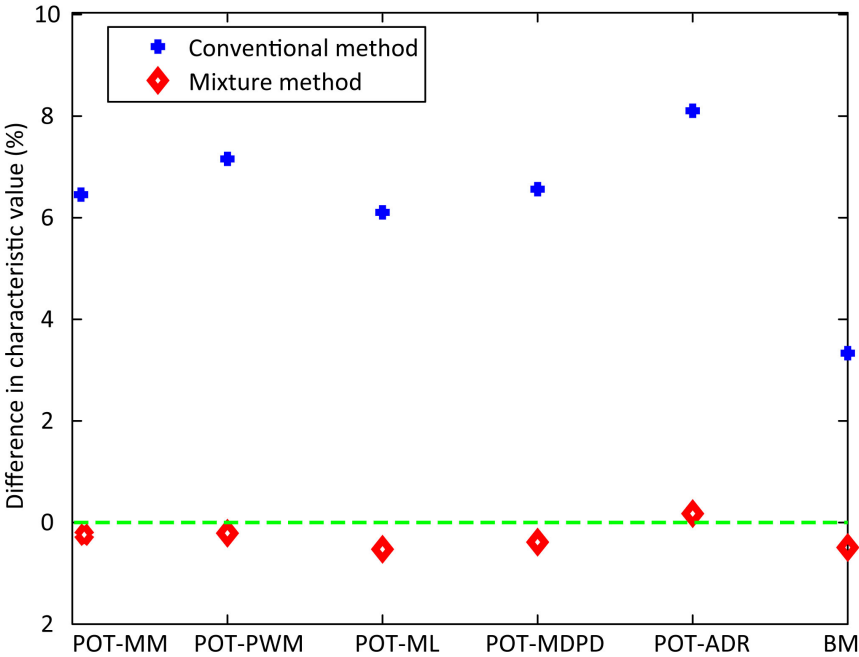


Figure 4.7: Comparison of estimates of characteristic value between conventional methods vs. mixture methods for Study 2, Example 2

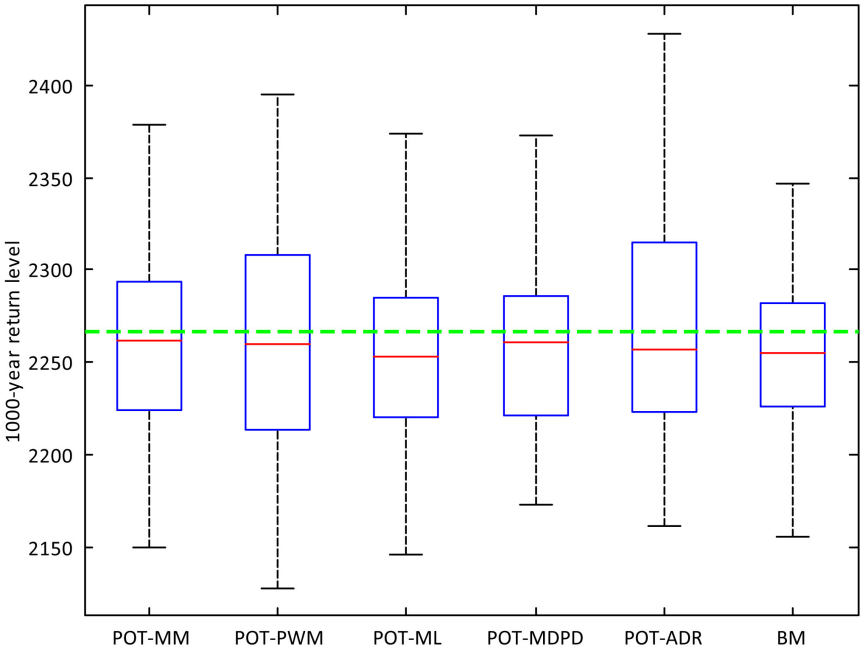


Figure 4.8: Estimated 1000-year return levels in boxplots for Study 2, Example 2

4.3.4 Study 3: Normal Distributed Sample

Normal distribution is a widely used distribution in bridge engineering, for example gross vehicle weights are usually assumed to follow multiple modal Normal distribution [Caprani, 2005]. In this study, the performance of MPOT method is evaluated through its application on a sample having a parent distribution of normal distribution. The parameters of the distribution are given in Table 4.6. The core distribution is $N(420, 30)$ with the relative frequency of occurrence $\varphi_1 = 0.9$, while the "contaminating" distribution is $N(380, 45)$. It is considered that 1000 events per day occur.

Table 4.6: Parameters of mechanisms for Study 3

Example	Event type number	Scale σ	Location μ	Probability of occurrence f_j	Daily number of events n_d
First	Type 1	30	420	0.90	1000
	Type 2	45	380	0.10	

Table 4.7: Parameter estimates for CPOT method by various estimators

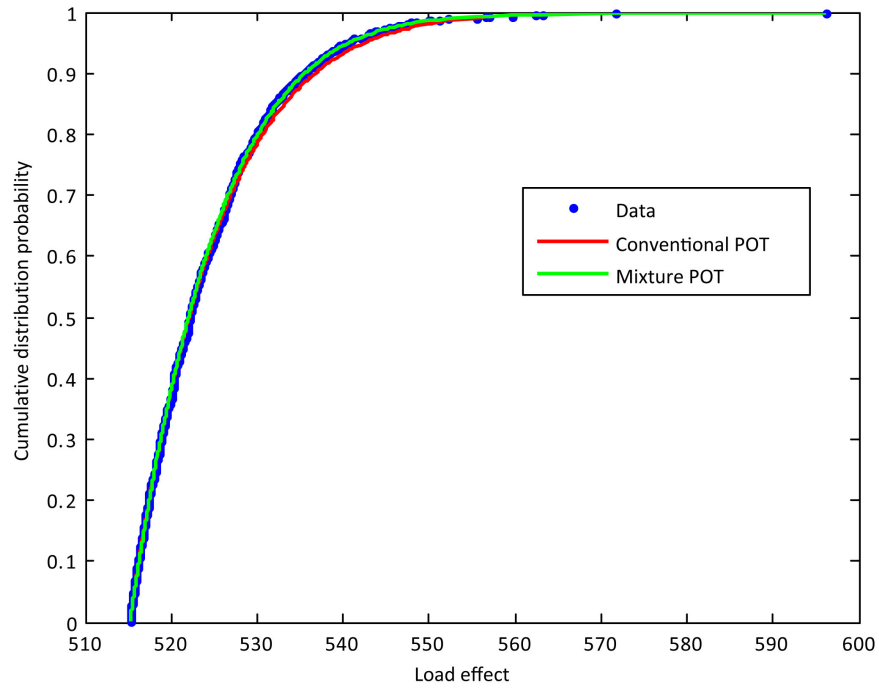
Estimator	Shape	Scale	Location	No. exceedances	KS, p-value
MM	-0.0767	10.21	510.52	1321	0.8823
PWM	-0.0930	10.37	510.52	1321	0.9735
ML	-0.0583	10.03	510.52	1321	0.6936
MDPD	-0.0760	10.20	510.52	1321	0.8726
ADR	-0.1059	10.46	510.52	1321	0.9420

Figure 4.9 displays an application of CPOT and MPOT method to the mixed normal distribution sample. Parameter estimates for CPOT method are obtained by the five previous mentioned estimators and listed in Table 4.7. The parameter estimates for mixture POT method are given in Table 4.8. Figure 4.9a provides the empirical CDF to show departures from very small values. Figure 4.9b shows the fitting in the log-scale, the goodness of the methods is apparently displayed. Both CPOT and MPOT methods capture the main part of the data very well, but the discrepancy between empirical distribution and fitted distribution becomes larger when getting close to the upper tail. The CDF obtained by MPOT captures the upper tail with significantly less bias than with the CPOT. Therefore the MPOT method has a better performance on modeling the upper tail data than the CPOT method, consistently with results of KS goodness-of-fit test as given in Table 4.8. After obtaining the upper tail distribution, it is straightforward to calculate the maximum value distribution function using equation. Daily maxima distributions are given in Figure 4.10 along with the true daily maximum value distribution obtained by equation. The result confirms the previous result that the mixture POT method estimates the daily maximum value distribution with good accuracy.

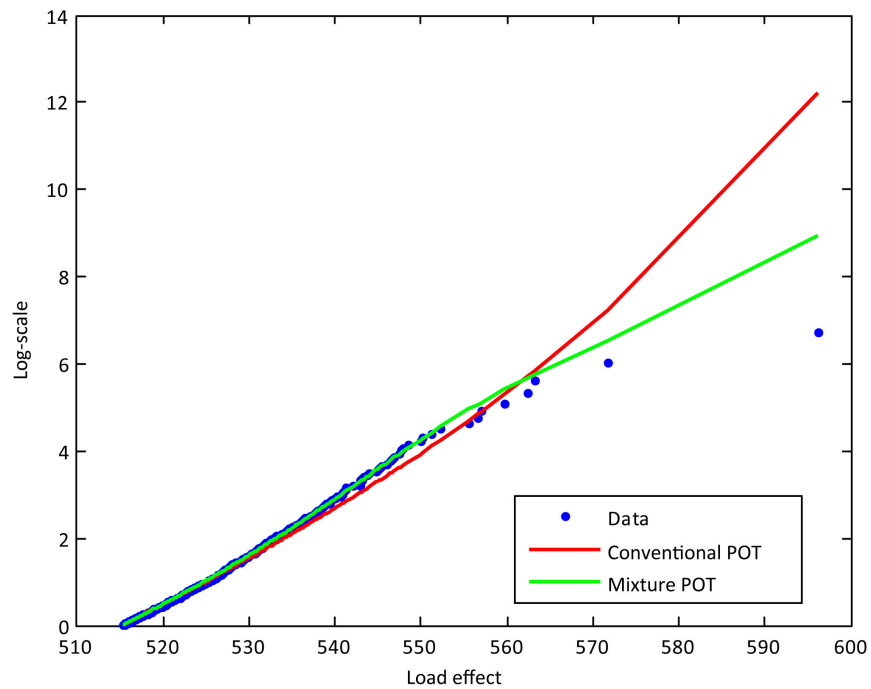
The full simulation results of quantile estimation for the sample sets obtained by applying the conventional and mixture POT methods are given in Figure 4.11. It indicates that both

Table 4.8: Parameter estimates for MPOT method by various estimators

Estimator	Component 1					Component 2					Mixture KS
	Shape	Scale	Location	No.	KS	Shape	Scale	Location	No.	KS	
MM	-0.173	9.9	515.2	707	0.908	-0.056	15.9	479.1	1371	0.926	0.964
PWM	-0.105	10.0	508.0	1500	0.909	-0.058	16.0	479.1	1371	0.903	0.866
ML	-0.177	10.0	515.2	707	0.922	-0.053	15.9	479.1	1371	0.945	0.979
MDPD	-0.177	10.0	515.2	707	0.922	-0.057	16.0	479.1	1371	0.918	0.974
ADR	-0.106	10.1	508.0	1500	0.937	-0.091	16.2	486.6	845	0.931	0.918



(a) Standard cumulative distribution probability plot.



(b) Gumbel scaled cumulative distribution probability plot.

Figure 4.9: These figures display the GPD fitting obtained by CPOT and MPOT approaches.

approaches have good performance on quantile estimation, with maximum error less than 2%, and the estimated return levels from conventional method are much closer to the true value. The results from the mixture GEV method are also obtained and approximate the true value with a small difference also, but the method does not work as well as POT methods.

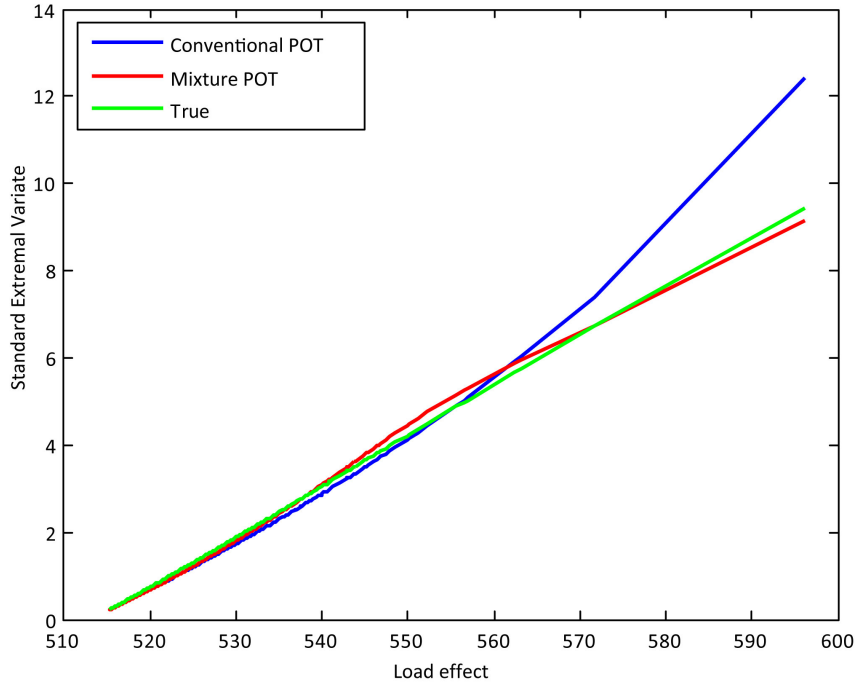


Figure 4.10: Extreme value distribution from conventional and mixture POT methods

4.4 Discussion

4.4.1 Effect of Sample Size

The study in Chapter 3 demonstrates that the sample size is important to extreme value modeling in application under standard manner. In this section, we intend to investigate the influence of sample size on MPOT method. The Example 1 of Study 2 is used to study the effect of different sizes of samples on quantile estimation as it represents the situation that threshold needs to be selected. Sample sizes of 200, 500, and 1000 are used as the basis of the procedure outlined previously. For each of these sample sizes, there are fitted GPDs for the mixture POT and conventional POT methods. As a comparison, the results of return level obtained from the mixture GEV and conventional GEV method are presented also.

Figure 4.12 presents the results using an error bar plot, displaying the mean values and the range of $[-\sigma, \sigma]$ for the return levels estimated from the different methods considered. It is clear that the mean value is consistently accurate, regardless of sample size for the mixture

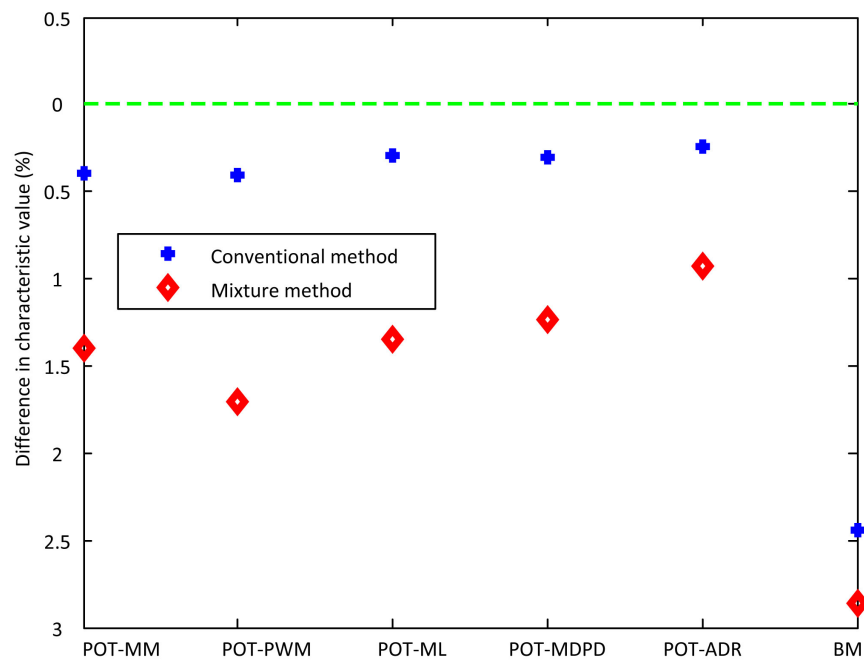


Figure 4.11: Comparison of estimates of characteristic value between conventional methods vs. mixture methods for Study 3

methods. Furthermore, the standard deviation decreases with increasing sample size. For smallest size of 200 considered in this study, the mixture POT method generally has a better performance as it provides smaller standard deviation. However, the mixture GEV method is more sensitive to the sample size; its performance remarkably improves with increasing sample size.

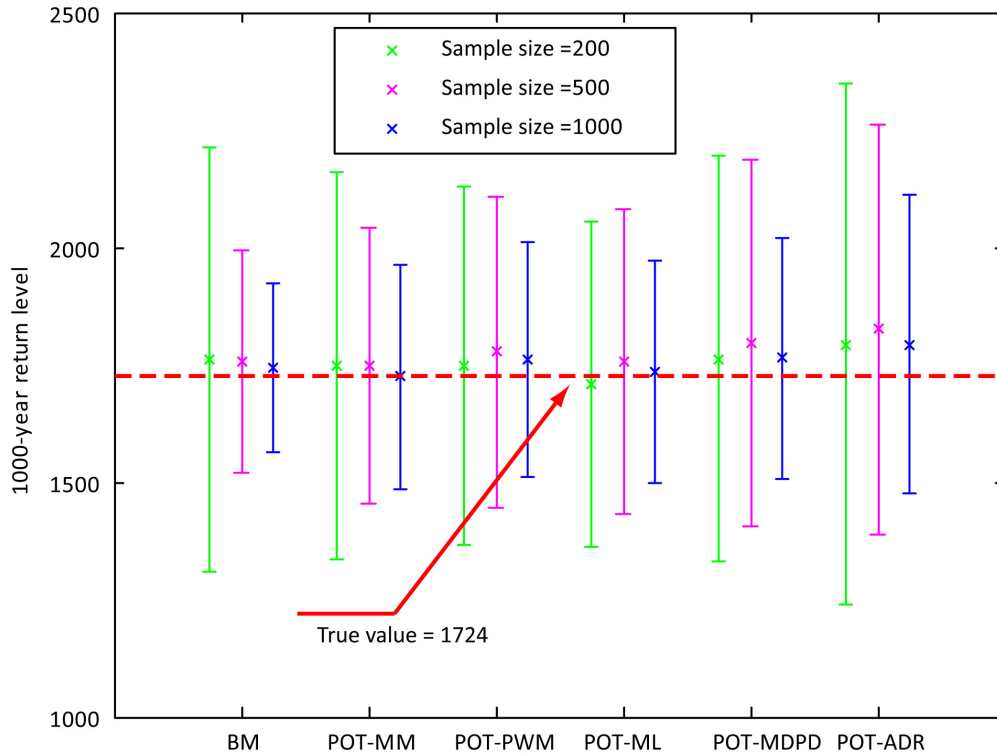


Figure 4.12: Error bar plot (mean \pm standard deviation) of 1000-year return level

4.4.2 Composition

The core distribution of previous samples is assume to be slightly contaminated by other distribution, in practice the core distribution can be severely contaminated by other distribution. In order to investigate the influence of proportion of contaminated distribution on quantile estimation, two additional studies have been carried out. The combination of core distribution and contaminated distribution and corresponding parameters are listed in Table 4.9. One sample is combined with two distributions having bounded limits, and the other is combined with bounded and unbounded distribution.

Figure 4.13 and Figure 4.14 show the mean and the coefficient of variation for the ratio that is calculated by dividing the quantile estimates from the mixture and conventional methods by the true value calculated by Eq. (4.11) and Eq. (1.13), respectively. It is clear that the mean value still is consistently accurate, regardless of the proportion of contaminated distribution

Table 4.9: Distribution parameters for Study 4 and Study 5

Study	Example	Event type	Shape	Scale	Location	Probability weight
4	1	1	-1/3	1	0	0.9
		2	-2/3	1	0	0.1
	2	1	-1/3	1	0	0.8
		2	-2/3	1	0	0.2
	3	1	-1/3	1	0	0.7
		2	-2/3	1	0	0.3
	4	1	-1/3	1	0	0.6
		2	-2/3	1	0	0.4
5	1	1	-0.1	1	0	0.9
		2	0.1	1	0	0.1
	2	1	-0.1	1	0	0.8
		2	0.1	1	0	0.2
	3	1	-0.1	1	0	0.7
		2	0.1	1	0	0.3
	4	1	-0.1	1	0	0.6
		2	0.1	1	0	0.4

for the MPOT method, whereas the CPOT method converges to an inaccurate estimated value. However, it should be noted that this effect of contamination ratio has negative influence on conventional method for the Study 5, but it has a positive influence on return levels obtained from the conventional method for the Study 6 as mean ratio approximates to true value with increasing proportion of contaminated distribution. Namely the governing event in Study 6 is Event 2, therefore the increasing of its proportion can improve the estimation. Further, the conclusion is confirmed as the coefficient of variation of the mixture method decreases with increasing proportion of contaminated distribution for Study 6, while the coefficient of variation remains in a stable level for Study 5. The results indicate that the increasing size of governing data can improve the quantile estimation.

4.5 Simulated Traffic Load Effects

4.5.1 Introduction

The time history of traffic load effects (e.g. bending moments, shear forces, deflections etc.) process includes many periods of zero or small load effects (see Figure 4.15), and majority of local maxima of load effect are due to cars or trucks which are relatively small. Hence many efforts can be saved by excluding consideration of these data to simplify the problem in analyzing extreme bridge traffic load effects as they have no contribution to extreme value. Vehicles with GVW greater than 3.5 tonnes are therefore commonly retained to study the traffic load effects on bridges. Moreover, Caprani [2005] only retains load effects induced by "significant crossing events" which are defined as events involving multiple trucks or a single

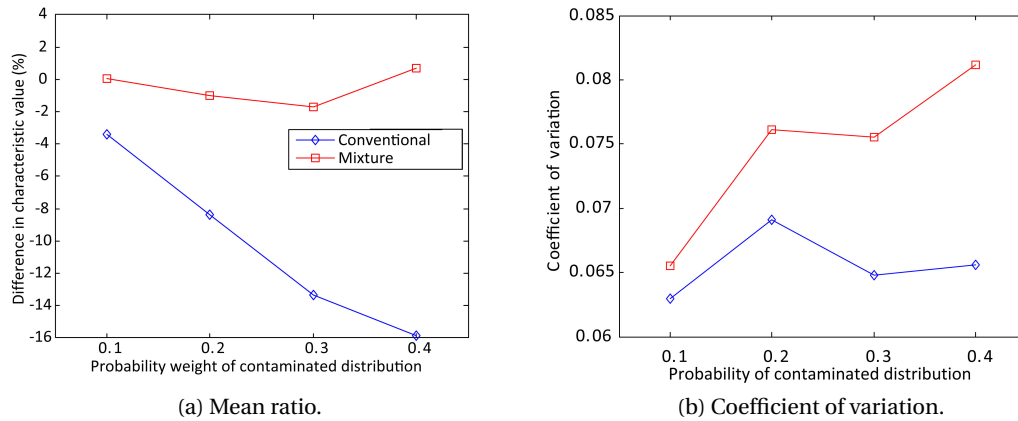


Figure 4.13: Results of proportion of contaminated distribution effect for Study 4.

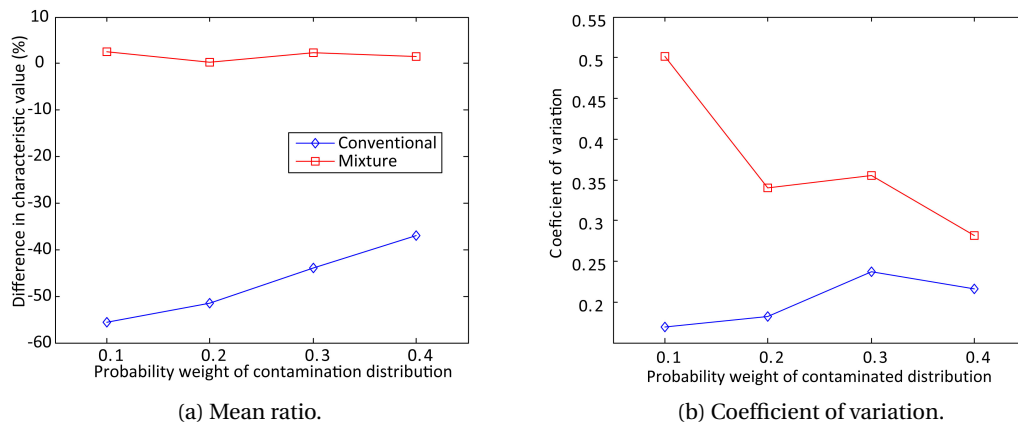


Figure 4.14: Results of proportion of contaminated distribution effect for Study 5.

truck with GVW in excess of 40 tonnes. It is effective for using block maxima method, which only deals with the maximum within a period or a block, to model extreme value. However, it may lose some information as the multiple-truck loading events may induce less load effect than single truck with GVW less than 40 tonnes. As shown in Figure 4.15, several single truck loading events induce larger load effect than those induced by 2-truck loading events. In order to use all possible relatively large load effects efficiently, the full time history of effect induced by traffic passing over the bridge is retained first, then the local extreme and its corresponding type of loading event (comprising the number of trucks) are identified. Figure 4.16 illustrates such a process, the time history of the traffic load effect is given in blue line, and the local extremes are marked with red star. The bridge experiences a complex traffic crossing sequence. At the beginning, one truck (1st truck) is on the bridge, then another truck (2nd truck) arrives on the bridge generating a 2-truck loading event, then the first arrived truck leaves the bridge and the loading event becomes to a single truck, then a new truck (3rd truck) enters the bridge and the loading events becomes to a 2-truck again, then the 2nd arrived truck exits the bridge,

then a new truck (4th truck) arrives to consist a new 2-truck loading event, then the 3rd truck exits the bridge and the loading event becomes single truck loading event. In this process, four trucks have arrived on the bridge and produced 4 single truck loading events and three 2-truck loading events. The local extremes for each loading event are identified and marked in the figure. Using this procedure, local peaks for various type of loading events are identified.

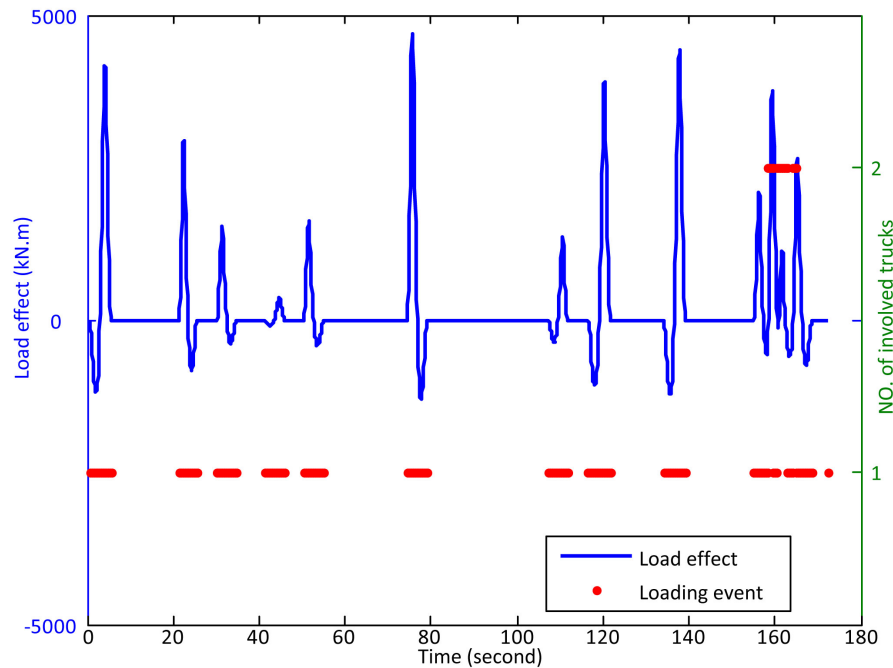


Figure 4.15: Time history of load effects

As shown in Figure 4.17, local extremes induced by different types of loading events consisting of different numbers of trucks are not identically and independently distributed data, and the standard extreme value theory can not be directly applied to these mixed data. Load effects should be classified by type of loading event Caprani et al. [2008]. Using traffic load effect simulation program BTLECS, which is described in Appendix B, developed in this research, local maxima of load effects can be identified and grouped by corresponding loading events. The proposed mixture peak-over-threshold (MPOT) method can be then used, and the performance of the method to the bridge traffic load problem are assessed in this section by comparing with conventional POT method and the mixture block maxima method proposed by Caprani et al. [2008].

Previous studies [O'Connor et al., 2001] have demonstrated that the critical influence lines for developing load model are bending moment at mid-span of a simply supported bridge, shear force at end-support of a simply supported bridge, and hogging moment at middle support of a two-span continuous bridge (see Table 4.10). In this study, these three types of load effect are studied with span lengths of 20, 30, 40 and 50 m. Considering the time consumption 1500-day

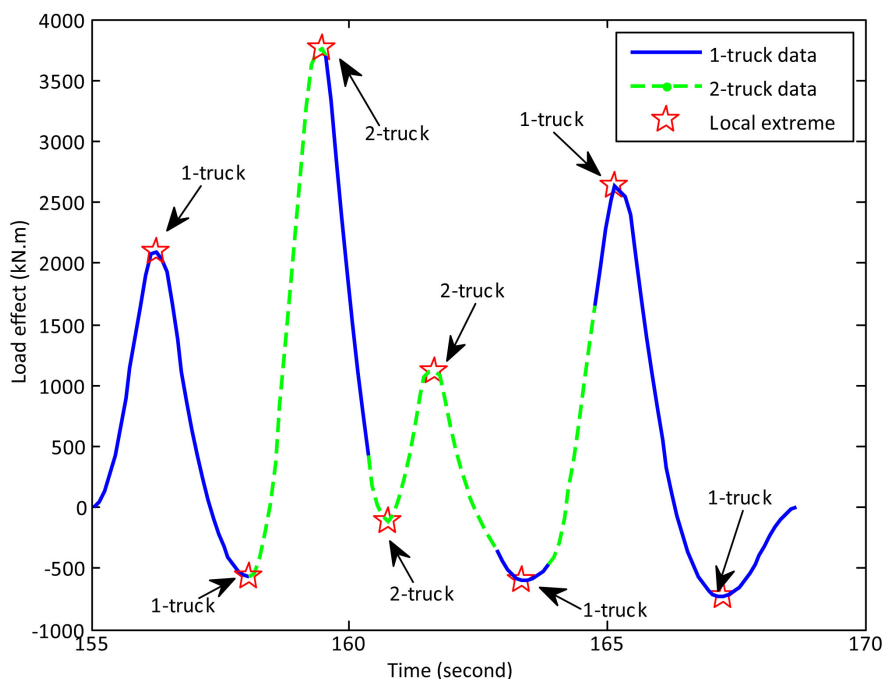


Figure 4.16: Detail of local extreme identification

were generated by BTLECS with statistic inputs based on measurements from Saint Jean de Védas (SJDV). The statistics of traffic data from SJDV are presented in Appendix A.

Table 4.10: Influence lines used in calculation of load effect

Item	Description Representation
I1	Bending moment at mid-span of a simply supported bridge
I2	Right-hand support shear force in a simply-supported bridge
I9	Bending moment at middle support of a two-span continuous bridge

4.5.2 Composition of Loading Event

Desrosiers and Grillo [1973] state that the multiple presence of trucks is primarily dependent upon the length of bridge and traffic volume but almost independent of other parameters like truck speed by studies conducted on several highway locations (Connecticut Route 5, I-91 at the Depot Hill Road, and I-91 at the Connecticut Route 68). This conclusion is also made by Gindy and Nassif [2007] who confirm that the probability of simultaneous presence of multiple truck increases as increasing of traffic density due to the increase of traffic volume using 11 years WIM data collected from 25 WIM sites at New Jersey between 1993 and 2003. Moreover, for different types of load effects, their sensitivities to multiple-truck presence are

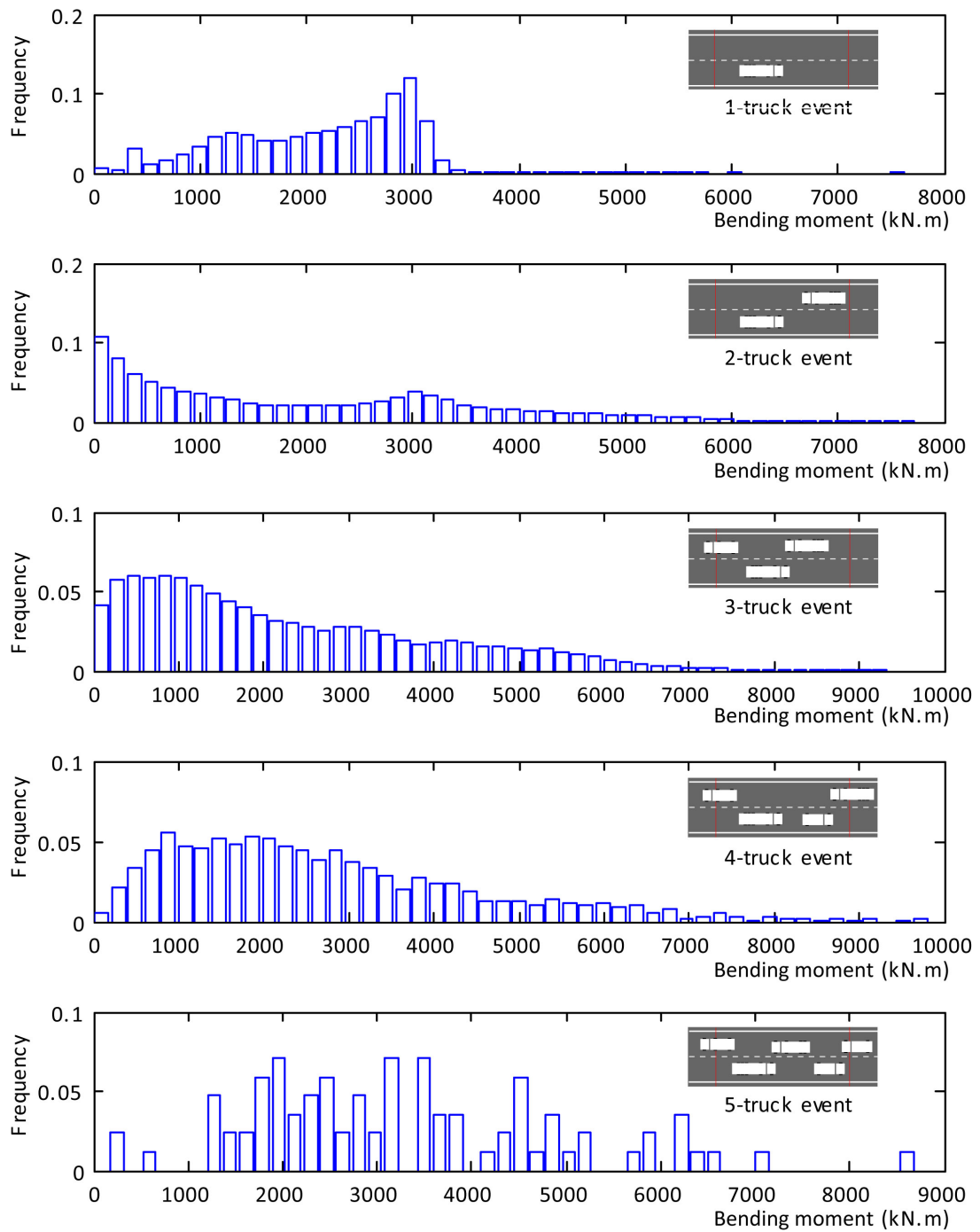


Figure 4.17: Histogram of load effects due to various type of loading event

different Harman and Davenport [1979]. In the following, we present the composition of type of loading event for the studied load effects.

For the three types of load effect, six categories of loading events have been identified from the simulation. These six categories of truck arrangements are 1-truck, 2-truck, 3-truck, 4-truck, 5-truck, and 6-truck loading events, but it should be noted that the 1-truck case includes the situation from one axle of the truck to the whole truck being on the bridge, 2-truck includes from one axle to all axles of each of two trucks being on the bridge simultaneously, and so on for other cases. Two sets of loading event composition are listed in Table 4.11 for the three types of load effect, with four types of bridge lengths. The first group is for load effect over 90th percentile, and the second group is for load effect above 95th percentile. Figure 4.18 shows the governing type of loading event changes with increasing bridge length. For a bridge length of 20 m, 2-truck and 3-truck loading events govern the upper tail. For a bridge length of 30 m, it can be seen from Figure 4.18a or Figure 4.18b that the governing event is 3-truck loading event. For bridge lengths of 40 and 50 m, 3-truck events are still the govern but some 4- and 5-truck events occur at the upper end of the simulation period. In addition, the composition of loading events are different between the data over 90th percentile and those over 95th percentile, it further confirm the importance to classify the load effects by loading events in the application of POT method.

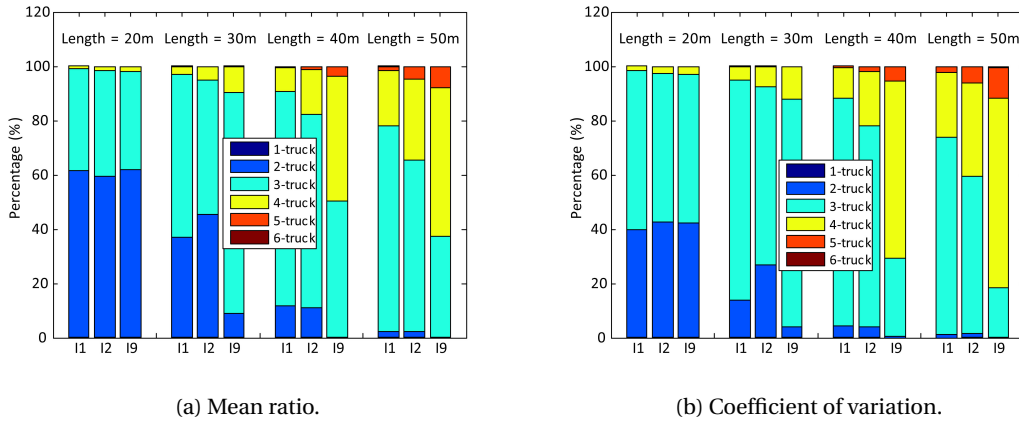


Figure 4.18: Probabilities for six types of loading events (left) over 90th and (right) 95th percentile.

4.5.3 Applicability of Conventional POT Method in Extreme Traffic Load Effect Modeling

The underlying non-identically distribution property of the data may lead to the availability problem of conventional POT method in estimating the distribution of extreme traffic load effect. In this section, we will compare the performance of the proposed mixture POT method and the conventional POT method on approximating the exceedances of traffic load effects for

Table 4.11: Probabilities for six categories of loading events for data above 90th and 95th percentile

Data	Type of loading event	20 m			30 m			40 m			50 m		
		I1	I2	I9	I1	I2	I9	I1	I2	I9	I1	I2	I9
$X_{0.90}$	1-truck	0.047	0.079	0.068	0.050	0.067	0.056	0.047	0.051	-	0.155	0.043	-
	2-truck	61.37	59.49	61.77	36.95	45.51	9.00	11.73	11.16	0.29	2.20	2.20	0.19
	3-truck	37.60	38.76	36.36	59.87	49.28	81.46	79.06	70.91	50.18	75.77	63.08	37.07
	4-truck	0.99	1.67	1.80	3.10	4.94	9.29	8.79	16.55	45.96	20.13	30.11	54.96
	5-truck	-	-	-	0.037	0.194	0.198	0.37	1.31	3.57	1.71	4.42	7.53
	6-truck	-	-	-	-	-	-	-	-	-	0.044	0.142	0.240
$X_{0.95}$	1-truck	0.094	0.079	0.136	0.100	0.073	0.113	0.094	0.081	-	-	0.085	-
	2-truck	39.87	42.38	41.97	13.72	26.73	3.87	4.25	4.07	0.57	1.38	1.59	0.29
	3-truck	58.38	54.98	55.00	81.11	65.50	83.99	84.04	73.84	28.86	72.35	57.96	18.02
	4-truck	1.67	2.55	2.89	5.03	7.37	11.74	11.18	20.04	65.14	23.92	34.24	69.99
	5-truck	-	-	-	0.050	0.328	0.282	0.44	1.94	5.43	2.26	5.87	11.31
	6-truck	-	-	-	-	-	-	-	-	-	0.089	0.255	0.384

Chapter 4. Mixture POT Approach to Model Extreme Bridge Traffic Load Effect

five thresholds at 90th, 92nd, 94th, 96th, and 98th percentiles. GPD parameters are estimated by MM, PWM, ML, MDPD and ADR methods that have been given in Chapter 3.

The quality of the estimated distributions can be checked by goodness-of-fit and graphical approach. Two types of goodness-of-fit tests are available for GPD. Choulakian and Stephens [2001] propose to check the fit by using the Cramer-von Mises statistic W^2 and the Anderson-Darling A^2 statistic. While Villasenor-Alva and Gonzalez-Estrada [2009] provide a goodness of fit test for the GPD in the situation that parametric estimators do not exist, the approach is to use the nonparametric bootstrap method. In this study, we use the method proposed by Choulakian and Stephens [2001] to evaluate the fitting. The procedure to use this goodness-of-fit test is as follows:

- Find the estimates of unknown parameters as described previously, and make the transformation $z_{(i)} = F(x_{(i)})$, for $i = 1, \dots, n$, using the estimates where necessary.
- Calculate statistics W^2 and A^2 as follows:

$$W^2 = \sum_{i=1}^n \left[z_{(i)} - \frac{2i-1}{2n} \right]^2 + \frac{1}{12n}$$

and

$$A^2 = -n - (1/n) \sum_{i=1}^n (2i-1) [\log z_{(i)} + \log 1 - z_{(n+1-i)}]$$

Table 4.12: Both shape parameter ξ and scale parameter σ unknown: upper tail asymptotic percentage points for W^2 of Cramer-von Mises test

$\xi \backslash p$	0.5	0.25	0.1	0.05	0.025	0.01	0.005	0.001
0.9	0.046	0.067	0.094	0.115	0.136	0.165	0.187	0.239
0.5	0.049	0.072	0.101	0.124	0.147	0.179	0.204	0.264
0.2	0.053	0.078	0.111	0.137	0.164	0.2	0.228	0.294
0.1	0.055	0.081	0.116	0.144	0.172	0.21	0.24	0.31
0	0.057	0.086	0.124	0.153	0.183	0.224	0.255	0.33
-0.1	0.059	0.089	0.129	0.16	0.192	0.236	0.27	0.351
-0.2	0.062	0.094	0.137	0.171	0.206	0.254	0.291	0.38
-0.3	0.065	0.1	0.147	0.184	0.223	0.276	0.317	0.415
-0.4	0.069	0.107	0.159	0.201	0.244	0.303	0.349	0.458
-0.5	0.074	0.116	0.174	0.222	0.271	0.338	0.39	0.513

Searching the critical value given in Table 4.12 and Table 4.13 for confidence percentage provided by Choulakian and Stephens [2001], the asymptotic 5% critical values z_5 for A^2 and W^2 for the estimate of the shape parameter ξ from conventional POT method can be obtained as given in Table 4.16. By comparing the critical values with the calculated EDF test statistics,

Table 4.13: Both shape parameter ξ and scale parameter σ unknown: upper tail asymptotic percentage points for A^2 of Anderson-Darling test

$\xi \backslash p$	0.5	0.25	0.1	0.05	0.025	0.01	0.005	0.001
0.9	0.339	0.471	0.641	0.771	0.905	1.086	1.226	1.559
0.5	0.356	0.499	0.685	0.83	0.978	1.18	1.336	1.707
0.2	0.376	0.534	0.741	0.903	1.069	1.296	1.471	1.893
0.1	0.386	0.55	0.766	0.935	1.11	1.348	1.532	1.966
0	0.397	0.569	0.796	0.974	1.158	1.409	1.603	2.064
-0.1	0.41	0.591	0.831	1.02	1.215	1.481	1.687	2.176
-0.2	0.426	0.617	0.873	1.074	1.283	1.567	1.788	2.314
-0.3	0.445	0.649	0.924	1.14	1.365	1.672	1.909	2.475
-0.4	0.468	0.688	0.985	1.221	1.465	1.799	2.058	2.674

the fitting quality can be revealed. For estimators, neither MM nor PWM estimated GPD do fit the dataset well at the considered threshold, in contrast, the ADR estimated GPD fits the dataset well as the test statistics are lower than the z_5 . While some of the ML or MDPD estimated GPDs fit the dataset well, they fail to fit in some cases.

Table 4.14: Critical value at various thresholds

Statistic	Threshold	MM	PWM	ML	MDPD	ADR
AD	$X_{0.90}$	1.03	1.04	1.07	1.06	1.01
	$X_{0.92}$	1.02	1.03	1.07	1.07	1.03
	$X_{0.94}$	1.04	1.04	1.05	1.05	1.01
	$X_{0.96}$	1.03	1.05	1.06	1.05	1.01
	$X_{0.98}$	1.02	1.05	1.07	1.07	1.03
CM	$X_{0.90}$	0.16	0.16	0.17	0.17	0.16
	$X_{0.92}$	0.16	0.16	0.17	0.17	0.16
	$X_{0.94}$	0.16	0.16	0.17	0.17	0.16
	$X_{0.96}$	0.16	0.17	0.17	0.17	0.16
	$X_{0.98}$	0.16	0.17	0.17	0.17	0.16

We use the traditional graphical method to further compare the performance of MPOT and CPOT. We present the probability diagnostic graphic in Figure 4.19, where the distribution parameters are estimated by maximum likelihood method. The left plots from subfigure (a) to subfigure (e) show the empirical survival function (black dots) fitted function with conventional POT estimates (red solid lines) and with mixture POT estimates (green dash lines) for various thresholds. The right plots from subfigure (a) to subfigure (e) show the previous mentioned survival function in logarithm scale. It can be seen that MPOT method approximates the exceedances over threshold with good accuracy. While the CPOT method approximate the majority of the data but has poor approximation for the high tail, but the high tail is extremely important in the extreme value analysis such for predicting high quantile. The results of root-mean-square-error reported in Table 4.16 confirm these conclusion that

Table 4.15: Empirical distribution function statistics for load effect of length 40m, Load effect I1

Statistic	Threshold	No.	MM	PWM	ML	MDPD	ADR
AD	$X_{0.90}$	6403	3 (1.01)	2.68 (1.44)	0.56 (0.38)	0.72 (0.56)	0.47 (0.27)
	$X_{0.92}$	5122	3.28 (1.27)	2.68 (1.4)	0.52 (0.43)	0.67 (0.62)	0.37 (0.26)
	$X_{0.94}$	3842	3.12 (0.83)	2.69 (1.95)	1.45 (0.33)	1.34 (0.69)	0.55 (0.33)
	$X_{0.96}$	2561	3.07 (0.84)	2.7 (1.7)	0.97 (0.34)	1.02 (0.67)	0.48 (0.3)
	$X_{0.98}$	1281	2.41 (0.81)	2.66 (1.27)	0.74 (0.34)	0.65 (0.64)	0.37 (0.26)
CM	$X_{0.90}$	6403	0.54 (0.24)	0.46 (0.29)	0.16 (0.14)	0.19 (0.16)	0.14 (0.12)
	$X_{0.92}$	5122	0.6 (0.29)	0.48 (0.3)	0.15 (0.15)	0.17 (0.18)	0.12 (0.12)
	$X_{0.94}$	3842	0.56 (0.2)	0.47 (0.35)	0.34 (0.12)	0.32 (0.17)	0.16 (0.14)
	$X_{0.96}$	2561	0.55 (0.2)	0.46 (0.31)	0.24 (0.12)	0.25 (0.17)	0.14 (0.13)
	$X_{0.98}$	1281	0.43 (0.2)	0.44 (0.25)	0.2 (0.13)	0.16 (0.17)	0.12 (0.12)

the mixture POT method improves the modeling as it provides lower goodness-of-fit statistics. Therefore, the MPOT has better performance than the CPOT method, and it can capture the tail well.

4.5.4 Threshold Selection Approach in the Use of Mixture POT method

An essential preliminary step is to determine an appropriate threshold u to each component of the mixture load effects for which the asymptotic GPD approximation. The threshold selection requires consideration of the trade-off between bias and variance: too high a threshold reduces the number of exceedances and thus increases the estimated variance, whereas too low a threshold will reduce a bias because the GPD will fit the exceedances poorly. The classical approaches use graphical diagnostics to select optimal threshold, for instance mean residual life plot. A crucial requirement on the use of these approaches is that they require practitioners to graphically inspect the data, understand their features and assess the model fit, when choosing the threshold, and it thus requires substantial expertise. Consequently the selected threshold will be rather subjective. Automated approach with appropriate measure is preferable to avoid subjective judgment. Statistics like root mean square error, goodness-of-fit test statistics are frequently used in automatic threshold selection method. Ferreira et al. [2003] determine the optimal threshold by minimizing the mean square error of the quantiles, while Dupuis [1999] provides a threshold selection guide based on goodness-of-fit test. Here we adopt automatic method to determine the optimal threshold, and the AD and CM goodness-of-fit test statistics proposed by Choulakian and Stephens [2001] are used as the measure. For example, the optimal thresholds selected for bending moment at mid-span of a simply supported bridge with span length of 40 m are given in Table 4.17.

In the case of mixture POT, there are two or more shape parameter estimates, therefore it is impossible to find the critical value and to assess whether the mixture GPD fits the dataset well or not. A nonparametric test is needed to evaluate the fitting quality; here we have used the

Table 4.16: Root mean square error at various threshold

Threshold	No.	MM	PWM	ML	MDPD	ADR
$X_{0.90}$	6403	0.0091 (0.004)	0.0083 (0.0059)	0.0035 (0.0032)	0.0066 (0.0062)	0.0095 (0.0084)
$X_{0.92}$	5122	0.0079 (0.0033)	0.0079 (0.0054)	0.0034 (0.0032)	0.0063 (0.0065)	0.0078 (0.0079)
$X_{0.94}$	3842	0.0099 (0.0061)	0.0083 (0.0079)	0.0064 (0.0042)	0.0099 (0.0071)	0.0107 (0.0096)
$X_{0.96}$	2561	0.0095 (0.0051)	0.0084 (0.0071)	0.0048 (0.0039)	0.0083 (0.0069)	0.0096 (0.0091)
$X_{0.98}$	1281	0.0086 (0.0035)	0.0086 (0.0059)	0.0041 (0.0033)	0.0061 (0.0068)	0.0079 (0.0081)

Table 4.17: Optimal threshold selection for 11 (bending moment at mid-span of simply supported bridge) with bridge length of 40m

Statistic	Estimator	2-truck			3-truck			4-truck			KS p-value
		Shape	Scale	Threshold	Shape	Scale	Threshold	Shape	Scale	Threshold	
AD	MM	0.0628	262.5	6540	-0.2185	830.4	6540	-0.1874	1114.0	6540	0.09
	PWM	0.0952	253.5	6540	-0.2056	821.6	6540	-0.1918	1118.2	6540	0.10
	ML	0.0725	259.9	6540	-0.2771	812.7	6864	-0.1887	1115.5	6540	0.74
	MDPD	0.0884	256.4	6540	-0.2728	808.9	6864	-0.1873	1113.9	6540	0.55
	ADR	0.1162	252.4	6540	-0.2116	829.0	6540	-0.1910	1116.0	6540	0.79
	MM	0.0536	269.8	6571	-0.2567	798.0	6864	-0.1874	1114.0	6540	0.66
	PWM	0.0952	253.5	6540	-0.2483	792.7	6864	-0.1918	1118.2	6540	0.48
	ML	0.0725	259.9	6540	-0.2813	803.3	6921	-0.1887	1115.5	6540	0.86
CM	MDPD	0.0884	256.4	6540	-0.2728	808.9	6864	-0.1873	1113.9	6540	0.55
	ADR	0.1162	252.4	6540	-0.2561	799.7	6864	-0.1910	1116.0	6540	0.70

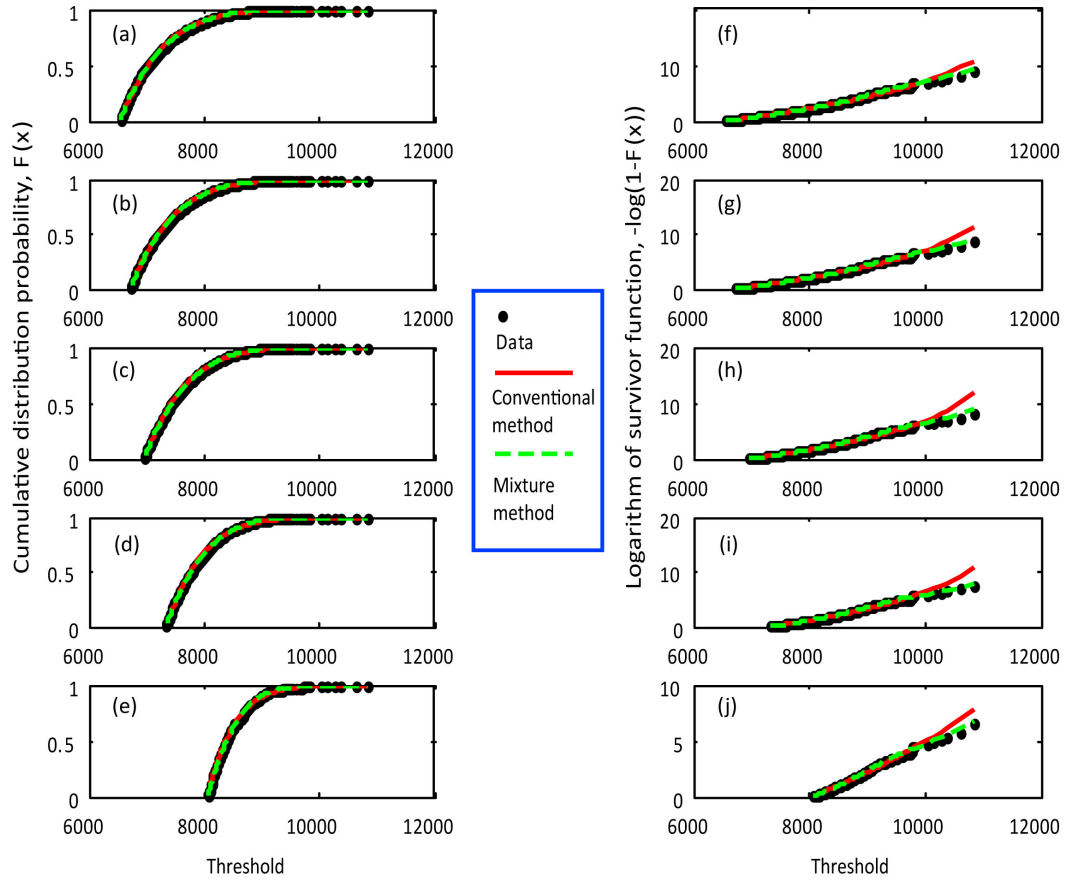


Figure 4.19: Diagnostic plot for threshold excess model fitted to load effect

Kolmogorov-Smirnov (KS) test. In statistics, the KS test is a nonparametric test, and qualifies a distance between the empirical distribution function of the sample and the cumulative distribution function of the reference distribution. The p-values for confidence level of 0.05 are given in Table 4.18 for the examined samples. Furthermore, the results indicate that the null hypothesis of modeling datasets with GDP or mixture GPD from conventional POT and mixture POT method are accepted as the p-values are greater than 0.05. It is illustrated in the QQ plots in Figure 4.20. Again, the results confirm the previous remark that the mixture POT fits the sample better than the conventional POT as the KS test statistics from mixture POT are greater than those from convention POT.

4.5.5 Results of Simulation

The previous study has demonstrated that the MPOT method can improve the modeling of tail distribution of traffic load effects. For the load effects and bridge lengths described, 100-year

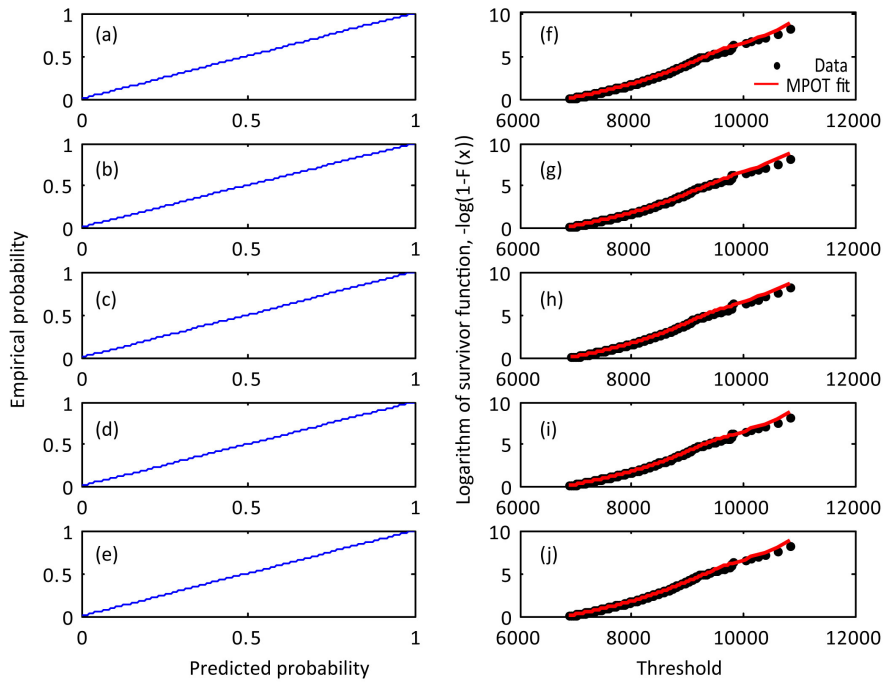
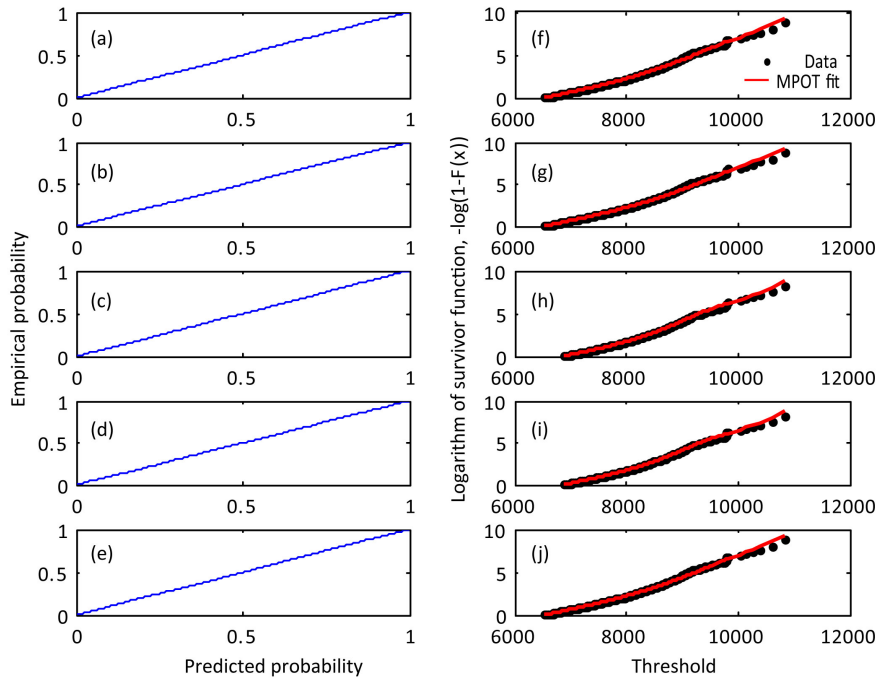


Figure 4.20: Diagnostic graphics

Table 4.18: KS test statistics for various thresholds and parameter estimation methods

Threshold	No.	MM	PWM	ML	MDPD	ADR
$X_{0.90}$	6403	0.072 (0.408)	0.014 (0.296)	0.12 (0.542)	0.1 (0.529)	0.164 (0.57)
$X_{0.92}$	5122	0.172 (0.453)	0.098 (0.208)	0.157 (0.146)	0.148 (0.239)	0.107 (0.42)
$X_{0.94}$	3842	0.65 (0.759)	0.644 (0.754)	0.339 (0.839)	0.567 (0.796)	0.737 (0.843)
$X_{0.96}$	2561	0.641 (0.718)	0.702 (0.673)	0.307 (0.867)	0.453 (0.829)	0.633 (0.778)
$X_{0.98}$	1281	0.422 (0.676)	0.697 (0.677)	0.087 (0.601)	0.173 (0.611)	0.537 (0.596)

and 1000-year return period characteristic values, calculated from the conventional block maxima method, the composite distribution statistic (CDS) approach proposed by Caprani et al. [2008], the CPOT approach and the MPOT approach, are presented in Table 4.19 and Table 4.20. The parameters for conventional method based distribution are estimated with mixed data, while the parameters for mixture method based distribution are estimated by fitting distribution to each grouped data. Due to the available data are relative small when classifying data by type of loading events, the data from events with less than 10% proportion are grouped together to reduce variance in the estimates of distribution parameters according to the conclusion made in theoretical study that slight contamination do not influence the parameter estimation when data having similar tail behavior. This includes among others the case of 6-truck event. Conversely, the load effect of bending moment at mid-span of a simply span bridge with span length of 40 m, the recorded 2-truck, 3-truck and 4-truck events are the core events with proportion greater than or around 10% (see Table 4.11), the distribution are thus divided into components from these three events and parameters are estimated for each components as listed in Table 4.17. The differences between return level estimates from conventional and mixture methods are listed in Table 4.19 and Table 4.20 for 100-year return period and 1000-year return period, respectively. The estimated return levels are given in Tables 4.22 and 4.23

The first conclusion can be made on performances of the methods for estimating 100-year and 1000-year return levels. The differences between conventional and mixture estimates are smaller for 100-year return level than for 1000-year return level. For example, the difference between convention method and mixture for 100-year return level of load effect I1 with span of 30 m shown in Table 4.19 is around 10%, while the difference for 1000-year return level in Table 4.20 is around 10% more. It confirms the common impression that the extrapolation to remote future is not stable.

It seems that the difference between conventional method and mixture method is smaller for load effects for shorter spans, either the BM or the POT. For instance, the difference is -8.49% for BM for 100-year return level of load effect I1 at length of 20 m in Table 4.19, but it increases to about 17% at span length of 50 m. It is due to the composition of loading events becoming more complex when span length increases.

Among the three types of load effects, the performances of the methods are different. The

Chapter 4. Mixture POT Approach to Model Extreme Bridge Traffic Load Effect

Table 4.19: Percentage difference of 100-year return level between conventional and mixture method (%)

Load effect	Length (m)	BM/GEV	POT/GPD				
			MM	PWM	ML	MDPD	ADR
I1	20	-8.49	0.11	0.43	0.19	0.17	-0.63
	30	-9.56	-6.31	-10.40	-8.18	-9.66	-13.25
	40	-14.63	-8.27	-7.90	-1.82	-7.19	-9.54
	50	-16.98	15.78	-2.71	20.32	21.18	24.61
I2	20	5.12	-0.47	1.54	0.20	0.36	-0.96
	30	-20.60	-3.02	-0.32	-6.33	-3.66	0.17
	40	-9.51	-3.02	-16.38	-16.02	-21.40	-25.99
	50	-11.22	0.08	-2.73	1.20	1.04	2.04
I9	20	-29.92	-4.55	-7.11	-1.63	-4.30	-16.47
	30	-15.22	-5.89	-9.69	-4.11	-5.92	-9.26
	40	-8.28	5.76	20.09	16.59	23.89	28.61
	50	-17.85	8.44	24.03	9.14	14.40	30.28

differences are larger for load effects of I9 than for the other two. As been stated by Harman and Davenport [1979], the load effect of I9 is more sensitive to the multiple presence of trucks. This shows that the differences for return level of type I9 load effect between convention method and mixture method becomes larger with increasing span length.

Moreover, comparisons of the 100-year return levels and the 1000-year return levels from mixture GEV distribution and mixture GP distribution are given in Table 4.21. The two methods seem to provide consistent results. In general, the differences are less than 10%, it can be concluded that the two methods have similar performance. However, it is also clear that some of the differences are significant, especially for longer span lengths.

4.6 Conclusion

A detailed analysis of load effect is presented in this chapter. This analysis assesses the two primary assumptions of extreme value theory with respect to bridge loading events. It is shown that bridge traffic load effects can be considered as independent but they are not identically distributed. A modification has been proposed in order to make it applicability of the extreme value modeling for bridge traffic load effects, and it helps to derive a new method - mixture peaks over threshold.

The MPOT method is shown to give results which differ from a conventional POT approach. From the analysis of load effect distributions presented, theoretical examples are developed through which the performance of the proposed method is assessed and compared with that of the conventional approach. It is shown that the violation of the assumption of identically distributed data by the conventional method, results in different predictions as compared to the MPOT method, especially when the components come from significantly different distri-

Table 4.20: Difference in 1000-year return level between conventional and mixture model (%)

Load effect	Length (m)	BM/GEV	POT/GPD				
			MM	PWM	ML	MDPD	ADR
I1	20	-10.62	0.24	0.64	0.30	0.28	-0.62
	30	-16.20	-13.50	-22.30	-22.38	-24.88	-25.21
	40	-29.67	-9.78	-11.11	-1.00	-9.44	-18.01
	50	-36.45	34.53	-1.39	44.65	46.16	53.06
I2	20	8.65	-0.80	1.93	0.05	0.28	-1.37
	30	-25.62	-8.36	-8.90	-11.17	-8.81	-4.43
	40	-11.39	-4.48	-36.71	-36.18	-42.90	-48.55
	50	-13.91	1.26	-2.68	2.69	2.58	3.80
I9	20	-41.27	-8.28	-12.52	-3.83	-7.92	-25.76
	30	-17.82	-7.10	-13.42	-6.72	-10.99	-19.27
	40	-10.21	9.40	34.22	28.00	40.81	47.71
	50	-17.65	15.34	40.60	16.50	24.94	51.36

butions. In addition, the proposed generalized Pareto distribution based MPOT is compared with the generalized extreme value distribution based method, which also acknowledges the differences in distribution of data, and the results show that the GPD based method has better performance than the GEV based method in terms of bias and standard deviation.

The MPOT method is applied to full traffic simulations on a range of bridge lengths and load effects. It is shown that some forms of loading events tend to govern certain lengths and load effects, and that this behavior is dependent on the physical nature of the bridge loading problem. The differences between the conventional and the mixture approach are great especially for longer span, it seems that the applications have greatest difference on the load effects for 40 m.

Table 4.2.1: Difference (mixture POT vs. mixture GEV)

Load effect	Length (m)	100-year					1000-year				
		MM	PWM	ML	MDPD	ADR	MM	PWM	ML	MDPD	ADR
I1	20	0.43	-0.65	-0.57	0.89	-4.16	0.48	-0.74	-0.65	1.02	-5.44
	30	2.14	0.13	1.22	9.21	-5.44	8.13	8.84	11.73	17.17	-14.59
	40	-0.14	-0.05	0.25	0.46	1.75	1.80	0.14	1.32	8.82	-1.71
	50	-1.78	0.50	-0.10	-1.38	17.33	-2.44	0.70	-0.14	-1.85	10.28
I2	20	0.13	-1.91	-1.38	1.74	7.33	0.08	-2.45	-1.79	2.14	3.26
	30	-3.81	3.98	0.60	-3.03	22.85	-0.92	3.74	0.41	-3.95	11.82
	40	16.27	15.95	23.47	32.22	4.78	51.41	50.41	67.44	87.83	-0.18
	50	2.79	-0.85	-0.99	-1.23	21.55	3.93	-1.07	-1.35	-1.53	17.72
I9	20	5.27	-4.12	-0.21	15.40	-1.25	8.39	-6.18	-0.32	25.15	-10.28
	30	3.34	-1.77	-0.06	2.40	-0.39	6.06	-0.29	4.23	13.06	-6.51
	40	-0.07	-0.72	0.00	5.57	4.22	-0.12	-1.28	-0.03	10.09	-11.32
	50	-5.15	1.49	0.36	-2.09	15.64	-7.19	2.18	0.51	-2.80	8.10

Table 4.22: Comparison of 100-year return levels (or characteristic values)

Load effect effect	Length (m)	Conventional/Mixed						Composite distribution statistics					
		GEV	GPD					GEV	GPD				ADR
			MM	PWM	ML	MDPD	ADR		MM	PWM	ML	MDPD	
I1 (kN.m)	20	4361	3717	3744	3696	3698	3722	4765	3713	3728	3688	3691	3746
	30	7353	7221	7054	7086	7048	7302	8130	7708	7873	7717	7802	8418
	40	10864	10489	10515	11220	10639	10390	12725	11434	11418	11428	11463	11486
	50	15058	19394	16006	20254	20277	20585	18138	16750	16452	16834	16733	16520
I2 (kN)	20	939	807	825	797	803	817	893	811	812	796	800	825
	30	1008	969	958	973	968	971	1269	999	961	1039	1005	969
	40	1055	1052	1055	1056	1053	1061	1166	1085	1261	1258	1339	1434
	50	1142	1169	1168	1172	1168	1177	1286	1168	1201	1158	1156	1154
I9 (kN.m)	20	-1696	-1105	-1132	-1092	-1106	-1116	-2420	-1158	-1219	-1110	-1155	-1336
	30	-1645	-1678	-1664	-1679	-1676	-1656	-1940	-1783	-1842	-1751	-1782	-1826
	40	-2463	-3114	-3534	-3408	-3648	-3998	-2685	-2945	-2943	-2923	-2945	-3109
	50	-3817	-4076	-4422	-4163	-4315	-4794	-4646	-3759	-3565	-3815	-3772	-3680

Table 4.23: Comparison of 1000-year return levels (or characteristic values)

Load effect	Length (m)	Conventional/Mixed							Composite distribution statistics						
		GEV	GPD					GEV	GPD						
			MM	PWM	ML	MDPD	ADR		MM	PWM	ML	MDPD	ADR		
I1 (kN.m)	20	4658	3772	3805	3746	3749	3777	5211	3763	3781	3735	3738	3801		
	30	7558	7381	7169	7209	7162	7477	9020	8533	9227	9288	9535	9998		
	40	11142	10679	10711	11733	10860	10560	15841	11836	12050	11852	11992	12880		
	50	15601	23973	17143	25957	26010	26771	24549	17820	17385	17945	17796	17490		
I2 (kN)	20	1033	837	860	823	830	850	951	843	844	823	828	861		
	30	1059	1006	991	1012	1005	1008	1423	1098	1088	1139	1102	1054		
	40	1089	1087	1091	1093	1088	1100	1230	1138	1724	1712	1906	2138		
	50	1181	1221	1220	1225	1220	1233	1372	1206	1253	1193	1190	1188		
I9 (kN.m)	20	-2253	-1169	-1208	-1150	-1169	-1184	-3836	-1274	-1381	-1195	-1270	-1595		
	30	-1684	-1765	-1744	-1767	-1762	-1734	-2049	-1900	-2015	-1894	-1980	-2148		
	40	-2621	-3786	-4640	-4373	-4872	-5628	-2919	-3461	-3457	-3416	-3460	-3810		
	50	-4190	-4638	-5247	-4787	-5050	-5916	-5088	-4021	-3732	-4109	-4042	-3908		

5 Effects of Distribution of Vehicle Lateral Position in Lane on Bridge Local Effects from WIM Measurements

5.1	Introduction	141
5.2	Related Research	142
5.3	Measurements	143
5.3.1	Vehicle Lateral Position Collection Device	143
5.3.2	Measurements of Transverse Location of Vehicles	144
5.4	Sensitivity of Local Effects to VLP Case I: RC Bridge Deck Slab	149
5.5	Sensitivity of Local Effects to VLP Case II: Orthotropic Bridge Deck	151
5.5.1	Results for Transverse Bending Moment	154
5.5.2	Discussion	156
5.5.3	Fatigue Damage Assessment	160
5.5.4	Induced Damage Localization	162
5.6	Conclusion	164

5.1 Introduction

The aim of this chapter is to investigate the influence of transverse location distribution of vehicles on bridge load effects. The transverse location of a vehicle (referring to the distance from centerline of the vehicle to the longitudinal centerline or outer edge of a bridge) on bridge is critical to bridge design as the effect of live load on the main longitudinal members is a function of the magnitude and location of wheel loads on the deck surface and of the response of the bridge to these loads [Huo et al., 2005]. In bridge engineering, the three-dimensional behavior of the structural system is usually simplified to be considered by an equivalent live load lateral distribution factor which assigns a proportion of the load effect to the structural elements depending on their position relative to the applied load. These factors are generally available for the longitudinal effects governed by gross vehicle weights (GVWs) [Bakht and Jaeger, 1983]. However, the attention regarding fatigue safety should consider both the transverse and longitudinal stresses. As in [Huo et al., 2005], load effects like stresses on decks [American Institute of Steel Construction, 1963; Troitsky and Foundation, 1987] are more sensitive to the transverse loading position in lane. The use of a relatively coarse vehicle transverse location for calculating longitudinal effects will lead to under- or over-estimation of the effects induced by an individual wheel load. Modern Weigh-in-Motion (WIM) systems permit the measurement of vehicle transverse position as well as vehicle track (the distance from the centerline of the tire pressure area on one side of an axle to the centerline on the other side). Using newly collected WIM data, this chapter intends to assess the influence of the distribution of transverse location of vehicle centerline in lane on the bridge traffic load effects. Two types of bridge have been utilized to evaluate the influence of transverse location of vehicle on traffic load effects. One is an orthotropic steel deck bridge [Gomes, 2012], and another is a reinforced concrete box-girder prestressed bridge [Treacy and Bruhwiler, 2012]. In the following, the term "transverse location of vehicle" refers to the transverse eccentricity of the centerline of a vehicle with respect to the longitudinal centerline of a lane where the vehicle is located.

Measurements of transverse location of vehicles on four French highways were collected by WIM systems in 2010 and 2011. The measurements showed different distribution models of transverse location of vehicle with the recommended model in EC1. In order to evaluate the influence of the distribution of transverse location of vehicle on load effects on bridge decks, finite element analysis have been performed to model an orthotropic steel deck bridge and a prestressed concrete box-girder bridge. The orthotropic steel deck case is extended further to assess the influence of transverse location on fatigue damage on details in bridge deck. The sensitivity of stress to the loading location was evaluated, and the influence surfaces of stresses for critical joints, which are susceptible of fatigue cracking, were obtained. Stress spectrum analysis and fatigue damage calculation were performed using the calculated stresses induced by traffic. By comparing the stresses and damages induced by different traffic patterns (through distributions of transverse location of vehicle), it was found that the histogram of stress spectrum and cumulative fatigue damage were significantly affected by the distribution.

Actually, knowing the precise distribution of transverse location of vehicles can not only avoid under- or over-estimation of the fatigue damage for details under consideration, but also helps to constitute the inspection program. Due to the large number of welded connection details in orthotropic steel decks, it is advisable to focus inspection of the most critical details prone to fatigue cracking [Connor et al., 2012]. Numerical analysis illustrates that integration finite element modeling and traffic data with distributions of transverse location of vehicles can help to make an accurate predetermination of which welded connections should be sampled to represent the health of the deck. Moreover, accounting for scatter related to this distribution of transverse load locations could also be made possible using probabilistic approaches.

5.2 Related Research

Orthotropic steel decks have become common components of major steel bridges because of their favorable characteristics such as high load-carrying capacity, light weight, and short installation time [Huo et al., 2005]. However, in the orthotropic steel decks subjected to many cycles of live load induced stresses, fatigue cracks may generate at the welded connections that locate between deck plate and the rib, and geometrical details [de Jong, 2004]. Among the various fatigue cracks observed in orthotropic decks with closed ribs, cracks in rib-to-deck (one sided) partial-joint-penetration welds are of particular concern [Pfeil et al., 2005; Sim and Uang, 2012; Xiao et al., 2006, 2008; Ya et al., 2010]. This type of welded joint is prone to fatigue cracking as it is subjected to a very localized out-of-plane bending moment, particularly in the transverse direction induced by wheel loads. The stress distribution in of orthotropic steel decks especially for rib-to-deck joints has been studied widely through lab testing [Ben and WanChun, 2005; Gomes, 2012; Tsakopoulos and Fisher, 2003], field measurements [Pfeil et al., 2005], and analytical modeling or finite element modeling [Cullimore and Smith, 1981; Gomes, 2012; Sim and Uang, 2012; Xiao et al., 2008]. Factors affecting the stress on the critical joints like deck plate and rib web thicknesses, surfacing layer properties, loading location have been studied [Ji et al., 2011; Sim and Uang, 2012; Xiao et al., 2008], but loading location in the transverse direction perhaps is the prominent one among them [Gomes, 2012; Xiao et al., 2008]. In order to consider the influence of the loading location on design these of types of joints, clauses are given in design codes. There exists difference among them: some recommend positioning the wheel to induce maximum stress at the detail under consideration like AASHTO, while some propose to use a random distribution of wheel path like EC3. Due to the randomness of driver behavior, setting the wheel path to a stochastic variable should be more reasonable even though some deterministic local influent factors should be accounted for. Finally, experimental evidence of effect lateral position of live loads is of out most importance to precisely document the stochastic variation of this load distribution, and forecast the consequence in terms of included stochastic effects.

5.3 Measurements

5.3.1 Vehicle Lateral Position Collection Device

To get a better understanding of the load effect on bridges, WIM devices were used to record and identify gross vehicle weights and axle weights as vehicles pass over the devices. A typical WIM systems has two transversal piezo-sensors (*A* and *B* in Figure 5.1). The voltage in the piezo-sensors changes due to the pressure on the sensor caused by a crossing vehicle axle, and the axle weights can thus be calculated based on such a change. This passing vehicle axle also interrupts the magnetic signal produced by the loop sensors, and therefore, the configuration information like the number of axles, the axle spacing and the number of vehicles can be determined [Jacob et al., 2000].

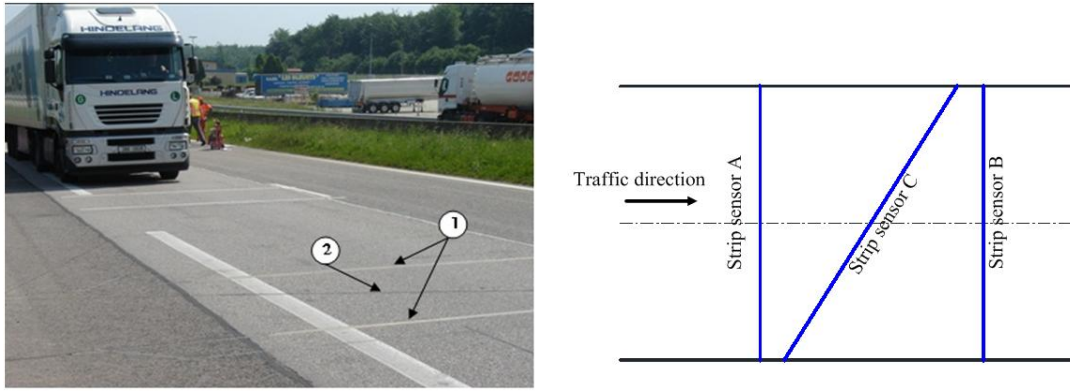


Figure 5.1: WIM device for collection of transverse vehicle position.

To measure vehicle lateral position (relative position with respect to the lane centerline), an additional sensor (*C*) was installed with an angle, θ , as shown in Figure 5.1. Assuming the vehicle runs over the device from left to right and in a straight line. The vehicle arrives at sensor *A* at time, t_a , and leaves the device at time, t_b , the speed of the vehicle can be determined from $v = d/(t_b - t_a)$ as the distance, d , between sensor *A* and *B* is known. When the left and right tires cross strip *C*, the associated times, $t_{c,left}$ and $t_{c,right}$, are registered respectively and the vehicle width, w , can be found from the formula:

$$w = \frac{v(t_{c,left} - t_{c,right})}{\tan \theta} \quad (5.1)$$

The lateral displacement of vehicle centerline in lane can be calculated basing on the known position of lane centerline, l_0 ,

$$e = l_0 - \frac{[v(t_{c,left} - t_a) - v(t_{c,right} - t_a)]}{2 \tan \theta} = l_0 - \frac{v(t_{c,left} - t_{c,right})}{2 \tan \theta} \quad (5.2)$$

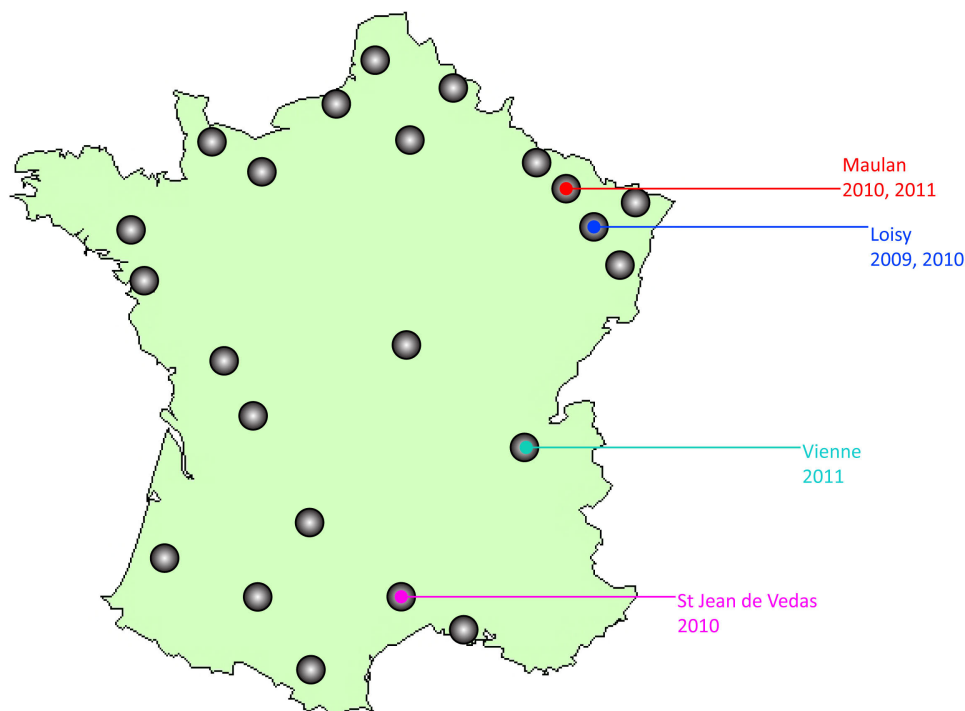
Thus, a negative value means that the vehicle shifts to left side and the positive value for right side. A field test of this system has been carried out on Maulan open experimental site, on RN4 highway, in France, and the test results are very homogeneous and consistent [Jacob et al.,

2008].

5.3.2 Measurements of Transverse Location of Vehicles

This type of WIM system has been installed on several highways to collect traffic information and data, and data collected from four of them between 2010 and 2011 were used in the present study. These four WIM stations (see Figure 5.3) were located at Vienne, Saint Jean de Védas, Loisy, and Maulan on the French motorways A7, A9, A31 and RN4 highways respectively, and the profile section of WIM stations are shown in Figure 5.2. These WIM systems provide high quality measurements as they were classified in class B (10) or C (15) according to the Cost 323 standard [Jacob et al., 2000]. However due to the dynamic nature of moving loads, low percentages of erroneous results can arise during everyday use, filtration is required to remove unreliable data before conducting the analysis [Sivakumar et al., 2011]. In the first step, unreasonable records with error in axle weights, axle spacing were eliminated according to filtration criteria proposed by Sivakumar et al. [2011]. In addition, the quality of WIM measurements can be further improved by using lateral position records [Klein et al., 2012] that vehicles driving outside the lane and unreasonable vehicle widths were excluded.

Figure 5.2: WIM station locations and measured period.



Heavy trucks are critical when modeling traffic load effects for bridge design or assessment and the majority of them drive in the right lane (also said slow lane) as most of European Union countries restrict them to the right lane, which is also required by traffic laws (<http://cga.ct.gov/2005/rpt/2005-R-0814.htm>). The trucks in the slow lane were used in the



Figure 5.3: Profile of WIM system on the four studied stations

following. Transverse locations of vehicle for the four sets are given in Figure 5.4a, and the EC1 recommended model is given in the figure also as a reference. In order to illustrate the variability in the measurements, error bar plots have been utilized to present the data. In Figure 5.4, the vertical red line is used to represent the lane centerline, therefore the negative value at left side means the vehicle shift to the left side of lane and the contrary for the vehicle shifting to right side. The EC1 model is symmetric with respect to axis at 0. For the four sites measurements, three of them have positive mean value except Maulan. It means that most of the trucks driving on highway at Maulan were prone to drive at left side of the lane, and the trucks running in the other sites preferred to drive near right side or outer edge of roadway. The differences of the mean values thus confirmed that the distribution of transverse location of trucks in lane is site-specific.

The severity of truck load effects on bridges is strongly related to the type of trucks [Wang et al., 2005], thus it is important to know whether the distribution of transverse locations of truck is type-specific or not. In EC1, the trucks on European routes are represented by five types of standard trucks that are extracted from traffic measurements collected mainly from Auxerre [Sedlacek et al., 2006]. To investigate this question, the measurements from Saint Jean de Védas were used as they contains more measurements than other three sites. The recorded trucks were classified by number of axles, and the mean value and standard deviation of transverse location of vehicle are obtained for each type of truck. All types of truck showed similar behavior: the mean value was positive, and the main part of truck in each class was prone to drive toward the right side as illustrated in Figure 5.4c. The error bar plot indicates

that the distribution of transverse location of trucks did not show significant vehicle-type feature (see Figure 5.4b), the mean value and standard deviation have slight difference (see Figure 5.5).

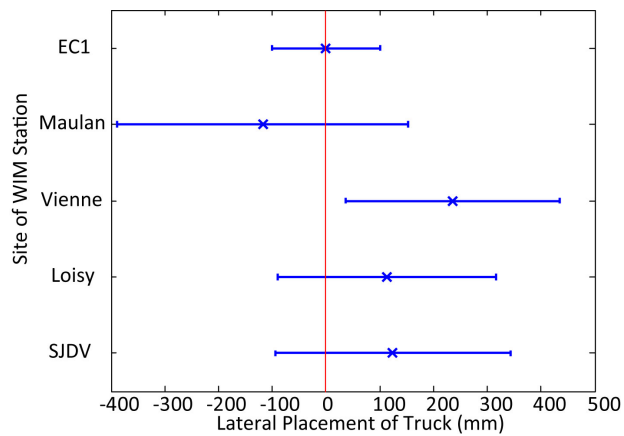
Figure 5.4c shows the relationship of the transverse location of vehicle with different vehicle speed. The measured trucks were grouped by their speeds into seven groups with mean value from 75 km/h to 135 km/h. The transverse locations of trucks in each group are presented with their mean values and standard deviations in error bar plot, in bottom axis of Figure 5.4c. The result indicates that higher speed leads to a concentration of the wheel paths closes to the lane centerline.

Although the speeds of the recorded trucks range from 65 km/h to 140 km/h, the measurements show that the majority of the trucks have a speed around 85 km/h. About 90% of trucks have speed in the range of 80 km/h to 100 km/h as shown in the histogram of speed in Figure 5.4c. Moreover, most European Union countries set maximum allowance speed at about 80 km/h for heavy good vehicles (generally defined as trucks with GVW greater than 3.5 t). Trucks with speeds between 80 and 100 km/h were thus used to further analyze statistical behaviour of measurements from French WIM stations. The frequency distributions in bar chart form (Figure 5.6) were prepared to show the pattern of transverse location of vehicles. In the figure, the ordinate shows the probability density and the abscissa is the distance from the centre of either wheel to the lane centre. The vertical line in the figure indicates the lane centre, and the positive value means the wheel centre deviates to the right side of the lane. The Gumbel or normal distribution fits the measurements very well, and it has a right skew shape that is different from the commonly used symmetric distribution in literature such as [Xiao et al., 2008]. The fitted parameters are given in Table 5.1 for the four sites.

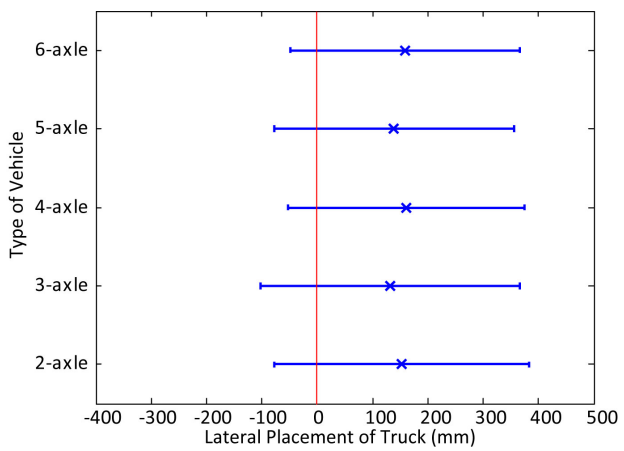
Table 5.1: Fitted distribution parameters

Parameter	SJDV, 2010	Loisy, 2010	Vienne, 2011	Maulan, 2011
Distribution type	Gumbel	Normal	Gumbel	Normal
Location, μ (mm)	244.6	101.1	326.5	-117.8
Scale, σ (mm)	181.7	202.1	156.9	270.8

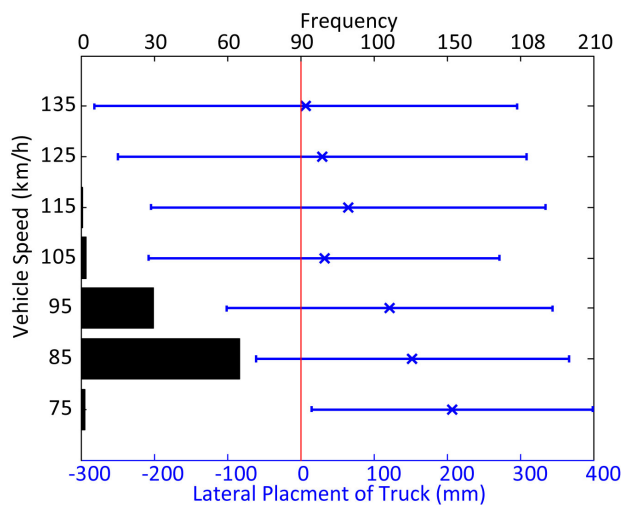
In the above investigation, the distribution of transverse locations of a vehicle in-lane position based on several sites measurements has been considered. Three aspects influencing the distribution of transverse location of vehicles were investigated including site location, vehicle type, and vehicle speed. The distribution is insensitive to the type of vehicles, but it is strongly related to site location and vehicle speed. For the aspect of site location, three of the four sites are located on expressway, and the Maulan is located on a national highway, RN4. The three sets of data from the expressway have a similar feature in which the majority of the trucks are shifted to the right side relatively to the lane center, while the distribution for the national highway is shifted to the left side. After a further investigation of the lane profile, the slow lane on the three expressways have a emergency lane at their right side, while the RN4 only has two driving lanes without an emergency lane. From a safety point of view,



(a) Various site.



(b) Type of vehicle.



(c) Speed.

Figure 5.4: Sensitivity analysis.

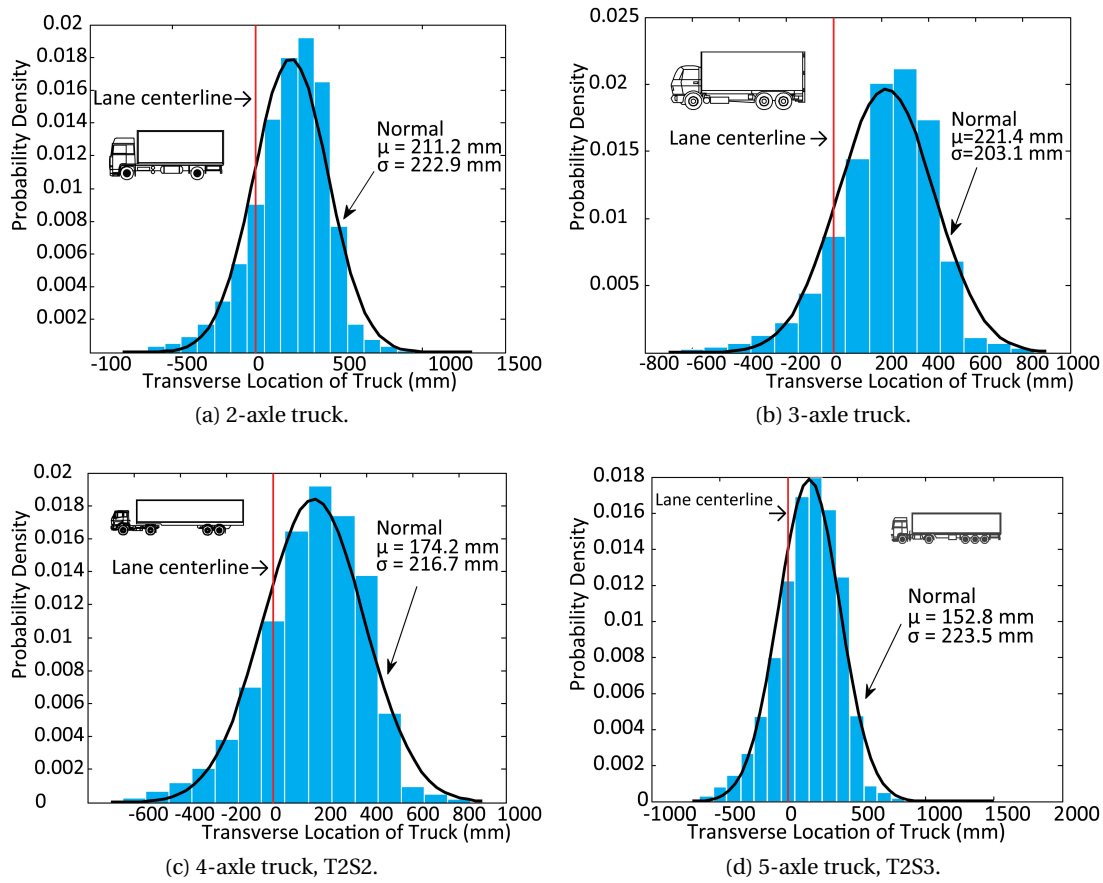


Figure 5.5: Distribution of transverse location of centre line of trucks for various types of truck.

drivers are more comfortable with wider lanes [Ma et al., 2008; Prem et al., 1999]. Therefore, differences in the transverse location distribution of vehicles among different sites may be considered to mainly arise from the profile of lane cross section. For the aspect of vehicle speed, as illustrated in Figure 5.4c, it is seen that higher speed vehicles prefer to drive along the lane center. Similar phenomena have been reported by Blab and Litzka [1995]. However, the measurements indicate that most of trucks travel at speeds ranging from 80 to 100 km/h, thus the distribution of transverse location of vehicle can be represented by these trucks. The Gumbel distribution is shown to fit the measurements of transverse location of vehicles well, which differs from the commonly used symmetric model such as the normal distribution. In the following, sensitivity of transverse load effects on two types of bridge decks is investigated.

5.4. Sensitivity of Local Effects to VLP Case I: RC Bridge Deck Slab

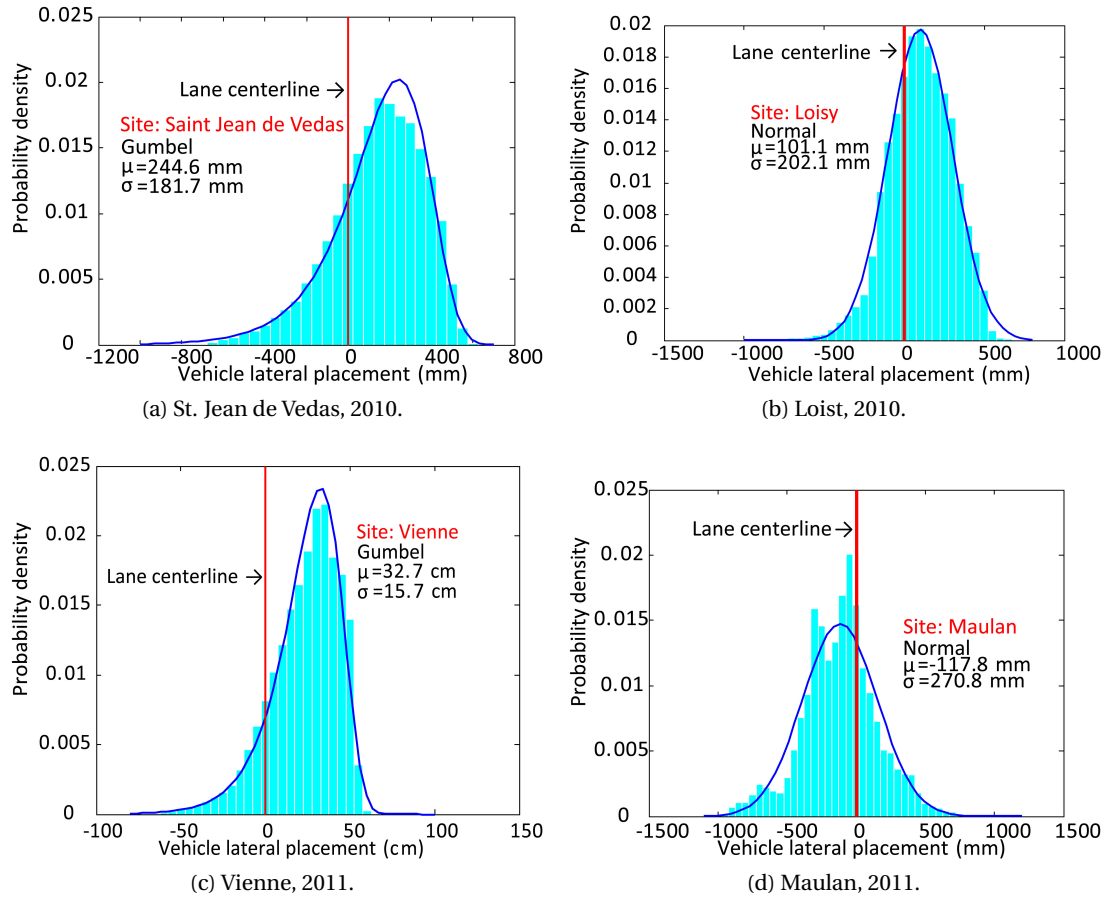


Figure 5.6: Distribution of transverse location of centre line of trucks on slow lane for various location

5.4 Sensitivity of Local Effects to Vehicle Lateral Position Case I: Reinforced Concrete Bridge Deck Slab

The influence of vehicle lateral position on bridge traffic load effects was first studied for a prestressed concrete bridge at Morge in Switzerland. The bridge is a three-span, twin box-girder structure with total span length of 110.5 m as shown in Figure 5.7(a). A monitoring system, described in detail in [Treacy and Bruhwiler, 2012], was installed in 2011. The bridge was equipped with a series of strain gauges on steel reinforcement bars in the deck slab. Two 10 mm diameter bars in the transversal direction and two 12 mm diameter bars in the longitudinal direction in the bottom layer of the deck slab reinforcement were instrumented. The three strain gauges arrangement on the transverse bars (S1a to S2c) shown in Figure 5.7(b) capture the movement in the positive transverse bending moment in the deck slab which is dependent on the vehicle lane position. The sensors S1c and S2c closest to the vehicle wheels experience very sharp strain peaks when directly exposed to each axle. Figures 5.7(c) and 5.7(d) illustrates an example of the passage of a 60 tonne truck passing over the bridge.

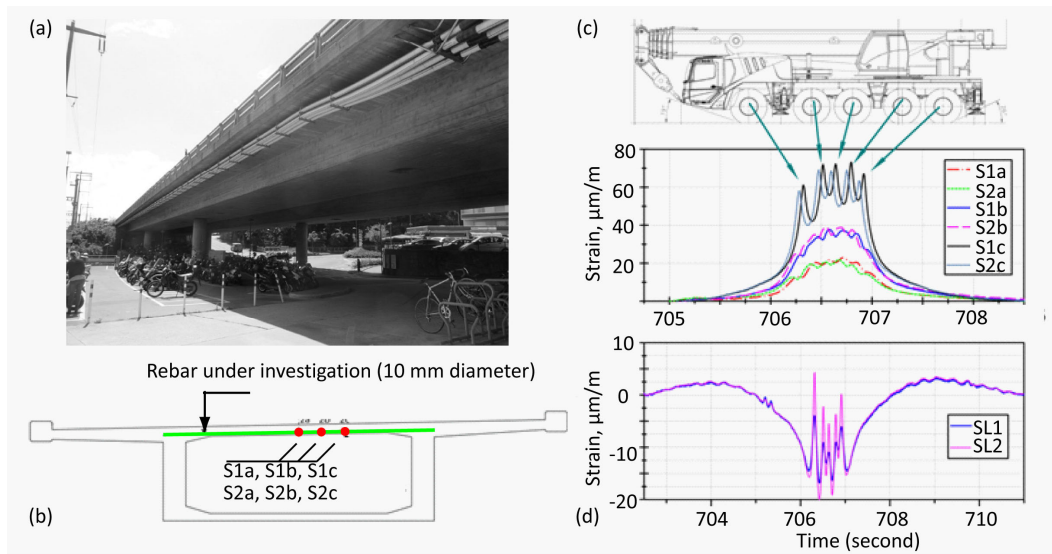


Figure 5.7: Signature of extreme vehicle seen as: (a) Morge Bridge, (b) Cross section of box-girder and gauge arrangement, (c) Influence on transverse reinforcing bar tensile strains and, (d) Influence on longitudinal bar strains, Reproduced from [Treacy and Bruhwiler, 2012]

Finite element software ANSYS was used to analyze the structure, and 8-node shell elements were used to mesh the concrete box-girder. In order to analyze the local effects, the model has been carefully meshed into element with size of 50 mm by 50 mm at the locations under investigation with a coarser mesh throughout the global model (see Figure 5.8). A unit load of 10 kN (approximately 1 tonne) was applied on the deck to a square area of 400mm x 400 mm to simulate a typical tire contact area, and the load moved along both longitudinal and lateral direction with a step of 0.1 m in the area close to sensor position and a larger step for area away from the sensor. Through this numerical analysis, the influence line of truck loads on stresses in rebars in the deck slab can be examined. In Figure 5.9, the transverse stress on the top face of deck is plotted at location of sensor S1a. The local concentration of the transverse stress is clearly shown, the track riding exactly over the sensor generates a larger transverse stress than other tracks. The strain is remarkably reduced when the loading position is away from the sensor position, a load positioned further than 2 m away has a negligible contribution to the effect. It should be noted that in the presented case the stress amplitude induced by the load is small compared to the strength of the reinforcement. For other cases of reinforced concrete bridge decks, Zanuy et al. [2011] report the risk of fatigue due to lightly reinforced concrete bridge decks; Fu et al. [2010] state that repeated truck wheel loads may cause cracks to become wider, longer, and more visible in concrete bridge decks, although the magnitude of transverse stress is low. Hence, it is an interesting task to further investigate the influence of vehicle lateral position on lightly reinforced concrete bridge decks or damaged reinforced concrete bridge decks.

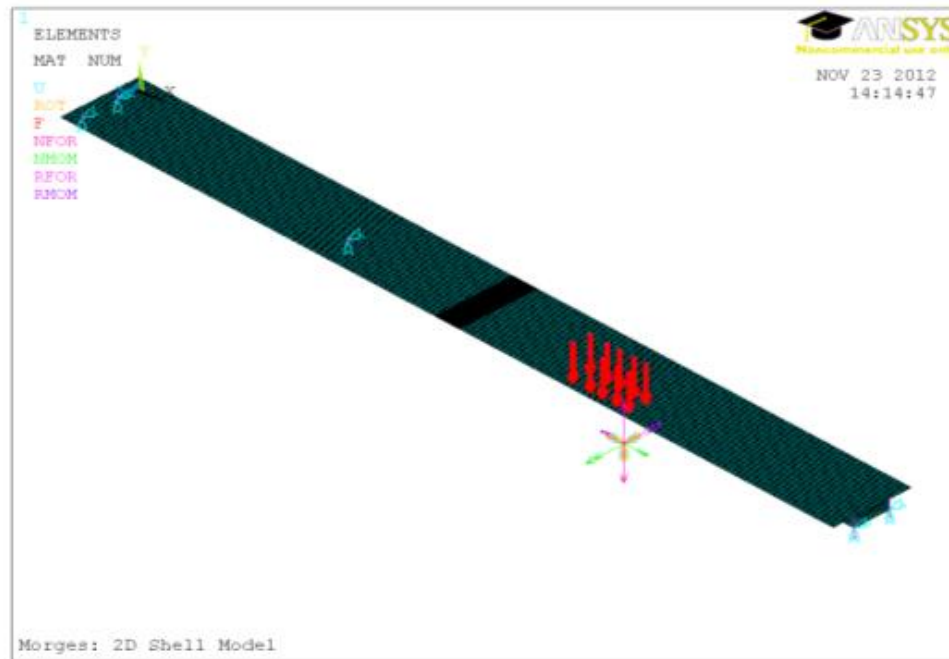


Figure 5.8: Finite element model for Morge bridge

5.5 Sensitivity of Local Effects to Vehicle Lateral Position Case II: Orthotropic Bridge Deck

The Millau Viaduct (Figure 5.10a) has been chosen as an example of an orthotropic steel deck. It is a multi-span cable-stayed bridge located in Southern France. The main girder was designed as a closed box with trapezoidal cross section with an all-welded orthotropic roadway deck, with a structural depth of 4.2 m and width of 32 m, which carries 2 lanes and an emergency lane in each direction (see Figure 5.10b for a cross-sectional view). The pavement overlay is composed of a 3 mm thick waterproofing layer and a 70 mm thick bituminous surfacing layer. The deck of the bridge consists of a deck plate of thickness, $t = 12 - 14$ mm (14 mm for deck under slow lane and $t=12$ mm for other lanes), and trough stiffeners with a wall thickness of 6 mm at a distance of 600 mm. The troughs are 300 mm wide at the top and 200 mm at the bottom, and they are 300 mm deep. Thus, the deck is uniformly supported every 300 mm by a trough wall in transversal direction and 4 m in longitudinal direction.

The transverse stress distribution in the deck is of interest in this study. It can be estimated with the third system described in American Institute of Steel Construction [1963], where a partial structure is modeled instead of the whole bridge structure. 3D shell elements are frequently used to carry out such structural analysis [Cullimore and Smith, 1981; Xiao et al., 2008]. FE model was developed for the deck under slow lane that consists of the seven trapezoidal ribs supported by four transverse floor beams. Figure 5.11 shows the model using the finite-element analysis software ANSYS. Troughs and decks were modeled by using linear elastic

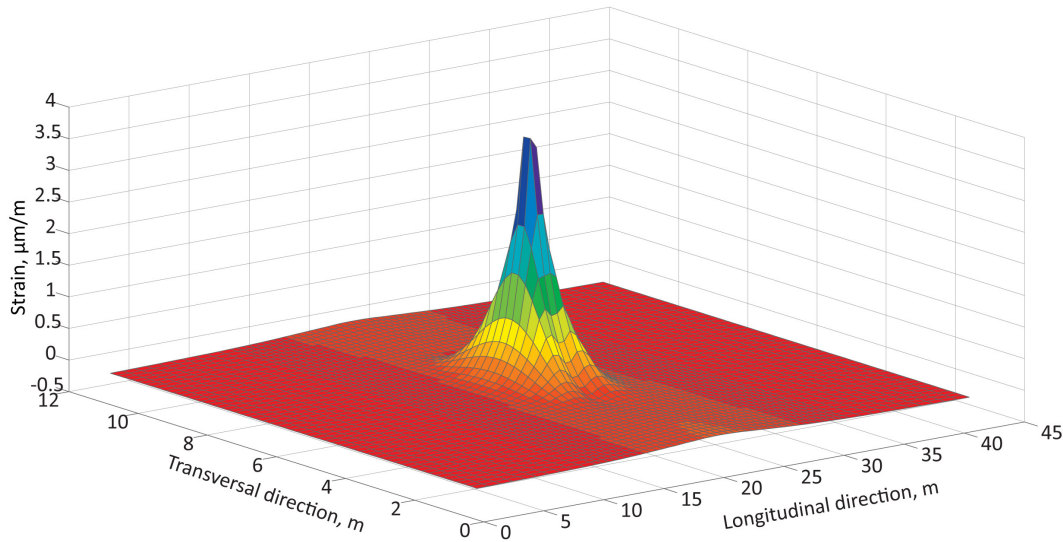


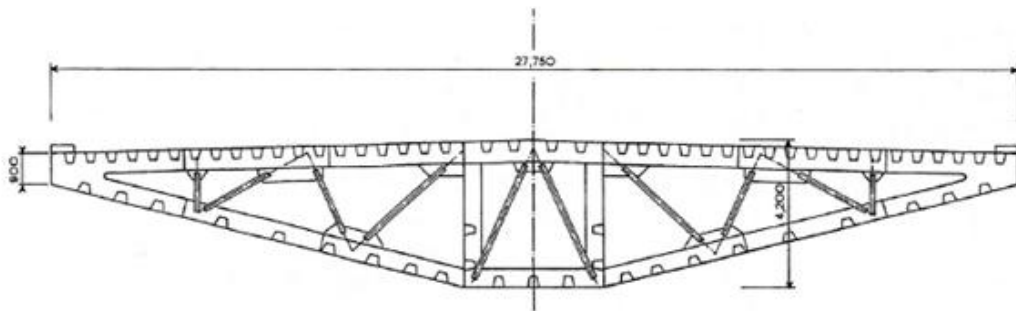
Figure 5.9: Change of transverse strain on the rebar at sensor position S1A

three-dimensional shell elements where four nodes placed in the same plane define a plate. The element is capable of accounting for in-plane tension/compression, in-plane/out-of-plane shear and out-of-plane bending behaviors. In balancing between computation time and result accuracy certain elements of the structure have been designed with a finer mesh. The three inner troughs and the deck between them are the focus of modeling and have been meshed with 25 mm by 25 mm elements. The other parts have been meshed with 50 mm by 50 mm elements. The steel has been considered as isotropic linear elastic with classical parameters values (Young's modulus of 210 GPa and a Poisson's ratio of 0.3). The deck plates were restrained for vertical translation (z-direction) at the two longitudinal boundaries and were allowed to rotate, they were restrained against vertical and transverse translations (z- and y-directions) and were allowed to rotate around the y-axis to model continuous or overhanging floor beams extending beyond girder webs.

This sensitivity study shows how the lateral eccentricity can benefit the examination of such structures. Three types of tire of single wheel for steer axle, dual wheel, and single wheel are very common for trucks on European roads, they correspond to different sizes of wheel loaded area. Assuming that the load distributes to the vertical in an angle of 45° and the 74 mm bituminous surfacing layer is rigid, the distribution area on the steel plate for the three tires are 368 mm by 450 mm, 688 mm by 450 mm, and 428 mm by 450 mm, respectively, see in Figure 5.12. To investigate the stress influence line for the locations of concern, two models of wheel load paths have been considered. One moves the wheel load along the longitudinal direction, and the other one runs along transverse direction. The wheel load is simulated crossing along 37 paths in the transverse direction and 99 tracks in the longitudinal direction on the deck, thus 3663 cases of wheel loads were considered for each type of wheel. Most of the load cases were distributed over the inner three ribs of the second span. In this particular area, the load has been moved with steps of 0.1 m in longitudinal direction and 0.075m in



(a) General view of Millau viaduct.



(b) Cross-sectional view of the steel deck of the Millau Viaduct.

Figure 5.10: Millau viaduct

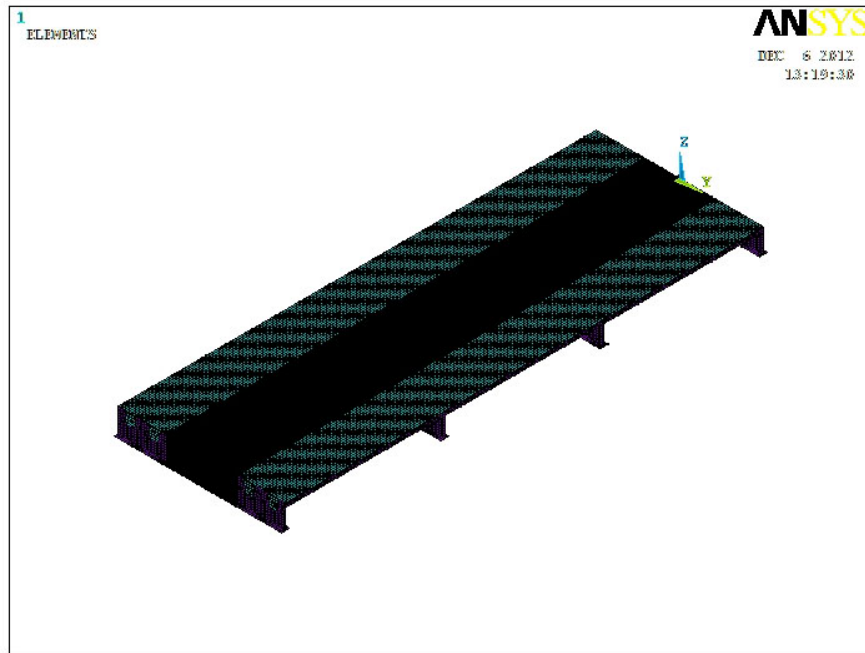


Figure 5.11: Simplified finite element model of an orthotropic steel deck

transverse direction.

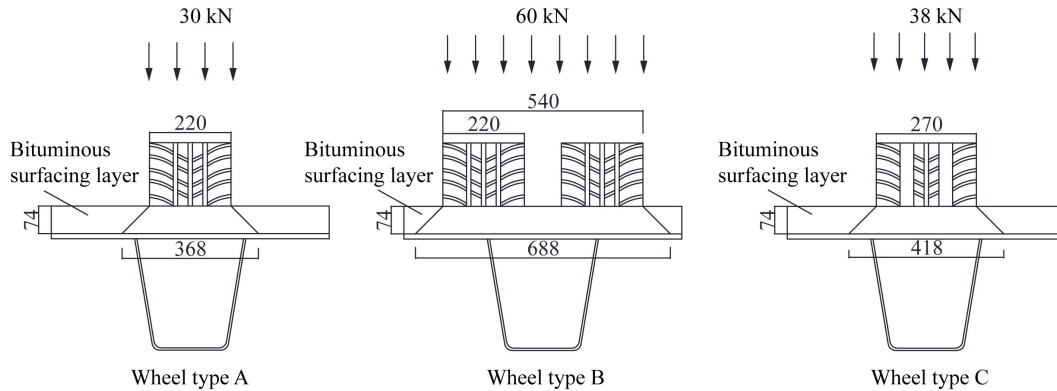


Figure 5.12: Load distribution through the wearing cover (unit: mm)

5.5.1 Results for Transverse Bending Moment

The longitudinal influence lines for several stresses at mid-span in between the second and third cross beam are presented in Figure 5.13. Similarly transverse stress we displayed on Figure 5.14. In the figure, the ordinate shows the stress in different parts of the deck and the abscissa is the load position along longitudinal direction. Previous studies have shown that the longitudinal influence lines have a similar shape for wheel load along different longitudinal

5.5. Sensitivity of Local Effects to VLP Case II: Orthotropic Bridge Deck

paths [Xiao et al., 2008], therefore, the influence lines under wheel loads riding over the joint were shown as the representatives. For the stress on the deck bottom surface, two locations were of interest as they may be susceptible to fatigue crack. "Deck Outer" in Figures 5.13 and 5.14 refers to the deck plate outside of the trough wall, while "Deck Inner" refers to the deck plate inside the trough wall. Stresses at the location "Deck Outer" may be associated with fatigue crack that initiates at the weld toe on the bottom surface of the deck plate and propagates upward into the deck plate. Stress at "Deck Inner" may be associated to fatigue cracks that initiate at the weld root and also propagate upward into the deck plate Kolstein [2007]. Three stresses on trough web were considered in this study. "Trough upper" in Figures 5.13 and 5.14 refers to trough wall at the trough-to-deck joint. Stresses at this location may be associated to fatigue cracks that initiate at the weld toe on the web. "Trough side" and "Trough bottom" refer to stiffener splice joint. Longitudinal stresses at these locations may be associated to fatigue cracks Kolstein [2007]. Usually cracks are initiated at the toe of the weld, but sometimes they can initiate at the root. The type of modeling approach is concerned with the global behavior and does not include the weld geometry in this work. The stresses presented later represent the stresses near rib-to-deck intersection rather than exact rib-to-deck joint.

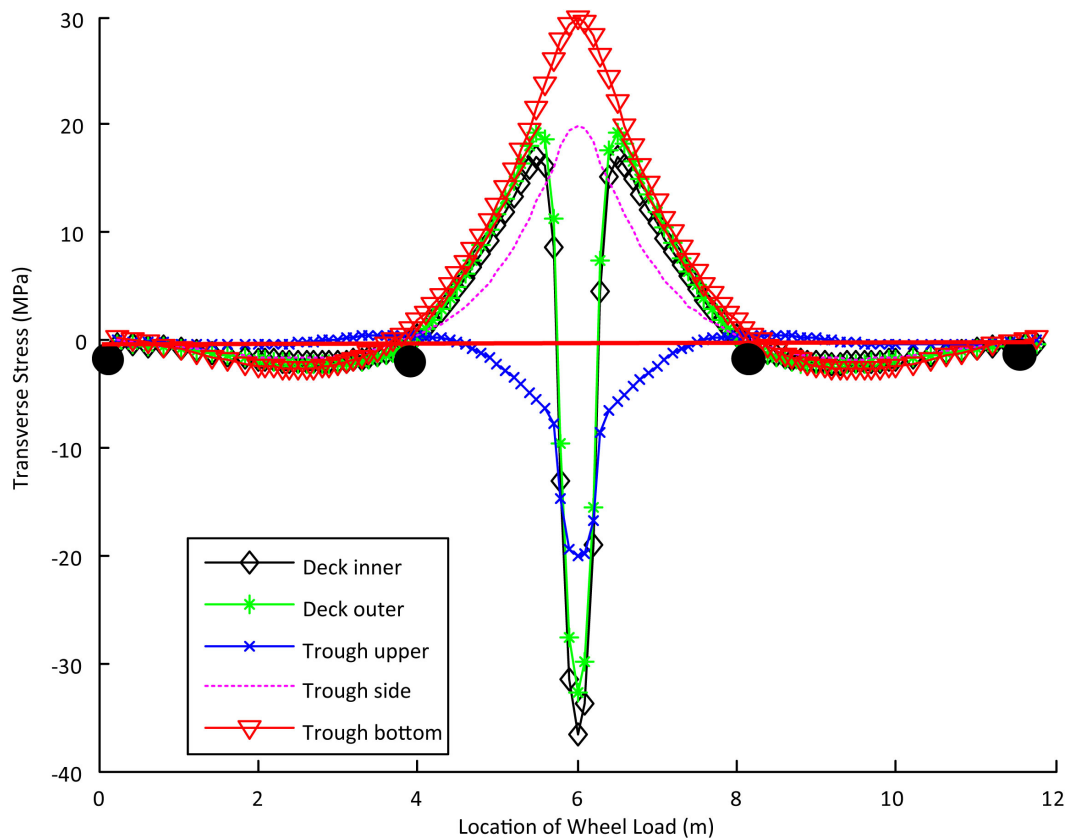


Figure 5.13: Longitudinal influence line

As shown in Figure 5.13 all the stresses longitudinal influence lines are very short, and the

stresses outside the range of middle span are small and can be neglected. The further the wheel load away from the considered joint, the smaller the stresses generated. The maximum stress range always occurs when the wheel load is close to the section. The stress completely change from tension to compression when the load gets close to the section. A stress range of 53.7 MPa has been obtained for "Deck Outer" under the over-rib wheel loads. The wave of the transverse stress at "Trough upper" has been given in the figure with green line for the over-rib loads. The stress range of 20.6 MPa is much smaller than those of the deck plate under the same load. The influence lines for stresses with respect to trough splice joint on "Trough side" and "Trough bottom" are also given in the figure.

In Figure 5.14 it is clearly indicated that the stresses in the trough web and the deck plate are significantly reduced as the loading location moves away from the object joint, and all the stresses become zero when the loading location is around 600 mm away. For the two stresses ("Deck Outer" and "Deck Inner") on deck plates' bottom surface, both stress ranges disappear rapidly as the loading location moves away from the joint. The over-rib wall loads ($e=0$) generate the largest stress or stress range. The stress wave on the trough wall at "Trough upper" due to wheel load's transversal move fluctuates significantly. The trough wall experiences compression when the loading is located at the left side of the trough wall, while a tensile stress is generated when the loading is at the right side. The maximum tension or compression stress occurs when the loading location is about 200 mm away from the rib-to-deck joint rather than when it is located just over the rib. The stress at "Trough side" and "Trough bottom" had similar feature as the stress on the deck plate near the joint that reaches peak values as the wheel load moves over the section of stress investigation, and significant stresses appear only when the wheel is rather close.

These results show that the loading location has a very significant influence on the investigated stresses. In order to quantify fluctuation of stress waves with loading location, the stress generated for various loading locations have been compared with those generated when the load is exactly located over the investigated object. While the load over the deck at the location considered generates peak values for the stresses at "Deck Outer", "Deck Inner", "Trough side", and "Trough bottom", the stresses are reduced when the loads moves away as displayed in Table 5.2. When the loading location is 300 mm away, the stress have been shown to be reduced by more or less half, and most of them reduced by 100% when the loading location is 450 mm away. In addition, the stresses reduce much faster when the load moves away in right (or inside trough) than in left (outside trough). The stress at "trough upper" is the most sensitive to the loading location among the five investigated.

5.5.2 Discussion

The longitudinal influence lines for the several joints frequently considered as susceptible to fatigue shown in Figure 5.13 emphasize the critical effect of wheel loads on orthotropic steel decks. Particularly, when a load crosses over, its transverse location has a significant

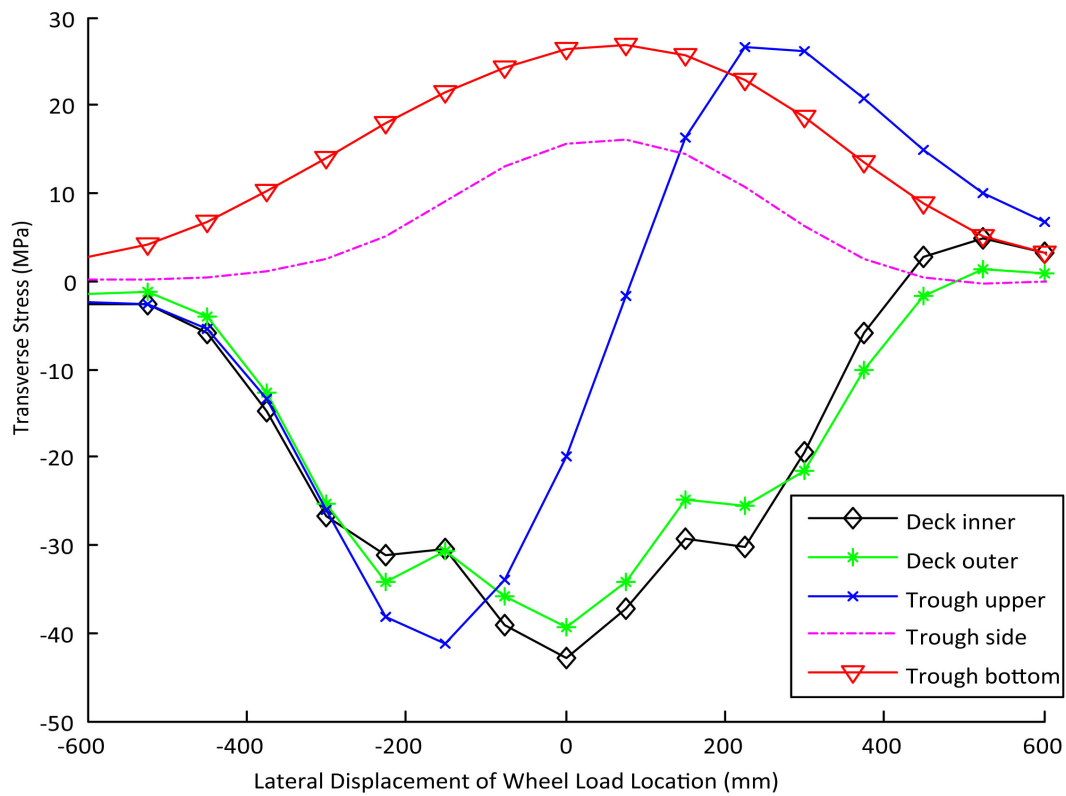


Figure 5.14: Transverse influence line

influence on the amplitude of the induced stress range. Namely, because of the localized stress concentration, it was used to weigh the vehicles passing over as a bridge weigh-in-motion (BWIM) system [Dempsey et al., 1998; Jacob et al., 2010]. In Figure 5.14, the stress on bottom surface of deck plate "Deck Inner" and "Deck Outer" that near rib-to-deck is subjected to large compression. The compression stress reduces as the loading moves away from the joint in transverse direction. The stress on trough wall near the rib-to-deck joint ("Trough upper") changes from tension to compression as the loading location varies from the joint. The trough wall is subjected to axial compression when the loading acts on the joint, thus the transverse stress is much smaller. The trough wall is subjected to positive or negative bending when the loading location is away from the joint position, thus the trough wall is subjected to tension or compression. The relative differences listed in Table 5.2 indicate that the loading location should be very precise, for instance, a 150 mm shift of the loading location leads the stress on deck plate to be reduced by about 40%. Therefore, the location of the loading should be known as accurately as possible for a safety assessment of such orthotropic bridge decks, otherwise the stresses are possibly either over- or under-estimated.

Fatigue resistance of rib-to-deck welded joints can be affected by several parameters, including loading location, deck and rib plate thicknesses, weld penetration ratio, fabrication procedure, and pavement topping layer [Sim and Uang, 2012; Xiao et al., 2008]. Among them the influence of loading location has been parametrically studied using the finite element model

Table 5.2: Stress (relative percentage difference, %)

Deviation (mm)	Deck Outer	Deck Inner	Trough upper	Trough side	Trough bottom
-600	-80.3	-84.6	-66.1	-98.6	-81.4
-450	-68.9	-75.2	-42.9	-91.4	-59.0
-300	-18.3	-16.4	59.9	-66.3	-30.2
-150	-22.1	-15.1	125.8	-20.4	-7.2
0	0	0	0	0	0
150	-38.5	-43.0	-202.7	-25.2	-15.8
300	-59.4	-44.0	-265.3	-70.9	-48.5
450	-114.8	-98.5	-206.1	-92.4	-77.3
600	-113.9	-104.5	-154.1	-96.5	-88.4

previously described. Moreover, load effects induced by the combination of traffic data and corresponding influence surface have been statistically analyzed. In the following, we use the traffic data collected from SJDV as a typical feature of highway traffic in France. For instance, the most standard 5-axle truck on European roads, the distribution of loads for each type of axle is presented in the form of a histogram (see Figure 5.15).

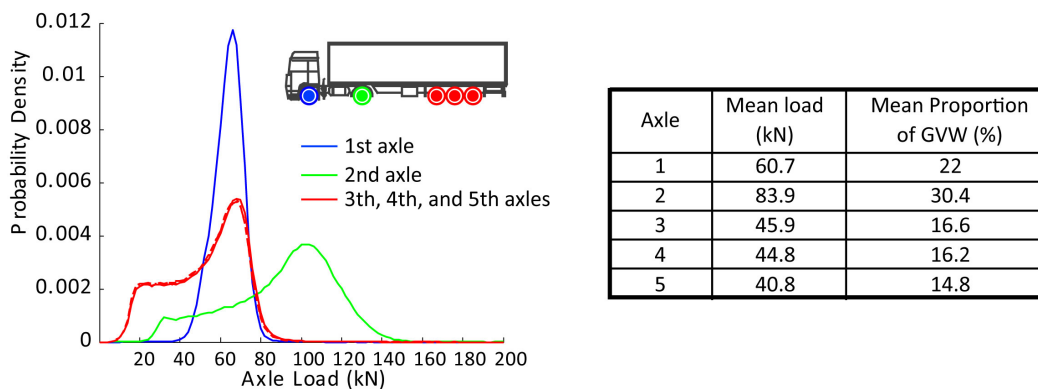


Figure 5.15: Histogram of individual axle loads for standard 5-axle truck

To identify the position of local damage on the steel deck caused by vehicle load for different distributions of transverse location, the peak points and valley points of the stress time-history for the fatigue susceptible points were first determined by simulation of vehicles crossing over the influence surface. By executing the rainflow cycle counting technique to the stress time history data, a stress spectrum was obtained. Figure 5.16 shows the histogram of the two stress spectra for "Deck Outer" attained from traffic with setting the mode of measured distribution and Eurocode recommended distribution of vehicle lateral placement at the same position above the rib-to-joint connection. It can be seen that traffic with EC1 vehicle lateral placement model generates more number of cycles for larger stress amplitude while the measured model provides more number of cycles for smaller stress amplitude. The comparison provides an evidence that the distribution model of transverse location of truck has noticeable influence on the calculated stress spectra.

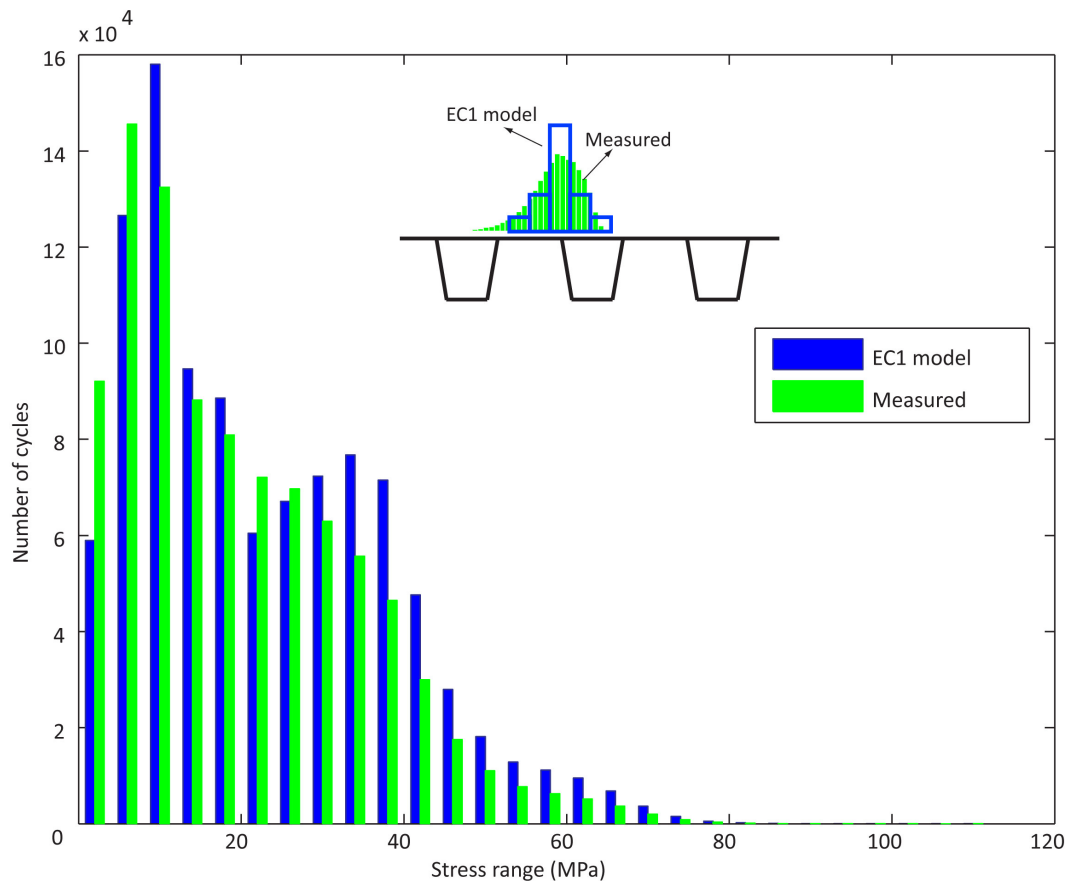


Figure 5.16: Histogram of stress spectra under traffic load with EC and measured vehicle lateral position model

According to Eurocode, the model of transverse location of vehicles should be centered to notional lanes assumed to be located anywhere on the carriageway for safety reasons, assessment has to be carried out with peak of the distribution located at the most critical location with respect to the effect considered. A sensitivity study was thus carried out to analyze the influence of notional lane position on the cycles of previous studied stress at "Deck outer". The centerline of notional lane moved from 25 cm left to 25 cm right to the considered rib-to-deck connection in a step of 5 cm. Histograms of stress spectra under traffic with EC and measured vehicle lateral placement model for each notional lane case are given in Figure 5.17. The Figures 5.17a and 5.17b give the results for the notional lane centerline at left side of the rib-to-deck connection and at right side, respectively, for Eurocode recommended transverse location model. The Figures 5.17c and 5.17d give similar results but from measured vehicle lateral position distribution model. In each figure, the histogram of stress spectra from wheel path located directly over the rib-to-deck connection is given as an reference. In general, the number of stress cycles reduces when the wheel load away from the considered rib-to-deck connection for both EC recommended and measured model of vehicle lateral position. However, differences can be found between EC1 and measured model as the EC1

has the almost the same influence between the notional lane shift to left and right, while the influence is different between left and right shift of notional lane for measured model.

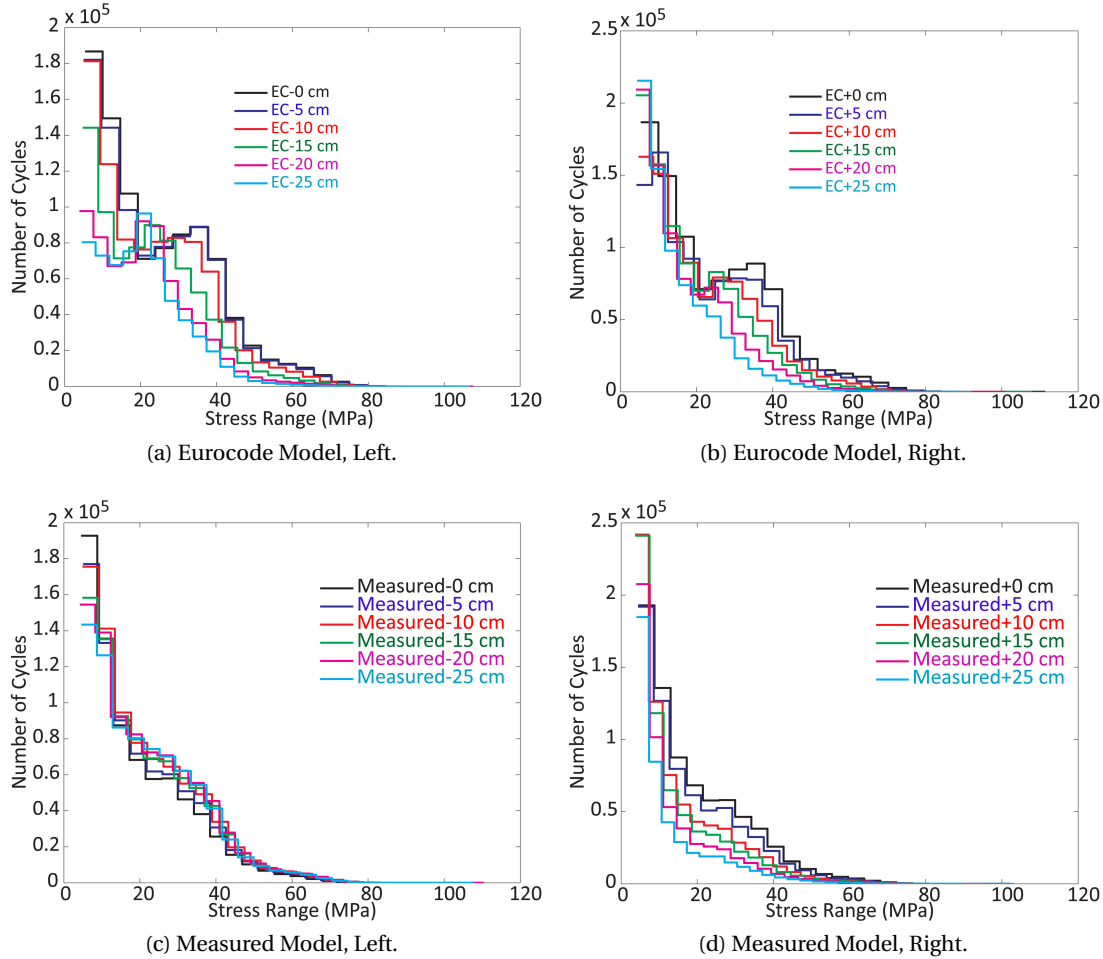


Figure 5.17: Comparison of histograms of stress spectra under traffic load with EC and measured vehicle lateral position model

5.5.3 Fatigue Damage Assessment

To examine the fatigue state of the joint when the distributions of transverse location of vehicle are different, the fatigue damage degree for the joint has been calculated by applying Miner's rule. In order to calculate the cumulative fatigue damage on a structural component by the Miner's rule, the number of repetitions to failure of the specified stress ranges is needed. This information is obtained from the S-N curves or S-N relationships, which are established from the experimental results for different materials and different categories of welded details. Each connection detail subject to fluctuation of stress should, where possible, have a particular class designated in EC3. The detail of the welded joint of rib-to-deck intersection is categorized as

5.5. Sensitivity of Local Effects to VLP Case II: Orthotropic Bridge Deck

class 50 or 71 in EC3 depending on the type of welding.

Five loading cases have been established by combining the distribution models of transverse location of vehicle and vehicle widths (Figure 5.18): (Case 1) Constant vehicle width and no deviation, (Case 2) Constant vehicle width and EC1 deviation, (Case 3) Measured vehicle width and EC1 deviation, (Case 4) Constant vehicle width and measured deviation, and (Case 5) Measured vehicle width and measured deviation. The wheel load measurements from SJDV were used to simulate the traffic load effects induced by these five cases. The array of peaks valleys were obtained by the rain flow counting method, and the cycles of stress range were counted for stress amplitude and the resulting histograms are given in Figure 5.19.

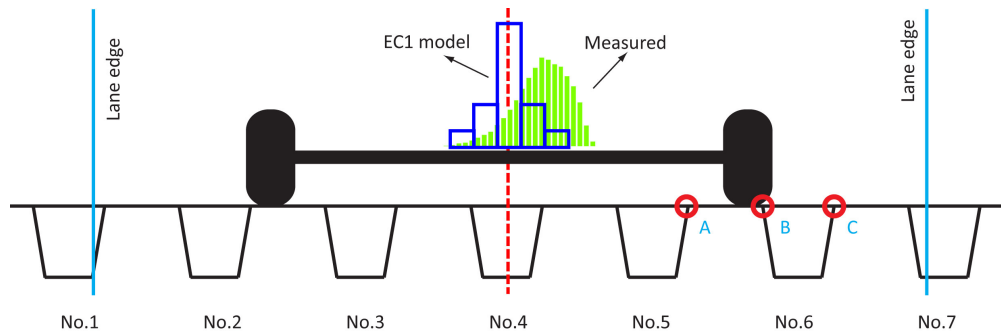


Figure 5.18: Transverse distribution of wheel path

Table 5.3: Cumulative fatigue damage in rib-to-deck joint under SJDV traffic

Case	Cumulative Fatigue Damage		Relative Difference (%)	
	Cat 50	Cat 71	Cat 50	Cat 71
1	1.32E-02	5.23E-03	40.6	52.44
2	9.36E-03	3.43E-03	0	0
3	9.10E-03	3.33E-03	-2.8	-2.87
4	4.46E-03	1.49E-03	-52.4	-56.57
5	4.26E-03	1.42E-03	-54.5	-58.69

Table 5.3 shows the cumulative fatigue damage for rib-to-deck joint ("Trough outer") under the five loading conditions, and the relative percentage difference of calculated cumulative fatigue damage between the Eurocode recommended loading condition and other four considered conditions are presented also. In general, the case of constant vehicle width and without deviation generates the largest damage in the joint, while the case of measured vehicle width and deviation generates the lowest damage in the joint. By comparison, for same distribution model of transverse location of vehicle, the damage caused with constant width is almost the same as that caused by measured vehicle widths, although the latter case generates somewhat smaller damage. For the same vehicle width model, the damage under EC1 model of transverse location of vehicle can be one time compared with that from measured model of transverse location of vehicle. In addition, the damage caused without consideration of transverse deviation is about 40% more than that under EC1 model. Therefore, it can be

concluded that distribution of transverse location of vehicle has an obvious influence on the fatigue life of the rib-to-deck joint.

5.5.4 Induced Damage Localization

Due to the large number of welded connection details, inspecting orthotropic bridges presents unique challenges as compared to other more common bridge types. It is prudent that a sampling of welds of representative orthotropic details receive periodic inspections. These predetermined details are then monitored over time to ascertain whether the detail is exhibiting any fatigue cracking [Connor et al., 2012; Ma et al., 2008]. The predetermined details mainly are those under the wheel path. In general, when there are no measurements of wheel path, the model of transverse distribution in the specification is used. However, it will over- or under-estimate damage as the stresses on orthotropic steel decks are very sensitive to the transverse loading location.

Table 5.4: Localization of cumulative fatigue damage

Category	Cumulative Fatigue Damage with different distribution models of transverse location of vehicle					
	EC1			Measured		
	A	B	C	A	B	C
Cat 50	2.11E-03	9.36E-03	1.32E-03	1.15E-03	4.26E-03	5.59E-03
Cat 71	5.17E-04	3.43E-03	3.51E-04	2.99E-04	1.42E-03	1.93E-03
Damage order	2	1	3	3	2	1

Three adjacent rib-to-deck joints, named A, B, and C in Figure 5.18, near the wheel location have been selected to evaluate the influence of transverse distribution on the damage induced. The wheel load measurements at SJDV combined with the two transverse distribution models have been used to simulate the traffic load effects. The arrays of peak points and valley points have been obtained by the rain flow counting method, and the cycles of stress ranges have been counted to calculate fatigue damage accumulation. The calculated cumulative damage levels by using Miner's rule for each joint are listed in Table 5.3. As expected, the fatigue damage levels are quite different between the two models for each joint. The EC1 model generates about two times larger damage on joint A and B, while the measured model induces around 4 times more damage on joint C. In addition, the largest damage for EC1 case is joint B, but joint C may be the first to experience fatigue cracking for a traffic distribution corresponding to SJDV measurements. For EC1 model, the damage is concentrated on the joint B, while the joints B and C have equivalent damage for measured model. It gives a significant different picture for these two transverse distribution models, thus it will generate quite different inspection program, should such calculations be used as part of an inspection approach.

5.5. Sensitivity of Local Effects to VLP Case II: Orthotropic Bridge Deck

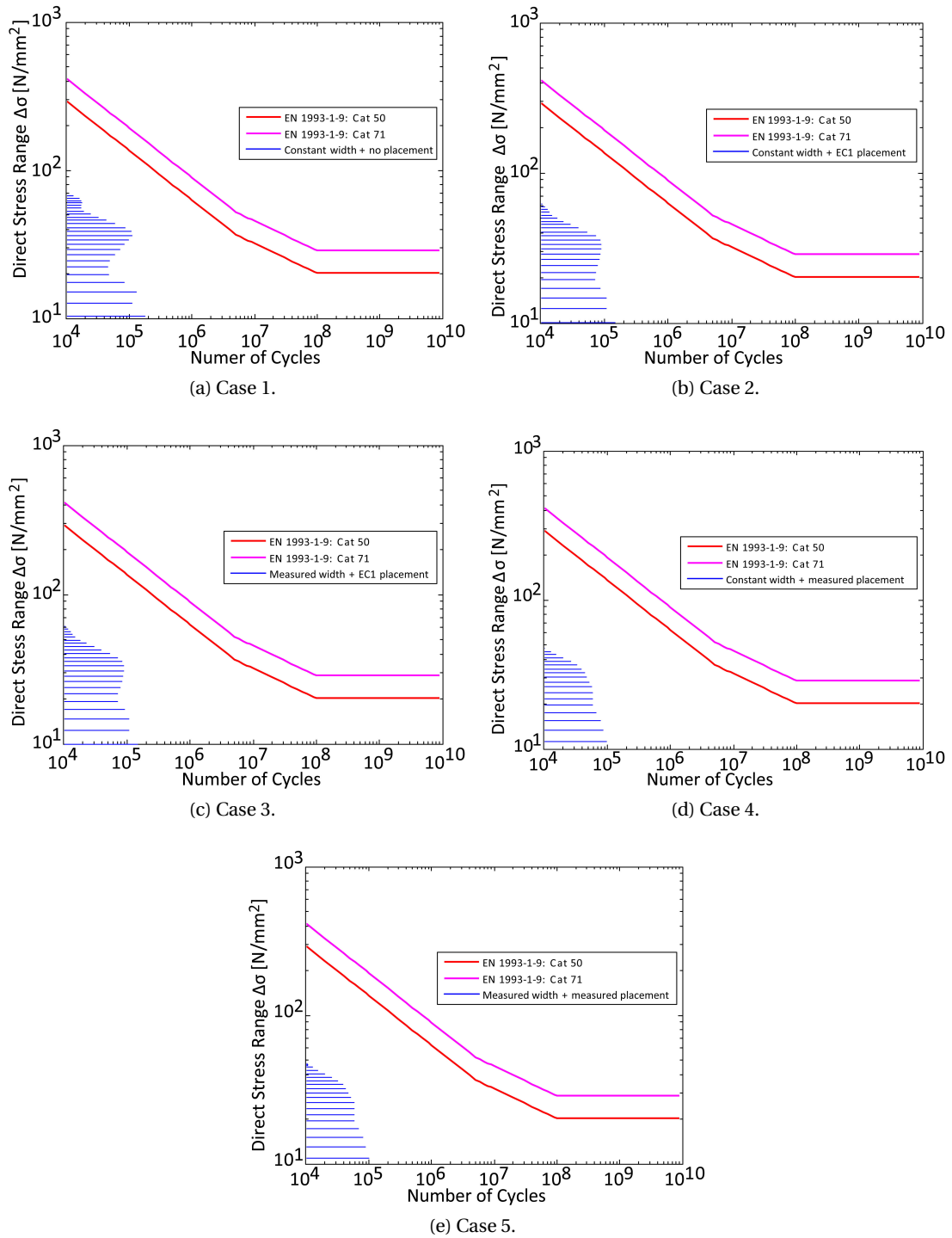


Figure 5.19: Stress histograms plotted on Eurocode S-N curves

5.6 Conclusion

Measured datasets of transverse location of vehicle center lines were collected from four highway sites in France using weigh-in-motion system. The measurements showed that the distribution of transverse location of vehicle center lines is different from the model recommended in EC1, and also different from the commonly used normal distribution in references. Three sets of data were from expressways, and the other was from a national highway. The three motorway datasets showed similar statistical feature such that the trucks tend to maintain a driving position towards to the right side with a shift from lane center line, while the data from national highway exhibits a contrary trend that trucks transverse locations shift to the left side of lane center line. The analysis indicates that the difference arises from the profile of lane cross section. Sensitivity analysis also showed that the transverse distribution is related to the vehicle speed but is insensitive to the type of vehicle. The number of sites available is inconclusive to provide generalized distributions of the lateral 'in lane' positioning of trucks but highlights the importance of obtaining local data and assessing local features of the road geometry and bridge environment in such analyses.

To investigate the influence of transverse distribution of vehicles on bridge traffic load effects, two types of bridge decks were selected. One is an orthotropic steel deck as the local effects in orthotropic steel decks are governed by wheel loads [Cullimore and Smith, 1981], the other is a reinforced concrete deck as fatigue assessment of such structures may be relevant [Fu et al., 2010]. Finite element analyses of the bridges have shown the localized stress/strain at loading location. However the amplitude of strain in the concrete deck reinforcement is very small because of design requirements for global behavior. A refined stress analysis was conducted on the orthotropic steel deck. Transverse distribution of loading was shown to generate significant out-of-plane bending moments at the rib-to-deck joint. Bending stresses were dominant on deck plate and rib. For the several frequently reported fatigue crack susceptible joints, the influence of transverse location of loading on their stresses has been evaluated. The transverse stress on rib wall near rib-to-deck is most sensitive to loading location.

By integrating measured traffic load and transverse location of centerline of vehicles on lane, the stresses induced by traffic considering vehicle lateral position were obtained. The statistical analysis performed on the stress spectra revealed that transverse distribution of wheel loads has a significant influence on fatigue damage induced by traffic. For instance, the damage on a rib-to-deck joint generated by using the transverse distribution of EC1 is twice as large as that with a measured transverse distribution model considering also the bias in mean vehicle position. Due to the large number of welded connection details, it may be relevant to identify. Sample connections prone to fatigue to represent the health of the deck. This can be achieved using realistic vehicle in-lane position simulations. From fatigue calculations of critical details, potential fatigue cracking connections can be identified by using precise transverse location of the wheel center although this identification may be quite sensitive to the traffic locations assumption. Knowing the distribution of transverse wheel location within lanes is thus important not only for assessing fatigue life of orthotropic decks but also

for developing maintenance strategies.



Conclusions and Perspectives

Conclusions of the Thesis	169
Perspectives for Future Research	171

This thesis presents a statistical analysis of traffic load effects for the evaluation of the structural safety of existing road bridges with the final goal of improving existing techniques for the management of bridges. The following tasks were carried out as steps to achieve this objective:

- Review current existing methods for modeling maximum traffic load effects and propose ways to improve some prediction methods to obtain more accurate estimates.
- Investigate the parameter estimation methods for generalized Pareto distribution, and give guidance for selecting estimations in applying POT methods to bridge traffic load effects.
- Develop a method to improve the statistical analyses for lifetime load effect when the loading events can be identified.
- Investigate the influence of distribution of transverse location of vehicles on bridge traffic load effects that governs the loading capacity and local safety.

Conclusions of the Thesis

Interesting results have been obtained during the work which was carried out in order to achieve the previously presented aims. The main results are given in this section with respect to these aims.

- Many different methods have been used in the literature to model bridge traffic load effects. These methods include fitting distribution (Normal, Gumbel, Weibull) to tail, extreme value modeling methods and level crossing method, and all of them concern the tail behavior. The early stage used method of fitting distribution to tail needs to pre-determine type of distribution, subjective judgments are thus involved in the estimation. The same problem exists in applying level crossing method to model bridge traffic load effect as it assumes the traffic load effect process to be stationary and Gaussian. In recent years, extreme value theory based block maximum method has gained a lot of attention and has been applied to model bridge traffic load effects. However, many applications of BM method have been found to fit extreme value distribution to upper tail of block maxima rather than the whole observed block maxima. It apparently lacks theoretical ground and needs subjective judgment to determine the fraction of tail to be fitted. Actually, another extreme value theory based method named peaks over threshold (POT) can achieve this goal with concrete theoretical support. The POT method has been widely used in other disciplines, in place of BM method for modeling extreme values but has less application in modeling bridge traffic load effect.
- To quantitatively evaluate performance of these existing methods on modeling extreme value distribution, numerical simulation sample from a Normal distribution and traffic load effect data generated by Monte Carlo simulation have been used. The evaluation is

based on 75-year characteristic value and annual probability of failure, and results are presented in Chapter 2. Although the results indicate that no one of the investigated methods provides accurate estimates for characteristic value or annual probability of failure, the approaches fitting distribution to tail have better performance than other methods for numerical sample and the POT method shows better performance for Monte Carlo simulated traffic load effects. Additionally, the methods generally have better performance on characteristic value estimation than annual probability of failure.

- As concluded in Chapter 2, POT method has the best performance for modeling extreme bridge traffic load effects. To further introduce the POT method and to improve its performance, a comparative study has been carried out in Chapter 3 on the performance of parameter estimation methods. Although maximum likelihood estimation is the most widely used method, other methods like method of moments actually have better performance in situations like samples with small size. A number of parameter estimation methods have been investigated, and numerical sample and traffic load effect data are used to evaluate their performance. Results presented in Chapter 3 show that no method has always better performance than others, but methods like MM, PWM, ML, PML and ADR have well performance. In additional, the MDPD method has better performance for bridge traffic load effect data than numerical samples.
- Literature has shown that load effects due to different compositions of loading event are not identically distributed, thus standard extreme value theory can not be used in its strict validity domain for modeling the maximum traffic load effects. A composite distribution statistics method has already been proposed in the literature based on block maxima method. In chapter 4, a new method termed mixture peaks over threshold has been developed which accounts for the different parent distribution of load effect, and combines them to determine the characteristic load effect.

Theoretical studies were firstly used to verify the mixture peaks over threshold (MPOT) approach against the conventional peaks over threshold (CPOT) approach. It was shown for several examples that the MPOT corresponds to the exact distribution far more closely than the CPOT approach. In addition, the MPOT approach was also compared with the composite statistics distribution method proposed by Caprani et al. [2008], the results indicate that these two methods have similar performance and provide more accurate results as compared to the traditional methods.

The MPOT method is applied to full traffic simulations on a range of bridge lengths and load effects. It is shown that some types of loading events tend to govern certain lengths and load effects, and that this result is dependent on the physical nature of the bridge loading problem. The differences between the conventional and the mixture approach are great especially for longer span, it seems that the applications have greatest difference on the load effects for 40 m span.

- Measurements of transverse location of vehicles on four French highways were collected by WIM systems in 2010 and 2011. The measurements showed a completely different

distribution model of transverse location of vehicle to that recommended in EC1. In order to evaluate the influence of the distribution of the transverse location of the vehicles on load effects of the bridge deck, finite element analyses were carried out to model the Millau Viaduct in France which has an orthotropic steel deck and a prestressed concrete box-girder bridge in Switzerland. The Millau case is extended further to assess the influence of transverse location on fatigue life. The sensitivity of stress to the loading location was evaluated, and the influence surface of stresses for critical joints, which are susceptible of fatigue cracking, is obtained. Stress spectrum analysis and fatigue damage calculation are performed using the calculated stresses induced by traffic. By comparing the stresses and damages induced by different traffic patterns (through distributions of transverse location of vehicles), it is found that the histogram of stress spectrum and cumulative fatigue damage are significantly affected by the distribution.

Perspectives for Future Research

The modeling of extreme bridge traffic load effects is a necessary part of the evaluation of existing highway bridges. There is thus space for further work which would complement this thesis:

- As it has been emphasized, POT method has been successfully used in disciplines like hydrology, insurance and etc., but limited study can be found on its application to bridge traffic load effects. The possible reasons are (i) the traffic load effects are not critical to bridge structures as such river level to reservoir design and assessment, (ii) the BM method is very easy to use. However, it deserves to introduce POT method to bridge traffic load effect. In this thesis, we have dealt with one of the critical issue, which is parameter estimation, in applying POT method to bridge traffic load effect. Alternative issues of threshold selection have not been deeply discussed, there is thus a need to study the choice of threshold.
- All the existing methods for modeling bridge traffic load effects ignore the time dependency and assume stationary of the process. However, it is widely reported that traffic is increasing year by year in forms of traffic volume and loaded weight of single truck. Meanwhile, the load carrying capacity of structures decreases with the environment aggressions, degradations and natural aging. Therefore, it is necessary to study the traffic load effects with consideration of time dependency. How are the methods affected by evolution of loadings with time, when non-stationary processes are assumed?
- Although a mixture peaks over threshold method was introduced for modeling traffic load effects due to mixed loading events, it should be noticed that it is always impossible or difficult to classify load effects by their originating loading events. Therefore the mixture peaks over threshold as well as composite statistic distribution methods are not available for monitoring data in practice when loading events can not be identified.

Conclusions and Perspectives

There is thus a need to introduce more efficient and robust parameter estimation methods similar to MDPD to estimate the distribution parameters for generalized extreme value distribution or generalized Pareto distribution.

Bibliography

- American Institute of Steel Construction (1963). *Design manual for orthotropic steel plate deck bridges*. American Institute of Steel Construction Inc, New York.
- Ashkar, F. and Nwentsa Tatsambon, C. (2007). Revisiting some estimation methods for the generalized Pareto distribution. *Journal of Hydrology*, 346(3-4):136–143.
- Ashkar, F. and Ouarda, T. B. M. J. (1996). On some methods of fitting the generalized Pareto distribution. *Journal of Hydrology*, 177(1):117–141.
- Bailey, S. F. (1996). *Basic principles and load models for the structural safety evaluation of existing road bridges*. PhD thesis, Department of Civil Engineering, École Polytechnique Fédéral de Lausanne, Lausanne, Switzerland.
- Bailey, S. F. and Bez, R. (1999). Site specific probability distribution of extreme traffic action effects. *Probabilistic Engineering Mechanics*, 14(1-2):19–26.
- Bakht, B. and Jaeger, L. G. (1983). Effect of vehicle eccentricity on longitudinal moments in bridges. *Canadian Journal of Civil Engineering*, 10(4):582–599.
- Bakht, B. and Jaeger, L. G. (1987). Multi-presence reduction factors for bridges. In *Bridge and transmission line structures*, pages 17–20, Orlando, Florida. ASCE Structures Congress.
- Basu, A., Harris, I. R., Hjort, N. L., and Jones, M. C. (1998). Robust and efficient estimation by minimising a density power divergence. *Biometrika*, 85(3):549–559.
- Ben, T. Y. and WanChun, J. (2005). Stress in orthotropic steel deck components due to vehicular loads. In *Structures Congress 2005*, pages 1–4. American Society of Civil Engineers.
- Blab, R. and Litzka, J. (1995). Measurements of the lateral distribution of heavy vehicles and its effects on the design of road pavements. In *4th International Symposium on Heavy Vehicle Weights and Dimensions*, pages 389–396, Paris, France.
- Bruls, A., Croce, P., Sanpaolesi, L., and Sedlacek, G. (1996). Env 1991 - part 3: Traffic loads on bridges. In *Proceedings of IABSE Colloquium*, pages 439–453, Delft.
- Bulinskaya, E. (1961). On the mean number of crossings of a level by a stationary gaussian process. *Theory of Probability & Its Applications*, 6(4):435–438.

Bibliography

- Butler, R. (1986). Predictive likelihood inference with applications. *Journal of the Royal Statistical Society. Series B (Methodological)*, 48(1):1–38.
- Caprani, C. C. (2005). *Probability analysis of highway bridge traffic loading*. PhD thesis, School of Architecture, Landscape and Civil Engineering, University College Dublin.
- Caprani, C. C., Grave, S. A., O'Brien, E. J., and O'Connor, A. J. (2002). Critical loading events for the assessment of medium span bridges. In Topping, B. H. V. and Bittnar, Z., editors, *Sixth International Conference on Computational Structures Technology*, pages 1–11, Stirling, Scotland. Civil-Comp Ltd.
- Caprani, C. C. and O'Brien, E. J. (2010). The use of predictive likelihood to estimate the distribution of extreme bridge traffic load effect. *Structural Safety*, 32(2):138–144.
- Caprani, C. C., Obrien, E. J., and McLachlan, G. J. (2008). Characteristic traffic load effects from a mixture of loading events on short to medium span bridges. *Structural Safety*, 30(5):394–404.
- Castillo, E. and Hadi, A. S. (1997). Fitting the generalized Pareto distribution to data. *Journal of American Statistical Association*, 92(440):1609–1620.
- Castillo, E., Hadi, A. S., Balakrishnan, N., and Sarabia, J. M. (2004). *Extreme Value and Related Models with Applications in Engineering and Science*. Wiley Series in Probability and Statistics. Wiley.
- Cebrian, A. C., Denuit, M., and Lambert, P. (2003). Generalized Pareto fit to the society of actuaries large claims database. *North American Actuarial Journal*, 7(3):18–36.
- Chaouche, A. and Bacro, J.-N. (2006). Statistical inference for the generalized Pareto distribution: Maximum likelihood revisited. *Communications in Statistics - Theory and Methods*, 35(5):785–802.
- Choulakian, V. and Stephens, M. A. (2001). Goodness-of-fit tests for the generalized Pareto distribution. *Technometrics*, 43(4):478–484.
- Coles, S. G. and Dixon, M. J. (1999). Likelihood-based inference for extreme value models. *EXTREMES*, 2(1):5–23.
- Connor, R., Fisher, J., Gatti, W., Gopalaratnam, V., Kozy, B., Leshko, B., McQuaid, D. L., Mdelock, R., Mertz, D., Murphy, T., Paterson, D., Sorensen, O., and Yadlosky, J. (2012). Manual for design construction and maintenance of orthotropic steel deck bridges. Technical Report FHWA-IF-12-027, HDR Engineering Inc.
- Cooper, D. I. (1997). Development of short span bridge-specific assessment live loading. In Das, P. C., editor, *The safety of bridges*, pages 64–89. Thomas Telford.
- COST 345 (2002a). Procedures required for assessing highway structures: Final report. Technical report, European Commission Directorate General Transport and Energy.

- COST 345 (2002b). Procedures required for assessing highway structures: Working group 1 report on the current stock of highway structures in european countries, the cost of their replacement and the annual costs of maintaining, replacing and renewing them. Technical report, European Commission Directorate General Transport and Energy.
- Cowan, R. J. (1975). Useful headway models. *Transportation Research*, 9(6):371–375.
- Cremona, C. (1995). Evaluation des effets extremes du trafic sur les haubans d'un pont. *Bulletin des LPC*, 199:71–80.
- Cremona, C. (2001). Optimal extrapolation of traffic load effects. *Structural Safety*, 23(1):31–46.
- Cremona, C. (2011). The surveillance of bridges in france. In *6th International Conference on Acoustical and Vibratory Surveillance Methods and Diagnostic Techniques*, pages 1–17, Paris, France.
- Cremona, C. and Carracilli, J. (1998). Evaluation of extreme traffic load effects in cable stayed and suspension bridges using wim records. In O'Brien, E. and Jacob, B., editors, *2nd European Conference on Weigh-in-motion of Road Vehicles*, pages 243–251.
- Crespo-Minguillon, C. and Casas, J. R. (1997). A comprehensive traffic load model for bridge safety checking. *Structural Safety*, 19(4):339–359.
- Cullimore, M. S. G. and Smith, J. W. (1981). Local stresses in orthotropic steel bridge decks caused by wheel loads. *Journal of Constructional Steel Research*, 1(2):17–26.
- Davison, A. C. and Smith, R. L. (1990). Models for exceedances over high thresholds. *Journal of the Royal Statistical Society. Series B (Methodological)*, 52(3):393–442.
- de Jong, F. B. P. (2004). Overview fatigue phenomenon in orthotropic bridge decks in the netherlands. In *2004 Orthotropic Bridge Conference*, pages 489–512, Sacramento, California.
- de Zea Bermudez, P. and Kotz, S. (2010). Parameter estimation of the generalized Pareto distribution-part I & II. *Journal of Statistical Planning and Inference*, 140(6):1353–1388.
- de Zea Bermudez, P. and Turkman, M. (2003). Bayesian approach to parameter estimation of the generalized Pareto distribution. *TEST*, 12(1):259–277.
- Deidda, R. (2010). A multiple threshold method for fitting the generalized Pareto distribution and a simple representation of the rainfall process. *Hydrol. Earth Syst. Sci. Discuss.*, 7(4):4957–4994. HESSD.
- Deidda, R. and Puliga, M. (2009). Performances of some parameter estimators of the generalized Pareto distribution over rounded-off samples. *Physics and Chemistry of the Earth, Parts A/B/C*, 34(10-12):626–634.
- Dempsey, A., Jacob, B., and Carracilli, J. (1998). Orthotropic bridge weigh-in-motion for determining axle and gross vehicle weights. In *2nd European conference on Weigh-in-Motion*, pages 435–444.

Bibliography

- Desrosiers, R. and Grillo, R. (1973). Estimating the frequency of multiple truck loadings on bridges: Final report. Technical report, University of Connecticut.
- Ditlevsen, O. (1994). Traffic loads on large bridges modeled as white noise fields. *Journal of Engineering Mechanics*, 120(4):681–694.
- Dupuis, D. J. (1996). Estimating the probability of obtaining nonfeasible parameter estimates of the generalized Pareto distribution. *Journal of Statistical Computation and Simulation*, 54(1-3):197–209.
- Dupuis, D. J. (1999). Exceedances over high thresholds: A guide to threshold selection. *EXTREMES*, 1(3):251–261.
- Dupuis, D. J. and Field, C. A. (1998). Robust estimation of extremes. *The Canadian Journal of Statistics / La Revue Canadienne de Statistique*, 26(2):199–215.
- Dupuis, D. J. and Tsao, M. (1998). A hybrid estimator for generalized Pareto and extreme-value distributions. *Communications in Statistics - Theory and Methods*, 27(4):925–941.
- Enright, B. (2010). *Simulation of traffic loading on highway bridges*. Doctoral thesis, School of Architecture, Landscape and Civil Engineering, University College Dublin.
- Enright, B. and O'Brien, E. J. (2011). Cleaning weigh-in-motion data: techniques and recommendations. International Society for Weigh-In-Motion.
- Enright, B. and O'Brien, E. J. (2012). Monte carlo simulation of extreme traffic loading on short and medium span bridges. *Structure and Infrastructure Engineering*, 1:1–16.
- Eugenia Castellanos, M. and Cabras, S. (2007). A default Bayesian procedure for the generalized Pareto distribution. *Journal of Statistical Planning and Inference*, 137(2):473–483.
- European Commission (2008). *European energy and transport: trends to 2030 - updated 2007*. Luxembourg: Office for Official Publications of the European Communities, Belgium.
- European Commission (2012). *EU Transport in Figures: Statistical Pocketbook*. Luxembourg Publications Office of the European Union.
- Eymard, R. and Jacob, B. (1989). Un nouveau logiciel: le programme castor pour le calcul des actions et sollicitations du trafic dans les ouvrages routiers. *Bulletin des LPC*, pages 64–77.
- Fekpe, E. (1997). Vehicle size and weight regulations and highway infrastructure management. *Journal of Infrastructure Systems*, 3(1):10–14.
- Ferreira, A., Haan, L. d., and Peng, L. (2003). On optimising the estimation of high quantiles of a probability distribution. *Journal of Theoretical and Applied Statistics*, 37(5):401–434.
- Fisher, R. (1973). *Statistical methods and scientific inference*. Hafner Press.

- Flint, A. and Jacob, B. (1996). Extreme traffic loads on road and target values for their effects for code calibration. In *Proceedings of IABSE Colloquium on Basis of Design and Actions on Structures*, pages 469–478, Delft.
- Fu, G. and van de Lindt, J. W. (2006). LRFD load calibration for state of Michigan trunkline bridges. Technical Report Report RC-1466, Wayne State University Colorado State University.
- Fu, G. and You, J. (2009). Truck loads and bridge capacity evaluation in China. *Journal of Bridge Engineering*, 14(5):327–335.
- Fu, G. and You, J. (2010). Extrapolation for future maximum load statistics. *Journal of Bridge Engineering*, 16(4):527–535.
- Fu, G., Zhuang, Y., and Feng, J. (2010). Behavior of reinforced concrete bridge decks on skewed steel superstructure under truck wheel loads. *Journal of Bridge Engineering*, 16(2):219–225.
- Getachew, A. (2003). *Traffic load effects on bridges - statistical analysis of collected and Monte Carlo simulated vehicle data*. Doctoral thesis, Department of structural engineering.
- Getachew, A. and O'Brien, E. J. (2007). Simplified site-specific traffic load models for bridge assessment. *Structure and Infrastructure Engineering*, 3(4):303–311.
- Ghosn, M. and Moses, F. (1985). Markov renewal model for maximum bridge loading. *Journal of Engineering Mechanics*, 111(9):1093–1104.
- Ghosn, M. and Moses, F. (2000). Effect of changing truck weight regulations on U.S. bridge network. *Journal of Bridge Engineering*, 5(4):304–310.
- Ghosn, M., Sivakumar, B., and Miao, F. (2012). Development of state-specific load and resistance factor rating method. *Journal of Bridge Engineering*, in print.
- Gindy, M. (2004). *Development of a reliability-based deflection limit state for steel girder bridges*. Doctoral thesis, Graduate School-New Brunswick.
- Gindy, M. and Nassif, H. H. (2006). Comparison of traffic load models based on simulation and measured data. In *Joint International Conference on Computing and Decision Making in Civil and Building Engineering*.
- Gindy, M. and Nassif, H. H. (2007). Multiple presence statistics for bridge live load based on weigh-in-motion data. *Transportation Research Record: Journal of the Transportation Research Board*, pages 125–135.
- Gomes, F. (2012). *Influence du revêtement sur le comportement en fatigue des dalles orthotropes: étude d'une solution en BFUP*. Phd thesis, École doctorale sciences ingénierie et environnement, Université Paris-Est.

Bibliography

- Grave, S., O'Brien, E. J., and O'Connor, A. J. (2000). The determination of site-specific imposed traffic loadings on existing bridges. In Ryall, M. J., Parke, G., and Harding, J. E., editors, *Bridge management 4 - inspection, maintenance, assessment and repair*, pages 442–449. Thomas Telford Limited.
- Greenwood, J. A., Landwehr, J. M., Matalas, N. C., and Wallis, J. R. (1979). Probability weighted moments: Definition and relation to parameters of several distributions expressible in inverse form. *Water Resour. Res.*, 15(5):1049–1054.
- Grimshaw, S. D. (1993). Computing maximum likelihood estimates for the generalized Pareto distribution. *Technometrics*, 35(2):185–191.
- Guo, T., Frangopol, D., Han, D., and Chen, Y. (2011). Probabilistic assessment of deteriorating prestressed concrete box-girder bridges under increased vehicle loads and aggressive environment. *Journal of Performance of Constructed Facilities*, 25(6):564–576.
- Harman, D. J. and Davenport, A. G. (1979). A statistical approach to traffic loading on highway bridges. *Canadian Journal of Civil Engineering*, 6(4):494–513.
- He, X. and Fung, W. K. (1999). Method of medians for lifetime data with weibull models. *Statistics in Medicine*, 18(15):1993–2009.
- Hewitt, J., Stephens, J., Smith, K., and Menuez, N. (1999). Infrastructure and economic impacts of changes in truck weight regulations in Montana. *Transportation Research Record: Journal of the Transportation Research Board*, 1653(1):42–51.
- Holmes, J. D. and Moriarty, W. W. (1999). Application of the generalized Pareto distribution to extreme value analysis in wind engineering. *Journal of Wind Engineering and Industrial Aerodynamics*, 83(13):1–10.
- Hosking, J. R. M. (1990). L-Moments: Analysis and estimation of distributions using linear combinations of order statistics. *Journal of the Royal Statistical Society. Series B (Methodological)*, 52(1):105–124.
- Hosking, J. R. M. and Wallis, J. R. (1987). Parameter and quantile estimation for the generalized Pareto distribution. *Technometrics*, 29(3).
- Huang, C., Lin, J.-G., and Ren, Y.-Y. (2012). Statistical inferences for generalized Pareto distribution based on interior penalty function algorithm and Bootstrap methods and applications in analyzing stock data. *Computational Economics*, 39(2):173–193.
- Huo, X., Wasserman, E., and Iqbal, R. (2005). Simplified method for calculating lateral distribution factors for live load shear. *Journal of Bridge Engineering*, 10(5):544–554.
- Husler, J., Li, D., and Raschke, M. (2011). Estimation for the generalized Pareto distribution using maximum likelihood and goodness of fit. *Communications in Statistics - Theory and Methods*, 40(14):2500–2510.

- Hyndman, R. J. and Koehler, A. B. (2006). Another look at measures of forecast accuracy. *International Journal of Forecasting*, 22(4):679–688.
- Iman, R. L. and Conover, W. J. (1982). A distribution-free approach to inducing rank correlation among input variables. *Communications in Statistics - Simulation and Computation*, 11(3):311–334.
- Ito, K. (1963). The expected number of zeros of continuous stationary gaussian processes. *Journal of Mathematics of Kyoto University*, 3(2):207–216.
- Ivanov, V. (1960). On the average number of crossings of a level by the sample functions of a stochastic process. *Theory of Probability & Its Applications*, 5(3):319–323.
- Jacob, B. (1991). Methods for the prediction of extreme vehicular loads and load effects. Technical report, LCPC.
- Jacob, B. (2000). Assessment of the accuracy and classification of weigh-in-motion systems part 1: Statistical background. *International Journal of Heavy Vehicle Systems*, 7(2):136–152.
- Jacob, B., Bouteldja, M., and Stanczyk, D. (2008). Installation and experimentation of MS-WIM systems with three strip sensor technologies - early results. In Jacob, B., editor, *5th International Conference on Weigh-In-Motion*, pages 149–158.
- Jacob, B., Hannachi, H., and Ieng, S. (2010). *Bridge weigh-in-motion on steel orthotropic decks - Millau viaduct and Autreville bridge*, pages 209–209. Bridge Maintenance, Safety and Management. CRC Press.
- Jacob, B. and Kretz, T. (1996). Calibration of bridge fatigue loads under real traffic conditions. In *Proceedings of IABSE Colloquium on Basis of Design and Actions on Structures*, pages 479–487, Delft.
- Jacob, B., Maillard, J., and Gorse, J. (1989). Probabilistic traffic load models and extreme loads on a bridge. In *5th International Conference on Structural Safety and Reliability*, pages 1973–1980.
- Jacob, B., O’Brien, E. J., and Newton, W. (2000). Assessment of the accuracy and classification of weigh-in-motion systems: Part 2. european specification. *Heavy Vehicle Systems*, 7(2-3):153–168.
- James, G. (2003). *Analysis of Traffic Load Effects on Railway Bridge*. PhD thesis, Structural Engineering Division.
- Jenkinson, A. F. (1955). The frequency distribution of the annual maximum (or minimum) values of meteorological elements. *Quarterly Journal of the Royal Meteorological Society*, 81(348):158–171.

Bibliography

- Ji, B., Chen, D., Ma, L., Jiang, Z., Shi, G., Lv, L., Xu, H., and Zhang, X. (2011). Research on stress spectrum of steel decks in suspension bridge considering measured traffic flow. *Journal of Performance of Constructed Facilities*, 26(1):65–75.
- Juárez, S. F. and Schucany, W. R. (2004). Robust and efficient estimation for the generalized Pareto distribution. *EXTREMES*, 7:237–251.
- Klein, E., Stanczyk, D., and Ieng, S.-S. (2012). Improvement of weigh-in-motion accuracy by taking into account vehicle lateral position. In Jacob, B., editor, *Interation Conference on Weigh-in-Motion, ICWIM6*, pages 206–213.
- Kolstein, M. H. (2007). *Fatigue classification of welded Jjoints in orthotropic steel bridge decks*. Doctoral thesis, Faculty of Civil Engineering and Geosciences, Delft University of Technology.
- Koubi, B. and Schmidt, F. (2009). LCPC-Pollux. Paris, France. Laboratoire Centrale des Ponts et Chaussée.
- Kozikowski, M. (2009). *WIM based live load model for bridge reliability*. Doctoral, Graduate College.
- Kwon, O., Kim, E., and Orton, S. (2011a). Calibration of live-load factor in LRFD bridge design specifications based on state-specific traffic environments. *Journal of Bridge Engineering*, 16(6):812–819.
- Kwon, O.-S., Kim, E., Orton, S., Salim, H., and Hazlet, T. (2011b). Calibration of the live load factors in LRFR design guidelines. Technical report, Missouri Transportation Institute and Missouri Department of Transportation.
- Leadbetter, R. M., Lindgren, G., and Rootzen, H. (1983). *Extremes and related properties of random sequences and processes*. Springer-Verlag, New York Heidelberg Berlin.
- L'Ecuyer, P., Simard, R., Chen, E. J., and Kelton, W. D. (2002). An object-oriented random-number package with many long streams and substreams. *Operations Research*, 50(6):1073–1075.
- Leutzbach, W. (1972). *Introduction to the theory of traffic flow*. Springer-Verlag, New York.
- Lindgren, G. (2006). *Lectures on stationary stochastic processes*. Lund University, Sweden.
- Luceno, A. (2006). Fitting the generalized Pareto distribution to data using maximum goodness-of-fit estimators. *Computational Statistics & Data Analysis*, 51(2):904–917.
- Ma, R., Zeng, Y., and Chen, A.-r. (2008). *Maintenance strategies for large span suspension bridges against fatigue and corrosion*, pages 513–518. CRC Press.
- Mackay, E. B. L., Challenor, P. G., and Bahaj, A. S. (2011). A comparison of estimators for the generalized Pareto distribution. *Ocean Engineering*, 38(11-12):1338–1346.

- Maes, M. A. (1995). Tail heaviness in structural reliability. In *International Conference on Applications of Statistics and Probability*, pages 997–1002.
- Mathiasen, P. E. (1979). Prediction functions. *Scandinavian Journal of Statistics*, 6(1):1–21.
- Melchers, R. E. (1987). *Structural reliability: analysis and prediction*. Ellis Horwood Series in Civil Engineering. Ellis horwood limited, England.
- Meshgi, A. and Khalili, D. (2009). Comprehensive evaluation of regional flood frequency analysis by L- and LH-moments. II. development of lh-moments parameters for the generalized Pareto and generalized logistic distributions. *Stochastic Environmental Research and Risk Assessment*, 23(1):137–152.
- Messervey, T. B., Frangopol, D. M., and Casciati, S. (2010). Application of the statistics of extremes to the reliability assessment and performance prediction of monitored highway bridges. *Structure and Infrastructure Engineering*, 7(1-2):87–99.
- Miao, T. J. and Chan, T. H. T. (2002). Bridge live load models from WIM data. *Engineering Structures*, 24(8):1071–1084.
- Moharram, S. H., Gosain, A. K., and Kapoor, P. N. (1993). A comparative study for the estimators of the generalized Pareto distribution. *Journal of Hydrology*, 150(1):169–185.
- Nowak, A. S. (1993). Live load model for highway bridges. *Structural Safety*, 13:53–66.
- Nowak, A. S. and Hong, Y.-K. (1991). Bridge live-load models. *Journal of Structural Engineering*, 117(9):2757–2767.
- Nowak, A. S., Nassif, H., and DeFrain, L. (1993). Effect of truck loads on bridges. *Journal of Transportation Engineering*, 119(6):853–867.
- O'Brien, E. and Caprani, C. C. (2005). Headway modelling for traffic load assessment of short to medium span bridges. *The Structural Engineer*, 86(16):33–36.
- O'Brien, E., Enright, B., and Caprani, C. (2008). Implications of future heavier trucks for Europe bridges. In Znidaric, A., editor, *Transport Research Arena Europe*. Slovenia National Building and Civil Engineering Institute.
- O'Brien, E., Enright, B., and Getachew, A. (2010). Importance of the tail in truck weight modeling for bridge assessment. *Journal of Bridge Engineering*, 15(2):210–213.
- O'Brien, E. J., Caprani, C. C., and O'Connell, G. J. (2006). Bridge assessment loading: a comparison of west and central/east europe. *Bridge Structures*, 2(1):25–33.
- O'Brien, E. J., Caprani, C. C., Znidaric, C. C., and Quilligan, M. (2003). Site-specific probabilistic bridge load assessment. In *Third International Conference on Current and Future Trends in Bridge Design, Construction and Maintenance*, pages 341–348. Thomas Telford Limited.

Bibliography

- O'Brien, E. J. and Enright, B. (2013). Using weigh-in-motion data to determine aggressiveness of traffic for bridge loading. *Journal of Bridge Engineering*, 18(3):232–239.
- O'Brien, E. J., Sloan, D. T., Bulter, K. M., and Kirkpatrick, J. (1995). Traffic load 'fingerprinting' of bridges for assessment purposes. *The Structural Engineer*, 73(19):320–324.
- O'Brien, E. J., Znidaric, A., Brady, K., González, A., and O'Connor, A. (2005). Procedures for the assessment of highway structures. *Proceedings of the ICE - Transport*, 158:17–25.
- O'Connor, A. and Eichinger, E. M. (2007). Site-specific traffic load modelling for bridge assessment. In *Proceedings of the ICE - Bridge Engineering*, volume 160, pages 185–194.
- O'Connor, A. and Enevoldsen, I. (2008). Probability based modelling and assessment of an existing post-tensioned concrete slab bridge. *Engineering Structures*, 30(5):1408–1416.
- O'Connor, A., Jacob, B., O'Brien, E., and Prat, M. (1998). Report of studies on performed on the normal load model, LM1, ENV 1991-3 Traffic Loads on Bridges. Technical report, LCPC.
- O'Connor, A., Jacob, B., O'Brien, E., and Prat, M. (2001). Report of current studies performed on normal load model of EC1. *Revue Francaise de Génie Civil*, 5(4):411–433.
- O'Connor, A. and O'Brien, E. J. (2005). Traffic load modelling and factors influencing the accuracy of predicted extremes. *Canadian Journal of Civil Engineering*, 32(1):270–278.
- O'Connor, A. J. (2001). *Probabilistic traffic load modelling for highway bridges*. Doctoral, Department of Civil Engineering.
- Pelphrey, J. and Higgins, C. (2006). Calibration of LRFR live load factors for Oregon stated-owned bridges using weigh-in-motion data. Technical report, Department of Civil Engineering, Oregon State University.
- Pelphrey, J., Higgins, C., Sivakumar, B., Groff, R., Hartman, B., Charbonneau, J., Rooper, J., and Johnson, B. (2008). State-specific LRFR live load factors using weigh-in-motion data. *Journal of Bridge Engineering*, 13(4):339–350.
- Peng, L. and Welsh, A. H. (2001). Robust estimation of the generalized Pareto distribution. *EXTREMES*, 4(1):53–65.
- Pfeil, M. S., Battista, R. C., and Mergulhao, A. J. R. (2005). Stress concentration in steel bridge orthotropic decks. *Journal of Constructional Steel Research*, 61(8):1172–1184.
- Pickands III, J. (1975). Statistical inference using extreme order statistics. *The Annals of Statistics*, 3(1):119–131.
- Pisarenko, V. F. and Sornette, D. (2003). Characterization of the frequency of extreme earthquake events by the generalized Pareto distribution. *Pure and Applied Geophysics*, 160(12):2343–2364.

- Prem, H., Austroads, Gleeson, B., ARRB Transport Research, George, R., Fletcher, C., and Ramsay, E. (1999). *Estimation of lane width requirements for heavy vehicles on straight paths*. ARRB Transport Research.
- Rasmussen, P. F. (2001). Generalized probability weighted moments: Application to the generalized Pareto distribution. *Water Resour. Res.*, 37(6):1745–1751.
- Reiss, R. D. and Thomas, M. (2007). *Statistical analysis of extreme values - with Applications to Insurance, Finance, Hydrology and Others Feilds*. Birkhauser, Boston.
- Rice, S. O. (1944). Mathematical analysis of random noise. *Bell Systems technical Journal*, 23:282–332.
- Rice, S. O. (1945). Mathematical analysis of random noise. *Bell Systems technical Journal*, 24:46–156.
- Scarrott, C. and MacDonald, A. (2012). A review of extreme value threshold estimation and uncertainty quantification. *REVSTAT - Statistical Journal*, 10(1):33–60.
- Sedlacek, G., Merzenich, G., Paschen, M., Bruls, A., Sanpaolesi, L., Croce, P., Calgaro, J. A., Pratt, M., Jacob, B., Leendertz, M., Boer, V. d., Vrouwenfelder, A., and Hanswille, G. (2006). Background document to EN 1991 - Part 2 - Traffic loads for road bridges - and consequences for the design. Technical report.
- Siegert, D., Estivin, M., Billo, J., Barin, F., and Toutlemonde, F. (2008). Extreme effects of the traffic loads on a prestressed concrete bridge. In Jacob, B., editor, *10th International Conference on Heavy Vehicle*, pages 379–387, Paris, France.
- Sim, H. and Uang, C. (2012). Stress analyses and parametric study on full-scale fatigue tests of rib-to-deck welded joints in steel orthotropic decks. *Journal of Bridge Engineering*, 17(5):765–773.
- Singh, V. P. and Ahmad, M. (2004). A comparative evaluation of the estimators of the three-parameter generalized Pareto distribution. *Journal of Statistical Computation and Simulation*, 74(2):91–106.
- Sivakumar, B. and Ghosn, M. (2009). Collecting and using weigh-in-motion data in LRFD bridge design. *Bridge Structures*, 5(4):151–158.
- Sivakumar, B., Ghosn, M., Moses, E., and TranSystems Corporation (2011). Protocols for collecting and using traffic data in bridge design. National Cooperative Highway Research Program (NCHRP) Report 683, Lichtenstein Consulting Engineers, Inc., Washington, D. C.
- Smith, R. (1984). *Threshold methods for sample extremes*, volume 131, chapter NATO Adv. Sci. Inst. Ser. C Math. Phys. Sci., pages 621–638. Reidel.
- Todorovic, P. and Zelenhasic, E. (1970). A stochastic model for flood analysis. *Water Resour. Res.*, 6(6):1641–1648.

Bibliography

- Treacy, M. A. and Bruhwiler, E. (2012). A monitoring system for determination of real deck slab behaviour in prestressed box girder bridges. In *Proceedings of 6th International Conference on Bridge Manitenance, Safety and Management*, pages 1495–1501, Stresa, Italy.
- Troitsky, S. and Foundation, J. F. L. A. W. (1987). *Orthotropic bridges theory and design*. James F. Lincoln Arc Welding Foundation.
- Tsakopoulos, P. and Fisher, J. (2003). Full-scale fatigue tests of steel orthotropic decks for the Williamsburg bridge. *Journal of Bridge Engineering*, 8(5):323–333.
- van de Lindt, J., Fu, G., Zhou, Y., and Pablo, R. (2005). Locality of truck loads and adequacy of bridge design load. *Journal of Bridge Engineering*, 10(5):622–629.
- van de Lindt, J. W., Fu, G., Pablo, R. M., and Zhou, Y. (2002). Investigation of the adequacy of current design loads in the state of Michigan. Technical Report Report RC-1143, Michigan Technological University Wayne State University.
- Victoria-Feser, M.-P. and Ronchetti, E. (1994). Robust methods for personal-income distribution models. *The Canadian Journal of Statistics / La Revue Canadienne de Statistique*, 22(2):247–258.
- Villasenor-Alva, J. A. and Gonzalez-Estrada, E. (2009). A bootstrap goodness of fit test for the generalized Pareto distribution. *Computational Statistics & Data Analysis*, 53(11):3835–3841.
- von Mises, R. (1936). La distribution de la plus grande de n valeurs. *Revue de l'Union Inter-balkanique*, 1:1–20.
- Wang, Q. J. (1997). LH moments for statistical analysis of extreme events. *Water Resour. Res.*, 33(12):2841–2848.
- Wang, T., Liu, C., Huang, D., and Shahawy, M. (2005). Truck loading and fatigue damage analysis for girder bridges based on weigh-in-motion data. *Journal of Bridge Engineering*, 10(1):12–20.
- Xiao, Z.-G., Yamada, K., Inoue, J., and Yamaguchi, K. (2006). Fatigue cracks in longitudinal ribs of steel orthotropic deck. *International Journal of Fatigue*, 28(4):409–416.
- Xiao, Z.-G., Yamada, K., Ya, S., and Zhao, X.-L. (2008). Stress analyses and fatigue evaluation of rib-to-deck joints in steel orthotropic decks. *International Journal of Fatigue*, 30(8):1387–1397.
- Ya, S., Yamada, K., and Ishikawa, T. (2010). Fatigue evaluation of rib-to-deck welded joints of orthotropic steel bridge deck. *Journal of Bridge Engineering*, 16(4):492–499.
- Ylvisaker, N. D. (1965). The expected number of zeros of a stationary gaussian processes. *Annals of Mathematical Statistics*, 36(3):1043–1046.

- Zanuy, C., Maya, L. F., Albajar, L., and de la Fuente, P. (2011). Transverse fatigue behaviour of lightly reinforced concrete bridge decks. *Engineering Structures*, 33(10):2839–2849.
- Zhang, J. (2007). Likelihood moment estimation for the generalized Pareto distribution. *Australian & New Zealand Journal of Statistics*, 49(1):69–77.
- Zhou, X. Y., Schmidt, F., and Jacob, B. (2012). Assessing confidence intervals of extreme traffic loads. In Jacob, B., McDonnell, A.-M., Schmidt, F., and Cunagin, W., editors, *6th International Conference on Weigh-in-Motion, ICWIM6*, pages 400–410. IFSTTAR.

A Weigh-in-Motion Data and its Statistical Analysis

A.1	WIM data	189
A.2	Cleaning Unreliable WIM Data	190
A.3	Statistical Description of WIM Data	192
A.3.1	Traffic Composition	192
A.3.2	Flow Rate	192
A.3.3	Gross Vehicle Weight	192
A.3.4	Axle Loads	194
A.3.5	Axle Spacing	195
A.3.6	Headway Distribution	196

A.1 WIM data

This work includes five sets of Weigh-in-Motion (WIM) data collected very recent years between 2009 and 2011 at four sites - Saint Jean de Vedas (SJDV), Loisy, Vienne and Maulan, on three motorways and one highway - A9, A31, A9 and RN4, respectively, in France. The locations and measured periods are shown in Figure A.1. An overview of the data is given in Table A.1. The WIM data are used to develop a model for simulating truck loading on highway bridges.

In SJDV, there are WIM sensors in the three lanes of the 6-lane highway, and data were col-

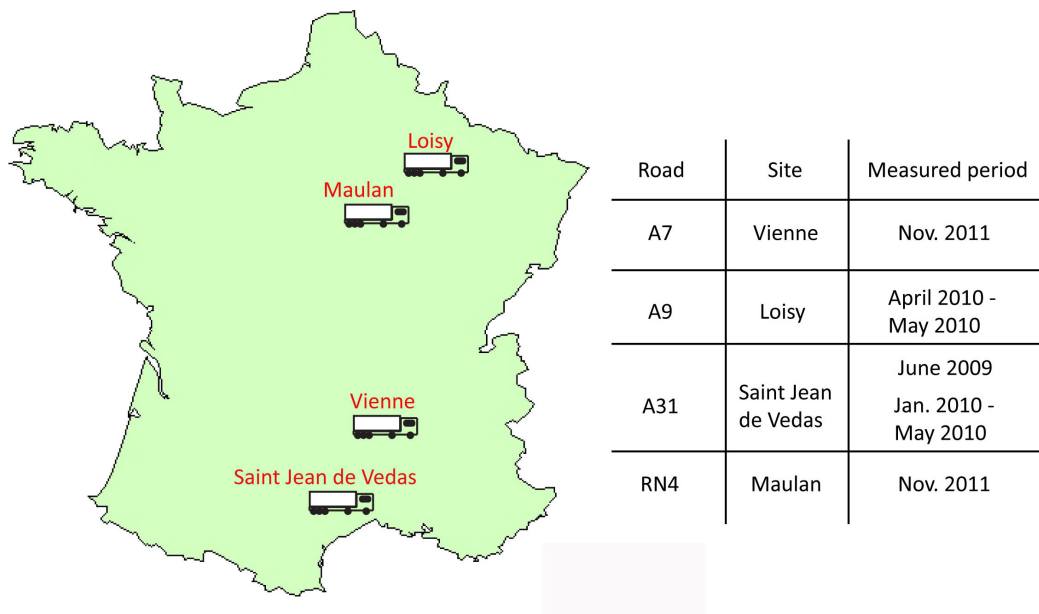


Figure A.1: The measurement locations and periods

lected during two periods. A total number of 841 609 trucks weighing 3.5 t or more with time stamps recorded with a precision of 0.01 second were recorded from 1st January to 31st May, 2010. And another set of data was provided for truck traffic in the two outer lanes, and a total of 841 786 vehicles weighing from 0.6 t were recorded in June, 2009, no measurements were provided for the fast lane.

In Loisy, there are WIM sensors in the two lanes of the 4-lane motorway. Data were recorded for truck traffic in these two lanes for the 61 days period from 1st April to 31st May, 2010. A total of 273 190 trucks weighing 3.5 t or more with time stamps recorded with a precision of 0.01 seconds.

In Vienne, there are WIM sensors in the three lanes of the 6-lane motorway. Data were recorded for truck traffic in these three lanes in Novembre 2011. A total of 180 252 trucks weighing 3.5 t or more were recorded with a precision of 0.01 seconds.

In Maulan, there are WIM sensors in the slow lane of the 4-lane highway. Data were provide for truck traffic in the lane for Novembre 2011. A total of 73 010 trucks weighing 3.5 t or more with time stamps recorded to a precision of 0.01 seconds.

Table A.1: Overview of WIM data

	St Jean de Vedas		Loisy	Vienne	Maulan
Road No.	A9		A31	A7	RN4
No. of lanes	2 × 3		2 × 2	2 × 3	2 × 2
Type of sensor	Piezoceramics		Piezoceramics	Piezoceramics	Piezoquartz
Measurement period	2010 Jan. - 2010 May	2009 Jun.	2010 Apr. - 2010 May	2011 Nov.	2011 Nov.
No. of days	138	28	61	30	30
No. of equipped lanes with WIM systems	3	2	2	3	1
No. of vehicles	841 609	841 786	273 190	180 252	73 010
The statistics below are based on cleaned data.					
No. of vehicles	757 969	144 579	263 328	149 930	64 546
No. of vehicles (Slow lane)	676 630	131 484	257 254	147 222	64 546
Average daily flow (Slow lane)	4903	4696	4217	4907	2152
Max. GVW (t)	74	73.9	90.3	86.9	99.9
Average GVW (t)	27.5	26.9	25.1	27.0	27.4
Average Speed (km/h)	89	89	86	82	86
Max. No. of axles	8	8	8	8	8
No. vehicles over 40t	46 638	8 391	21 987	9 140	4 709
No. vehicles over 44t	3 308	743	2 298	1 055	358
No. vehicles over 60t	96	29	26	44	10

A.2 Cleaning Unreliable WIM Data

Although weigh-in-motion techniques have significantly advanced in this decade, the recorded data still include some unreliable observations due to the roughness of pavement where the WIM system is located, the environment, the unstability of WIM system and etc. Therefore it is important to examine the WIM data to remove unreliable data containing unlikely trucks to ensure that only quality data is used to model traffic load Enright and O'Brien [2011]; Sivakumar et al. [2011]. WIM data cleaning rules have been recommended by Enright and O'Brien [2011]; Sivakumar et al. [2011]. However, the feature of traffic data, the type of WIM system are different from country to country. In this thesis, some modifications are made on these two recommended rules with respect to the French WIM data. The cleaning techniques used in this thesis are listed in Table A.2 and compared with others [Enright and O'Brien, 2011; Getachew, 2003; Sivakumar et al., 2011].

Table A.2: Comparison of data cleaning rules

Getachew [2003]	Enright and O'Brien [2011]	Sivakumar et al. [2011]	This thesis
Accept one axle vehicles with length less than 12 m	At least 2 axles; and no upper limitation	Total number of axles less than 3 or greater than 12	Exclude vehicles with less than 2 axles; and the observed maximum number of axle is 8.
–	Exclude if speed below 20 to 60 km/h varies with site.	Speed below 16 km/h	Clean if speed below 40 km/h
–	Exclude if speed above 120 km/h.	Speed above 160 km/h	Clean if speed above 120 km/h
–	–	Truck length greater than 36 m	Truck length greater than 30 m and GVW greater than 20 t
–	Exclude if sum of axle spacing greater than length of truck	Sum of axle spacing greater than length of truck	Sum of axle spacing greater than length of truck or less than 65% of truck length
–	Exclude if sum of the axle weights differs from the GVW by more than 0.05t	Sum of the axle weights differs from the GVW by more than 10%	Exclude if the sum of axle weights differs from the GVW by more than 10%
–	GVW less than 3.5 t are excluded	GVW less than 5.4 t	–
–	Vehicles with individual axle greater than 40 t are excluded.	Individual axle weight greater than 32 t	Exclude vehicles if the proportion of axle weight is greater than 85% of GVW
–	–	Steer axle greater than 11.3 t	–
–	–	Steer axle less than 2.7 t	–
Exclude if distance between the first axle and last axle is less than 3 meters for four axle vehicles	–	First axle spacing less than 1.5 m	–
Any axle spacing less than 1 m for five or more axle vehicles	Any axle spacing less than 0.4 m	Any axle spacing less than 1 m	–
–	–	Any individual axle less than 1 t	Keep only vehicles with axle weight greater than 0.6 t
–	–	–	Exclude if lateral position outside the notional lane

A.3 Statistical Description of WIM Data

A.3.1 Traffic Composition

A common rule to define the class of truck is the number of axles [Caprani, 2005; Enright and O'Brien, 2012]. Although this classification is very efficient in use, it may not be reasonable. For truck with same number of axles, the loading capacity is different between rigid connection truck and articulate connection ones, and also the load distribution is different. Therefore they lead to various aggressions to bridge structure or components especially those are sensitive to axle load. A more refined classification was applied in some studies [Bailey, 1996; O'Connor and O'Brien, 2005]. Coupling with French WIM data, a further subclassification of trucks has been used in this thesis as given in Figure A.2. The trucks were firstly classified by their number of axles in a traditional way, the composition is shown in Figure A.3. Then the data were further classified by axle configurations, and the classification is given in Table A.3.



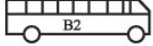
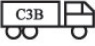

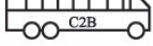


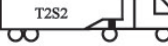





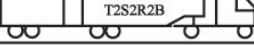
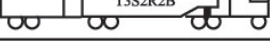

2-axle	 	
3-axle	 	 
4-axle	 	
5-axle	 	 
6-axle		
7-axle		
8-axle		

Figure A.2: Truck classification

A.3.2 Flow Rate

Truck traffic has evident variation, the hourly average truck flow for traffic at Saint Jean de Vedas is calculated and shown in Figure A.4. It can be found that the fast lane and the slow one have similar variation during the day, it indicates that the hourly average truck flow reaches its highest level between 10 am and 15 pm.

A.3.3 Gross Vehicle Weight

Many models for GVW have been used by authors. Bailey [1996] has used a Beta distribution to model the weights of axle groups (tandems and tridem) and has built up the GVW from

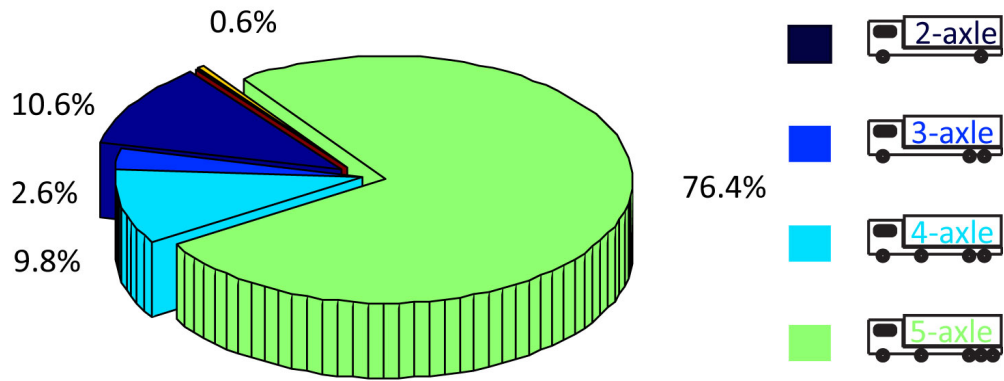


Figure A.3: Traffic composition

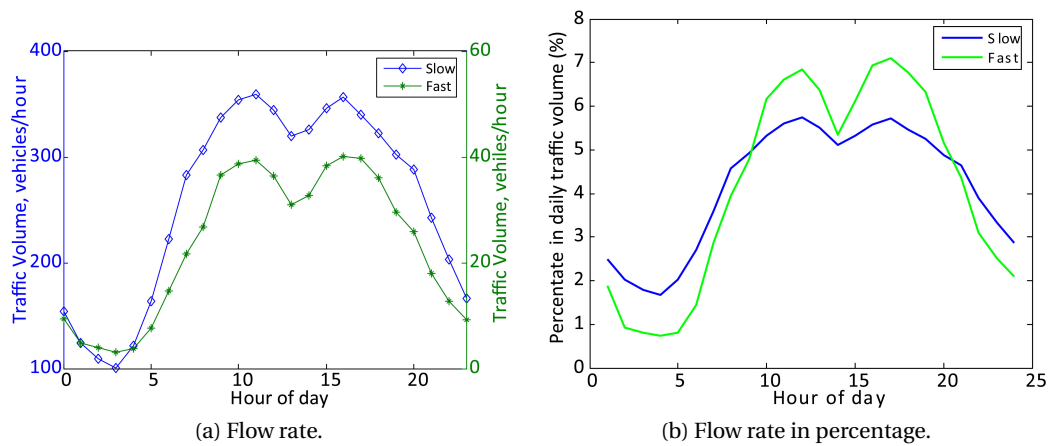


Figure A.4: Flow rate and percentage

this. Crespo-Minguillon and Casas [1997] use the measured empirical distribution as the basis for performing simulation. Enright and O'Brien [2012] has used a semi-parametric approach to model GVW. For GVWs up to a certain value, an empirical bivariate distribution, which is a function of GVW and number of axles, is used to fit the data. Above the threshold, GVW is modeled by a bivariate normal distribution. Caprani [2005] has used bimodal or trimodal normal distribution to model the GVW of each truck class.

In this thesis, we have adopted uni-, bi- and tri-modal normal distributions to model GVW of each subclass. It is found that the range of GVW is quite different for various subclass of vehicle, even if they have the same number of axles. Figures A.5 to A.8 illustrate the GVW distribution fitting for traffic data collected at Saint Jean de Vedas.

Table A.3: Classification of truck and traffic composition

Class		Subclass			
2-axle	Category	C2	B2	U2	
	Percentage	60	22	18	
3-axle	Category	C3B	T2S1	B3	U2R1
	Percentage	41	16	24	19
4-axle	Category	T2S2	C2R2B	U2R2	
	Percentage	65	31	4	
5-axle	Category	T2S3	C2R3B	C3BR2A, C3BR2B	
	Percentage	95	2	3	
6-axle	Category	T2S2R2B			
	Percentage	100			
7-axle	Category	T3S2R2B			
	Percentage	100			
8-axle	Category	T3S3R2B	T3S3R2A		
	Percentage	93	7		

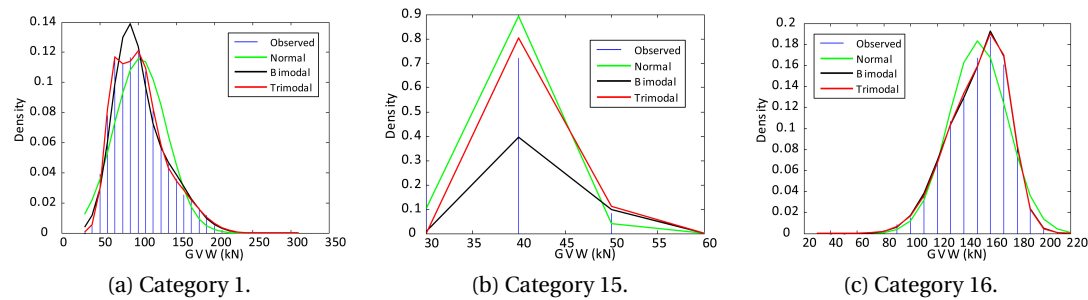


Figure A.5: GVW histogram and fitting for 2-axle trucks

A.3.4 Axle Loads

For short- to medium span bridges, the axle loads are particularly important. Various methods have been proposed in the literature to model the axle loads. Caprani [2005]; O'Brien et al. [2006] have used a mixture of Normal, bimodal Normal and trimodal Normal distributions to each class of truck. Enright and O'Brien [2012] have used a bimodal Normal distribution. Bailey [1996] has used a bimodal Beta distribution for axle groups, and normal distribution for single axles. As the multi-modal Normal distribution is extensively used to model axle wght. In this study, the percentage of the GVW carried by each axle is modelled using uni-, bi- and tri-modal normal distributions. Sample distributions are shown in Figure A.9 for category 5 of 5-axle trucks.

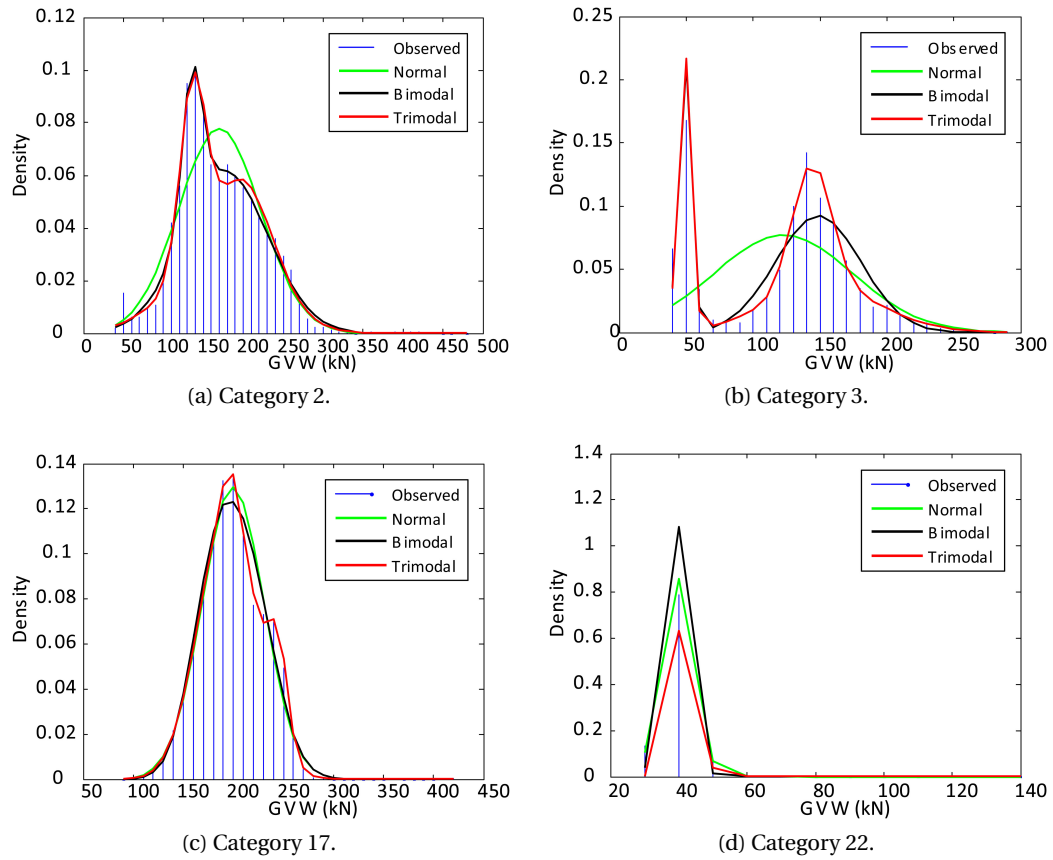


Figure A.6: GVW histogram and fitting for 3-axle trucks

A.3.5 Axle Spacing

As the axle loads, the axle spacing is vital important to short- to medium span bridge. Particular attention have been paid on modeling axle spacing in the literature. For axle spacing, each vehicle class is modeled seperatedly. Caprani [2005] have used bi- or tri-modal Normal distributions to model the measurements. Bailey [1996] have used Beta distributions to model the distance between axle groups and the front and rear vehicle overhangs. Enright and O'Brien [2012] have proposed to focus on the maximum axle spacing for each vehicle. For each vehilce measured, all axle spacings are ranked in descending order, starting with the maximum. Then an empirical distribution is used to model the maximum axle spacing for each vehicle class, and trimodal Normal distributions are used to model other spacings. Simultaneously, the authors have modeled the position of each of the ranked spacings on the vehicle by using empirical distributions for all spacings in each axle class. In this study, it is not necessary to rank the axle spacings to find the maximum axle spacing for each vehicle as the vehicles are classified by their silhoutte as given in Figure A.2. For each vehicle class, the axle spacings are almost constant value corresponding to their positions on the vehcile as the histograms of axle spacing always has very sharp shape, which indicates a small standard

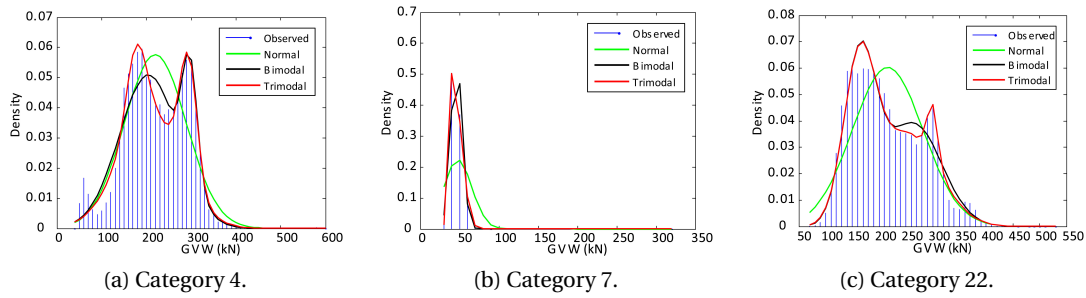


Figure A.7: GVW histogram and fitting for 4-axle truck

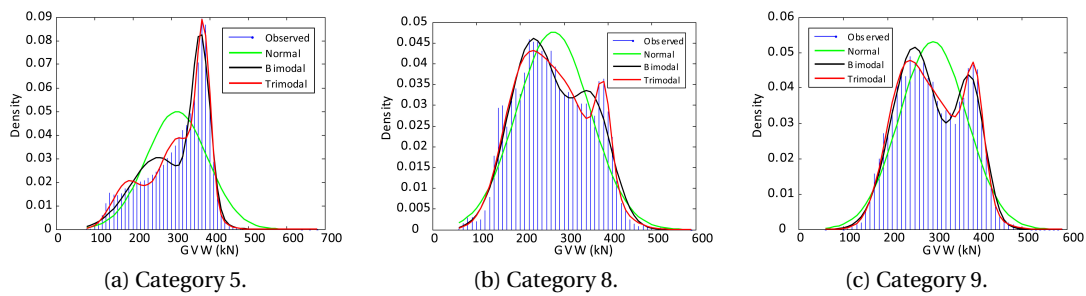


Figure A.8: GVW histogram and fitting for 5-axle trucks

deviation, see for example in Figure A.10. Uni- bi- or trimodal Normal distributions are used to model the measured axle spacing for each vehicle class.

A.3.6 Headway Distribution

Headway is a measurement of the distance or time between successive vehicles, it is an important factor to describe traffic flow. A lot of investigations and studies have been carried out about the headway distribution. Most of distribution formulae are derived from probability statistics. These formulae can be categorized into two classes. One is under the assumption of free traffic flow, the other is developed for congest traffic flow. For short- to medium span bridge, the free flowing is deemed to be the governing traffic condition [Bakht and Jaeger, 1987]. Especial focus have been given on two trucks following or side-by-side situations in many studies [Nowak and Hong, 1991; Nowak et al., 1993] during the development of AASHTO. According to the scope of this thesis, the free flowing traffic is concerned. The most used model is that assuming the arrival of vehicles is Poisson process, and the corresponding time interval between two successive arrivals are exponential distribution Leutzbach [1972]. The Poisson and exponential distribution are valid only when traffic flows are light. Moreover, the headway can be zero if the exponential distribution is used, which in practice is impossible. Therefore, a shifted exponential distribution has been proposed by Cowan [1975] with a minimum time interval between successive vehicles. Bailey [1996] has used the shifted exponential distribution to describe the free flowing traffic with a minimum headway of 0.25 s.

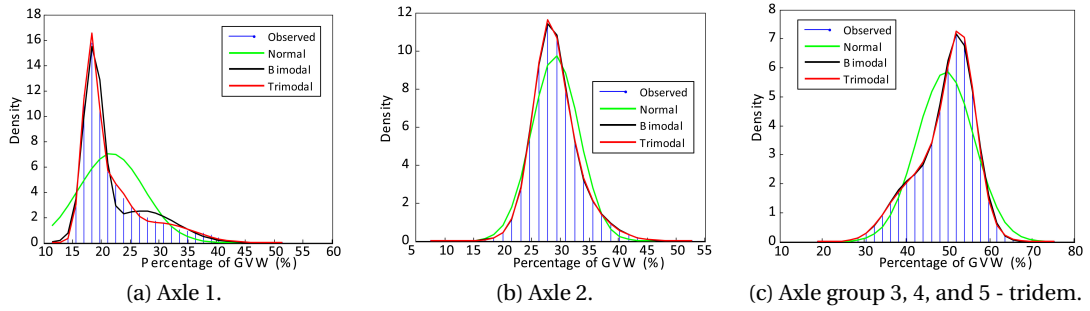


Figure A.9: Percentage of GVW carried by each axle for 5-axle trucks, category 5

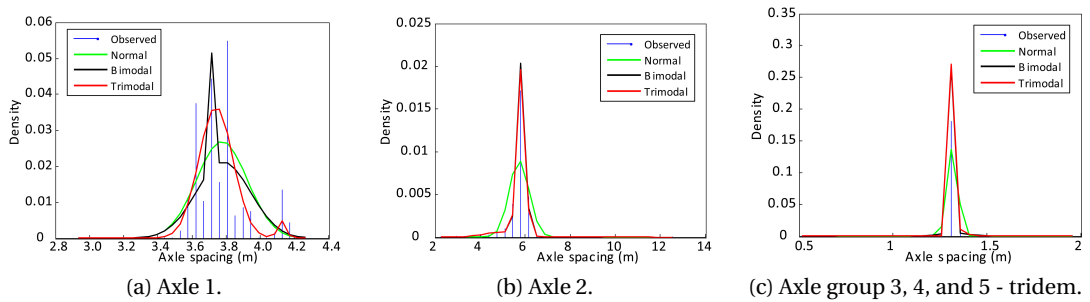


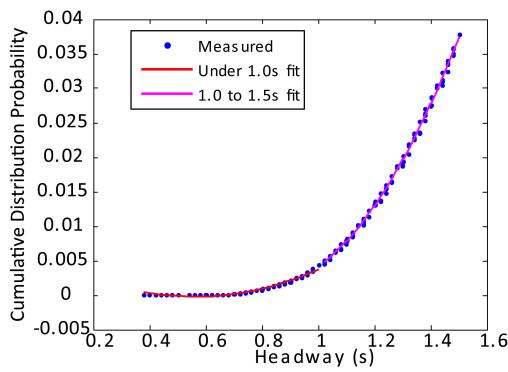
Figure A.10: Percentage of GVW carried by each axle for 5-axle trucks, category 5

Although the shifted exponential distribution model considers the traffic more reasonable, it still can not fit the heavy traffic flow well. Vehicles need frequently adjust their speeds to that of a vehicles in front in heavy traffic situation, Leutzbach [1972] has found that the Erlang distribution can describe the headway in heavy traffic. Other models like using Pearson type III distribution, log-normal distribution are aslo used to model heavy traffic.

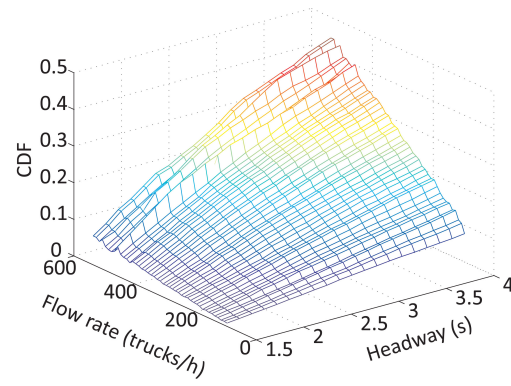
For a given traffic, the density of traffic is mixture as shown in Figure A.4. The traffic is heavy between 10 h to 20 h, and the traffic is light in other time. A mixture model can therefore describe the traffic more accurately. Basing their measurements of five days WIM data from Auxerre in France, O'Brien and Caprani [2005] have proposed a mixture model, which consists of a flow dependent sub-model and a flow independent sub-model, to describe headway distribution. For headways of less than 1.5 seconds, a flow independent model has used. For headways greater than 1.5 seconds, a flow dependent model has proposed, but two sub-models have been considered. For headways between 1.5 and 4 seconds, the other is used to headways greater than 4 seconds. Enright and O'Brien [2012] has used the model proposed by O'Brien and Caprani [2005] in similar manner but with two modifications. One is to use gap instead of headway to eliminate the influence of vehicle length on headway. The gap is the time between the rear axle of the front tuck and the front axle of the following truck. The other is to allow for different gap distributions for different flow rates at very small gaps like less than 1.0 second.

Appendix A. Weigh-in-Motion Data and its Statistical Analysis

In this thesis, we also adopt the model described by O'Brien and Caprani [2005] to model headways used for single-lane traffic in each direction, and the headway is same as the gap used by Enright and O'Brien [2012]. Measurements from Saint Jean de Vedas is used to illustrate the modeling processing. The cumulative distribution probability of headways less than 1.5 seconds are plotted in Figure A.11a. The measured distribution is fitted with two quadratic equations, one for less than 1 second, and another between 1 and 1.5 seconds. For measured headways between 1.5 and 4 seconds, they are categorized by hourly flow in intervals of 10 trucks/h. The resulting cumulative distribution functions are illustrated in Figure A.11b. A quadratic equation is fitted to each grouped data with respect to average hourly flow. For headways greater than 4 seconds, an average hourly flow based shifted exponential distribution is used.



(a) Less than 1.5 s.



(b) Between 1.5 s and 4 s.

Figure A.11: Cumulative distribution function for headway

B Bridge Traffic Load Effect Calculation and Simulation Program

B.1	Introduction	201
B.2	Program Description	201
B.2.1	Algorithm for Traffic Load Effect Calculation	201
B.2.2	Flowchart	202
B.3	Traffic Files	206
B.3.1	Traffic Composition and Flow	206
B.3.2	Axle Spacing	206
B.3.3	Axle Weight	207
B.3.4	Gross Vehicle Weight	207
B.3.5	Headway	208
B.4	Output	209
B.4.1	Time History File	209
B.4.2	Histograms of Value, Level Crossing, Rainflow Cycle Counting	210
B.4.3	Block Maximum Vehicle Files	213
B.4.4	Peaks over Threshold	216

B.1 Introduction

This appendix presents the function and use of the bridge traffic load effect calculation and simulation (BTLECS) program developed as part of this research. The model for traffic load effect is based on a program named CASTOR developed by Eymard and Jacob [1989] and updated by Koubi and Schmidt [2009] under the name LCPC-Pollux. The CASTOR software was written in FORTRAN, and it is a procedural oriented programming, which is not easy to be extended to carry out traffic load effect extreme value analysis by using block maxima method or peaks over threshold approach. Furthermore, the CASTOR or LCPC-POLLUX software can only be used to calculate traffic load effects by using collected traffic data like from WIM, but it is impossible to conduct a Monte Carlo Simulation to extend the available traffic files. Therefore, the new program, BTLECS, was developed, the program is object-orientated and was written in C++ language.

B.2 Program Description

B.2.1 Algorithm for Traffic Load Effect Calculation

Using influence surfaces, $S(x, y)$, or lines $L(x, y)$ to calculate the load effect at a certain point (x, y) is an extensively way in the purpose of bridge design and assessment. The influence surface can be decomposed into longitudinal influence line $L(x)$ and transversal influence line $T(y)$ as:

$$S(x, y) = L(x) \cdot T(y) \quad (\text{B.1})$$

$$T(x, y) = \frac{1}{2} (S(x, y - e) + S(x, y + e)) \quad (\text{B.2})$$

For calculating load effect induced by the passage of vehicles, the leading vehicle is assumed to move in a time step Δt . At each step, the program counts the number of vehicles, N , which is the total number of vehicles currently on the bridge. Then the load effect induced by these N vehicles can be obtained by using:

$$X_n = \sum_{j=1}^N C(y_j) \sum_{k=1}^{s(j)} P_{(j,k)} L_{i(j)} [V_j(t_n - t_j) - d_{(j,k)}] \quad (\text{B.3})$$

N : number of vehicle,

j : index of j th vehicle,

y_j : transversal location of j th vehicle,

V_j : speed of j th vehicle,

t_j : time that the first axle of j th vehicle passes over the position $x = 0$,

Appendix B. Bridge Traffic Load Effect Calculation and Simulation Program

$i(j)$: number of lane of j th vehicle,

$s(j)$: number of axles of j th vehicle,

$P_{(j,k)}$: axle load of k th of j th vehicle,

$d_{(j,k)}$: distance between steering axle to k th axle of j th vehicle.

In each step of the calculation, we assume that the involved vehicles keep constant speed and lateral position during the time interval Δt . The process of the calculation is to carry out a N times loop for the vehicles currently on the bridge. The loop starts from the leading vehicle to the N^{th} vehicle. The information of number of axles $s(j)$, axle loads $P_{(j,k)}$, axle spacings $d_{(j,k)}$, and speed V_j associated to the j^{th} vehicle are used to obtain: (i) the longitudinal position of each axle $x(j, k)$ that is used to determine the value on influence line, (ii) the contribution to total load effect. The influence line can be obtained by theoretical analysis (see Figure B.1a) or measurement (see Figure B.1b). At the end of each step, the program needs to judge whether the leading vehicle is still on the bridge or not. If it exits the bridge then it will be eliminated and another vehicle will be appointed to be the leading vehicle. This process is carried out until all the input vehicles from WIM data or generated by Monte Carlo simulation crossing over the bridge be considered.

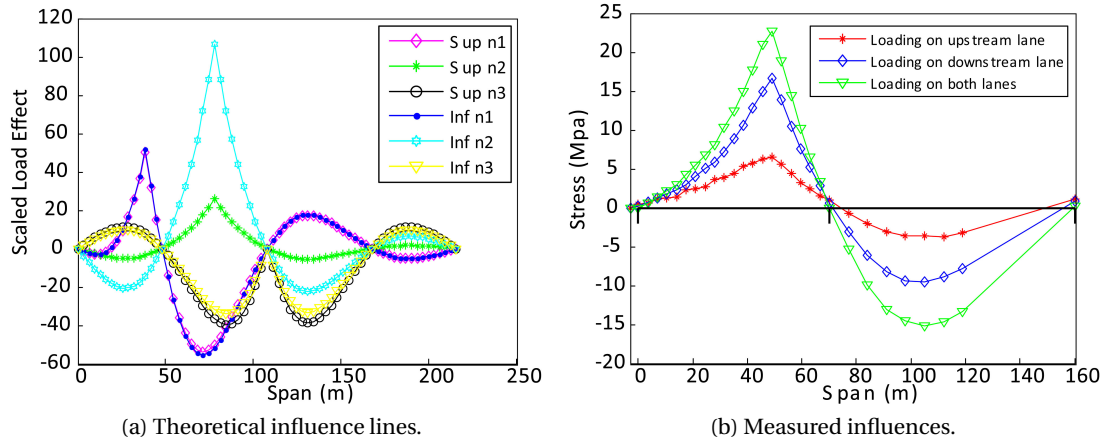


Figure B.1: Influence lines.

B.2.2 Flowchart

The flowchart in Figure B.2 shows the various modules of the simulation program, which are described below.

Module of generation The program provides two options to input traffic data. One is read from a file, and another is generated by Monte Carlo simulation.

If the traffic data input mode is read from an existing file, the file should be prepared in a certain format as shown in the Table B.1. An example of the input of traffic data is given in Figure B.3.

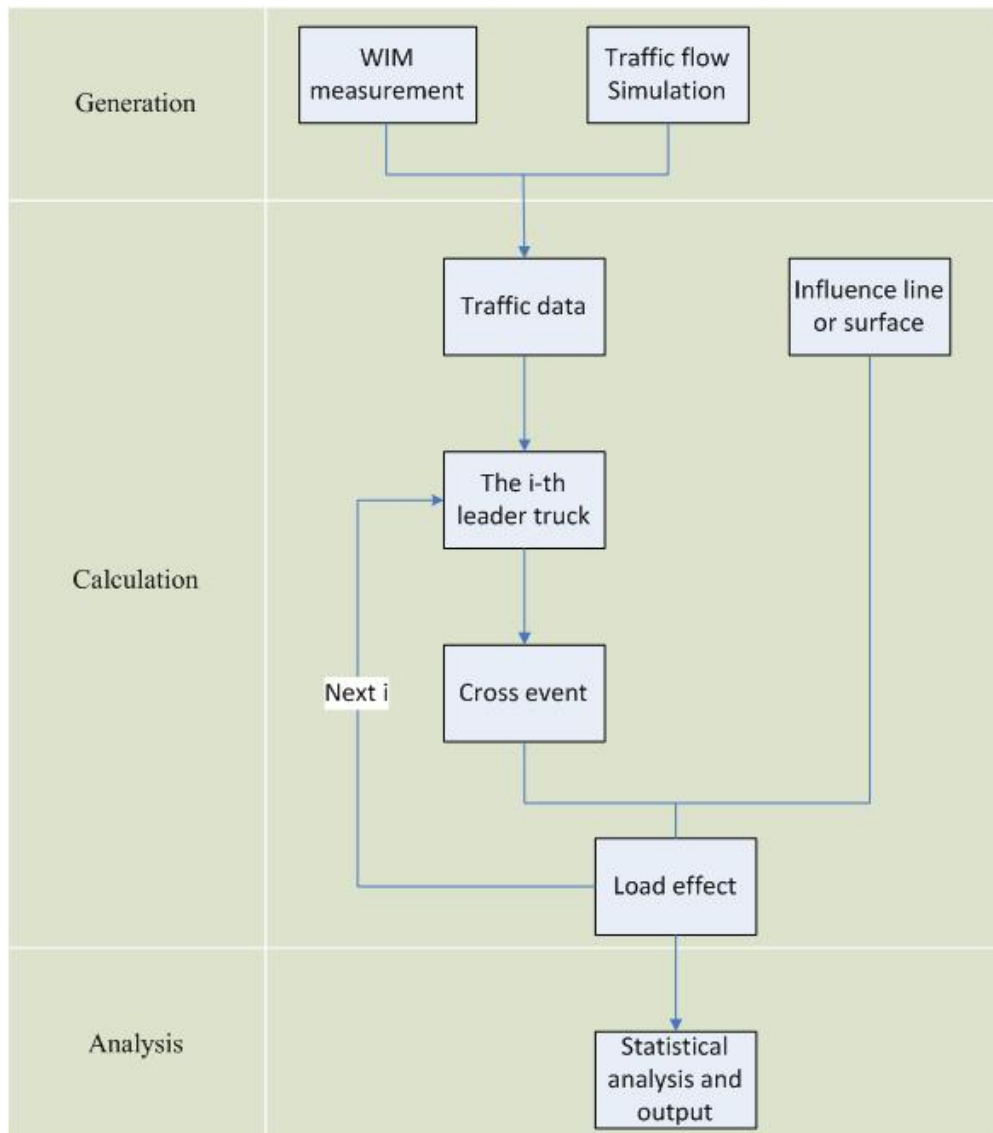


Figure B.2: Flowchart of BTLECS Program

```

0000001200020501201030000071209003131690505001220408500000153330690361092060305101320520132051
0000002200020501201030000286008902581720505000720609200000153330600362074060304001310420131045
0000003200020501201030000295408902821710505101821108900000153330600362077061304901320510132046
0000004200020501201030000335408902141670505102120206700000153330550372058058703301310350131034
0000005200010501201030000373608903611700505000519908600000153330660372099058406401310650133068
000000620001050120103000050340900149146040410212090770000001522054038104405730250132026
0000007200020501201030001075808902841640505105420009400000153330710371093058404101340390131042
0000008200020501201030001135808901721350505101321505500000153330550414047042902301310240134024
000000920002050120103000137440930299207040700062000850000001122065054110808330590137068
  
```

Figure B.3: Sample of input traffic data file

Appendix B. Bridge Traffic Load Effect Calculation and Simulation Program

Table B.1: Traffic data file format

Description	Unit	Format
Order		I7
Head		I4
Lane		I1
Day		I2
Month		I2
Year		I4
Week		I1
Hour		I2
Minute		I2
Second		I2
Second/100		I2
Speed	km/h	I3
Gross Vehicle Weight - GVW	dt	I4
Length	dm	I3
Number of axles		I2
Category of vehicle		I2
Transverse deviation in lane	cm	I3
Width of vehicle	cm	I3
Bumper	cm	I3
Type of axle		I10
Load - axle 1	dt	I3
Spacing - axle 1 - axle 2	cm	I4
Load - axle 2	dt	I3
⋮	⋮	⋮
Load - axle $n - 1$	dt	I3
Spacing - axle $n - 1$ - axle n	cm	I4
Load - axle n	dt	I3

If the traffic data is assigned to be generated by MC simulation, and the program activates the module of MC simulation. To carry out the simulation, basic information on the traffic is required. It includes the information on traffic namely traffic composition, flow rate and headway, and the information of vehicles of axle load, axle spacing, gross vehicle weight and speed. These traffic information files should be prepared according to the specific format. Details on the input files for performing Monte Carlo simulation of traffic flow are given in Section B.3. The programs generate traffic day by day until the required number of days is achieved. The random number is produced by the random number generator provided by L'Ecuyer et al. [2002]. The simulation procedure is as follows:

- For each day, the program firstly generates a number for daily traffic volume according to the input statistical distribution of traffic volume, then the hourly traffic volume can automatically be obtained with the input flow rate information.
- Secondly, the program combines the assigned hourly traffic volume with the input headway model to generate the traffic flow that gives arrival time to each vehicle.
- Thirdly, the feature of each vehicle is assigned by using the information of traffic composition, axle load, axle spacing, gross vehicle weight and speed.

Module of calculation Each randomly generated daily traffic is superimposed on structures of interest. Effects are thus calculated combining the loads and positions of vehicle stored in the traffic flow with the given influence function (line or surface). Traffic is stepped over a bridge by incrementing the vehicle positions, the traffic flow is stepped as a function of the speed of vehicles. When an vehicle is stepped off the influence line or surface being considered, it is deleted from the traffic flow, and a new vehicle is assigned to be leading vehicle.

Module of statistical analysis At the end of each crossing event, the load effect time history during this crossing event is passed to the statistical analysis module to obtain statistics of interest. The statistics includes histogram of value, histogram of level crossing counting, histogram of rainflow cycle counting, block maxima and peaks over threshold. Details on these statistics are presented in Section B.4.

Module of output results At the end of the simulation of the defined number of days the statistics of calculated traffic load effects are written to files. These statistics are output in tables. Samples of the results are given in Section B.4.

B.3 Traffic Files

B.3.1 Traffic Composition and Flow

The files of traffic composition hold the data of percentage of trucks in each class that is named by number of axles, and for percentage of trucks in each subclass that is grouped by their silhouette mainly the types of connection that is rigid or articular. An example is given and explained in Table B.2.

Table B.2: Traffic composition input file

Class	Percentage	Subclass			
		1	2	3	4
2-axle	10.57	0.6288	0.2127	0.1586	0
3-axle	2.64	0.4284	0.1618	0.2258	0.1839
4-axle	9.82	0.6544	0.3064	0.0392	0
5-axle	76.35	0.9547	0.0189	0.0264	0
6-axle	0.55	0.4935	0.5065	0	0
7-axle	0.05	1	0	0	0
8-axle	0.01	0.0889	0.9111	0	0

The file for flow rate holds the average number of trucks, for the hour under consideration, for each lane. An example is given in Table B.3.

Table B.3: Flow rate input file

Time	0	1	2	3	4	5
Slow lane	148.7	121	105.1	96.5	116.4	154.6
Fast lane	9.1	4.6	3.6	2.9	3.5	7.1
Time	6	7	8	9	10	11
Slow lane	209	264.9	288.8	317.3	335.5	339.9
Fast lane	13.4	20.2	24.9	34.5	36.1	37
Time	12	13	14	15	16	17
Slow lane	328.3	304.5	312.4	328.2	338	325.3
Fast lane	34.3	29.5	31.1	36.1	37.6	37.8
Time	18	19	20	21	22	23
Slow lane	309.8	288.3	272.7	228.8	191.6	161.9
Fast lane	34.6	27.9	24.4	16.8	12	9.1

B.3.2 Axle Spacing

This file stores the axle spacing data for all classes of trucks measured on the site. As described, the axle spacings are modeled by uni- or multi-modal normal distribution, therefore there are three parameters required for each of the modes: the weight, the mean, and the standard

deviation. An example for 2-axle is given in Table B.4.

Table B.4: Axle spacing input file for 2-axle truck

Mode	Category 1			Category 2			Category 3		
	Mean	Std	Weight	Mean	Std	Weight	Mean	Std	Weight
Mode 1	386	39	0.1965	382	42	0.8027	591	10	0.1601
Mode 2	508	59	0.5246	407	4	0.1973	614	10	0.5925
Mode 3	624	37	0.2790	-	-	-	683	11	0.2473

B.3.3 Axle Weight

In order to avoid the summation of generated axle weights greater than the gross vehicle weight, here the axle weight is presented as a ratio of the gross vehicle weight. Axle weight data may be fitted by a mix of a number of Normal distributions; that is, the data may be multi-modally normally distributed. There are three parameters required for each of the modes: the weight, the mean and the standard deviation. The maximum number of modes allowed in the program is three; hence the 3×3 tabular format of the data. An example is given in Table B.5.

Table B.5: Axle weight input file for 2-axle truck

Axle	Mode	Category 1			Category 2			Category 3		
		Mean	Std	Weight	Mean	Std	Weight	Mean	Std	Weight
1 st	Mode 1	0.6987	0.0267	0.029	0.4363	0.054	1	0.3639	0.0254	1
	Mode 2	0.4321	0.0649	0.971	-	-	-	-	-	-
	Mode 3	-	-	-	-	-	-	-	-	-
2 nd	Mode 1	0.3045	0.0266	0.0289	0.5695	0.0541	1	0.6378	0.0254	1
	Mode 2	0.5706	0.0649	0.9711	-	-	-	-	-	-
	Mode 3	-	-	-	-	-	-	-	-	-

B.3.4 Gross Vehicle Weight

The file contains the parameters of the distributions that characterize the GVW for each class of trucks. Again the distribution of GVW is assumed to be a multimodal normal distribution, and an example is given in Table B.6.

Table B.6: GVW input file for 2-axle truck

Mode	Category 1			Category 2			Category 3		
	Mean	Std	Weight	Mean	Std	Weight	Mean	Std	Weight
Mode 1	6.73	1.11	0.2363	3.91	0.44	1	14.31	2.17	0.6708
Mode 2	9.89	1.85	0.4749	-	-	-	16.61	1.11	0.3292
Mode 3	13.83	3.34	0.2888	-	-	-	-	-	-

Appendix B. Bridge Traffic Load Effect Calculation and Simulation Program

B.3.5 Headway

The headway model proposed by O'Brien and Caprani [2005] is adopted here. This model includes three parts, the first two are represented by 2nd ordered polynomes that are independent on flowrate or traffic volume, and the third part is assumed to be a flow rate dependent 2nd order polynomial function. An example is given in Table B.7, in which Line 1 indicates the number of flow dependent headway models. Line 2 and 3 give the parameters of the quadratic-fit headway CDF for under 1.0 s and between 1.0 s and 1.5 s respectively. The following lines return the parameters of the quadratic fit to the headway CDF for that flow of the first column.

Table B.7: Headway

49	0	0	0				
0	0.020977	-0.023663	0.0064589				
0	0.074462	-0.11972	0.049445				
76.494	-0.005048	0.03664	-0.03753	326.49	-0.0088234	0.14493	-0.15758
86.494	-0.003435	0.03725	-0.04142	336.49	-0.0098058	0.15188	-0.16346
96.494	-0.001821	0.037858	-0.045312	346.49	-0.012647	0.17339	-0.18853
106.49	-0.00020793	0.038469	-0.049201	356.49	-0.011238	0.16607	-0.17909
116.49	0.00014333	0.038854	-0.050425	366.49	-0.012221	0.17531	-0.18756
126.49	0.00071673	0.043011	-0.054727	376.49	-0.012819	0.18111	-0.19447
136.49	0.0019588	0.035748	-0.045866	386.49	-0.013319	0.18528	-0.1951
146.49	-0.0024351	0.064459	-0.077179	396.49	-0.013467	0.18543	-0.19307
156.49	-0.0037983	0.072362	-0.08712	406.49	-0.011538	0.17933	-0.18754
166.49	-0.002969	0.068716	-0.081166	416.49	-0.015111	0.20076	-0.21707
176.49	-0.0035484	0.075985	-0.091239	426.49	-0.012236	0.18559	-0.19269
186.49	-0.0024476	0.074726	-0.088546	436.49	-0.013004	0.19368	-0.20524
196.49	-0.0031514	0.084054	-0.098513	446.49	-0.013614	0.19991	-0.20832
206.49	-0.0026836	0.081375	-0.095341	456.49	-0.027381	0.27029	-0.25708
216.49	-0.001686	0.077476	-0.088758	466.49	-0.018902	0.23881	-0.26091
226.49	-0.00087772	0.07778	-0.090408	476.49	-0.017222	0.22718	-0.24762
236.49	-0.0061718	0.10843	-0.1256	486.49	-0.022359	0.2607	-0.28449
246.49	-0.0032954	0.096443	-0.11098	496.49	-0.039003	0.34888	-0.37748
256.49	-0.0063687	0.11365	-0.12688	506.49	-0.02307	0.28119	-0.30551
266.49	-0.0077585	0.1234	-0.1387	516.49	-0.018633	0.23902	-0.24853
276.49	-0.0074835	0.12469	-0.13685	526.49	-0.016264	0.23547	-0.23677
286.49	-0.009353	0.13932	-0.15657	536.49	-0.016264	0.23547	-0.23677
296.49	-0.0068702	0.12611	-0.14018	546.49	-0.016264	0.23547	-0.23677
306.49	-0.0091684	0.14265	-0.16066	556.49	-0.016264	0.23547	-0.23677
316.49	-0.0095783	0.14991	-0.16679				

B.4 Output

B.4.1 Time History File

Full time history files present all information of the calculated load effects, they include the information of the leading trucks like position on the bridge, number of involved trucks for inducing the load effect, and the value of load effect. Due to the numerous information which are included, it is an extremely large file for a long run simulation. Although the full time history is not used very often in bridge traffic load effect analysis, it is necessary to be generated to check the program.

In the program, the full time history file can be generated when the specific option is selected, and the program creates a single file named: *01_TotEff.txt*. A sample is given:

Line	No. trucks	No. invovled trucks	Time (second)	Effect (kN.m)
1	0	1	89.21	801.408
2	0	1	89.31	565.968
3	0	1	89.41	401.396
4	0	1	89.51	268.961
5	0	1	89.61	136.526
6	0	1	89.71	62.2444
7	0	1	89.81	4.4145
8	0	1	89.91	0
9	1	1	232.14	0
10	1	1	232.24	79.4201
11	1	1	232.34	218.24
12	1	1	232.44	422.124
13	1	1	232.54	630.669
14	1	1	232.64	937.44
15	1	1	232.74	1342.44
16	1	1	232.84	1749.02

The format is:

- Column 1: The order of leading truck;
- Column 2: The number of trucks currently on the bridge;
- Column 3: The current time counted from the arrival of the first truck;
- Column 4: The value of the load effect induced by the truck configuration on the bridge.

An example output is given showing the number of trucks on the bridge and the corresponding value of load effects. As can be seen, the main loading event is a single truck whilst 2-truck event occurs.

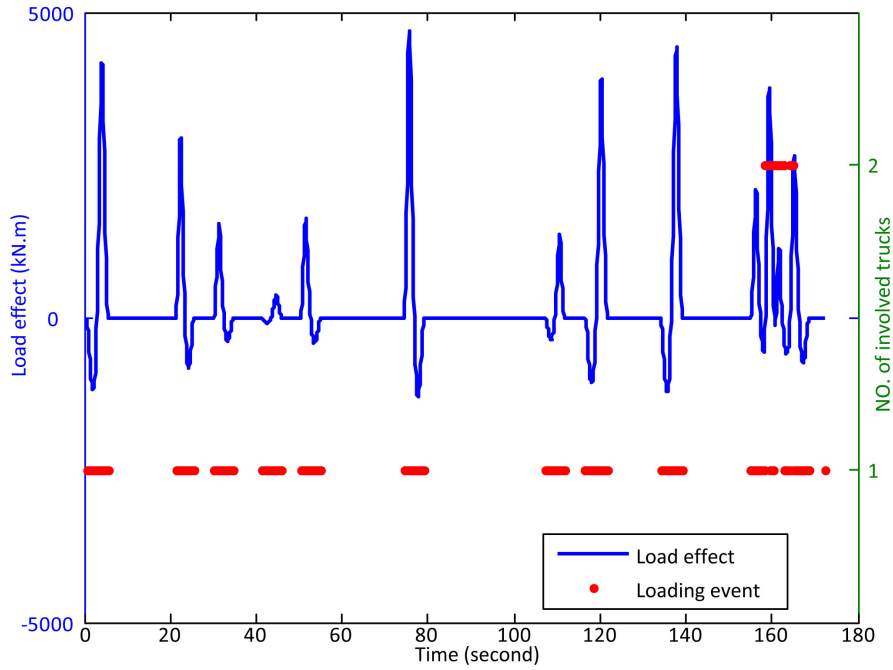


Figure B.4: Full time history

B.4.2 Histograms of Value, Level Crossing, Rainflow Cycle Counting

During the calculation process, several useful statistics, including histogram of values, histogram of level crossing and histogram of rainflow cycle counting of the load effects can be produced simultaneously if the corresponding options are activated.

These three types of histograms have a common requirement that the bin value or number of bins should be determined before conducting calculation. In the CASTOR and LCPC-Pollux, the minimum and maximum are needed to input for all in table two. However, it is impossible to know the exact minimum and maximum before the calculation, therefore the inputs of minimum and maximum are problematic. In BTLECS, the minimum V_{min} and maximum V_{max} are given by an automatic procedure. Before implementing the calculation, a two days of traffic is used to get the 2-days minimum and maximum, and the possible minimum and maximum for the simulation period are estimated on the basis of pre-calculated 2-days values such as multiplying by a factor like 2.

After knowing the minimum V_{min} and maximum V_{max} , another important issue to construct histograms is to determine the number of bins N_b or the bin width h . There is no optimal number of bins, and different bin sizes can reveal different features of the data. Some suggestions have been proposed to determine an optimal number of bins, but almost all of them are based on known the total data, which is impossible during the calculation process, such as Sturge's

formula suggests that the optimal number of bins for a sample of n data is $N_b = \log_2 n + 1$. In this program, we propose to set the bin size as large as possible such as 200, because it is possible to merge like two bins to one when the amount of data is large, but it will be problematic if we want to decompose one bin to two bins if the pre-set bin size has been taken too small. The bin width is thus:

$$\Delta h = \frac{V_{max} - V_{min}}{N_b} \quad (B.4)$$

Histogram of value

For arbitrary E_n , it can be classified to the i^{th} according to

$$i = \text{int} \left(\frac{X_n - V_{min}}{\Delta h} \right) \quad (B.5)$$

as $X_n \in [V_{min} + i \cdot \Delta h, V_{min} + (i + 1) \cdot \Delta h]$. An example of histogram of values is given in Figure B.7.

Histogram of Rainflow cycle counting

In fatigue applications it is generally agreed that the shape of the curve connecting two intermediate local extremes in the load is of no importance, and that only the values of the local maximum and minima of the load sequence influence the life time. A load process can thus, for fatigue applications, be characterized by its sequence of local extremes, also called turning points. For the load effect process X_t with a finite number of local extremes occurring at the time time points t_1, t_2, \dots . For simplicity, we assume that the first local extreme is a minimum, then we can denoted the sequence of turning points by

$$TP(\{X_t\}) = \{X_{t_1}, X_{t_2}, X_{t_3}, X_{t_4}, X_{t_5}, \dots\} = \{m_0, M_0, m_1, M_1, m_2, M_2, \dots\}$$

where m_k denotes a minimum and M_k a maximum, see Figure B.5.

A rainflow cycle is defined as (see also Figure B.6): Let $X(t)$, $0 \leq t \leq T$, be a function with finitely many local maxima of height M_k occuring at times t_k . For the k^{th} maxima at time t_k define the following left and right minima

$$\begin{aligned} m_k^- &= \inf\{X(t) : t_k^- < t < t_k\} \\ m_k^+ &= \inf\{X(t) : t_k < t < t_k^+\} \end{aligned}$$

where

$$t_k^- = \begin{cases} \sup\{t \in [0, t_k] : X(t) > X(t_k)\}, & \text{if } X(t) > X(t_k) \text{ for some } t \in [0, t_k], \\ 0 & \text{otherwise,} \end{cases}$$

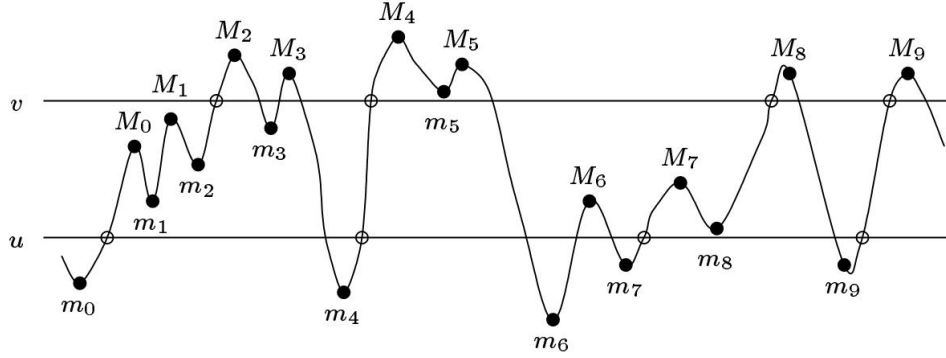


Figure B.5: The local minima and maxima (marked by dots) for a stochastic process.

$$t_k^+ = \begin{cases} \inf\{t \in [t_k, T] : X(t) \geq X(t_k)\}, & \text{if } X(t) > X(t_k) \text{ for some } t \in [t_k, T], \\ T & \text{otherwise.} \end{cases}$$

Then, the k^{th} rainflow cycle is defined as (m_k^{rfc}, M_k) , where

$$m_k^{rfc} = \begin{cases} \max(m_k^-, m_k^+), & \text{if } t_k^+ < T, \\ m_k^- & \text{if } t_k^+ = T. \end{cases}$$

The three typical statistics in fatigue applications are therefore defined as:

$$\begin{aligned} \text{amplitude} &= (M_k - m_k^{rfc})/2 \\ \text{range} &= M_k - m_k^{rfc} \\ \text{mean} &= (M_k + m_k^{rfc})/2 \end{aligned}$$

see also Figure B.6. From these definitions and the rainflow counting algorithm, a histogram

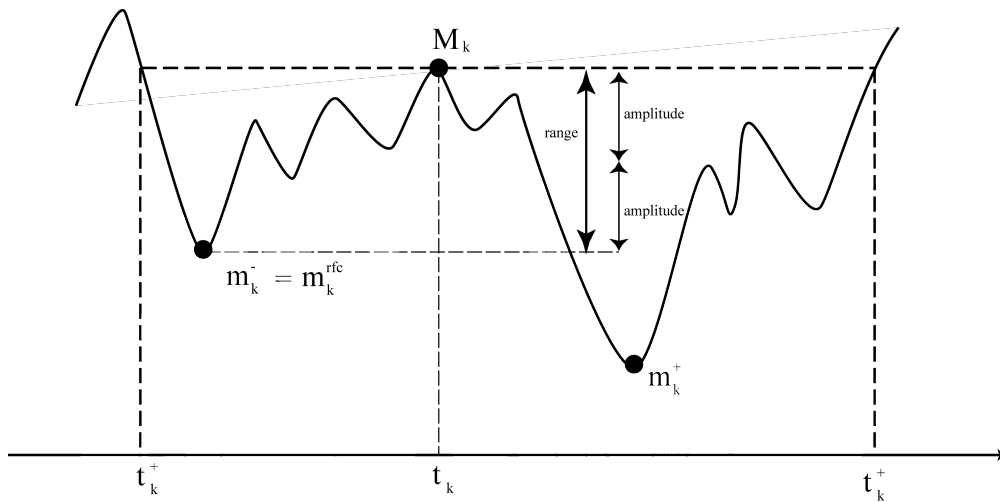


Figure B.6: The definition of rainflow cycle

of rainflow cycles generated is shown in Figure B.9.

Histogram of level crossing counting

The definition and details of level crossing is given in Section 1.2.3. An example of histogram for level crossing counting is given in Figure B.8.

Example

An example of output file for these histogram is given:

Line	Bin value	Level crossing	No.	Rainflow
1	0	50866	152582	155
2	49.0705	51423	62132	77
3	98.141	51866	43396	114
4	147.212	52172	36957	103.5
5	196.282	52402	39518	128
6	245.353	52621	37109	203.5
7	294.423	52741	33216	948
8	343.494	51972	29193	621.5
9	392.564	51503	29037	270.5
10	441.635	51490	28286	219
11	490.705	51473	26288	271.5
12	539.776	51391	24683	292.5
13	588.846	51300	23528	351
14	637.917	51182	22605	361
15	686.987	51001	21700	342.5
16	736.058	50818	20618	407
17	785.128	50593	19788	419
18	834.199	50329	19496	499
19	883.269	49995	19265	532
20	932.34	49595	18537	570
21	981.41	49166	18360	631.5
22	1030.48	48675	18207	689
23	1079.55	48081	18044	780.5
24	1128.62	47396	17644	856
25	1177.69	46609	17050	893.5

B.4.3 Block Maximum Vehicle Files

Two types of block maximum can be obtained from this program. One is the traditional daily maximum that is taken out of the full data regardless of the type of loading events, and another type of daily maximum is drawn with respect to the type of loading event that is classified by

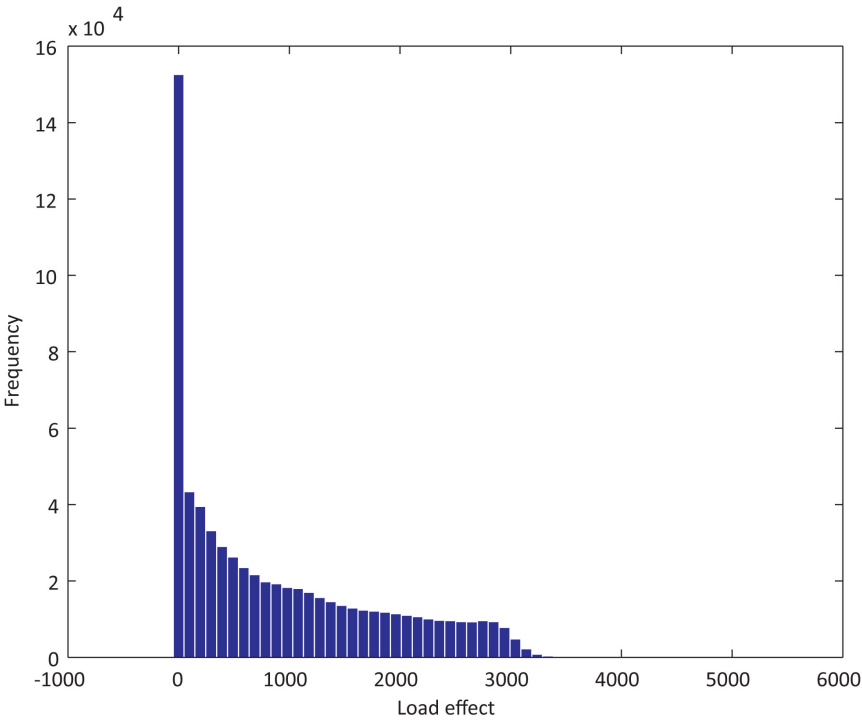


Figure B.7: Standard histogram

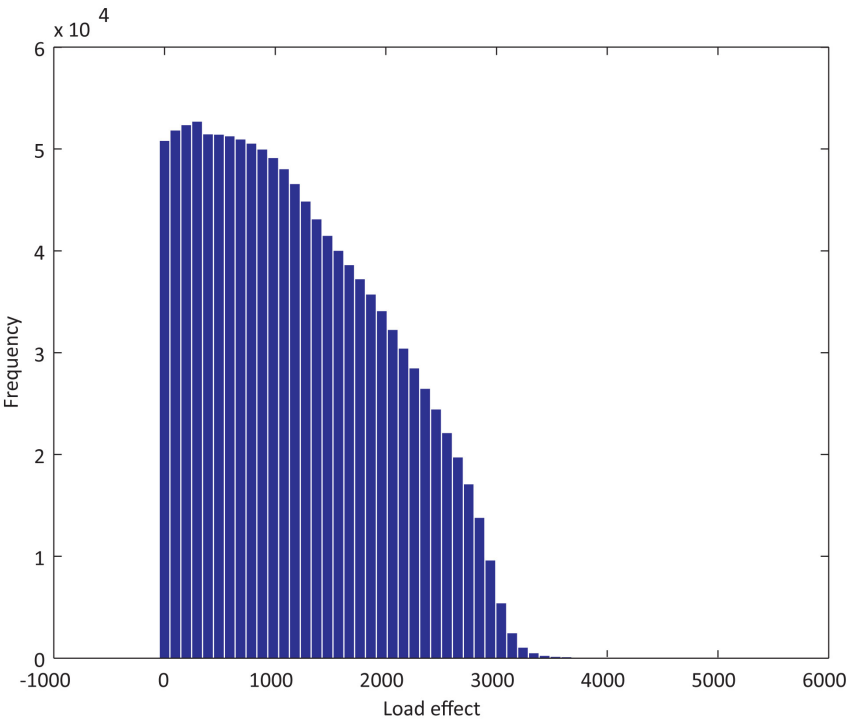


Figure B.8: Level up-crossing histogram

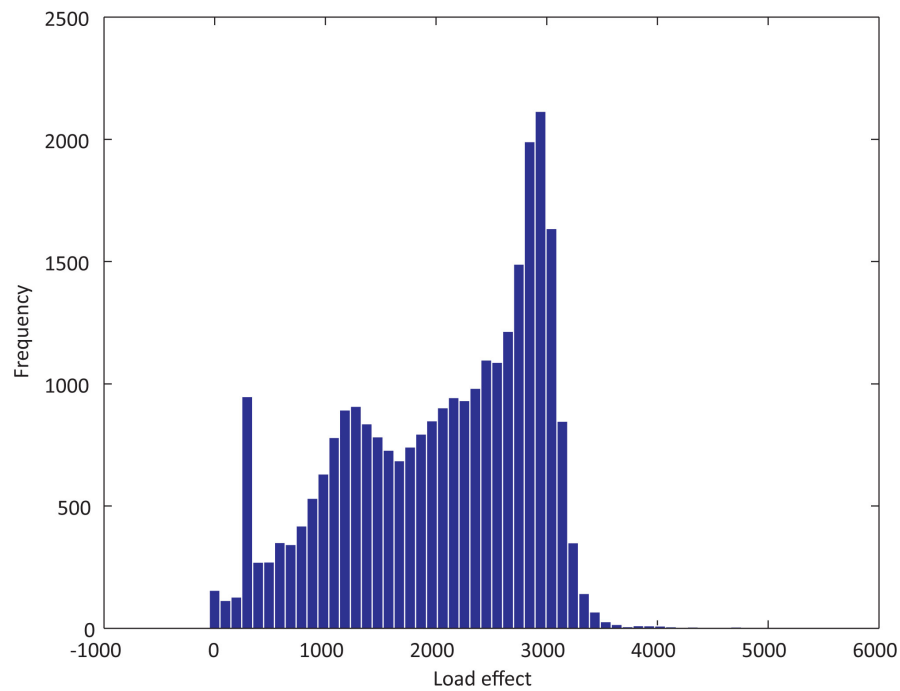


Figure B.9: Rainflow cycle counting histogram

the number of involved trucks. Sample output files are given, and a sample of the Gumbel probability paper for the block maxima is presented in Figure B.10.

	No. involved trucks	Time	Position	Effect (kN.m)
Day 1	1	72607.9	10.6678	4728.27
Day 2	2	24475	18.9944	5802.9
Day 3	2	66844.9	19.96	5789.66
Day 4	2	54157.8	20.4478	4716.15
Day 5	2	70650.5	19.68	4897.4
Day 6	2	25604	23.04	4390.7
Day 7	1	72119.7	9.75111	4819.12
Day 8	1	60144.7	12.8189	4756.69
Day 9	2	49056.3	22.2667	4732.47
Day 10	2	71432.9	20.4856	4936.96

	1-truck	2-truck	3-truck
Day 1	4728.27	4716.16	3239.17
Day 2	4332.16	5802.9	4852.12
Day 3	5215.37	5789.66	1117.7
Day 4	4587.94	4716.15	3526.49
Day 5	4276.61	4897.4	
Day 6	4260.94	4390.7	2956.42
Day 7	4819.12	4643.44	1998.82
Day 8	4756.69	4433.81	2564.87
Day 9	4050.06	4732.47	
Day 10	4432.9	4936.96	2902.31

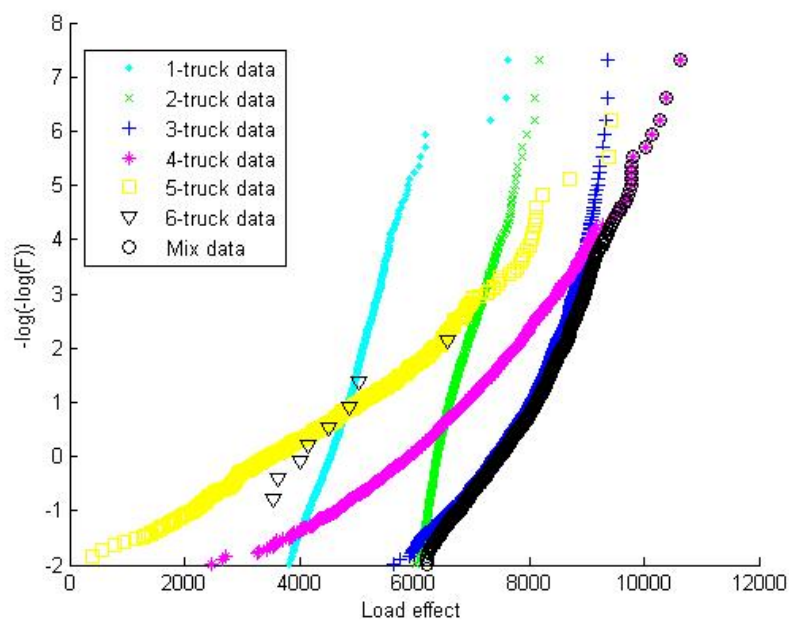


Figure B.10: Mixed daily maxima and maxima for individual loading event

B.4.4 Peaks over Threshold

If peaks over threshold files are required to be output, BTLECS creates two files. One is for negative load effects like hogging moment at middle support of a two-span continuous bridge, and another is for positive load effects like bending moment at mid-span of a simply supported bridge. A sample output is given:

Line	No. involved trucks	Effect (kN.m)
1	2	3482.46
2	1	3478.91
3	2	4716.16
4	2	3459.95
5	1	3687.64
6	2	3492.83
7	1	3534.15
8	1	3536.53
9	1	3446.75
10	1	3585.69
11	2	4438.47
12	1	3462.49
13	2	4137.03
14	2	3822.01
15	2	3824.27

A sample of mean excess plot for the recorded peaks over threshold is shown in Figure B.11.

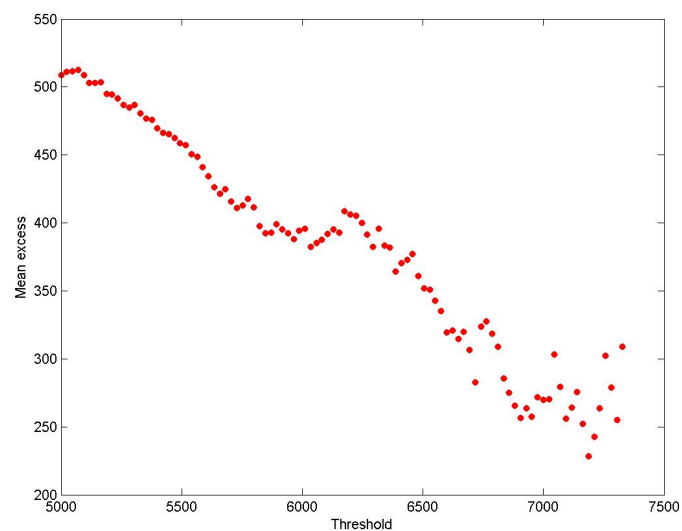


Figure B.11: Mean excess plot

C Mixture Peaks over Threshold Method

The following plots display the diagnosis of GPD obtained by MPOT and conventional POT. The left plots show the comparison in standard probability paper, and the right plots show the comparison in log-scale CDF. In the plots, the black dots represent the observations, the red line represents the GPD fitting from conventional POT method, and the green line represents the GPD fitting from MPOT method. From the top to bottom, the threshold is increased from 90th quantile to 98th quantile. Five parameter estimators (MM, PWM, ML, ADR and MDPD) were used to estimate the GPD parameter.

The legend used in the graphic diagnosis plots is given by Figure C.1.



Figure C.1: Legend for the graphic diagnosis plots of the following figures

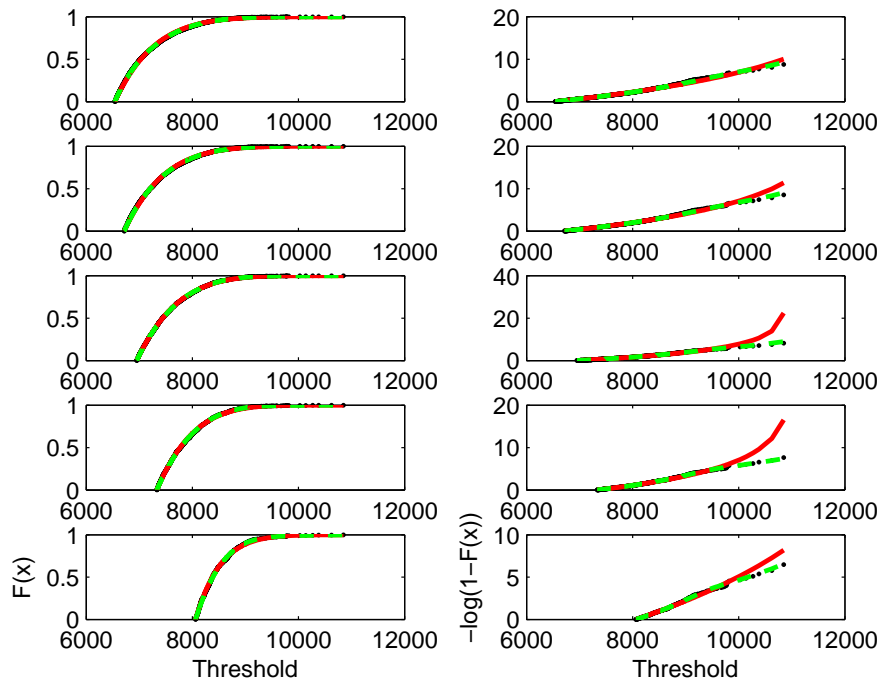


Figure C.2: Diagnosis plot, LE I1, 40 m, MM estimator

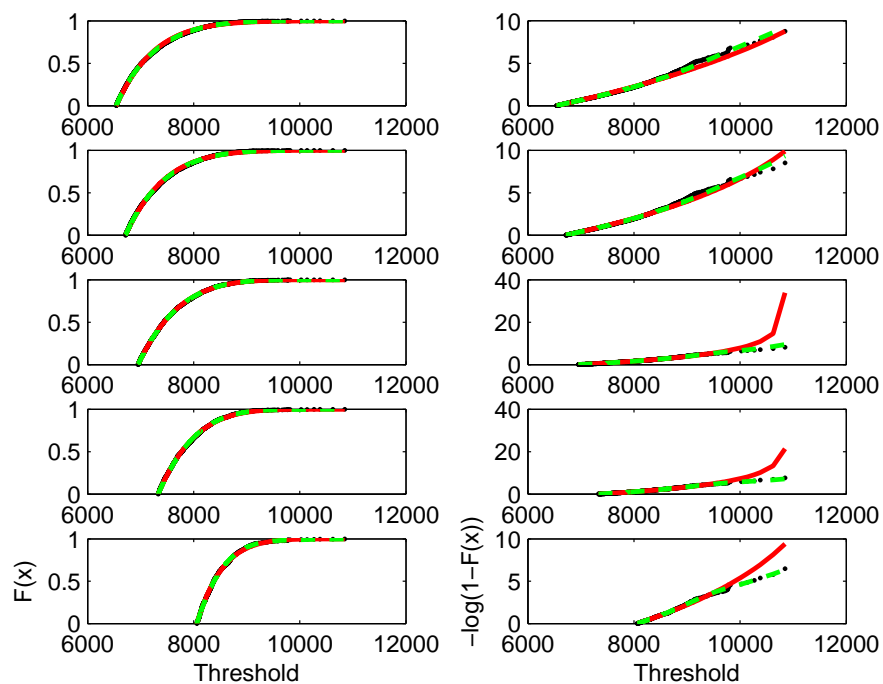


Figure C.3: Diagnosis plot, LE II, 40 m, PWM estimator

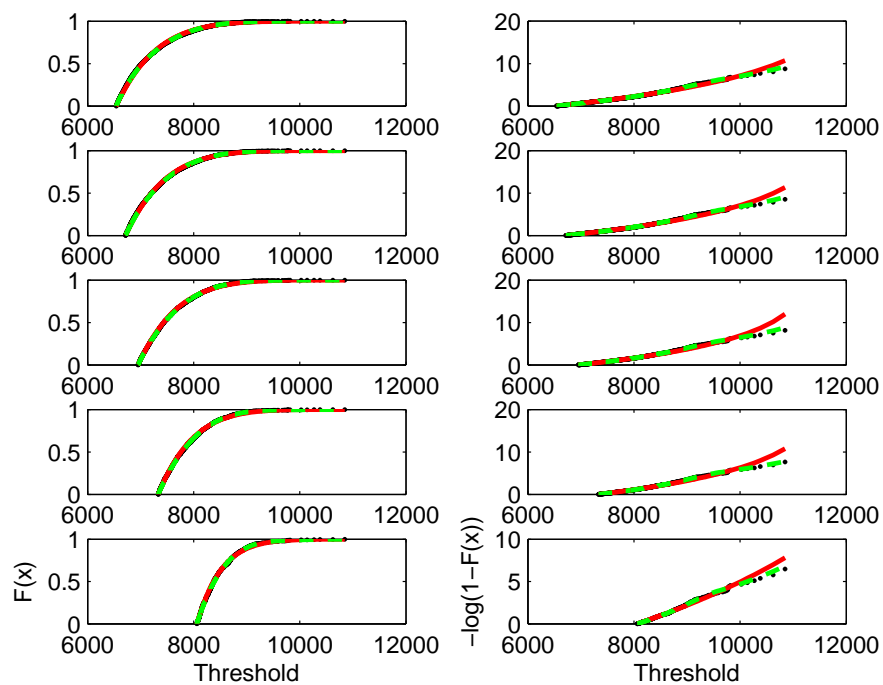


Figure C.4: Diagnosis plot, LE II, 40 m, ML estimator

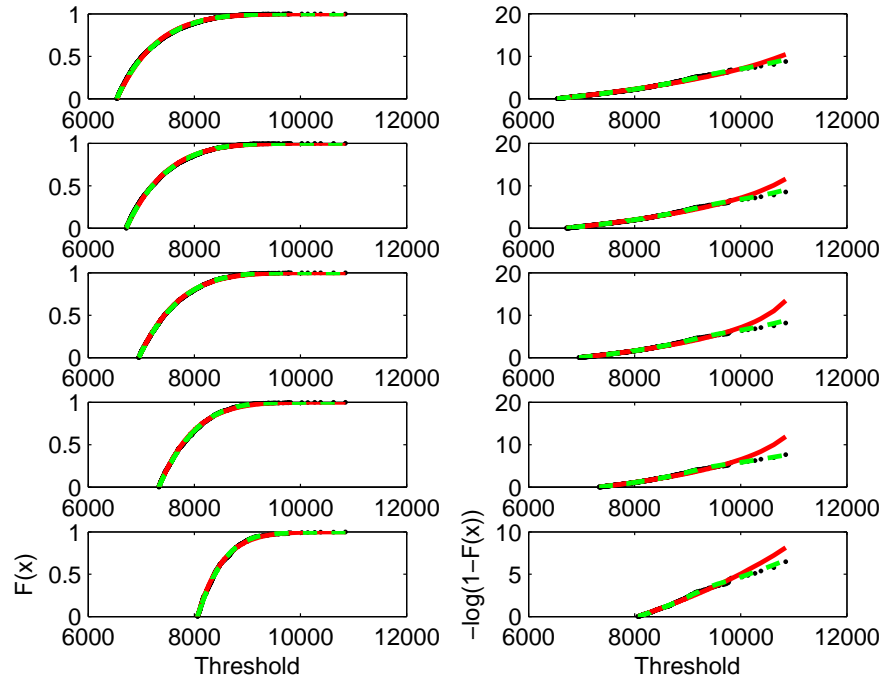


Figure C.5: Diagnosis plot, LE I1, 40 m, MDPD estimator

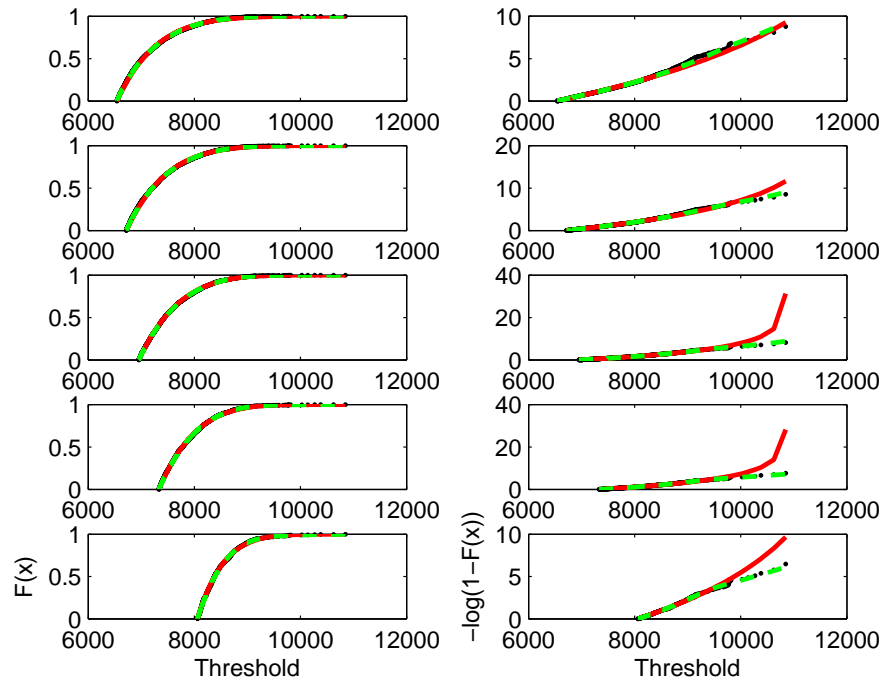


Figure C.6: Diagnosis plot, LE I1, 40 m, ADR estimator

Résumé Long

Une grande majorité (85%) des ponts français a une portée inférieure à 50m. Pour ce type d'ouvrages, la charge de trafic peut être déterminante pour la conception et la vérification. Or, en Europe, le fret routier a augmenté de 36.2% en t.km entre 1995 et 2010, et la croissance annuelle du volume transporté par la route a été estimée à 1.7% en t.km entre 2005 et 2030. Il est donc essentiel de s'assurer que les infrastructures européennes sont en mesure de supporter cette demande croissante en capacité des ouvrages. Pour les ouvrages neufs, les modèles de trafic dans les normes ou les législations pour la conception des ponts incluent une marge de sécurité suffisante pour que la croissance du trafic soit prise en compte sans dommage par ces ouvrages. Mais pour les ouvrages existants, la résistance structurelle aux trafics actuels et futurs est à vérifier et une priorisation des mesures doit être faite pour assurer leur intégrité structurelle et leur sécurité. De plus, afin de préserver leur infrastructure tout en ne menaçant pas leur compétitivité nationale, certains pays réfléchissent à l'introduction de poids lourds plus longs, plus lourds, ce qui permet de réduire le nombre de véhicules pour un volume ou un tonnage donné, ainsi que d'autres coûts (carurant, personnel, ..), ce qui justifie encore plus les études menées.

Le traitement de la problématique de l'accroissement du trafic dépend de notre degré de connaissance des charges de trafic et de leurs effets sur les ouvrages. En effet, dans le cadre du recalcul d'ouvrages existants, on considèrera dans le cas déterministe qu'un ouvrage est en sécurité quand sa capacité de résistance est supérieure aux actions qu'il doit supporter. Par contre, dans l'approche probabiliste, il faut que la résistance soit supérieure avec une probabilité donnée. Ceci signifie que quelle que soit l'approche choisie (déterministe ou probabiliste), la capacité de résistance structurelle et les actions appliquées à la structure doivent être connues le plus exactement possible. Ces dernières années, la modélisation des résistances a largement évolué, réduisant les incertitudes inhérentes. A contrario, l'étude des actions du trafic appliquées aux ouvrages n'a pas reçu autant d'attention jusqu'à ces dernières années. Pourtant, évaluer les effets extrêmes rencontrés par un ouvrage au cours de sa durée de vie est crucial pour sa sécurité. Ceci peut être réalisé de diverses manières, par des mesures empiriques de longue durée, des simulations de Monte Carlo et des analyses statistiques. Pourtant, même si les données relevées sur le terrain sont de plus en plus précises grâce aux avancées dans le domaine du pesage en marche, des enregistrements de longue durée, sans interruption, sont difficiles à recueillir. De même, les simulations pour méthode de

Monte Carlo peuvent générer un très grand nombre de données, mais des paramètres d'entrée erronés ou des hypothèses non vérifiées peuvent entraîner des résultats faux.

Grâce à des développements théoriques, même des enregistrements de relative neuf courte durée peuvent permettre de modéliser correctement l'évolution du trafic. Donc des modélisations de trafic sont connues depuis longtemps, mais les méthodes d'extrapolation n'ont été introduites que récemment. Pourtant, la théorie des valeurs extrêmes a été utilisée dans beaucoup de domaines depuis les 50 dernières années, pour la détermination de crues fluviales, l'estimation des variations des valeurs boursières, le calcul de la résistance de rupture de matériaux La théorie des valeurs extrêmes vise à estimer les probabilités d'événements rares dont certains ne seront probablement jamais observés physiquement. Ainsi modéliser les queues de distributions et les chargements extrêmes est important pour la conception des ponts et les calculs fiabilistes d'ouvrages. Les modèles donnent une approximation des queues de distribution tout en restant flexible sur les formes de queues de distribution. De plus, cette théorie des valeurs extrêmes donne un socle mathématique et statistique suffisamment concret pour justifier l'utilisation de modèles paramétriques, relativement simples, et permet d'obtenir des extrapolations à long terme à moindres frais.

Cette théorie des valeurs extrêmes permet d'évaluer des extrêmes de charges ou d'effets de charges, comme par exemple le niveau de période de retour de 1000 ans. Pourtant appliquer cette théorie se heurte à certains problèmes comme la dépendance entre événements extrêmes. Un autre problème provient de caractère rare des événements extrêmes, ce qui entraîne des difficultés d'identification du modèle et de ses paramètres, en particulier pour une structure complexe. Les effets du trafic sont complexes et difficiles à analyser avec des flux journaliers variables d'un jour sur l'autre. Se posent aussi la question de l'échantillonnage des extrêmes ou le choix des seuils. Ce doctorat se propose de répondre à certaines de ces questions.

Différentes méthodes d'extrapolation ont déjà été utilisées pour modéliser les effets extrêmes du trafic et déterminer les effets caractéristiques pour de grandes périodes de retour. Parmi celles-ci, citons l'ajustement d'une gaussienne ou d'une loi de Gumbel sur la queue de distribution empirique, la formule de Rice appliquée à l'histogramme des dépassements de niveaux, la méthode des maxima par blocs ou celle des dépassements de seuils élevés. Chaque méthode a ses avantages et ses inconvénients. Par exemple, la méthode d'adaptation d'une loi normale ou de Gumbel aux données est simple à comprendre, mais le choix du seuil de la queue de distribution est assez empirique. Ce choix n'est pas requis pour la méthode des maxima de blocs, mais il est nécessaire de choisir la taille des blocs. Une revue de ces méthodes et leurs hypothèses est faite dans le chapitre 1. Au chapitre 2, une étude quantitative est réalisée pour investiguer les différences entre les méthodes : deux calculs sont réalisés, l'un basé sur un échantillon numérique simulé et l'autre utilisant des enregistrements d'effets du trafic réel. La précision des méthodes investiguées est évaluée à l'aide de statistiques connues, le biais et l'erreur quadratique moyennée. En général, les méthodes donnent de moins bons résultats pour les probabilités de défaillance qu'aux valeurs caractéristiques, mais ceci n'est

peut-être qu'une conséquence des faibles probabilités recherchées (10^{-6} par an). Aucune des méthodes ne donne des résultats vraiment corrects en utilisant 1000 jours de données, mais les méthodes utilisant la queue de distribution, et en particulier celle des dépassements de seuil, donnent les meilleurs résultats. Plus de détails peuvent être trouvés au chapitre 2.

Les chapitres 1 et 2 indiquent que la méthode des dépassements de seuils donne de meilleurs résultats, donc nous l'avons utilisée au chapitre 3. Cette méthode n'a été que très peu utilisée dans le domaine des effets du trafic sur les ouvrages. La théorie mathématique nous indique que les dépassements de seuils correctement choisis, peuvent être assimilés à une distribution statistique de la famille de Pareto généralisée. Le choix du seuil, la taille et la précision des données disponibles, les critères pour identifier les pics indépendants impactent la précision des résultats obtenus. Les autres méthodes les plus connues sont celles du maximum de vraisemblance, la méthode des moments et la méthode des moments pondérés, qui ont chacune leurs avantages et inconvénients. La méthode des moments est facile à utiliser mais se limite à des distributions dont le paramètre de forme est inférieur à 0.5. Le chapitre 3 présente les conditions, hypothèses, avantages et inconvénients de ces méthodes, et leur applicabilité au phénomène des effets du trafic dans les ouvrages. Outre les méthodes déjà citées, nous étudions le maximum de vraisemblance pénalisé, le minimum de divergence de la densité, la méthode du fractile empirique, le maximum d'ajustement, le moment de vraisemblance. Pour illustrer le comportement et la précision de ces méthodes, trois études ont été conduites: sur des données issues de simulations numériques, des effets du trafic simulés par méthode de Monte Carlo et des effets du trafic mesurés sur un ouvrage réel. Des comparaisons sont faites. Les estimateurs ont des performances différentes et les performances d'un même estimateur diffèrent selon l'étude considérée. La conclusion générale est qu'aucune méthode n'est meilleure que toutes les autres dans tous les cas. Mais des recommandations peuvent être faites : pour une étude sur des données numériques, la méthode des moments et celle des moments pondérés sont conseillées pour des distributions avec des paramètres de forme négatifs, en particulier si la taille de l'échantillon est faible (<200), alors que la méthode du maximum de vraisemblance est recommandée pour des paramètres de forme positifs. Pour les effets du trafic simulés, le maximum de vraisemblance et le maximum de vraisemblance pénalisé donnent de meilleures estimations de la valeur de retour de 1000 ans quand le nombre de dépassements du seuil est supérieur à 100, alors que la méthode des moments et celle des moments pondérés sont meilleures pour des tailles d'échantillon inférieures à 100. Finalement, l'application aux données de trafic mesurées montre que les données aberrantes ont un impact significatif sur les estimations. Les résultats et commentaires sont présentés dans le chapitre 3.

Une autre difficulté provient du mélange de deux sous-populations distinctes. Ces sous-populations correspondent notamment, dans le cas des effets du trafic dans les ouvrages, aux phénomènes de croisement ou dépassement de plusieurs véhicules. Ceci contredit l'hypothèse d'événements identiquement distribués, nécessaire à l'application des théories des valeurs extrêmes. Des méthodes utilisant des distributions multi-modales (gaussiennes ou valeurs extrêmes généralisées) ont été proposées dans la littérature pour modéliser les

effets extrêmes du trafic.

Ce chapitre 4 propose une généralisation de la méthode des dépassements de seuils nommée dépassement des seuils mixés. Cette nouvelle méthode permet non seulement de modéliser correctement la queue de distribution, mais également de tenir compte des différentes sous-populations. Une évaluation de cette méthode est réalisée à l'aide de données issues de simulations numériques. Une étude de robustesse vis-à-vis de données erronées est également réalisée. Les résultats indiquent que la méthode des dépassements de seuils mixés est plus flexible que la méthode conventionnelle. De plus, en utilisant des effets du trafic simulés sur divers ouvrages de différentes portées, il semblerait que la divergence entre ces deux méthodes augmente quand la portée augmente. Ceci s'explique par le fait que lorsque la portée augmente, le nombre de véhicules impliqués peut changer plus facilement.

Pour des ouvrages de portée supérieure à 50m, le scénario conditionnant les effets extrêmes est la congestion qui ne nous intéresse pas ici. Pour certains ouvrages, l'effet du trafic peut aussi provoquer la fatigue. Au chapitre 5, nous étudions l'effet du trafic sur les ouvrages de longue portée pour des effets locaux, notamment l'effet de la position latérale des véhicules. Des enregistrements de trafic ont été utilisés et ont montré des différences avec la distribution du trafic recommandée par l'Eurocode 1. L'effet de ces différences a été analysé pour un pont à dalle orthotrope (la prenant l'exemple du viaduc de Millau). Il a été montré que la localisation transversale des véhicules affecte de manière significative les effets induits dans les ponts. La connaissance de la localisation transversale des véhicules permet donc de déterminer plus précisément les soudures qui seront fragilisées en premier, et donc les besoins d'inspection d'ouvrages prioritaires.

En conclusion, une méthode d'extrapolation innovante, permettant de traiter des sous-populations mixtes a été développée. Aucune méthode d'extrapolation n'est supérieure aux autres dans tous les cas, mais il semblerait pourtant que la méthode des dépassements de seuils sont la plus performante. Pourtant il faudrait généraliser l'acquisition de données du trafic, précises et sur des durées suffisantes. Ces données peuvent être obtenues par les stations de pesage en marche, dont un réseau est actuellement installé et opérationnel en France. Une évaluation correcte de l'état actuel des ouvrages existants vis-à-vis des effets actuels et futurs du trafic devient alors possible.

List of Figures

1.1	Maximum value distribution PDF for varying N	12
1.2	GEV distribution	14
1.3	Extreme value modeling methods: block maxima and peaks over threshold . .	15
1.4	Cumulative distribution function for generalized Pareto distribution	16
1.5	Principal parameters of a stochastic proces	18
1.6	CDF of moment and shear effect on normal probability paper. Reproduced from [Nowak and Hong, 1991]	23
1.7	Fitting normal distribution to upper tail of GVW histogram. Reproduced from [O'Brien et al., 2010]	24
1.8	Extrapolation with nonparametric fit. Reproduced from [Kozikowski, 2009] . .	24
1.9	Cumulative distribution maximum load effect of single lane events for different return periods. Reproduced from [Sivakumar et al., 2011]	25
1.10	Daily maximua CDF fitted to Gumbel distribution (Reproduced from [Cooper, 1997])	25
1.11	Gumbel extrapolation for the Foyle bridge, Reproduced from [O'Brien et al., 1995]	27
1.12	Gumbel extrapolation for the strain, Reproduced from [Grave et al., 2000] . . .	28
1.13	Gumbel plot of load effect, Reproduced from [Caprani et al., 2002]	28
1.14	A comparison of extrapolated PDF by NCHRP 12-76 method and the two steps block maxima method for load effect, Reproduced from [Fu and You, 2010] . .	29
1.15	Histograms of load effect for different loading events, (a)-(e) represent 1- to 5-truck events, Reproduced from [Harman and Davenport, 1979]	31
1.16	Mixture model of loading events, Reproduced from [Caprani et al., 2008]	32

List of Figures

1.17 Example of fitting a generalized Pareto distribution, Reproduced from [Crespo-Minguillon and Casas, 1997]	34
1.18 Application of POT to load effect for a 20 m span, Reproduced from [James, 2003].	35
1.19 Principles of optimal fitting. Reproduced from [Cremona, 2001]	36
1.20 Application of fitting Rice's formula to level crossing histogram. For queue length of 25 meters. Each value is a yearly maximum value, therefore the figure shows values that represent 3805 years' signal with one year interval. Reproduced from [Getachew, 2003]	37
2.1 Symmetrizing probability density function of load effect to obtain probability density function of resistance	42
2.2 Fit of the estimated generalized extreme value distribution for annual maxima from 5000 years of simulation	44
2.3 Error bar plot for inferred 75-year characteristic values	47
2.4 Error bar plot for inferred probabilities of failure	47
2.5 Daily maxima of load effects for 20 sets of 1000 days of simulation on Gumbel probability paper	49
2.6 Boxplots for 75-year return levels from 1000 days of simulation	51
2.7 Boxplots for annual probabilities of failure from 1000 days of simulation	52
2.8 Estimated distribution for maxima taken out of various time intervals for data from 1000 days of simulation	54
2.9 Estimated annual maximum distribution from distributions fitted to block maxima taken out of various time intervals for data from 1000 days of simulation .	55
2.10 Boxplots for 75-year return levels for annual maximum distribution from different time intervals	56
3.1 Comparison of simulated and observed load effects on ME plot	87
3.2 View of the instrumented Roberval Bridge	89
3.3 Instrumented span, after Siegert et al. [2008]	90
3.4 Histogram of the measured bending deformations	90

4.1	RMSE of quantile estimators.	106
4.2	Bias of quantile estimators.	106
4.3	Mean of quantile estimators.	107
4.4	Standard deviation of quantile estimators.	107
4.5	Comparison of estimates of characteristic value between conventional methods vs. mixture methods for Study 2, Example 1	110
4.6	Estimated 1000-year return levels in boxplots for Study 2, Example 1	111
4.7	Comparison of estimates of characteristic value between conventional methods vs. mixture methods for Study 2, Example 2	112
4.8	Estimated 1000-year return levels in boxplots for Study 2, Example 2	112
4.9	These figures display the GPD fitting obtained by CPOT and MPOT approaches.	115
4.10	Extreme value distribution from conventional and mixture POT methods	116
4.11	Comparison of estimates of characteristic value between conventional methods vs. mixture methods for Study 3	117
4.12	Error bar plot (mean \pm standard deviation) of 1000-year return level	118
4.13	Results of proportion of contaminated distribution effect for Study 4.	120
4.14	Results of proportion of contaminated distribution effect for Study 5.	120
4.15	Time history of load effects	121
4.16	Detail of local extreme identification	122
4.17	Histogram of load effects due to various type of loading event	123
4.18	Probabilities for six types of loading events (left) over 90 th and (right) 95 th per- centile.	124
4.19	Diagnostic plot for threshold excess model fitted to load effect	131
4.20	Diagnostic graphics	132
5.1	WIM device for collection of transverse vehicle position.	143
5.2	WIM station locations and measured period.	144
5.3	Profile of WIM system on the four studied stations	145

List of Figures

5.4	Sensitivity analysis.	147
5.5	Distribution of transverse location of centre line of trucks for various types of truck.	148
5.6	Distribution of transverse location of centre line of trucks on slow lane for various location	149
5.7	Signature of extreme vehicle seen as: (a) Morge Bridge, (b) Cross section of box-girder and gauge arrangement, (c)Influence on transverse reinforcing bar tensile strains and, (d) Influence on longitudinal bar strains, Reproduced from [Treacy and Bruhwiler, 2012]	150
5.8	Finite element model for Morge bridge	151
5.9	Change of transverse strain on the rebar at sensor position S1A	152
5.10	Millau viaduct	153
5.11	Simplified finite element model of an orthotropic steel deck	154
5.12	Load distribution through the wearing cover (unit: mm)	154
5.13	Longitudinal influence line	155
5.14	Transverse influence line	157
5.15	Histogram of individual axle loads for standard 5-axle truck	158
5.16	Histogram of stress spectra under traffic load with EC and measured vehicle lateral position model	159
5.17	Comparison of histograms of stress spectra under traffic load with EC and measured vehicle lateral position model	160
5.18	Transverse distribution of wheel path	161
5.19	Stress histograms plotted on Eurocode S-N curves	163
A.1	The measurement locations and periods	189
A.2	Truck classification	192
A.3	Traffic composition	193
A.4	Flow rate and percentage	193
A.5	GVW histogram and fitting for 2-axle trucks	194

A.6	GVW histogram and fitting for 3-axle trucks	195
A.7	GVW histogram and fitting for 4-axle truck	196
A.8	GVW histogram and fitting for 5-axle trucks	196
A.9	Percentage of GVW carried by each axle for 5-axle trucks, category 5	197
A.10	Percentage of GVW carried by each axle for 5-axle trucks, category 5	197
A.11	Cumulative distribution function for headway	198
B.1	Influence lines.	202
B.2	Flowchart of BTLECS Program	203
B.3	Sample of input traffic data file	203
B.4	Full time history	210
B.5	The local minima and maxima (marked by dots) for a stochastic process.	212
B.6	The definition of rainflow cycle	212
B.7	Standard histogram	214
B.8	Level up-crossing histogram	214
B.9	Rainflow cycle counting histogram	215
B.10	Mixed daily maxima and maxima for individual loading event	216
B.11	Mean excess plot	217
C.1	Legend for the graphic diagnosis plots of the following figures	221
C.2	Diagnosis plot, LE I1, 40 m, MM estimator	221
C.3	Diagnosis plot, LE I1, 40 m, PWM estimator	222
C.4	Diagnosis plot, LE I1, 40 m, ML estimator	222
C.5	Diagnosis plot, LE I1, 40 m, MDPD estimator	223
C.6	Diagnosis plot, LE I1, 40 m, ADR estimator	223

List of Tables

1.1	Domains of Attraction of the Most Common Distributions [Castillo et al., 2004]	13
2.1	Statistics (distribution parameters, symmetry axis, 75-year return level) of annual maximum traffic load effects from 5000 years of simulation	45
2.2	Percentage differences in 75-year return levels for various time intervals (%) . .	53
3.1	Three classical EDF statistics	69
3.2	Modified Anderson-Darling statistics	69
3.3	Computational forms for the EDF statistics	69
3.4	Bias of estimators of shape parameter for GPD	78
3.5	Bias of estimators of scale parameter for GPD	79
3.6	Bias of estimators of quantile at non-exceedance probability of 0.9	80
3.7	Bias of estimators of quantile at non-exceedance probability of 0.999	81
3.8	RMSE of estimators of shape parameter for GPD	82
3.9	RMSE of estimators of scale parameter for GPD	83
3.10	RMSE of estimators of quantile at non-exceedance probability of 0.9	84
3.11	RMSE of estimators of quantile at non-exceedance probability of 0.999	85
3.12	Mean absolute scaled error for the competition of estimators traffic load effect data	88
3.13	Inconsistency rate for each method of parameter estimation	91
3.14	Measurements of Roberval bridge: mean and standard deviation of estimated shape and scale parameters	93

List of Tables

3.15 Measurements of Roberval bridge: mean of return levels for various return periods ($\mu m/m$)	94
3.16 Measurements of Roberval bridge: standard deviation of return levels for various return periods ($\mu m/m$)	95
4.1 Simulation results for the estimation methods of MM, PWM, ML, MDPD and ADR. The results presented are the RMSEs over 500 replicates.	105
4.2 Simulation results for the estimation methods of MM, PWM, ML, MDPD and ADR. The results presented are the biases over 500 replicates.	106
4.3 Simulation results for the estimation methods of MM, PWM, ML, MDPD and ADR. The results presented are the means over 500 replicates.	107
4.4 Simulation results for the estimation methods of MM, PWM, ML, MDPD and ADR. The results presented are the standard deviations (STDs) over 500 replicates.	108
4.5 Parameters of mechanisms for Study 2	109
4.6 Parameters of mechanisms for Study 3	113
4.7 Parameter estimates for CPOT method by various estimators	113
4.8 Parameter estimates for MPOT method by various estimators	114
4.9 Distribution parameters for Study 4 and Study 5	119
4.10 Influence lines used in calculation of load effect	122
4.11 Probabilities for six categories of loading events for data above 90 th and 95 th percentile	125
4.12 Both shape parameter ξ and scale parameter σ unknown: upper tail asymptotic percentage points for W^2 of Cramer-von Mises test	126
4.13 Both shape parameter ξ and scale parameter σ unknown: upper tail asymptotic percentage points for A^2 of Anderson-Darling test	127
4.14 Critical value at various thresholds	127
4.15 Empirical distribution function statistics for load effect of length 40m, Load effect I1	128
4.16 Root mean square error at various threshold	129
4.17 Optimal threshold selection for I1 (bending moment at mid-span of simply supported bridge) with bridge length of 40m	130

4.18	KS test statistics for various thresholds and parameter estimation methods . . .	133
4.19	Percentage difference of 100-year return level between conventional and mixture method (%)	134
4.20	Difference in 1000-year return level between conventional and mixture model (%)	135
4.21	Difference (mixture POT vs. mixture GEV)	136
4.22	Comparison of 100-year return levels (or characteristic values)	137
4.23	Comparison of 1000-year return levels (or characteristic values)	138
5.1	Fitted distribution parameters	146
5.2	Stress (relative percentage difference, %)	158
5.3	Cumulative fatigue damage in rib-to-deck joint under SJDV traffic	161
5.4	Localization of cumulative fatigue damage	162
A.1	Overview of WIM data	190
A.2	Comparison of data cleaning rules	191
A.3	Classification of truck and traffic composition	194
B.1	Traffic data file format	204
B.2	Traffic composition input file	206
B.3	Flow rate input file	206
B.4	Axle spacing input file for 2-axle truck	207
B.5	Axle weight input file for 2-axle truck	207
B.6	GVW input file for 2-axle truck	207
B.7	Headway	208

Curriculum Vitae

Mr. Xiaoyi Zhou was born in 1982 in Yushan, Jiangxi Province, China. He has pursued the doctoral degree in École Doctorale Sciences Ingénierie et Environnement at Université Paris-Est since 2010. He had got his Master of Engineering degree from Department of Bridge and Tunnel Engineering at Tongji University, China, in 2008, and Bachelor of Science degree from College of Civil Engineering and Architecture at Zhejiang University of Technology, China, in 2005.

Mr. Zhou has worked as a Marie Curie Early Stage Researcher at IFSTTAR (former LCPC) since May 2010. From 2005 to 2010, Mr. Zhou worked as a Graduate Research Assistant at Tongji University, China.

Mr. Zhou has been involved in research in several areas, and his research interests are: structural reliability-based assessment, bridge structure maintenance, rehabilitation, management, modeling extreme bridge traffic load effect and extreme value theory. His publications and communications during doctoral period are listed below:

1. Zhou, X., Schmidt, F., Toutlemonde, F. and Jacob, B. (2013) Applying weigh-in-motion traffic data to reliability based assessment of bridge structures, 11th International Conference on Structural Safety & Reliability, New York, June 16-20, 2013.
2. Zhou, X., Schmidt, F. and Jacob, B. (2012) Application of generalized Pareto distribution to bridge traffic load effect, Journées des doctorants (Workshop), Lille, 9-11 May, 2012 (presented).
3. Zhou, X., Schmidt, F. and Jacob, B. (2012) Assessing confidence intervals on extreme traffic loads, 6th International Conference on Weigh-in-Motion, 3-7 June, Dallas, 2012.
4. Zhou, X., Schmidt, F. and Jacob, B. (2012) Extrapolation of traffic data for development of traffic load models: assessment of methods used during background works of the Eurocode, 6th International Conference on Bridge Maintenance, Safety and Management, 7-11 July, Stresa, 2012 (presented).
5. Zhou, X., Toutlemonde, F., Jacob, B. and Schmidt, F. (2012) Estimation statistique des charges extrêmes de trafic sur les ouvrages d'art, Journées Ouvrages d'Art, 9-11 May, Sourdun, 2012 (presented).
6. Zhou, X., Schmidt, F. and Toutlemonde, F. (2012) Practical extreme value modeling of traffic load effects on bridges, Entretiens 2012 du Réseau Génie Civil et Urbain (Workshop), 4 October, Paris, 2012 (poster).
7. O'Brien, E., Schmidt, F., Hajializadeh, D., Zhou, X., Enright, B., Caprani, C., Wilson, S. and Sheils, E., A review of probabilistic methods of assessment of load effects in bridges, Structural Safety (under review).

8. Ruan, X., Zhou, X. and Guo J. (2012) Bridge traffic load effect simulation and extrapolation based on synthetic vehicle flow, Journal of Tongji University (Natural Science), Vol. 10, 2012 (in Chinese).
9. Chen, A., Ruan, X., Zhou, X., Guo J., Ma, R. and Wang, D. (2011) Random traffic flow simulation system, Registered software (No. 20115R048844), China, 2011.